UNIVERSITY OF SOUTHAMPTON

FACULTY OF ENGINEERING AND THE ENVIRONMENT

Civil and Environmental Engineering

Laboratory Element Tests and Numerical Modelling to Investigate the Performance of Composite Sprayed Concrete Lined Tunnels in Soft Ground

by

Jiang Su

Thesis for the degree of Doctor of Philosophy

May 2015

UNIVERSITY OF SOUTHAMPTON

ABSTRACT

FACULTY OF ENGINEERING AND THE ENVIRONMENT

Civil Engineering

Thesis for the degree of Doctor of Philosophy

LABORATORY ELEMENT TESTS AND NUMERICAL MODELLING TO INVESTIGATE THE PERFORMANCE OF COMPOSITE SPRAYED CONCRETE LINED TUNNELS IN SOFT GROUND

Jiang Su

This thesis investigates the behaviour of composite sprayed concrete lined tunnels via laboratory experimental work and numerical modelling. The composite spayed lining consists of two layers of shotcrete separated by a spray applied waterproofing membrane. The primary aims of the research were three-fold. The first was to examine whether there is composite action between the three layers. The second objective was to assess the factors controlling composite action. The third objective was to explore a design methodology for producing an efficient and robust composite SCL tunnel lining.

A three-stage research programme was undertaken at the University of Southampton, UK. The first part of this research consisted of a large number of short and long-term compression, tension and shear tests on samples cut from composite shell test panels, in order to measure the interface parameters. The second part included a series of short-term four-point bending tests on samples cut from the same composite shell test panels and the development of corresponding numerical models. This was to confirm the interface parameters and verify a numerical modelling approach using Finite Difference numerical analysis package FLAC (Fast Lagrangian Analysis Continua) ready for the third stage. The third part of the research programme was an extensive numerical study investigating the impact of variations in interface properties and primary/secondary lining thickness ratios on the performance of composite SCL tunnels under practical loadings.

The overall conclusion of the project is that there can be significant composite action in composite SCL tunnel linings, the overall lining thickness can be

significantly reduced by utilising composite action and the sprayed membrane interface is robust enough to maintain the integrity of CSL tunnels under most loading scenarios.

Table of Contents

List of Tables

List of Figures

DECLARATION OF AUTHORSHIP

I, JIANG SU, declare that this thesis and the work presented in it are my own and have been generated by me as the result of my own original research.

Laboratory Element Tests and Numerical Modelling to Investigate the Performance of Composite Sprayed Concrete Lined Tunnels in Soft Ground

I confirm that:

1. This work was done wholly or mainly while in candidature for a research degree at this University;
2. Where any part of this thesis has previously been submitted for a degree or any other qualification at this University or any other institution, this has been clearly stated;
3. Where I have consulted the published work of others, this is always clearly attributed;
4. Where I have quoted from the work of others, the source is always given. With the exception of such quotations, this thesis is entirely my own work;
5. I have acknowledged all main sources of help;
6. Where the thesis is based on work done by myself jointly with others, I have made clear exactly what was done by others and what I have contributed myself;
7. Parts of this work have been published as:

(1) Su, J. Design of sprayed concrete lining in soft ground – a UK perspective. Underground. The Way to the Future. *Proceedings of the World Tunnel Congress 2013* Abingdon, GB, CRC Press. 593-600.

(2) Su, J., Bloodworth, A. and Haig, B. Experimental Investigation into the Interface Properties of Composite Concrete Lined Structures, *The Way to the Future. Proceedings of the World Tunnel Congress 2013* Abingdon, GB, CRC Press. 1518-1525.

(3) Su, J. and Bloodworth, A. Experimental and Numerical Investigation of Composite Action in Composite Shell Linings, *Proceedings of 7th International Symposium on Sprayed Concrete*, Sandefjord, Norway, 361-374.

Signed:.....

Date: .....

Acknowledgements

First of all, I would like to express my sincere thanks for my supervisors Dr. Alan Bloodworth and Professor Chris Clayton for their direction, encouragement and assistance throughout the period of this work.

I would also like to express my gratitude to Ross Dimmock for his inspiration of this project and continuous encouragement and help, Chris Pound for this assistance and advice and Matt Lane for proof-reading my thesis.

Special thanks go to Mott MacDonald for sponsoring me for this PhD research and Tam-Normet for providing me the testing samples.

I would like to thank Dave Lynock and Harvey Skinner for all his help in the lab and their expertise in making all the special testing equipment.

Many thanks are due to all my colleagues and friends for their contribution in numerous ways and particularly to Tony Deane, Alun Thomas, Yusheng Hsu, Ringo Tan and Bethan Haig.

Finally, I would like to thank my parents and my wife, Xu Sun, for their immense and endless support and encouragement during my whole studies.

Definitions and Abbreviations

ASCE: American Society of Civil Engineers

BCH: Bench

BSI: British Standard Institution

CSL: Composite shell lining

CTRL: Channel tunnel rail link

DSL: Double shell lining

EFNARC: European Federation of National Associations Representing for Concrete

FLAC: Fast Lagrangian Analysis Continua

GT ratio: ratio between the clear distance between the nearby construction and tunnel extrados to the tunnel diameter.

HEX: Heathrow Express

HME: Hypothetical Modulus of Elasticity

HSE: Health and Safety Executive

H&S: Health & Safety

ICE: Institution of Civil Engineers

INV: Invert

JLE: Jubilee Line Extension

JRC: Joint roughness coefficient

LU: London Underground

NATM: New Austrian Tunnelling Method

P/S ratio: Primary lining to secondary lining thickness ratio

SCL: Sprayed concrete lining

SSL: Single shell lining

TH: Top heading

VSU: Victoria station upgrade

Chapter 1: Introduction

1.1 General background

During the reference and detailed design stages of the Crossrail project for London Underground, it was recognised that there was a lack of knowledge on the tensile and, especially, the shear parameters at the sprayed concrete-membrane interface (Crossrail 2010). This prevented tunnel engineers from designing composite sprayed concrete lined (SCL) tunnel and hence limited the optimisation of lining thickness that could be achieved in soft ground. An industry sponsored research project was undertaken at the University of Southampton, funded by both Mott MacDonald and Tam-Normet, to investigate the composite action in SCL tunnel linings with sandwiched spray applied waterproofing membrane, by means of laboratory experimentation and numerical modelling. This thesis presents the research carried out, its findings, and evaluates the significance of composite action for SCL tunnel design.

1.2 Introduction to SCL tunnels

A SCL tunnel is one which uses sprayed concrete as its main ground support measure. Its biggest advantage over the segmental lined tunnelling method is its ability to construct non-circular shape tunnels. Depending on the preference of designers and contractors and the specific ground conditions encountered, different excavation sequences can be adopted to construct SCL tunnels in different sizes and shapes.

For a typical SCL tunnel construction, following the excavation of the ground for a given advance (*e.g.* top heading), the sprayed concrete is immediately applied to the face to stabilise the exposed ground. After completion of a certain number of following steps (*e.g.* bench and invert), a completed ring is formed, acting as a load bearing shell structure for either short or long-term support. This is usually followed by the installation of either a sheet or sprayed waterproofing membrane, before the construction of a permanent cast *in situ* or sprayed concrete secondary lining.

1.3 History and development of SCL tunnels

1.3.1 The early days of sprayed concrete

The sprayed concrete technique, which can be dated back to 1911 in the USA, was first used by Carl E. Akeley (Austin and Robins 1995) to make models of animals in a museum. As a means of tunnel support, SCL was first used in 1914 in the Bruceton Experimental Mine in the USA and by the 1920s had been used in several tunnels across Europe (Jones 2007). By the 1950s, SCL had become the primary means of support and controlling rock pressures and deformations in rock tunnels and mines (Kovari, 2003a, 2003b). The seminal work of the SCL technique was mostly attributed to two Austrians, Rabcewicz (1954a, 1954b 1964a, 1964b, 1965, 1969a, 1969b, 1969c) and then Golser (Rabcewicz and Golser 1973, 1974a, 1974b; Golser 1976, 1978) in the second half of the 20th century. In particular, Rabcewicz rebranded this technique as the 'New Austrian Tunnelling Method' (NATM). In 1969 the city of Frankfurt decided to test the NATM for driving metro tunnels, and the subsequent successful construction of underground stations in the 1970s demonstrated the principles apply equally well to soft ground (Babendererde 1980).

The NATM has many definitions (Rabcewicz 1964a, 1964b, Müller-Salzburg 1977, Sauer 1988, Kovari 1994). There is also a debate about whether NATM is a tunnelling philosophy or a set of excavation and support techniques (Golser 1978, Brown 1990, Hagenhofer 1990, Barton and Grimstad 1994, ICE 1996). To avoid any confusion, in this report 'SCL tunnelling' will be used to describe the tunnel excavation and support technique.

1.3.2 SCL tunnelling in the UK

The exact date of the first SCL tunnel built in the UK is still debated. However, it is widely acknowledged that the first extensive use of SCL in the UK was the Channel Tunnel in 1989. The first SCL tunnel successfully built within London was the Heathrow Express (HEX) Trial Tunnel in 1992. In 1994, SCL tunnelling experienced its biggest crisis in the UK as an SCL tunnel collapsed during its construction at Heathrow. All SCL works, including HEX and Jubilee Line Extension (JLE) projects, were halted. In 1996, the Institution of Civil Engineers (ICE) published a report (ICE 1996) on SCL tunnelling, concluding that this method can

be safely used in soft ground. In this thesis, soft ground is in comparison to hard rock.

In 2000, HSE published its investigation report (HSE 2000) into the HEX collapse, concluding that the main contributing factor lay in the poor quality of construction, rather than an inherent fault in the concept or defective design. Subsequently, the SCL technique has been more widely used and is recognised as a very efficient tunnelling method for tunnels of short length in soft ground.

It is not only useful for new tunnel construction but also suitable for the upgrading of existing underground stations. Figure 1-1 shows the extremely complex site conditions faced on the Victoria Station Upgrade (VSU) project where construction is taking place adjacent to or beneath existing building foundations, tunnels, pipelines and cable systems. At the time of writing this thesis, several projects in London are currently utilising the SCL technique, including the £14.6 billion Crossrail project and a number of other stations forming the London Underground Station Upgrade Programme, including Bond Street, Tottenham Court Road and Bank Stations. The SCL technique has also been adopted for Thames Water's £4.1 billion Thames Tunnel (Lee Tunnel) super sewer projects.

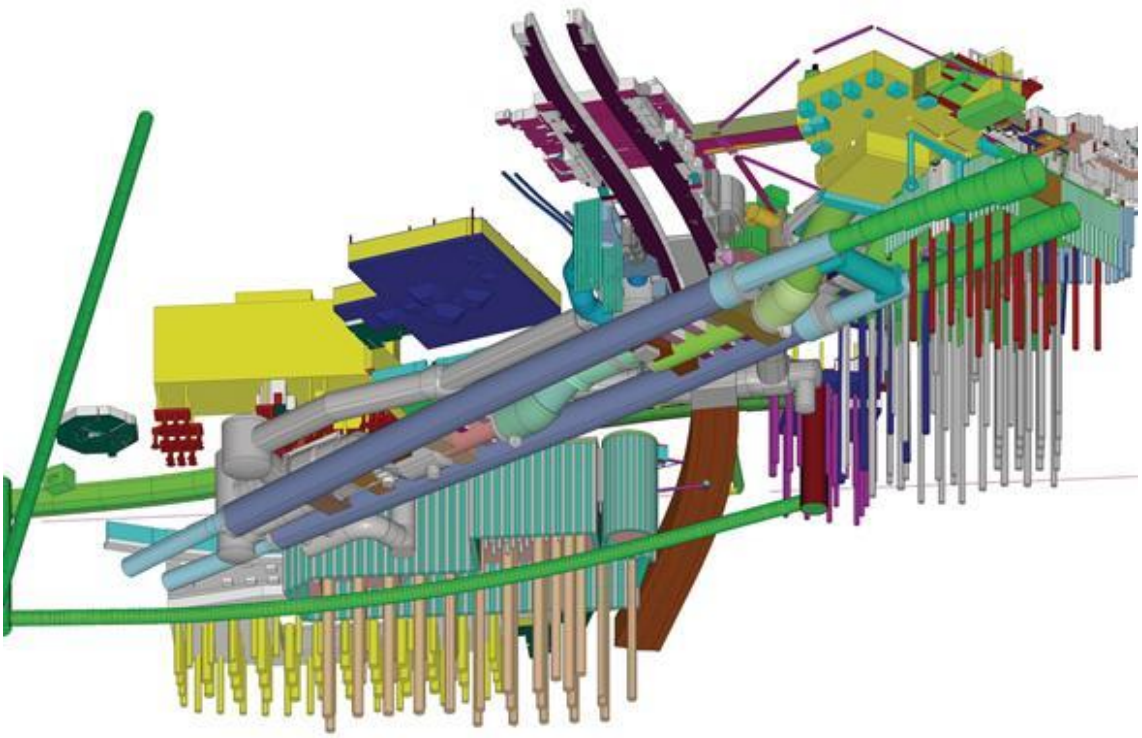

Figure 1-1 'Worm's eye' view of VSU project (Courtesy of Mott MacDonald)

1.3.3 Development of SCL in the UK

The development of SCL in the UK over the past twenty years can be divided into three stages. The first stage saw SCL tunnel configuration dominated by the sacrificial primary lining (SPL). The SPL, consisting of a layer of sprayed concrete primary lining, a layer of sheet waterproofing membrane and a layer of cast *in situ* concrete secondary lining, was adopted on the JLE project's Waterloo and London Bridge underground stations (Mair and Jardine 2001) as well as the HEX Terminal 4 project (Deane *et al.* 1997). The main drawback of SPL was its waste of material as the whole primary lining was treated as sacrificial in the long-term. A typical SPL is shown in Figure 1-2 (a).

The second stage saw the development of the single shell lining (SSL). The SSL, consisting of a layer of high-performance watertight permanent sprayed concrete lining without any waterproofing layer, was adopted in several projects in London, such as the Heathrow Baggage Transfer Tunnel (Grose and Eddie 1996) and the Channel Tunnel Rail Link (CTRL) North Downs Tunnel (Watson *et al.* 1999). The purpose of the SSL was to achieve both lining watertightness and material economics through a single pass lining. However, it was found that the cracks in the SSL could not be fully controlled, jeopardising the lining's long-term watertightness and durability (TRL 1998). A typical SSL is shown in Figure 1-2 (b).

The third development, which represents the current state-of-the-art technique, is the so-called double shell lining (DSL). In terms of tunnel construction, this is very similar to a composite shell lining (CSL) – a layer of spray applied waterproofing membrane is sandwiched between a layer of permanent sprayed concrete primary lining and a layer of permanent sprayed concrete secondary lining. The difference between the two approaches lies in the assumptions made about the structural interaction between the concrete and the membrane. The CSL assumes that a certain degree of adhesion and shear bond exists across the sprayed concrete-membrane interface. In response to a lack of reliable parameters to adequately describe this structural interface, the DSL approach was developed conservatively ignoring any such bond. This difference means the two lining options behave in very different ways when subjected to the design soil and water pressures. The DSL option has been used in the design of the Crossrail SCL tunnels (Pickett 2013). A typical CSL is shown in Figure 1-2 (c). So far, CSL tunnels have only been adopted in soft ground conditions, the reason of which is explained in the following section.

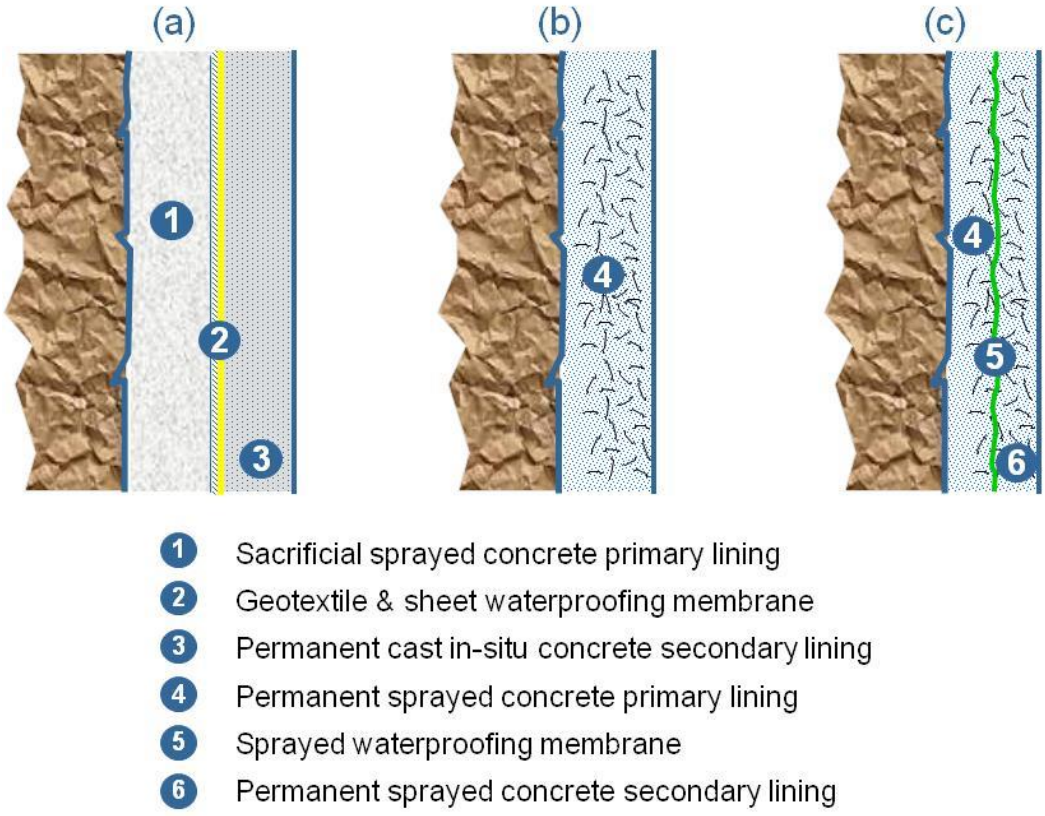

Figure 1-2 Typical longitudinal section of SPL (a), SSL (b) and CSL (c) (Courtesy of Mott MacDonald)

1.3.4 Development of composite SCL

Historically speaking, SCL has mostly been used in rock tunnels, where a relatively thin layer of sprayed concrete primary lining is used together with rock bolts and reinforcement meshes. The SCL undergoes large deformation after its application, and thus has been treated only as a temporary structure mostly due to a concern on its long-term durability. In comparison, a relatively thick sprayed concrete primary lining is used in soft ground SCL tunnelling to minimise ground surface settlement (*i.e.* mobilise less ground strength). This layer of sprayed concrete lining has recently been considered started to be accepted as a permanent structure due to improved long-term durability (Thomas and Pickett 2011). This advancement together with the adoption of spray-applied waterproofing membrane has enabled the conceptualisation of CSL tunnel, which is developed solely to be used in soft ground. So far there have only a few example projects for CSL tunnels, all of which are in Europe (Holter and Nermoen, 2011). No literature has been found on CSL tunnel projects in either North

America or Asia. Therefore, this thesis focuses on CSL tunnel in soft ground, with a particular interest in the UK.

In order to validate the CSL design approach, thus achieving further lining thickness design efficiency, the UK tunnelling industry has been asking for the investigation of composite action for SCL tunnel linings sandwiched by sprayed waterproofing membrane. In response to this call, a research programme has been undertaken at the University of Southampton to tackle this urgent issue.

1.4 Challenges and uncertainties in CSL design

Whilst significant conceptual development of CSL has been made, very limited laboratory testing and numerical modelling has been carried out to investigate the interface properties and the performance of CSL, preventing the development of efficient CSL tunnel design. This research aims to address this gap. For CSL tunnels, there are several outstanding questions of most interest to the tunnelling industry:

- How does the long-term stress relaxation affect the aforementioned stiffnesses?
- Which parameters matter, in terms of controlling composite behaviour?
- What affects these controlling parameters?
- Can these controlling parameters be measured reliably, and what values are to be expected?
- How can these parameters be used in a full analysis of a CSL tunnel?
- Is the behaviour of a CSL tunnel sensitive to the variation of these parameters?
- How can the degree of composite action be quantified?
- What is the impact of different interface stiffnesses on the load sharing between the primary and secondary lining and its lining and interface capacities?
- Can overall lining thickness reduction be achieved by utilising composite action?
- Is the interface sufficiently strong to maintain the integrity of CSL under practical loading?

1.5 Research aims and objectives

To answer the aforementioned questions, the overall aims are:

- To examine whether there is composite action in SCL tunnels with sandwiched sprayed waterproofing membrane;
- To identify and assess the factors that may control composite action;
- To explore the efficiency and robustness CSL tunnel design.

The objectives of the research are therefore:

- To carry out a critical literature review on the membrane interface properties and the performance of composite SCL tunnels.
- To identify the range of key interface parameters and the appropriate testing methods to obtain these parameters.
- To validate the selected testing methods by carrying out laboratory tests.
- To determine the interface strength and stiffness parameters in compression, tension and shear (for a typical spray applied membrane) by means of laboratory experiments.
- To understand the influence of primary lining surface finish (interface roughness) and measured waterproofing membrane thickness on the short and long-term interface parameters by means of laboratory experiments.
- To assess the repeatability of successfully measuring interface properties by examining the statistical results of laboratory experiments.
- To derive a set of interface parameters that can be used for the full numerical analysis of a CSL tunnel.
- To develop and validate a numerical modelling technique that can then be used for modelling whole CSL tunnels by simulating the behaviour of composite SCL beams cut from sprayed test panels.
- To develop a method of quantification for the degree of composite action and carry out a numerical sensitivity study on the impact of interface parameters on the degree of composite action for composite beams in the laboratory four-point bending test configuration.
- To evaluate the numerical predicted performance of a typical CSL tunnel in soft ground by comparing its load sharing with the full CSL (*i.e.* CSL tunnel with full composite action) and a non CSL (DSL) tunnels with the same

dimensions.

- To understand the impact of varying interface stiffness and primary/ secondary lining thickness ratios on the load sharing between the primary and secondary linings for the CSL tunnel by means of numerical modelling.
- To evaluate the lining and interface capacities for analysed scenarios.
- To investigate whether a tensile and/or shear bond failures could occur at the sprayed concrete-membrane interface of a CSL tunnel under the influence of nearby construction by means of numerical modelling.

1.6 Structure of thesis

The structure of the remaining Chapters of this thesis is as outlined below.

Chapter 2: Background

This Chapter comprises two parts. The first part is a detailed description of the developments in SCL tunnelling and its design method in soft ground in the UK. This is to give readers a clear picture of how SCL tunnelling has developed from the SPL, through the SSL and to the current DSL. The second part is a literature review, focusing on the laboratory tests on composite element samples sandwiched by another non-resin based spray applied waterproofing membrane and a subsequent numerical investigation on the behaviour of composite shell structures. Following this review, the gap between the current knowledge on the sprayed concrete-membrane interface properties and the ability to design CSL tunnels is identified.

Chapter 3: Research methodology and testing plan

This Chapter comprises three parts. The first introduces the research methodology adopted for this research. The rationale behind the proposed laboratory testing and numerical modelling is discussed. The second part describes the preparation of testing panels and samples. The sprayed concrete mix, variations in primary lining surface finish (interface roughness) and measured membrane thickness between panels are presented. The third section details the laboratory testing programme and the procedures to be adopted for the short and long-term compression, direct tension and direct shear tests on element samples cut from sprayed concrete panels, both with and without waterproofing membrane.

Chapter 4: Presentation and discussion of testing results

The results from the element laboratory tests described in Chapter 3 are presented and evaluated by comparing with the available literature and standards. A statistical analysis of test results for samples with various primary lining surface finishes and measured membrane thicknesses from different tests is carried out. Interim conclusions regarding test results are made at the end of this Chapter.

Chapter 5: Calibration of interface parameters

This Chapter firstly presents two rounds of calibrations. The first round calibration includes laboratory four-point bending tests and corresponding numerical modelling analyses using software package FLAC2D for both pure shotcrete and composite beams, from which discrepancies between test results and numerical analysis are identified. The second round calibration investigates the discrepancies by undertaking laboratory test on additional pure shotcrete beams and a steel beam with standard cross section, from which the influence of the machine compliance was understood. This is followed by laboratory tests and corresponding numerical modelling analyses on additional composite beams to verify the modelling approaches and interface parameters. After the verification, a sensitivity study was carried out investigating the impact of interface parameters on the degree of composite action for composite beams. A quantification method for the degree of composite action is proposed and applied to the composite beams in the sensitivity studies.

Chapter 6: Numerical Modelling of Composite Shell Lined Tunnels

This Chapter firstly describes a numerical modelling exercise for a typical CSL tunnel in soft ground using the modelling techniques and interface parameters validated in Chapter 5. The modelling results are presented and compared with those from a full CSL (*i.e.* CSL tunnel with full composite action) and a non CSL (DSL) tunnel with the same dimensions and in the same ground to quantify its degree of composite action. Subsequently, a series of parametric studies of the CSL tunnel is carried out to understand the effect of interface properties and the primary/secondary lining thickness ratios on the load sharing between the primary and secondary linings. The lining and interface capacities are also evaluated. Parametric studies, in which the interface stresses are compared with

the interface strength, are undertaken as a result of nearby construction activities to find out whether interface debonding or slippage could occur.

Chapter 7: Summary of discussions

This Chapter summarises the research carried out and findings in the context of verifying the interface parameters, predicting the behaviour of the composite beam under four-point bending tests, and understanding the performance of CSL tunnels with differing interface parameters and under different external loads.

Chapter 8: Conclusions and recommendations

This Chapter brings together all the various findings from Chapters two to seven and identifies opportunities for further research work.

Chapter 2: Literature Review

2.1 Introduction

This Chapter comprises two parts. The first part (Section 2.2) describes how the design requirements and analysis methods of SCL tunnels have changed with the development of the lining from a purely temporary to a permanent structure. Readers are given an insight into how and why SCL tunnels have developed to the current status.

The second section outlines the findings of existing laboratory tests (Sections 2.3) on the interface properties of a non-resin based sprayed membrane BASF MasterSeal 345 and associated numerical modelling (Section 2.4). This part aims to inform readers of the current knowledge on the sprayed waterproofing membrane interface and the behaviour of composite shell structures.

2.2 Sprayed concrete lining – the development

2.2.1 SCL as a temporary structure

Until recently, SCL tunnels, consisting of a layer of temporary sprayed primary lining, a layer of sheet waterproofing membrane and another layer of permanent cast secondary lining, dominated the market; mainly because of concerns over safety, watertightness and durability (Lyons *et al.* 2014, Spyridis *et al.* 2013). For the purpose of this thesis, this is called sacrificial primary lined (SPL) tunnel. The reasons why the SCL was only treated as a temporary structure were twofold: limitations of both the sprayed concrete technology itself and of the existing SCL design method. These factors are discussed separately in the following Sections.

2.2.2 Sprayed concrete technology for the temporary SCL

Twenty years ago the desire to achieve early-age strength development and hence effective ground support meant many other properties had to be compromised. Consequently SCL was treated only as a temporary structure. The main concerns at that time from the tunnelling industry about the SCL method included:

- Low final strength in the long-term due to accelerator dosage (Kusterle 1997)
- Long-term durability issues due to "shadows" behind steel reinforcement (Thomas 2008)
- Poor quality control due to use of the dry-mix process and manual spraying (Austin and Robins 1995)

2.2.3 Design method limitations for the temporary SCL

The lack of reliable design methods was another reason why SCL was perceived only as a temporary structure, especially in soft ground strata, such as London Clay. Tunnelling used to be an experience-based industry where empirical methods were widely adopted, such as using the Gaussian curve to predict the ground surface settlement profile (Peck 1969). However, the empirical methods for soft ground were mostly based on the assessment of previous local practices and lacked universal acceptance (ICE 2004).

Closed-form analytical methods were also developed for tunnelling design. However, most of them are not suitable for SCL tunnels as the complex soil-structure interaction caused by the multi-step SCL construction sequence could not be properly modelled. The famous closed-form Curtis-Muir Wood formula (Muir-Wood 1975, Curtis 1976), originally developed to confirm the design of segments for the Channel Tunnel project (Curtis 2010), could only be used as a check for SCL tunnels since it assumes that the lining is installed immediately after the tunnel is excavated and that full-overburden is applied to the tunnel lining, leading to an overestimate of the lining stress (BTS 2004). The convergence-confinement method (Hoek and Brown 1980; Brown *et al*. 1983), purposely developed for tunnels constructed in discontinuous media, such as rock, is not suitable for SCL tunnels in soft ground, which is a continuum media. For the beam-spring model, the loads to be applied to the lining are evaluated separately from the spring stiffness, disconnecting the interaction between soil and structures (ASCE 1984).

Numerical modelling was not considered as a viable design tool for SCL tunnels in soft ground until the 1990s, mainly due to insufficient computing capacity. The Heathrow Express Trial Tunnel, the first soft ground SCL tunnel constructed in London (in 1992), was designed by using finite difference software package

FLAC2D (Deane and Bassett 1995). This project represented the most advanced design at that time in the UK. The main features were:

- A conservative approach using mean and the worst case parameters for London Clay was adopted due to the absence of prior local projects
- A small strain stiffness non-linear isotropic model was used to model the pre-peak behaviour of London Clay
- A strain softening stress-strain relationship was adopted for its post-peak behaviour
- The Hypothetical Modulus of Elasticity (HME) approach was used to model the early-age sprayed concrete and the 3D tunnel face effect. Despite some attempts to give it a theoretical basis, the HME is effectively an empirical correction factor (Thomas 2008) – a very useful one but theoretical nonetheless.

The success of the Heathrow Express Trial Tunnel gave the industry significant confidence in building SCL tunnels in soft ground in London. However, the Heathrow Express project still posed a much bigger challenge to the designers as it comprised three large-diameter parallel SCL tunnels, in a close proximity under the terminal building (Van der Berg *et al.* 2003). There were also cross-passage connections between these tunnels. There were four major challenges:

- Little prior experience of additional loading to the SCL tunnels caused by compensation grouting (Linney and Essler 1994)
- Difficulty in estimating potential building damage due to SCL tunnelling induced ground movement
- Lack of knowledge on the extra loading on the adjacent SCL tunnels caused by the construction of new SCL tunnels
- Scarce data available to estimate the stress concentrations around the junctions due to the construction of the cross-passages

To ensure safety, designers adopted an extremely conservative approach by putting a large quantity of reinforcement in the SCL tunnels. For a 9m diameter platform tunnel, the temporary primary lining consisted of 300mm of sprayed concrete lining, reinforced by two layers of 8mm diameter mesh and full section lattice girders, leading to a reinforcement ratio at 0.23%. This quantity of

reinforcement made the spraying very difficult, leading to concerns of quality control and long-term durability of the lining.

It could be argued that the perception of SCL as only temporary structures was driven not only by insufficient development of the sprayed concrete technology, but also by the lack of efficient design methods. As an aside, it should be noted that, despite the limitations of the design, the causes for the collapse at Heathrow stemmed from failures in the construction management, particularly quality control and interpretation of monitoring data (HSE 2000).

2.2.4 Other issues with the temporary SCL

Until the mid-1990s in the UK, most spraying was carried out using the dry mix method. The high levels of dust generated and the need for tunnel workers to stand very close to the tunnel face during the spraying operation resulted in significant health and safety issues (ITA 1996). In addition, the sacrificial nature of the lining caused serious concerns of material waste, cost inefficiency and negative environmental impact.

2.2.5 SCL as a permanent structure

Significant efforts have been made by different parts of the tunnelling industry, including material suppliers, machinery manufacturers, designers and contractors. To improve the performance of SCL tunnels, several advances have made the use of SCL as a permanent structure possible:

- The shift in producing SCL from the dry mix process to a wet mix process substantially improved the quality control, productivity and Health and Safety benefits (Austin and Robins 1995)
- The adoption of alkali free accelerators enabled rapid setting, improved early and final strengths, reduced environmental impact and enhanced safety for tunnel workers (Kusterle 1997)
- The use of fibre reinforcement instead of mesh reinforcement eliminated the concern of “shadows” (*i.e.* voids behind reinforcement bars), shortened construction programme and saved overall cost (Thomas 2008)
- The shift from hand spraying to robotic spraying achieved a shorter programme and less material waste. It also complies with increasingly

strict Health and Safety laws in the UK (Franzén 1992)

- The use of total stations instead of lattice girders to profile the tunnel excavation and control the lining thickness has accelerated construction. This has been demonstrated "in the field" on projects such as Heathrow Terminal 5 project and Crossrail C510 contract, which also adopted an inclined "LaserShell" tunnel face, as developed by Morgan Est (Jones *et al*. 2008, Mar and Eddie 2013)
- The improvement in the quality of sprayed concrete has enabled the matured sprayed concrete to be treated as normal cast *in situ* concrete, with the same long-term strength development, low permeability (in the order of 10^{-12} to 10^{-14} m/s) and durability performance (Annett *et al*. 1997)

Permanent sprayed concrete has been widely accepted in certain sectors – most notably hydropower projects – and particular countries (*e.g*. Norway) for many years. It has only recently gained this acceptance more widely in the world and in soft ground applications. For soft ground SCL tunnelling in the UK, the latest design option is called unbonded DSL. This consists of a layer of permanent sprayed concrete primary lining, a layer of spray applied waterproofing membrane and a layer of sprayed or cast secondary lining, with no adhesion and shear bond assumed at the sprayed concrete-membrane interfaces (Mott MacDonald 2009a, 2013a). This design assumption was made due to the lack of evidence on the existence of long-term tensile and shear bonds and thus no bond is assumed across the interface. Steel fibres are used as the main reinforcement, and no steel bars and meshes are used except at the secondary lining inverts, large caverns and tunnel junctions (Mott MacDonald 2011, 2012). Lattice girders are eliminated and the tunnel profile is controlled by the total station (GE 2013). This design option has been adopted on several landmark projects, such as A3 Hindhead (Holter and Nermoen 2011) and Crossrail.

2.2.6 Design requirements for the permanent SCL

In the latest design option, the permanent sprayed primary lining is designed to take any loading that occurs before the installation of the secondary lining including that of the soil, water and any other pressures, such as surface surcharge and compensation grouting. The primary lining is assumed to stand up to a maximum of two years before additional support is installed. This is

determined by the fact that the stiff clay is assumed to be impermeable within two years in an undrained short-term analysis. This assumption is consistent with the work of Wongsaroj *et al*. (2007) who found that the clay's permeability should be in the region of 10^{-10} to 10^{-11} m/s to replicate the observed behaviour in the JLE Green Park field. It is also consistent with Addenbrooke's (1996) back-analysis of the running tunnels under the same field which indicated that the ground took between 10-20 years for most of the movements due to water flow to cease.

In the case of London clay, the long-term increase in soil pressure and surface surcharge are shared between the two linings and the long-term water pressure is assumed to apply solely to the secondary lining in a drained long-term analysis. This is due to the assumption that ground water can always find a way to pass through the primary lining via cracks or construction joints (Crossrail 2010). This has been a significant point of contention within the tunnelling industry as to where the water pressure should apply.

An initial layer of primary lining, normally between 25-75mm, is designed as sacrificial and disregarded in the long-term design case (Mott MacDonald 2010a). As it is assumed that the quality of this layer of sprayed concrete will not be as good as the following layers. Additionally the sacrificial layer is considered to resist the chemicals in the groundwater, particularly sulphates, which would cause corrosion to the steel fibres, leading to a reduction in the effective primary lining thickness in the long-term. The thickness of the sacrificial layer is determined mainly by the type and density of chemicals in the groundwater. Arguably 75mm is a quite conservative assumption.

A moderate strength of sprayed concrete should be specified in the design and used in the construction (Mott MacDonald 2009a). The lower limit of characteristic cylinder compressive strength for both linings are 28N/mm^2 at 28 days and 32N/mm^2 at 90 days respectively, and should exceed a modified J2 curve (Crossrail 2009a) within the first 24 hours, as shown in Figure 2-1. The sprayed concrete class is explained in Table 2-1. The specification of the lower limit of compressive strength of sprayed concrete is to guarantee that the lining would fulfil its functional requirement. Another reason for specifying a sprayed concrete of moderate strength is to achieve the desired ductile failure mode, rather than the unfavourable brittle failure mode, which is usually associated with high strength sprayed concrete (Bernard 2004). Although structural synthetic fibres are more economic and better in resisting corrosion (Bernard 2008), steel

fibres have been chosen as the reinforcement mainly due to the better performance in resisting long-term creep in tension (Bernard 2004). A 50mm fire proofing sprayed concrete layer mixed with micro synthetic fibres is designed inside of the secondary lining to reduce the spalling of concrete in a fire situation (Shuttleworth 2001).

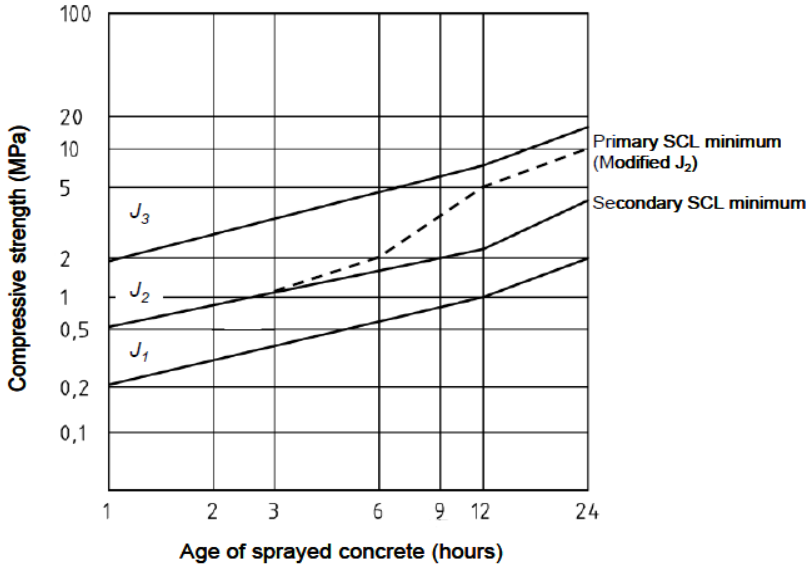

Figure 2-1 Early strength classes of young shotcrete (Crossrail 2009a)

Table 2-1 Sprayed concrete classes (Austrian sprayed concrete specification 1997)

Sprayed Concrete Class	Application
J_1	Sprayed concrete suitable for the placing of thin layers on a dry base without special load bearing requirements to be met during the first hours after placing; it offers the advantages of low dust formation and rebound.
J_2	Sprayed concrete that is required to be placed as quickly as possible in thick layers (including overhead). Additionally, sprayed concrete can be applied to water bearing ground, and sections of lining that are immediately adjacent to construction operations involving immediate stress and strain changes, such as new excavations or spiling. In normal tunnel conditions J_2 should not be exceeded.
J_3	Sprayed concrete for support to highly friable rock or excessive ingress of water. Due to the high level of dust and rebound, this class should only be used in limited areas.

2.2.7 Design methods for the permanent SCL

Since numerical modelling is now widely applied in the design of SCL tunnels, it can be considered that the way to improve the design depends on the accuracy of the constitutive models used. There are three main areas where numerical

modelling results could be improved: the constitutive model for the ground, the constitutive model for the sprayed concrete, and calibration of modelling approach.

As previously discussed, the CSL tunnel was developed to be used in soft ground, the behaviour of which varies significantly in different scenarios (*e.g.* static vs dynamic, small strain vs large strain). A realistic model of the ground is an essential consideration issue for the estimation of the magnitude and distribution of lining forces and deformations. It is therefore important to first understand the properties of soft ground including weak rock and soils (Bolton 1991). This influences the choice of constitutive model and parameters to simulate the soft ground behaviour for CSL tunnel design using numerical methods. The weak rock usually can be considered as soil like material due to the weathering effect (Fuenkajorn 2011). A large number of constitutive models have been proposed for soils. Two traditional models (*i.e.* Mohr-Coulomb, Modified Cam Clay) are supplemented by four further models of different complexity (*i.e.* isotropic and anisotropic nonlinear elastic with perfect plasticity, combined isotropic and kinematic hardening plasticity and hypoplasticity) (Masin and Herle 2005). The Mohr-Coulomb model is a linear elastic-perfectly plastic model. The basic parameters include Young's modulus and Poisson's ratio for the elastic behaviour and cohesion, friction angles and dilation angle for plastic behaviour. A simple non-linear elastic model combined with the Mohr-Coulomb failure criterion using six parameters can be used for the non-linear behaviour. To model the complex soil behaviour, additional parameters are introduced into the soil constitutive model. (Atkinson 2007, Yamamuro and Kaliakin 2005). The selected constitutive model should be able to simulate the key characteristics of the ground for the particular question.

London Clay ground conditions are referred to in this research. The higher small-strain stiffness of London Clay and its degradation with increased strain is very important for predicting the behaviour of CSL tunnel in London Clay. Therefore, the selected constitutive model should be able to accurately simulate these characteristics. Currently, several advanced constitutive models can simulate this key behaviour, such as the BRICK model (Simpson 1993) and MIT-E3 model (Whittle and Kavvadas 1994). However, they all require the input of many parameters, some of which are physically meaningless and difficult to be

obtained by laboratory tests. However, for tunnelling projects, the parameters used in the selected constitutive models should be easy to obtain and verify.

Industry and academia have spent significant efforts in collecting field and laboratory test data to develop constitutive models for ground strata such as London Clay (Gaspare 2005, Jardine *et al.* 1984, 1986). It could be argued that the constitutive models for London Clay have developed to a point where doubling the time and resource input may only improve the results very slightly. Hence, it relies on the designers' judgement to balance the accuracy of the results with the input resource for the modelling work. It should also be borne in mind that numerical modelling is just an approximation of reality, and its accuracy will be affected significantly by variation in workmanship and uncertainties of the ground (Thomas 2008).

For recent projects a high small strain stiffness non-linear elastic model has been adopted to simulate the behaviour of London Clay at the strains appropriate to tunnelling (Atkinson 2000, Addenbrooke 1996, Addenbrooke *et al.* 1997), especially for cases where several tunnels are close together. The Tresca and Mohr-Coulomb failure criteria and an associated plastic flow rule have been adopted to model the undrained and drained ground behaviour at failure and beyond. The model and failure criteria are both well known in industry and academia and backed by significant historical data. Besides, the parameters used in these models are relatively easy to obtain, and the computing time is modest compared with that using more sophisticated models. A typical high small strain stiffness nonlinear model for London Clay, which is called the A* model, is shown in Figure 2-2. The Figure shows the stiffness of London Clay degrades when its axial strain increases. The basis for the A* model is outlined in a paper by Eadington and O'Brien (2011). The benefit of this model is that a very wide range of ground investigation data, both *in situ* and laboratory data, can be used to develop stiffness degradation curves which are representative of *in situ* behaviour. Hence, it avoids over reliance on a small number of laboratory tests which may be affected by the sampling disturbance, which generally becomes more significant as depth increases. The method is also less reliant on the estimation of mean effective stress, which itself is subject to subjective interpretation of lateral earth pressures. More importantly, the A* parameters have been calibrated against a set of laboratory tests and show a good degree of match.

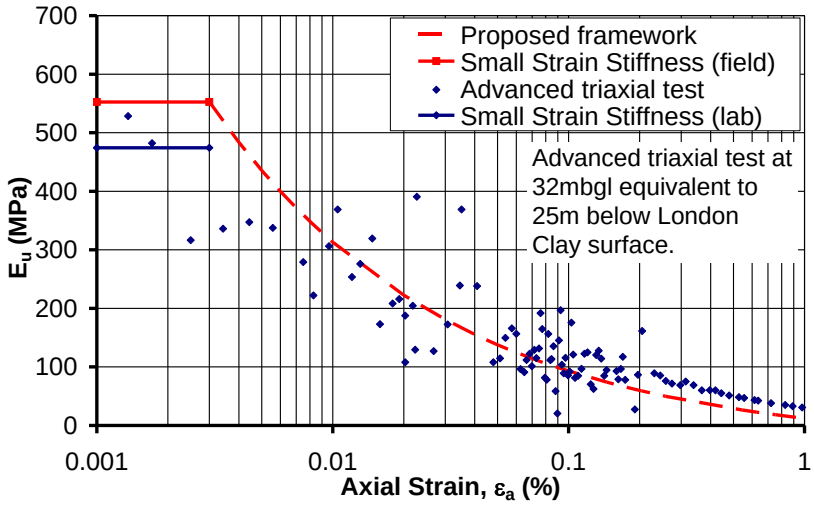

Figure 2-2 Typical A* model with variation of stiffness non-linearity of London Clay used in Crossrail SCL tunnel design (Eadington and O'Brien 2011)

In contrast to the universally accepted design method and criteria for cast *in situ* concrete, variations in SCL mix design and workmanship in different countries for different projects affect the strength and stiffness development significantly. Tests on sprayed concrete at both early-age and long-term have been carried out, leading to various stiffness/strength development equations (Thomas 2008). Therefore, where possible it is best to base the constitutive models on testing results from a similar, recently completed SCL projects. For Crossrail SCL tunnel design, an age-dependent strength curve for sprayed concrete was developed based on the modified J2 curve up to 24 hours (derived from previous SCL projects) and Chang and Stille approach (1993) thereafter. The stiffness of sprayed concrete at each age was also derived from Chang and Stille's stress-stiffness equation. The data of sprayed concrete stiffness and strength from Heathrow T5 project and A3 Hindhead were used to check the inputs.

Eurocode 2 (BSI 2004) has defined the compressive strain in the concrete at peak stress (ε_c) as 0.2% and ultimate compressive strain (ε_{cu}) as 0.35%. There is currently no universally accepted stress-strain relationship for the concrete in the tension area as the tensile stress is usually very small and hence not taken into account in the structural analysis. Pure concrete is a brittle material and will only exhibit a certain degree of ductility in tension with rebar reinforcement or structural fibres. Therefore, tensile stress-strain relationships for fibre reinforced sprayed concrete from different standards and design guides should be reviewed and carefully selected for routine SCL tunnel design.

2.2.8 Numerical modelling for SCL tunnel design

It is widely acknowledged that 3D modelling is far better than 2D modelling for SCL tunnels (Thomas 2003, Jones 2007) as the former can model the complicated construction sequence and three-dimensional stress redistribution around the tunnel face explicitly. For Crossrail SCL tunnel design, 3D modelling has been extensively used for compensation grouting and tunnel junction studies, as well as for tunnels in faulted ground and with irregular shapes (Mott MacDonald 2011, 2012, 2013b). The 3D model and the construction of the Whitechapel junction enlargement are shown below in Figure 2-3. However, it must be recognised that, compared with a 2D modelling approach, 3D modelling is very time consuming and should be used only if it can be seen to improve the accuracy of results significantly.

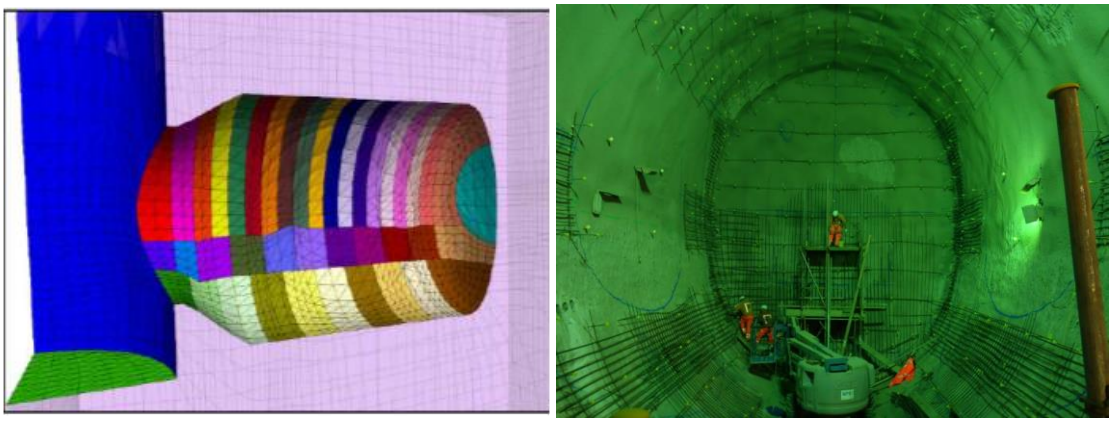

Figure 2-3 3D Model (left) and the construction (right) of the Whitechapel junction enlargement using permanent SCL

Most Crossrail SCL tunnels are still modelled by 2D analysis. Depending on the time and budget, either complicated coupled consolidation analysis or simply fully permeable analysis could be carried out for the drained long-term analysis in a numerical model. In total more than 100 2D primary and secondary lining sections have been analysed. Extensive calibration studies, including those against the Jubilee Line Extension (JLE) London Bridge Station, Heathrow T5 and Kings Cross Station, were carried out at the beginning of design in order to verify the constitutive models and input parameters for the ground and sprayed concrete (Mott MacDonald 2010b, 2010c and 2010d). Subsequently, a valid 2D modelling methodology was formulated and adopted for routine 2D analysis.

2.3 Sprayed waterproofing membrane

2.3.1 Performance criteria for sprayed waterproofing membrane

Historically, sheet membrane was used for waterproofing purposes, without providing any other structural functions. It was therefore assumed that all long-term water loads acted on the sheet membrane and thus to the secondary lining. It was only very recently that sprayed membrane emerged as a waterproofing material, with possibilities of providing composite action for the primary and secondary linings (Dimmock *et al.* 2011). This section provides background information about the sprayed membrane.

There are currently two main categories of sprayed waterproofing membrane systems (Crossrail 2009b):

- Non-resin based systems: Ethylene vinyl acetate powder based products, where water is added during the spraying process.
- Reactive resin based systems: Methacrylate reactive resins based products.

Crossrail (2009b) introduced and compared three sprayed waterproofing membrane systems: the Minova UK system, BASF MasterSeal 345, (both non-resin based systems) and Sterling Lloyd Intergritank HF, a reactive resin based system, along with sheet waterproofing membrane systems. The curing time for the non-resin and reactive resin based systems are 48 and 1-2 hours respectively. Although the reactive resin based systems have a much shorter curing time, there is a concern that the sprayed secondary lining, which is usually sprayed a few weeks or even months after the application of sprayed membrane, may not be able to bond to the reactive resin based waterproofing membrane as it completes its reaction too fast. Therefore, the non-resin based system is most commonly used at the moment. The International Tunnelling Association (ITA) has published guidance for the design of sprayed applied waterproofing membranes (ITA 2013). This outlines a number of key performance criteria:

- Permeability/water pressure resistance
- Elongation/Crack Bridging
- Bond Strength
- Minimum Thickness

- Tensile Strength
- Fire Rating

Whilst some benefit may be achieved if sufficient adhesive and shear bond strengths can be demonstrated permitting composite action between the lining layers, the existing guidance does not provide a detailed design method for such a case.

There is also a limitation on the use of sprayed waterproofing membrane: It is not possible to apply the membrane effectively in areas with active water ingress through the substrate. Quite low rates of seepage can result in water pressure developing at the concrete/membrane interface causing it to fail before it has cured sufficiently to achieve adequate adhesion. Active water should be either pre-sealed, or managed by drained systems, such as installation of a drainage fleece (Mott MacDonald 2008).

Since the sprayed membrane TamSeal 800 is non-resin based and is the product used for this research, the following sections therefore present some laboratory tests on a similar non-resin based BASF MasterSeal 345 waterproofing membrane. This includes discussion of the testing methods, procedures and results which informed the testing plan of this research.

2.3.2 Tests at BASF laboratory

Three point bending tests on small size pure sprayed concrete and composite beams were carried out according to EN 12390-5:2000 by BASF (BASF 2008). Nine specimens in total were prepared with dimensions 40x40x120mm. The specimens were six months old and fully cured when tested; with measured membrane thickness between 2.5 and 4mm. Specimens were categorized into three groups and their average stress-strain curves are shown in Figure 2-4.

Whilst the specimens in groups 1 and 2 demonstrate similar maximum flexural strengths, those in the latter group only deflected half as much as those in the former. This is probably caused by a more pronounced 'deep beam' effect (*i.e.* a beam with a small span/depth ratio fails in shear rather than in bending) for specimens in group 2. The specimens in group 3 exhibit a stiffer response than those in group 1 for a given loading level. This result is not convincing as the composite beam should behave 'softer' than the pure sprayed concrete beam.

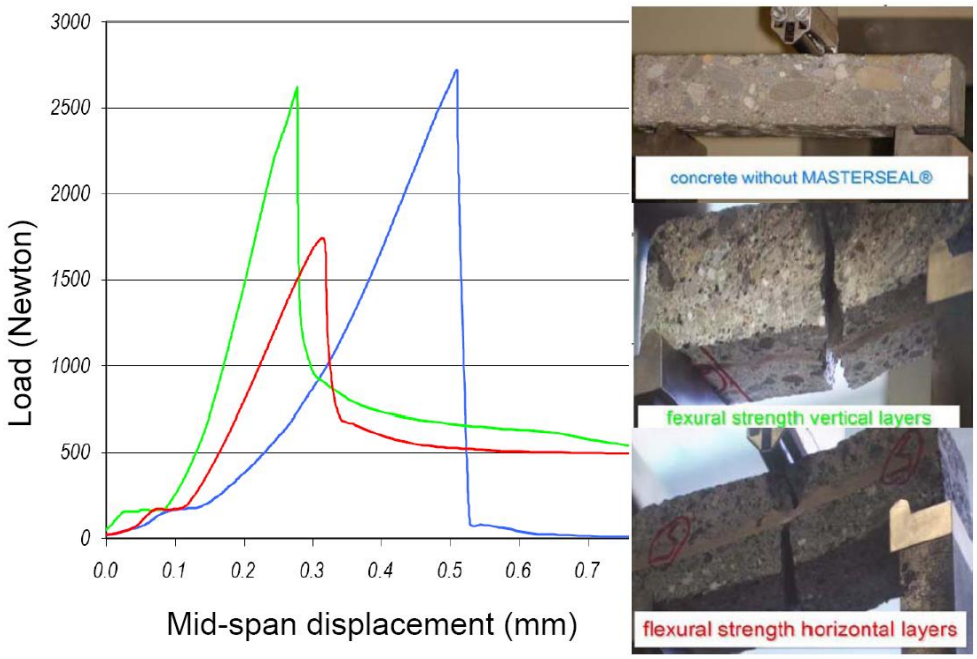

Figure 2-4 Testing specimen layout and results (courtesy of BASF)

2.3.3 Tests at the Graz University of Technology

Compression and shear tests were carried out using a shear box at the Graz University of Technology as requested by BASF (Graz 2008). The purpose of these tests was to understand the response of the sandwiched membrane to the compressive and shear stresses. Two specimens, both measuring 150x150x150mm, were cut with a diamond saw from panel sprayed by BASF. The two specimens 00 and 03 had a membrane thickness of 2 and 5 mm and a joint roughness coefficient (JRC) (Barton and Choubey 1977) of 0 and 20 respectively, as shown in Figure 2-5. The tests were performed using a servo hydraulic MTS System Corporation direct shear test system. The shear box is shown in Figure 2-6.

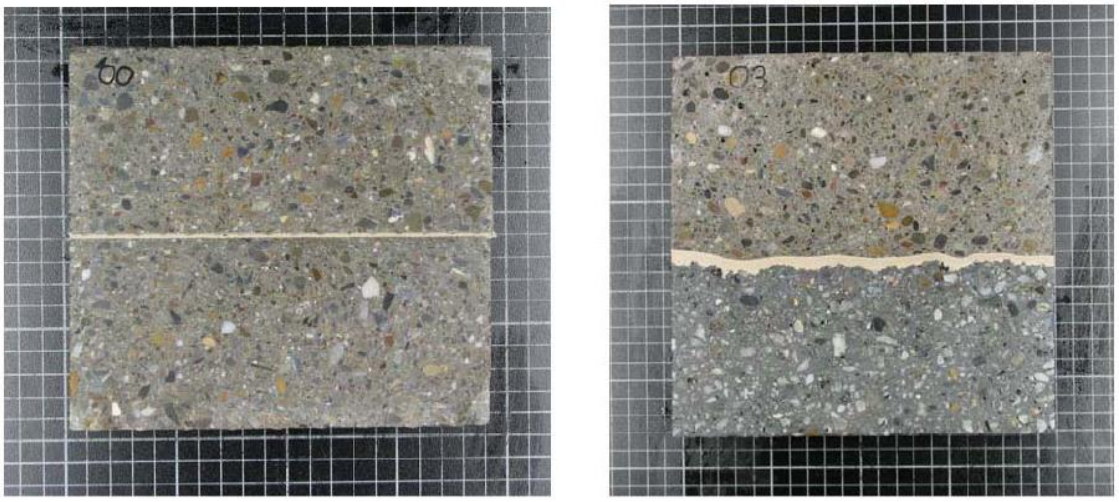

Specimen No. 00 Test 188.1 Specimen No. 03 Test 188.2

Figure 2-5 Two direct shear test specimens with varied membrane thickness and interface roughness (Graz 2008)

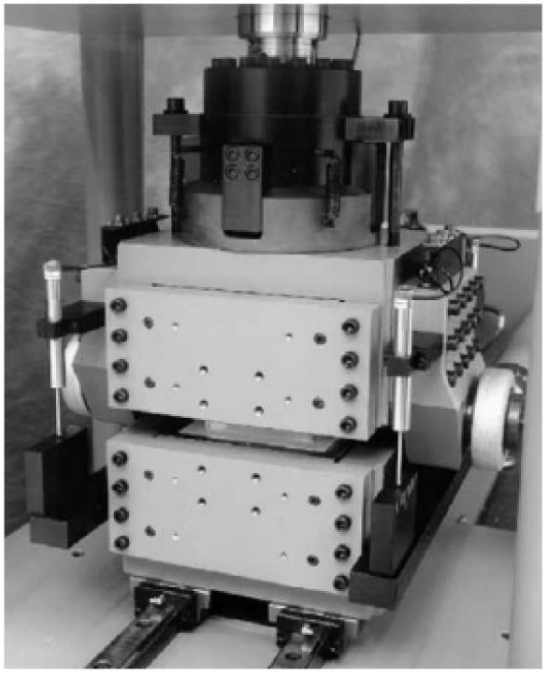

Figure 2-6 Shear Box for direct shear testing (Graz 2008)

In the compression and shear tests, stiffness was examined by applying small multiple load-unload cycles vertically and horizontally, respectively. The shear loading loops were applied in both directions. For the direct shear test, a normal stress of 0.26MPa was applied and shearing was carried out at a constant horizontal displacement rate of 0.2mm/min. In order to obtain a failure envelope from one test, infinite vertical stiffness was used in the direct shear tests. The test results are shown below in Table 2-2 and are discussed in Section 2.3.5.

Table 2-2 Summary of results from testing of the MasterSeal 345 membrane undertaken at the Graz University of Technology

	Specimen 00	Specimen 03
Membrane thickness	2mm	5mm
Interface roughness	Plane saw cut	As-sprayed
JRC (Joint Roughness Coefficient)	0	20
Compressive Modulus (first loading)	34.5MPa	32MPa
Compressive Modulus (cyclic loading)	56MPa	40MPa
Shear modulus (cyclical loading)	7.2MPa	17.5MPa
Shear strength	1.01MPa	1.76MPa
Cohesion, c	0.5MPa	1.05MPa
Internal Friction Angle, ϕ	24°	43°

2.3.4 Tests at the University of Innsbruck

In 2003, BASF commissioned the University of Innsbruck to carry out tests on element samples sandwiched by MasterSeal 345 (Lukas 2003). The mechanical test plan is shown in Figure 2-7 and the test results are shown in Table 2-3.

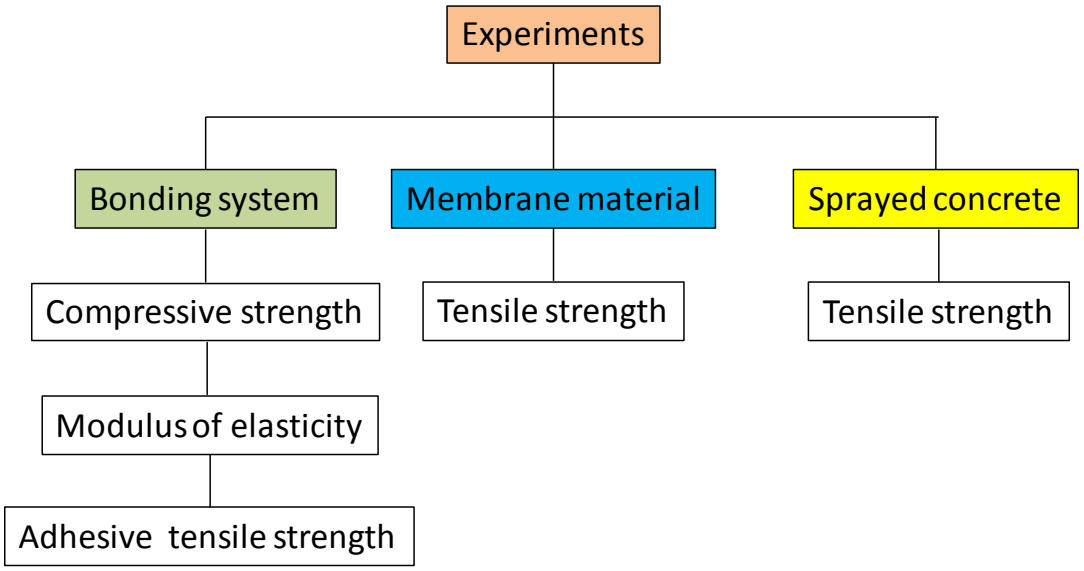

Figure 2-7 Plan for mechanical property tests system (Lukas 2003)

Table 2-3 Summary of test results for the MasterSeal 345 membrane

Test properties	Sample (mm)	Result
Compressive Strength – sprayed concrete	Ø=100 / h=100	40MPa
Compressive Strength – bonding system	Ø =100 / h=150	24MPa
Modulus of elasticity	Ø =100 / h=150	45MPa
Adhesive strength of the bonding system	Ø =100 / h=150	0.8MPa
Tensile strength of the membrane at 20ºC	30x90x3.2	2.6MPa
Elongation of the membrane at 20ºC	30x90x3.2	105%

The test results showed that the existence of sandwiched sprayed membrane had a certain influence on the compressive strength when compared with that of a pure sprayed concrete cylinder (40% compressive strength reduction).

It is also noteworthy that a description of the information on adhesive strength testing methodology, which may affect the results, was missing in the report. Three types of fracture of the tensile samples were outlined in the reports:

- Tensile failure in the sprayed concrete
- Adhesion break between the sprayed concrete and sealing material
- Tensile failure within the sealing material

However, the information about the actual fracture modes for these tensile tests was missing in the report.

2.3.5 Discussion of MasterSeal 345 membrane test programme

The only test carried out at both Graz University of Technology and the University of Innsbruck was for the compressive modulus, as shown below in Table 2-4. The test values showed a certain degree of similarity. However, it is difficult to compare the results as the membrane thickness, interface roughness (JRC) and testing procedures were all different. These issues are addressed as shown in Chapter 4.

Table 2-4 Comparison of test results for the compressive modulus

	Specimen 00	Specimen 03	Panel Result
Membrane thickness	2mm	5mm	3.2mm
Interface roughness	Plane saw cut	As-sprayed	As-sprayed
JRC	0	20	Not Known
Interface compressive Modulus (first loading)	34.5 MPa	32 MPa	45 MPa

2.4 Numerical modelling of a composite structure

Mott MacDonald was commissioned by BASF to carry out a preliminary numerical modelling investigation on the impact of sprayed membrane interface stiffness on the performance of a composite structure, which consisted of two layers of sprayed concrete linings sandwiched by a layer of sprayed membrane. No surrounding ground was included in the model. The analysis was carried out using FLAC3D (Mott MacDonald 2009b).

A series of analyses was carried out on a base model that contained one quarter of the ring with a longitudinal length of 1m as shown in Figure 2-8. For the model, the upper boundary in z-y plane, the lower boundary in x-y plane and the sides of the model were fixed. The average sizes of the blocks are 56×100×60mm for the primary lining and 29×100×51mm for the secondary lining.

The behaviour of the primary and secondary linings was described by a linear elastic material model. The concrete grade was assumed to be C40/50 MPa at 28 days. The creep coefficient was taken as 2.0 in accordance with Eurocode 2. The membrane was defined as an interface between the sprayed concrete layers and, as shown in Figure 2-9, its shear strength was modelled by the Mohr-Coulomb failure criterion defined by the interface cohesion and friction angle. The properties of the interfaces were taken from the back-analysis of direct shear test data from Graz (2008) as outlined in Section 2.3.3.

In the analyses, a loading of 500kPa effective vertical stress, 1000kPa effective horizontal stress and 250kPa water pressure was used. The full water pressure

was applied on the membrane layer, while the loadings derived from soil cover were applied to the primary lining.

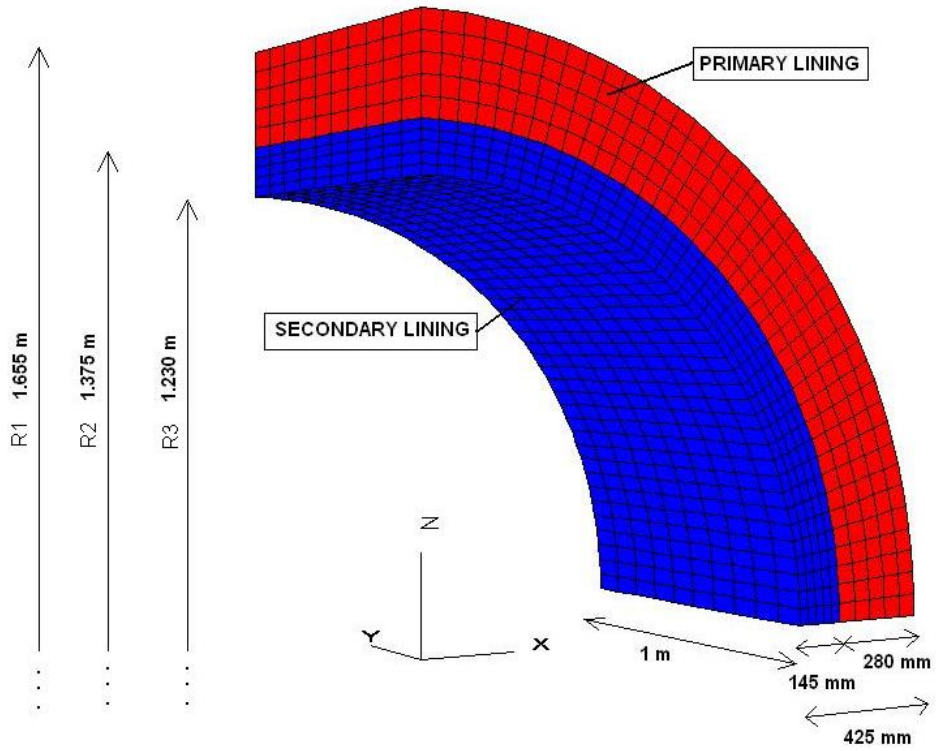

Figure 2-8 Base model geometry (Mott MacDonald 2009b)

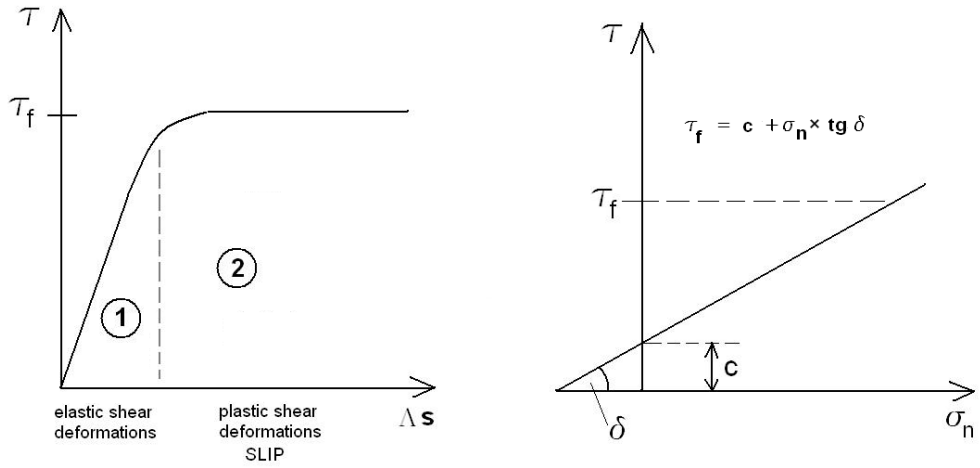

Figure 2-9 Behaviour of the interface under shear (left) and tension (right) (Mott MacDonald 2009b)

Eight models were analysed for interface properties between the extreme cases of no slip, through partial slip to full slip, *i.e.* from an SSL through CSL to DSL and the lining displacement results are shown in Figure 2-10. The results show that

the bigger the shear interface stiffness, the less interface shear displacement (but higher shear stress). Based on the numerical modelling study, it can be stated that there is a successful load sharing between the two layers of lining and no shear failure occurs on the interface, even under extreme loadings.

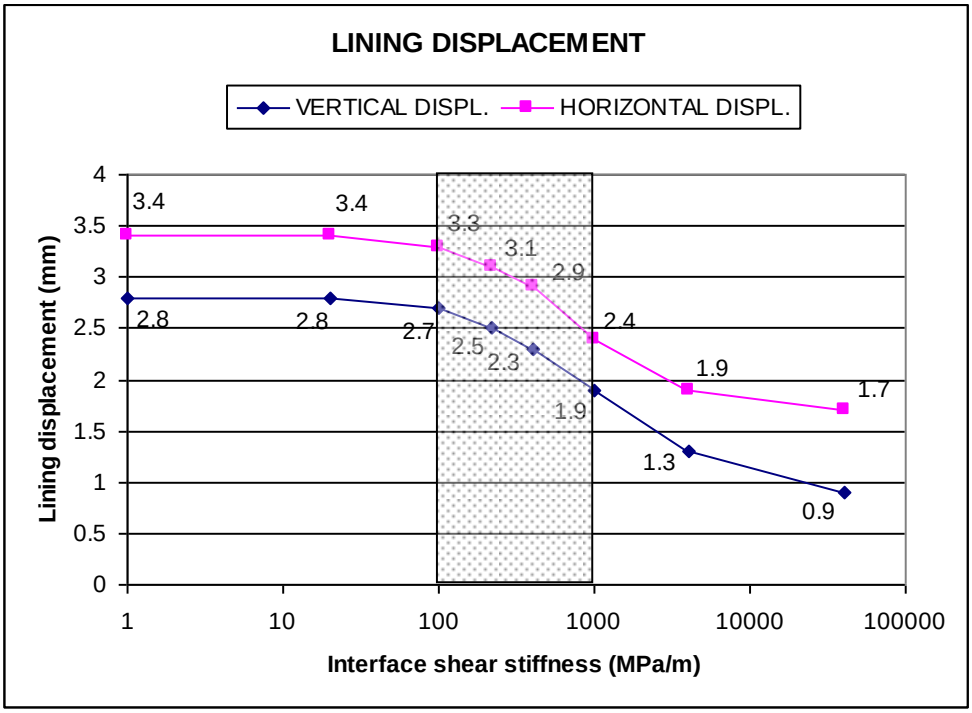

Figure 2-10 Lining displacement versus interface shear stiffness (Mott MacDonald 2009b)

There are several deficiencies in the model and its parameters which limit the level of confidence which can be placed in the results. Firstly, the input interface properties obtained from Graz (2008) were not correct as they used the infinite stiffness test method which overestimated the shear stiffness under normal loading. Secondly, the report confused the interface properties between the smooth interface and the rough interface specimens, labelling the smooth interface properties as latter and vice versa. Thirdly, no consideration was given to effects of complex soil-structure interaction, stage construction and long-term ground consolidation. Therefore, it is considered the results of this study lack credibility and more realistic numerical modelling needs to be carried out which takes into consideration of these issues.

2.5 Summary

This Chapter has reviewed key literature on different aspects of SCL tunnelling in soft ground. The key findings are:

(1) Sprayed concrete lining has developed from a temporary structure to a permanent structure, with the advances of both material technologies and design methods.

(2) Substantial knowledge of the behaviour of soft ground and SCL tunnel lining has been obtained through previous research, which has given the industry significant confidence in designing and constructing SCL tunnels in soft ground.

(3) In order to achieve lining efficiency, there is an urgent demand to establish a sound understanding of sprayed concrete-membrane interface properties and the behaviour of CSL tunnels in soft ground.

(4) Several independent laboratory tests on the sprayed concrete-membrane behaviour were carried out at different locations including universities and industrial laboratories on non-resin based BASF MasterSeal 345. However, these test results cannot be used directly in the design of CSL tunnels due to:

   a) Insufficient information on the testing methods

   b) Insufficient number of long-term testing results

   c) Lack of verification using other methods

(5) Only one numerical study was found for composite structures, in which only one quarter of CSL tunnel was modelled without surrounding ground. The analysis did not take into account soil-structure interaction, sequential excavation and the complex long-term ground consolidation behaviour due to the dissipation of excessive pore water pressure around the tunnel. It therefore does not reflect the true behaviour of CSL tunnels in soft ground.

Chapter 3: Research Methodology and Testing Plan

This Chapter first outlines the adopted research methodology. It then goes on to describe the sample preparation works, including the spraying process for sample panels and the specification of testing samples. Thirdly, the testing programme and procedures for element tests (*i.e.* uniaxial compression, direct tension and direct shear tests) are detailed. The testing programme and procedures for beam tests is introduced in Chapter 5.

3.1 Research methodology

In order to address the gap between the existing knowledge of sprayed concrete-membrane interface properties and the desire to design CSL tunnels, a research programme has been undertaken in the Infrastructure Research Division of the Faculty of Engineering and the Environment at the University of Southampton. Four stages were planned for this research project, as shown in Figure 3-1.

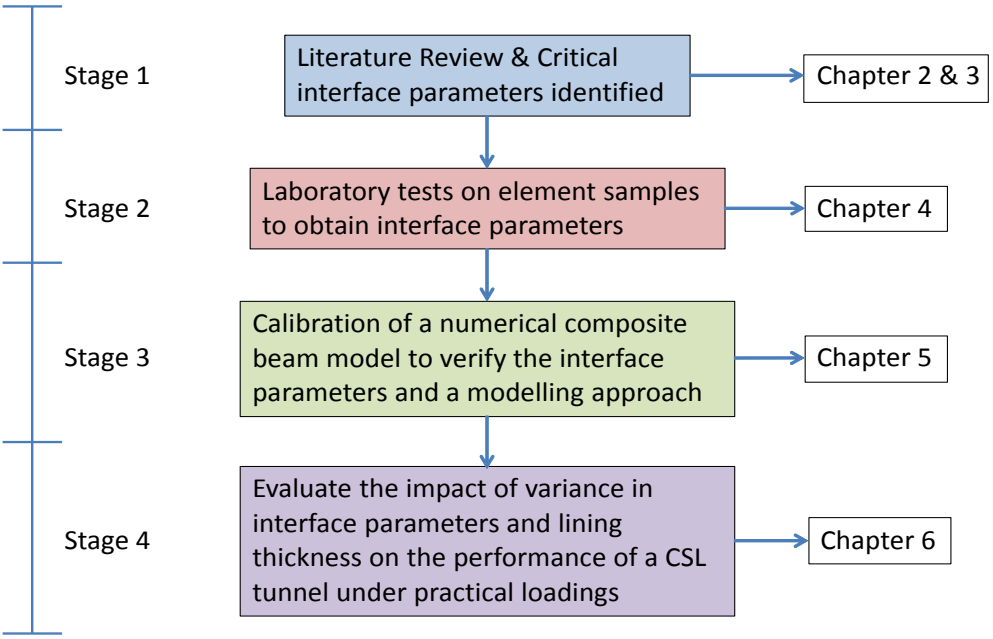

Figure 3-1 Research methodology flow chart

3.2 Sample preparations

3.2.1 Sample Panel Spraying

TAM International commissioned SCL contractor 'Sprayed Concrete' to produce a total of 15 panels, from which the test samples were cored and cut. Seven types of panels were sprayed, as shown in Table 3-1. The number in the brackets in Table 3-1 is the targeted membrane thickness while the range stated is that of the actual measured membrane thickness. This discrepancy arises from the natural variations inherent in this type of application. The main differences between these panels are their primary lining surface finish and measured membrane thicknesses. Both are the factors contributing to the interface properties (Meriam and Kraige 2011) and the effect of which is investigated in Chapter 4. In Table 3-1, a regulating layer is a thin layer of finer aggregate materials without structural steel fibres to smooth the 'as-sprayed' rough primary lining surface, creating a better substrate for the sprayed membrane and preventing the sprayed membrane from being penetrated by protruding steel fibres.

Table 3-1 Description of panel types and membrane thickness for SCL panels

Panel Type No.	Interface type	Membrane thickness (mm)	Number of panels produced
1	Smooth	1-4 (3)	2
2	Regulating layer	1-4 (3)	2
3	Rough (as-sprayed)	1-4 (3)	2
4	Smooth	4-12 (6)	2
5	Regulating layer	4-12 (6)	2
6	Rough (as-sprayed)	4-12 (6)	2
7	No interface	0	1

The panels were manufactured over a month as per the spraying sequence outlined in Table 3-2. After each spray, the boxes were covered with plastic sheeting to prevent exposure to sunshine or cold air, simulating a realistic

environment for sprayed concrete curing in the underground. The spraying and curing were carried out during the summer season between June and September 2011. The weather was as per the seasonal average with daytime temperature around 20-25 degrees Celsius. The panels were covered by plastic sheets and left outside in the yard whilst curing. No extremely cold weather was recorded during this period and the curing was generally recognised as comparable to the real site conditions in terms of temperature and humidity.

Table 3-2 Dates and actions for spraying SCL test panels

Action No.	Spraying Action	Date
1	Primary lining	14th June 2011
2	Regulating layer	16th June 2011
3	1st layer of waterproofing membrane	08th July 2011
4	2nd layer of waterproofing membrane	12th July 2011
5	Secondary lining	14th July 2011
6	Sample curing and cutting	07th Sep 2011

3.2.2 Primary lining surface finish

Figure 3-2 shows three different types of primary lining surface finished. Figure 3-2 (a) shows an 'as-sprayed' surface finish, to which the sprayed membrane can be applied directly, but the quality and the thickness of the membrane may be more difficult to regulate, resulting in high consumption of materials. Figure 3-2 (b) shows a surface that has been covered by a layer of regulating layer. Figure 3-2 (c) shows a completely smooth surface finish (*i.e.* screeded surface), which creates an ideal substrate for the application of sprayed membrane. However, it may be impractical to achieve such a finish in large tunnels and would increase the extent of working at height.

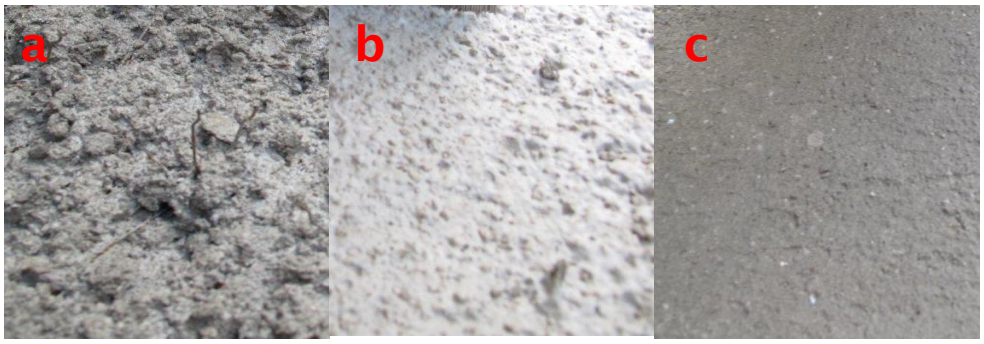

Figure 3-2 Surface roughness (a) 'as-sprayed' rough surface (b) regulated surface (c) smooth surface

The waterproofing membrane was sprayed in two layers. The first layer, which included red pigment, is shown in Figure 3-3 (a). This layer was then covered by a second grey layer as shown in Figure 3-3 (b). Applying the sprayed membrane in a two pass system offers two key advantages:

(1) the second layer will cover any shrinkage-induced pin holes arising from the first layer application
(2) a more effective visual inspection is facilitated, helping to ensure complete membrane coverage

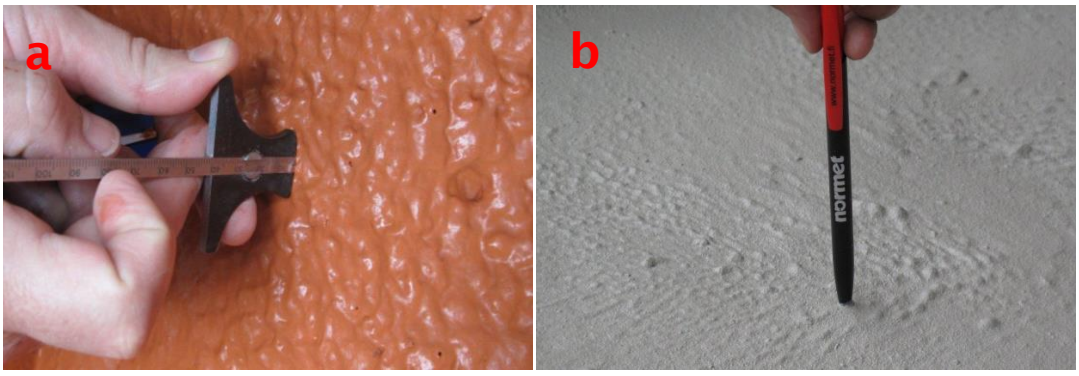

Figure 3-3 The first layer (a) and the second layer (b) of sprayed membrane.

3.2.3 Sprayed concrete mix

The mix specification and design for the primary and secondary linings are shown below in Table 3-3 and Table 3-4 respectively. The waterproofing membrane used in the spraying is TamSeal 800 from Tam-Normet and its detailed information is available from its product method statement (TAM-Normet 2011). TamShot 80AF accelerator was added at 6% by weight of cement and TamCem60 superplasticiser was also used.

Once spraying and curing were completed, the panels were cored and cut to obtain cylinder, block and beam samples. The samples were then transported to the University of Southampton and stacked and labelled ready for testing.

Table 3-3 Mix specification for primary and secondary lining sprayed concrete

Mix	Description	Agg Size (mm)	Cement Type	Target Slump	Target Strength
20080778	SCL mix	10	CEM1	S3	40MPa

Table 3-4 Mix design for primary and secondary lining sprayed concrete

Materials		Dry Batch Weights kg/m^3
Type	Source	
CEM1	Cemex- Rugby	450
0/4 MP Sand	Cemex - Northfleet	1300
4/10 Gravel	Cemex - Northfleet	550
Water reducing admixture	Cemex – CP105 (ml)	2250
FREE W/C		0.40

3.2.4 Testing sample dimensions

Testing samples were cut from the 15 panels using a diamond saw in accordance with the panel spraying and sample cutting plan attached in Appendix A. The number of each type of sample is given in Table 3-5. Concrete is a complex material that usually a large number of test samples are needed to determine its properties. The number of test samples in previous research ranges from hundreds (Zhang & Morgan 2014) to tens of thousands (Raphael 1984), depending on the main objective of each research. As aforementioned, the main objective of this research is not to create a large number of samples and carry out exhaustive laboratory tests to obtain statistically significant values of interface parameters. On the contrary, the main objective is to create a certain number of samples that covers a wide range of interface properties within the practical range, and understand whether the composite SCL tunnel design is sensitive to this practical range of interface parameters. Therefore, a limited number of

samples with wide range of interface properties were created to achieve the main objective of this research.

The standard dimensions of concrete cylinders for compression testing are 100mm in diameter and 200mm in height, as recommended by the BS EN 12390-1 (BSI 2000). However, due to the cutting of the uneven top surfaces, the height of the sprayed concrete cylinder samples generally varied between 180-190mm. This height difference should only make 2% of difference in test results when compared with those from samples of standard dimensions (Neville 1995). Due to the use of automatic spraying machines, the variance in lining thickness can be controlled within 10% for SCL tunnels with constant cross section.

The targeted dimensions of block and beam samples were 150×150×150mm and 900mm×150mm×150mm respectively. The typical testing samples are shown in Figure 3-4.

3.2.5 Sample designation

Test samples were designated with two numbers. The first, the Sample Type, indicates the combination of interface finish and measured membrane thickness (Table 3-1) and the second the number of the sample within its Type, for example, Sample 2-6 is the 6th of the Type 2 samples.

Table 3-5 Numbers of testing samples cut from panels

Type No.	Number of Cylinders	Number of blocks	Number of Beams
1	8	8	4
2	8	24	4
3	8	8	4
4	8	8	4
5	8	8	4
6	8	8	4
7	9	0	4
In total	57	64	28

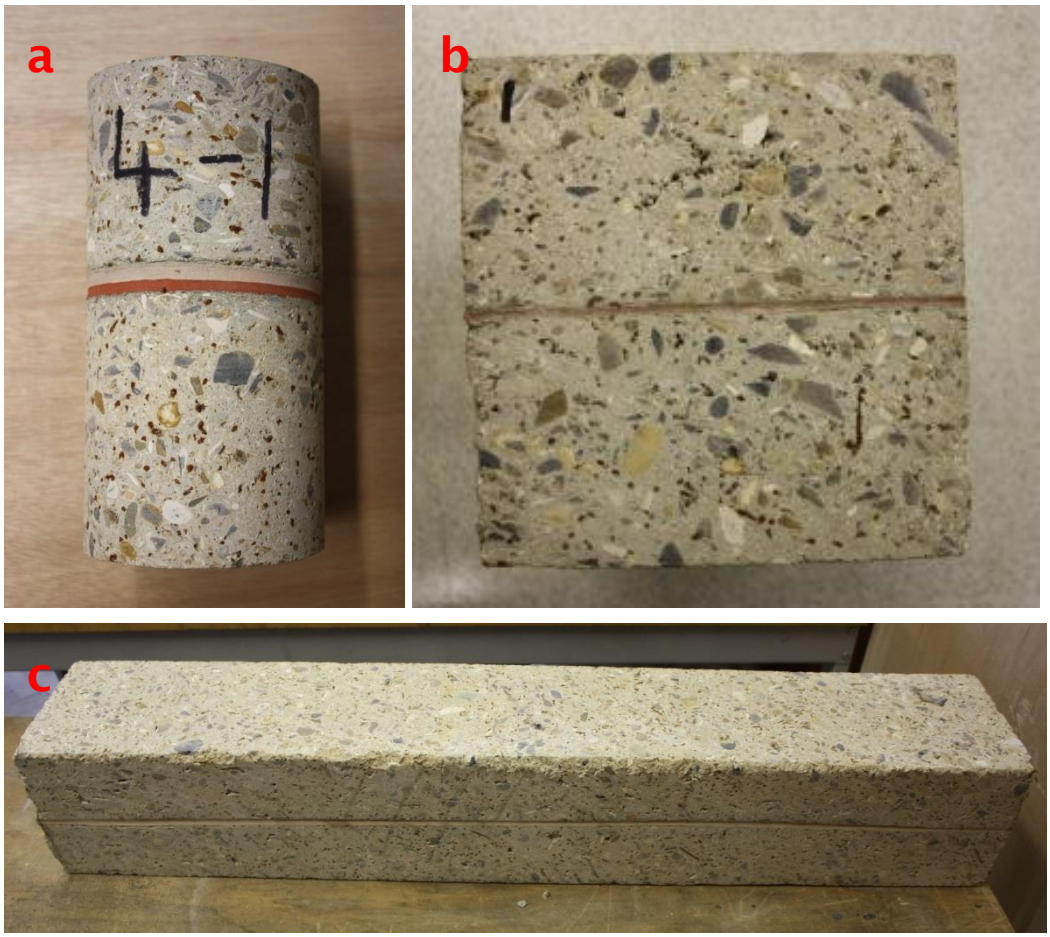

Figure 3-4 Typical Cylinder Sample (a), Block Sample (b) and Beam Sample (c)

3.3 Testing programme for element samples

3.3.1 Testing programme for short-term tests

Tests were carried out on element samples (*i.e.* cylinder and block) to determine the short and long-term interface parameters. Beam tests were subsequently carried out. Their testing methods and configurations are introduced in Chapter 5. The testing plan flow chart detailing the different short-term tests and desired interface properties is shown in Figure 3-5.

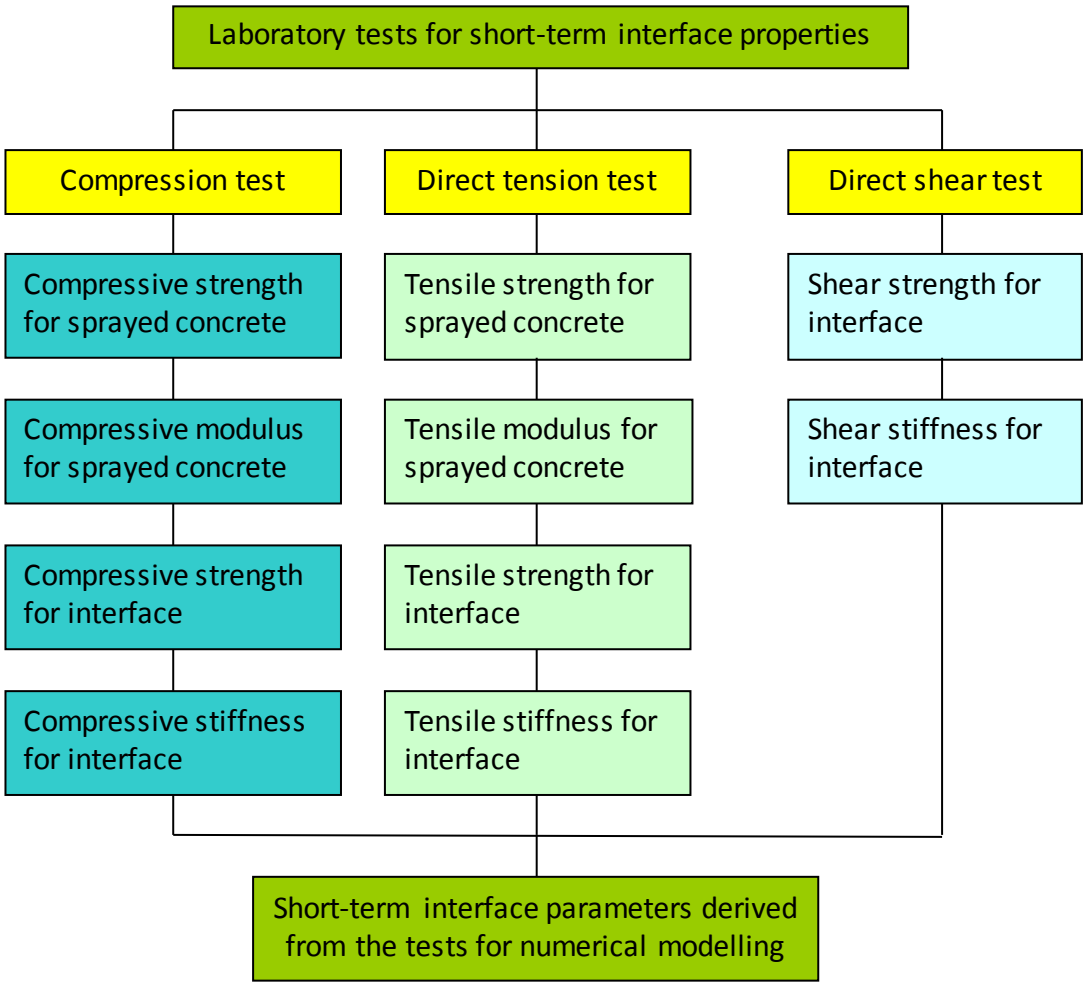

Figure 3-5 Short-term testing plan flow chart

21 short-term uniaxial compression tests and 21 short-term direct tension tests were planned to be carried out using cylinder samples, with 3 samples from each of the 7 panel types for each test.

Short-term direct shear tests were carried out under three different normal stresses, simulating the realistic ground and water pressures experienced by SCL tunnels in soft ground. Soft ground SCL tunnels are usually 20-40m (axis level) below the ground surface, leading to long-term full overburden between 400-800kPa. Historical site monitoring data suggests the loads on the lining could vary between 30% - 80% of full overburden pressure after one year (Powell, *et al.* 1997; Jones 2007), with the possibility of further increases. Therefore, three normal stresses at 250kPa, 500kPa and 750kPa were selected for the direct shear tests.

A regulated interface with thin (*i.e.* 1–4mm) membrane is generally considered a good compromise between surface finish quality and required working effort. It has therefore been recommended by both designers and manufacturers and has been specified in recent major projects, such as Crossrail. Type 2 regulated interface is therefore considered the main focus of this research and hence a reduced number of tests were carried out for other interface types under the two "extreme" normal pressures at 250kPa and 750kPa. The number of tests under each normal stress is shown in Table 3-6. The extra cylinder and block samples were kept as back-ups.

Table 3-6 Numbers of short-term direct shear tests planned

Type No.	250kPa normal stress	500kPa normal stress	750kPa normal stress
1	3	3	
2	3	3	3
3		3	
4	3	3	
5	3	3	
6		3	
7			
In total	12	18	3

3.3.2 Testing programme for long-term tests

The long-term testing plan flow chart is shown in Figure 3-6. The long-term interface parameters are used as the input for the numerical modelling of CSL tunnels in Chapter 6.

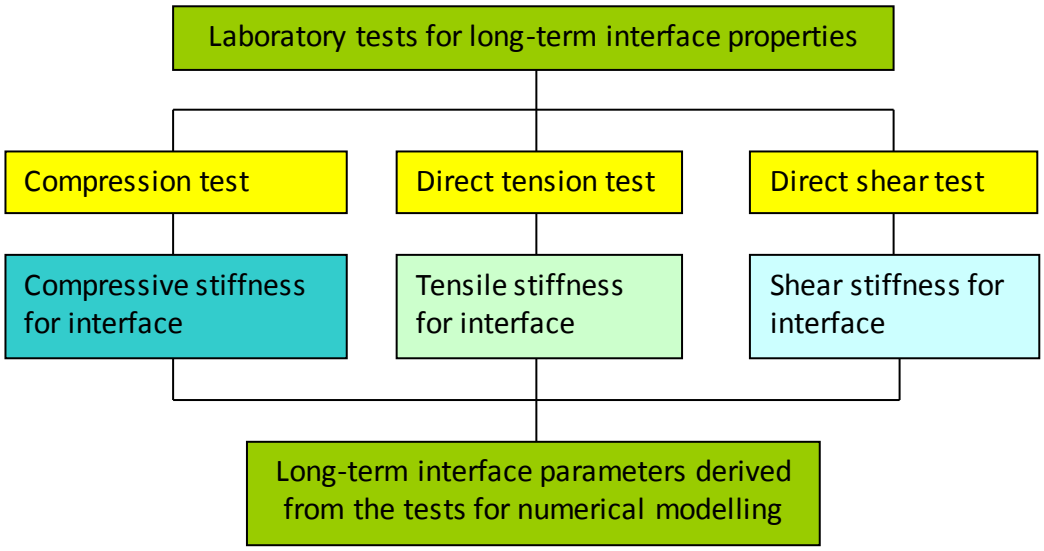

Figure 3-6 Long-term testing plan flow chart

Table 3-7 Number of long-term compression and tension tests

Type No.	Uniaxial Compression Test	Direct Tension Test
1	3*	0
2	0	1

* Tests were performed on the same sample

Table 3-8 Description of testing samples for the long-term direct shear test

Type No.	250kPa vertical pressure	500kPa vertical pressure	750kPa vertical pressure
2	1	1	0

3.4 Testing methods

This Section describes the machinery used during testing, including the instruments used to measure local displacements. This is followed by an outline of the testing procedures for both the short and long-term tests.

3.4.1 Uniaxial Compression Test

The uniaxial compression test was carried out using a DMG servo hydraulic loading machine with a maximum force of 600kN, as shown in Figure 3-7. The two steel plates on the lower part of the machine were used for the uniaxial compression test, whilst the steel grips on the upper part of the machine were used for the direct tension test. Machine load and stroke were scanned once every second and recorded automatically by a Vishay 5000 Series data logger. For each test, three potentiometers were clamped between two aluminium rings so as to measure the actual shortening of samples over the gauge length, as shown in Figure 3-8 (the third potentiometer is located behind the pictured sample). The potentiometers were first calibrated using an electronic length gauge and then linked to the data logger and scanned once per second.

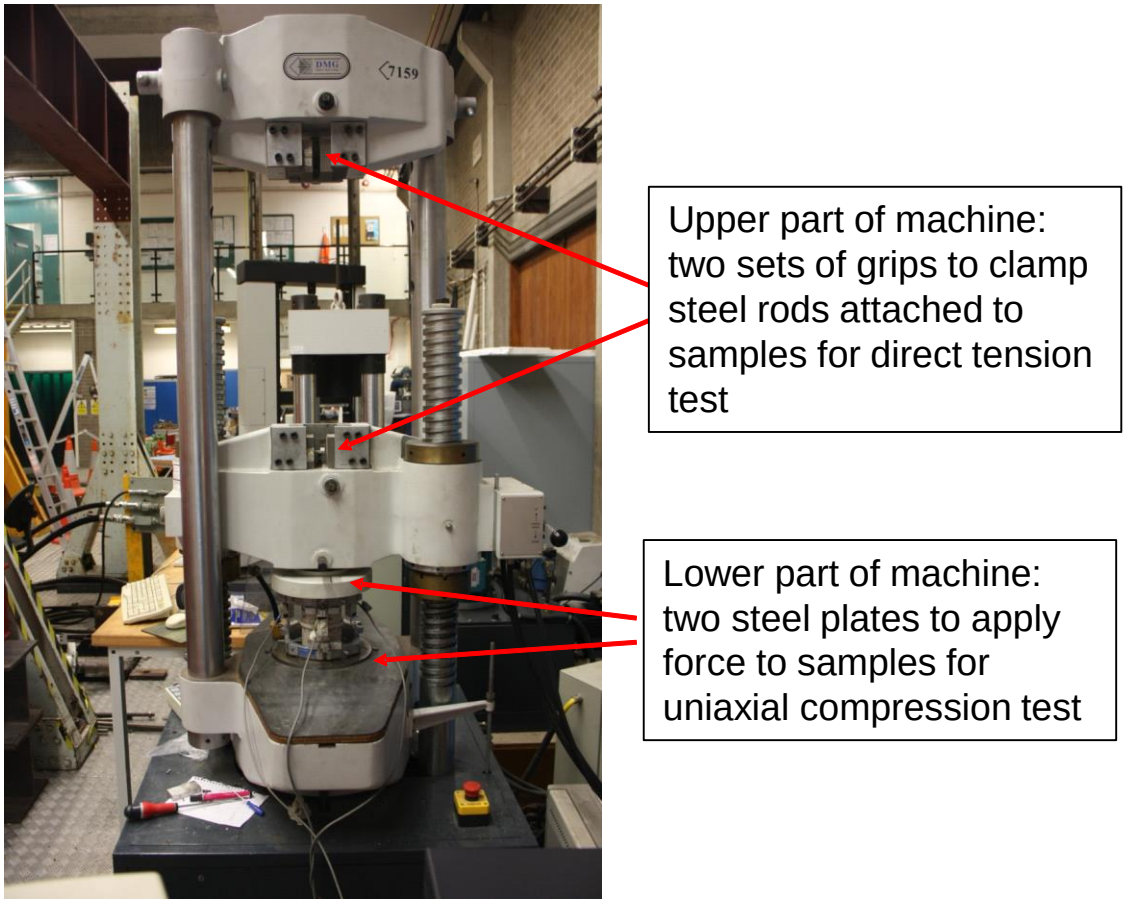

Figure 3-7 DMG servo hydraulic loading machine

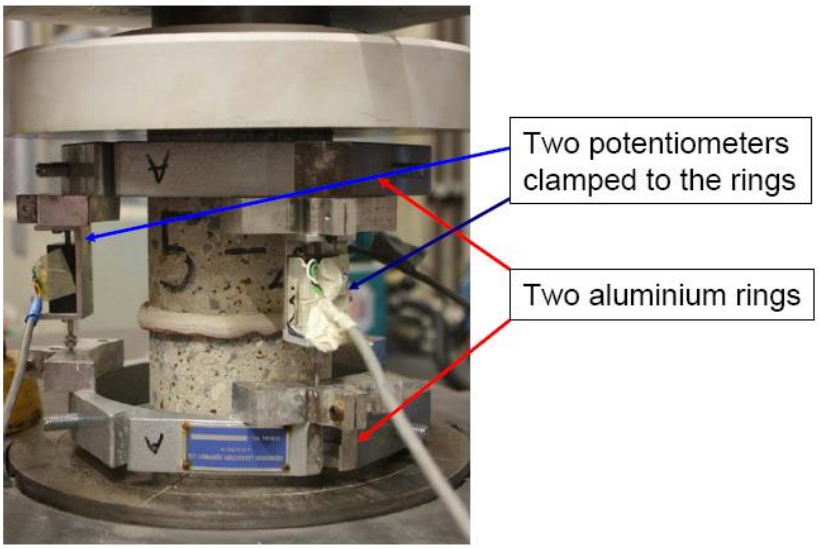

Figure 3-8 Typical compression test set-up

The distance between the two rings was around 160mm and the exact distance was measured before each test. The use of potentiometers as a local strain measurement instrument eliminated the impact of the compliance of the whole machine from the machine reading.

There were two stages to the short-term test. At the first stage, one sample from each sample type was loaded in compression up to 10MPa (upper bound cyclic loading compressive stress for the first loading sample) to obtain the first loading compressive stiffness. The stress was then reduced to approximately 2MPa (lower bound cyclic loading compressive stress for the first loading sample) and then back to 10MPa so as to complete a loading/unloading cycle to obtain its cyclic loading compressive stiffness and check if there was any hysteresis. Three cycles were applied in order to obtain an average value of cyclic loading stiffness. Subsequently, the stress was increased to the stage when the samples started to fail and the stress started to drop. Usually, SCL tunnels experience loading during their construction and operation but unloading when an adjacent underground structure is constructed nearby. Therefore, a cyclic loading test was carried out to understand if there is any difference between interface stiffnesses during loading and unloading.

Following the first stage of testing, an understanding was gained of the general behaviour and compressive strength for each type of sample. In the second stage, for the second and third samples of each type, the test procedure was almost the same except the upper and lower bounds of loading/unloading cycle were adjusted to 50% and 10% respectively of their compressive strength as

determined by the loading for the first sample. The test stroke rate was kept constant at 0.01mm/s.

A single Type 1 sample was selected for the long-term compression test. The sample was loaded to 3MPa, 6MPa and 20MPa respectively. Once the sample was loaded to its respective stress, the distance between the two steel plates was held constant, allowing stress relaxation to happen gradually within the sample. Each long-term compression test was sustained for one week during which the laboratory temperature was recorded by a temperature probe adjacent to the sample.

3.4.2 Direct Tension Test

The direct tension test was performed using the same machine and local displacement measurement instruments as the compression test. Steel plates were fixed to the end of the samples with epoxy adhesive. These two steel plates were of the same dimensions (100mm diameter and 20mm thickness) with a steel rod welded perpendicularly to the centre of each steel plate. The rods were each clamped tightly by the grips on the machine so as to apply the tensile force to the sample. The test stroke rate was kept constant at 0.01mm/s. A typical direct tension test setup is shown in Figure 3-9.

Only one test was carried out in the long-term testing, on a Type 2 sample, as interface roughness and membrane thickness had already been found to have little impact on the tensile stiffness, as discussed in Section 4.5. The sample was firstly loaded up to 0.5MPa and then the distance between two grips kept constant, allowing stress relaxation to happen gradually within the sample. It is understood that SCL tunnels in soft ground are usually between 20-40m (axis level) below the ground surface, therefore the invert should not be more than 50m below the ground surface. A 0.5MPa tensile stress is therefore sufficient to test the long-term behaviour of interface when subjected to long-term water pressure. The long-term tension test lasted for two weeks and the laboratory temperature was recorded by a temperature probe adjacent to the sample throughout.

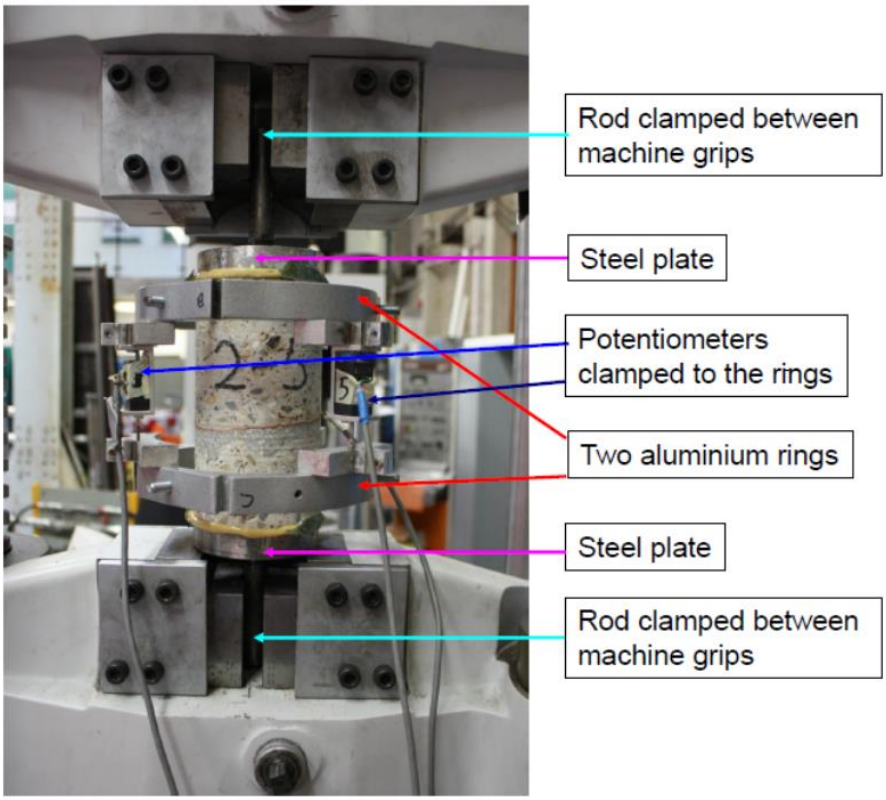

Figure 3-9 Typical direct tension test set-up

3.4.3 Direct Shear Test

The direct shear test was carried out using a Sercomp 7 special hydraulic controller system with WF large shear box. The shear box has two loading systems, one for normal (vertical) stress and one for shear (horizontal) stress. The maximum controllable horizontal shear load is 100kN and the minimum controllable vertical pressure is 0.025MPa (2.25kN on a 300mm shear box). The horizontal shear stress rate control is from 0.001MPa/s to 1000MPa/s. The whole direct shear test system is shown in Figure 3-10. The shear box comprises two parts. The upper box is fixed stationary to the machine and the lower box pushed by two hydraulic rams to generate shear stress in the test samples. A loading ring is positioned between two hydraulic rams to the back of the machine. Six LVDTs were calibrated and used to record test data. One LVDT was positioned within the loading ring to record the shear load and another was positioned at the back of the lower shear box to measure its horizontal displacement. Four LVTDs were positioned on the four corners of the top cap to measure the vertical dilation during the test. The normal force applied by the cross beam was recorded by the machine automatically.

Because the sample size was smaller than the box size, it was necessary to pack between the sample and the box in the direction of loading. Provided the stiffness of the packing material was much greater than the expected stiffness of the membrane interface in shear, the additional compliance of the test setup as a result of the packing would not affect the recorded membrane stiffness significantly. After consideration, timber was selected as the packing material, mostly due to its wide availability and ease of machining. In order to accommodate the small variance in sample dimensions, timber wedges in different thickness were machined and used to restrict the relative movement between the sprayed concrete layers and respective shear boxes, forcing the shear stress and displacement to occur at the membrane interface. The Young's modulus of timber is around 10GPa, leading to a stiffness for a 150mm combined length timber wedge of 6.66GPa/m, which is much higher than the first loading stiffness of the membrane interface, which is between 0.5–1.0GPa/m, as shown in Table 4-5 on page 71. A diagram of the shearing process is shown in Figure 3-11.

Figure 3-10 Sercomp 7 hydraulic controller system with WF large shear box

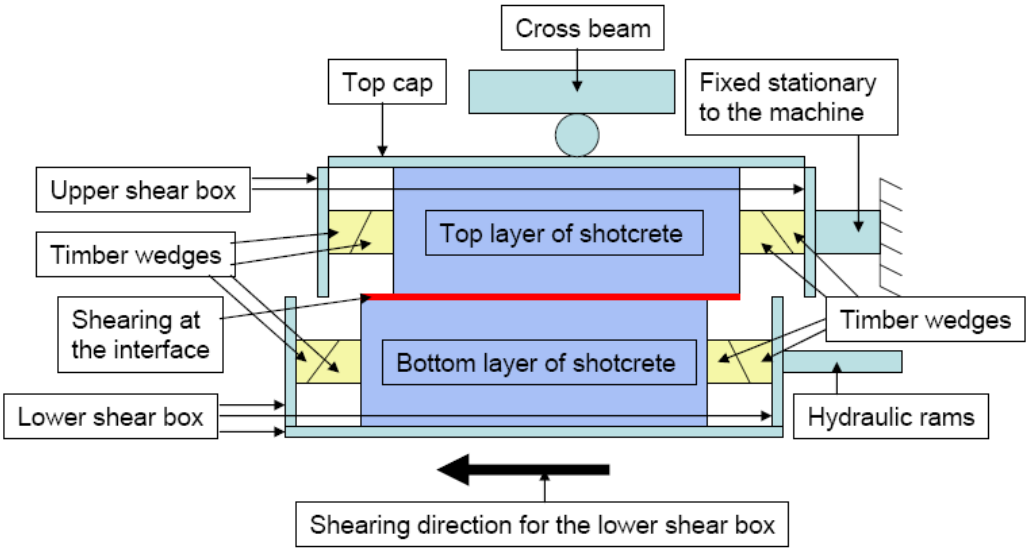

Figure 3-11 Cross-Section of the shearing process

In the short-term testing, once the specified vertical pressure was engaged, the shear stress started to be applied. The test procedure was similar to previous tests. The upper and lower bound cyclic loading shear stresses for all the testing samples were set at 0.7MP and 0.25MPa respectively. The test shear stroke rate was 0.2mm/min throughout.

Two Type 2 samples were tested in the long-term testing under 250kPa and 500kPa normal pressures. The samples were firstly sheared to 1MPa and then the shear displacement was kept constant, allowing the stress relaxation to happen gradually at the interface.

The long-term direct shear test stress of 1MPa was selected because it was approximately half of the maximum short-term shear interface stress. This would be of similar magnitude to the design shear strength after the average test results were factored down appropriately. Each long-term shear test last for two weeks and the laboratory temperature was recorded throughout by a temperature probe adjacent to the shear box.

3.5 Post-processing and presentation of results

Test results are presented in stress-deformation format using the following relationships, to indicate interface stiffness and failure stress and how they are influenced by interface roughness and membrane thickness.

$\sigma_n = F_n/A$ Equation 3-1

$\sigma_s = F_s/A$ Equation 3-2

$K_n = \sigma_n/\delta_n$ Equation 3-3

$K_s = \sigma_s/\delta_s$ Equation 3-4

Where:

F_n: Applied normal load

F_s: Applied shear load

A: Loading area

σ_n: Applied normal stress

σ_s: Applied shear stress

δ_n: Interface deformation in the normal direction

δ_s: Interface deformation in the shear (tangential) direction

K_n: Interface compressive/tensile stiffness

K_s: Interface shear stiffness

The direct shear tests measured the shear displacements externally, which were affected by the compliance of the testing machine and the rotation of the shear samples during the test. In order to compensate these impacts, the raw cyclic loading shear stiffness data was adjusted – this is reported in Chapter 4 and used in Chapter 5 for the calibration of the composite beam models.

The post-processing of the raw cyclic loading shear stiffness data is described with an example in Appendix B.

Chapter 4: Interpretation and Discussion of Element Test Results

4.1 Introduction

This Chapter first presents the short-term test results from the uniaxial compression tests, direct tension tests and direct shear tests for sprayed concrete samples with and without sandwiched membrane. The influence of interface roughness and measured membrane thickness are discussed for each type of test. Relationships between peak stress, first and cyclic loading stiffnesses, measured membrane thickness and the type of interface are proposed. Results from the three long-term relaxation tests on composite samples are then presented and the relationship between relaxation percentage and time for each type of test is proposed. A summary of the results is presented at the end of this chapter. All test samples were more than 90 days old when tested. All membrane thickness discussed in this and the following Chapters is measured thickness. For pure sprayed concrete samples, the strain was calculated over the gauge length. For composite samples, the strain was calculated over the measured membrane thickness.

4.2 Short-term compression tests on pure sprayed concrete cylinder samples

4.2.1 Test results for pure sprayed concrete samples

Uniaxial compression tests for three pure sprayed concrete cylinder samples were carried out to examine the response of sprayed concrete in compression. All samples were cyclically loaded three times between 5-20MPa and then loaded up to the failure stage. The test showed that all three samples failed in transverse tension, demonstrated by cracks developing vertically, as shown in Figure 4-1, fulfilling the requirement for a satisfactory failure given in the BS EN 12390-3 (BSI 2009).

The stress-strain relationships for three samples are shown below in Figure 4-2. The compressive strengths obtained for the three samples were 39MPa, 38MPa

and 37MPa respectively. The proportional limit was reached at about 80% of their respective compressive strengths with the secant modulus of elasticity before the proportional limit around 20-22GPa. The compressive strains at peak stress were between 0.18%-0.25% and there was no hysteresis during the cyclic loading.

Figure 4-1 Typical failure mode under compression test

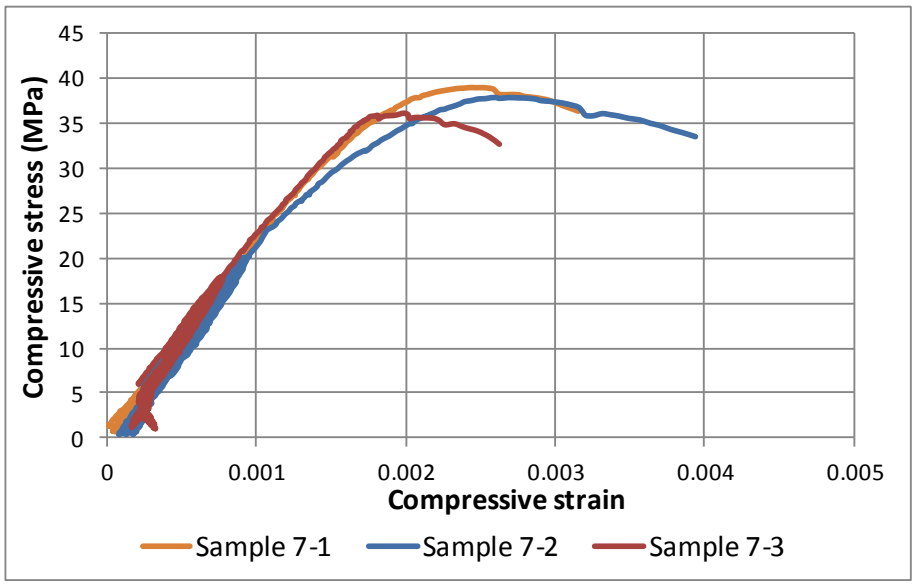

Figure 4-2 Stress-strain relationships for pure sprayed concrete cylinder samples under uniaxial compression

4.2.2 Evaluation of test results

The test results were compared with properties of cast *in situ* concrete in Eurocode 2 (BSI 2004) and sprayed concrete in RILEM code (RILEM 2003). The mean value of compressive strength for three samples was approximately 38MPa, with a standard deviation of 1MPa. If they were cast *in situ* concrete samples, based on the Table 3-1 in Eurocode 2 (BSI 2004), the corresponding secant modulus of elasticity would be around 33GPa, significantly higher than the test results of between 20-22GPa, and the associated proportional limit would be only 40%, much lower than the test results at 80%.

The compressive strain at peak stress for the sprayed concrete samples was between 0.18%-0.25%, close to the EC 2 specified range between 0.175%-0.22%. Eurocode 2 has only specified the ultimate compressive strain of 0.35% for a cross section under bending. For a cross section subjected to pure axial compression, the ultimate compressive strain should be limited to 0.2%, as specified by the RILEM code. All three samples achieved 35MPa compressive strength at the strain 0.2% with little variance, demonstrating consistency in test results.

The discrepancies in material response in compression between the sprayed concrete samples and expected behaviour of cast *in situ* concrete may be attributed to the different respective aggregate sizes. The larger aggregates used in typical cast *in situ* concrete may result in a higher compressive modulus (Neville 1995). On the other hand, the rounder and smaller aggregates used in typical sprayed concrete mixes lead to a lower concentration of stress at the aggregate/cement interface, thus postponing crack formation to a much later stage. This enables the sprayed concrete to perform elastically to a higher level of its compressive strength.

Based on the comparisons between the sprayed and cast *in situ* concrete properties, it is considered that the test results obtained from the uniaxial compression test are reasonable and can be used as a basis for the following investigation.

4.3 Short-term compression on composite cylinder samples

4.3.1 Testing overview

Compression tests were carried out to investigate the interface response in compression, especially the impact of interface roughness and measured membrane thickness. In line with the testing plan, a total of 18 samples were due to be tested, with 3 samples from each panel Type 1 to 6. In reality, only 17 samples were tested – a single Type 4 sample was omitted due to damage sustained prior to testing. It is noted that the Type 1 to 3 samples are of thin membrane interface with measured membrane thickness between 1-4mm. The Type 4 to 6 samples are of thick membrane interface with measured membrane thickness between 4-12mm.

4.3.2 Compressive interface stress-deformation relationships

Interface stress-deformation graphs for samples with thin (Type 1 to 3) and thick (Type 4 to 6) membranes are shown in Figure 4-3 and Figure 4-4 respectively.

The peak compressive stress of five out of six Type 1 & 2 interfaces was between 35-40MPa. Only one interface, 2-1, showed a lower peak compressive stress and lower corresponding strain, possibly due to defects inside the sample.

The peak compressive stress for all three Type 3 interfaces was much lower, between 14-25MPa. For thick membrane interfaces, the large variance in membrane thickness and difference in interface roughness had significant impact on the peak compressive stress of each interface. The peak compressive stress for three out of eight interfaces was between 20-25MPa while the other five interfaces were in the range of 12-17MPa.

Figure 4-3 and Figure 4-4 show that all interfaces failed in a brittle manner after reaching their peak stresses. There was no obvious increase in cyclic stiffness with increase in stress level. Numerical data and statistical analysis are presented in Table 4-1 and Table 4-2 respectively.

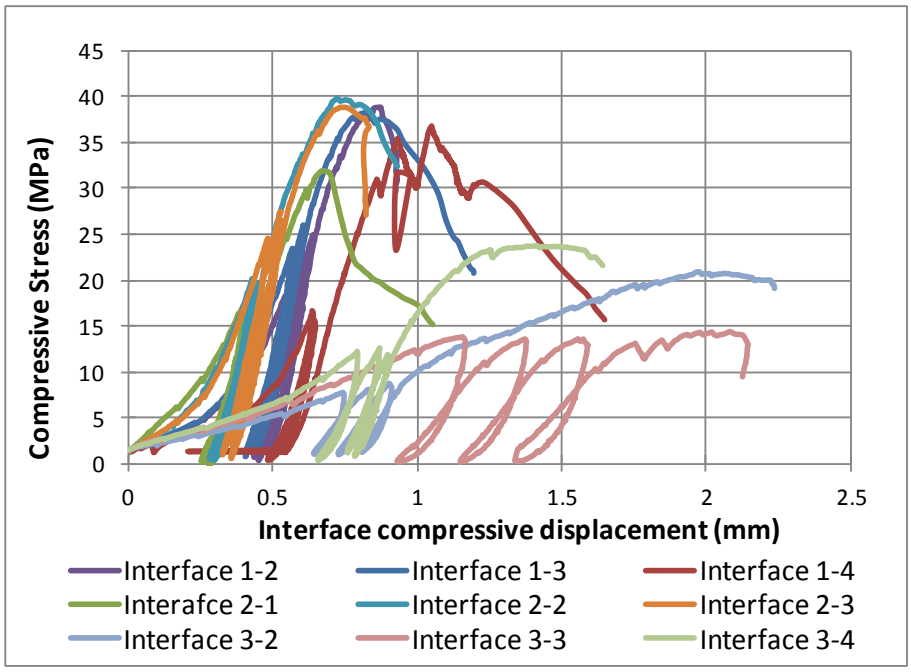

Figure 4–3 Thin membrane interface behaviour under uniaxial compression tests

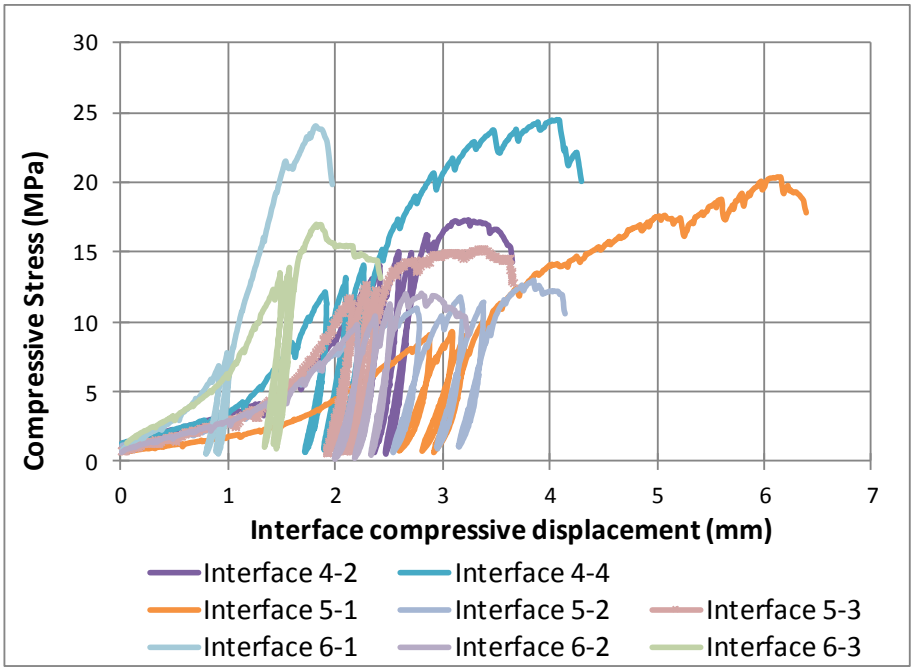

Figure 4–4 Thick membrane interface behaviour under uniaxial compression test

Table 4-1 Uniaxial compression test results

Interface Number	Membrane thickness (mm)	Peak Stress (MPa)	First loading stiffness (GPa/m)	Cyclic loading stiffness (GPa/m)
1-2	2.0	38	11.5	63.8
1-3	2.5	38	11.6	62.5
1-4	3.0	37	13.6	78.4
2-1	3.0	32	27.8	57.9
2-2	2.5	39	15.6	66.6
2-3	2.5	38	13.8	71.6
3-2	4.0	20	8.7	77.2
3-3	3.5	14	5.5	29.4
3-4	4.0	24	8.1	70.1
4-2	9.5	17	2.6	33.3
4-3	9.0	24	3.3	31.4
5-1	12.0	20	2.2	21.2
5-2	11.5	13	2.3	30.8
5-3	9.0	15	2.9	33.5
6-1	6.0	24	7.0	81.1
6-2	8.5	12	2.8	39.5
6-3	6.5	17	4.3	63.7

Table 4-2 Statistical analysis of uniaxial compression test results

Interface Type	Peak stress		First loading stiffness		Cyclic loading stiffness	
	Mean (MPa)	Standard deviation (MPa)	Mean (GPa/m)	Standard deviation (GPa/m)	Mean (GPa/m)	Standard deviation (GPa/m)
Type 1	37.7	0.6	12.2	1.2	68.2	8.8
Type 2	36.3	3.8	19.1[a]	7.6[a]	65.4	6.9
Type 3	19.3	5.0	7.4	1.7	58.9	25.8
Type 4	20.5	4.9	2.9	0.5	32.4	1.4
Type 5	16.0	3.6	2.4	0.4	28.5	6.5
Type 6	17.7	6.0	4.7	2.1	61.5	20.9

[a] Mean and standard deviation of first loading stiffness become 14.7 GPa/m and 0.8 GPa/m respectively if Interface 2-1 is excluded

4.3.3 Peak compressive stress

The relationship between peak compressive stress, measured membrane thickness and the type of interface roughness is shown in Figure 4-5, suggesting that:

(1) Smooth and regulated interface have similar impact on the peak stress

(2) As-sprayed rough interface reduces the peak compressive stress significantly (approximately 50%) for thin membrane interfaces (Type 3)

(3) Thick membrane thickness reduces the compressive peak stress significantly (approximately 50%) and the influence of interface roughness becomes less important (Types 4 to 6)

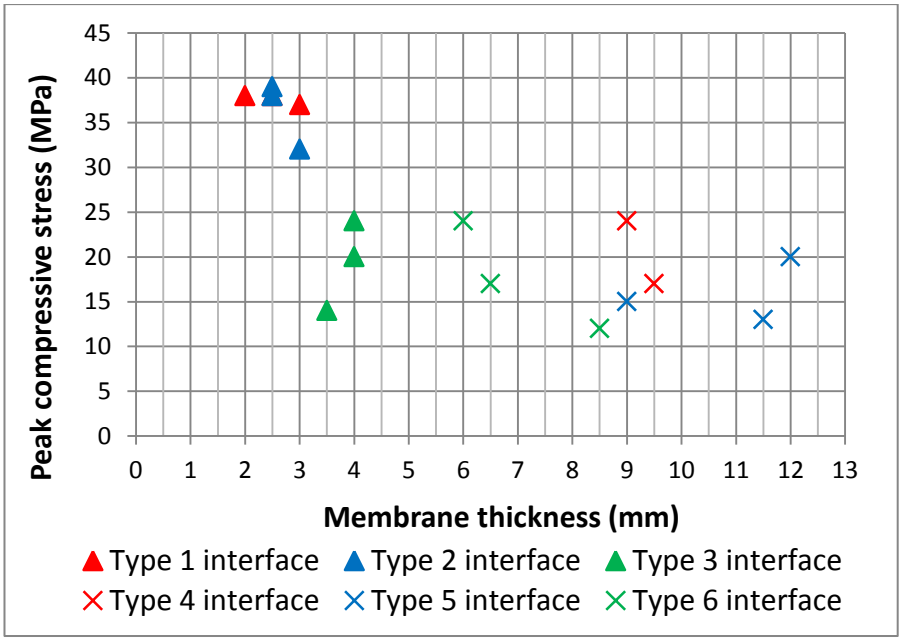

Figure 4-5 Relationship between peak compressive stress, membrane thickness and type of interface

4.3.4 First and cyclic loading compressive stiffnesses

The relationship between first loading compressive stiffness, membrane thickness and type of interface is shown in Figure 4-6. The first loading stiffness increases with reduced membrane thickness and reduced interface roughness, over the range 2GPa/m to 16GPa approximately (excluding the outlier interface 2-1). The relationship between cyclic loading compressive stiffness, membrane thickness and type of interface is shown in Figure 4-7. The cyclic loading

stiffness increases with reduced membrane thickness, over the range 20GPa/m to 80GPa/m, but is little affected by the interface roughness. The conclusions are very similar to those for compressive peak stress.

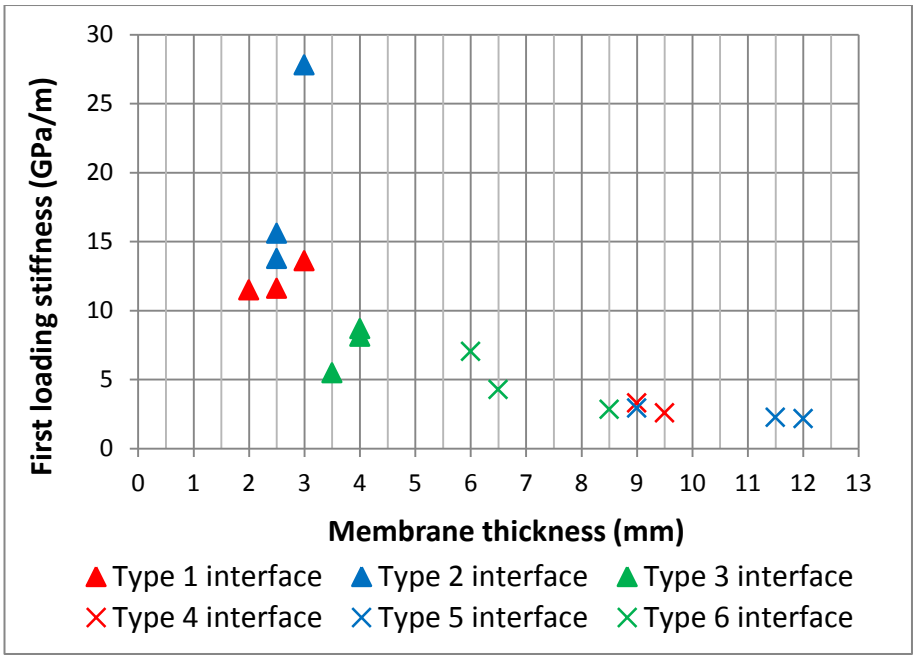

Figure 4-6 Relationship between first loading compressive stiffness, membrane thickness and type of interface

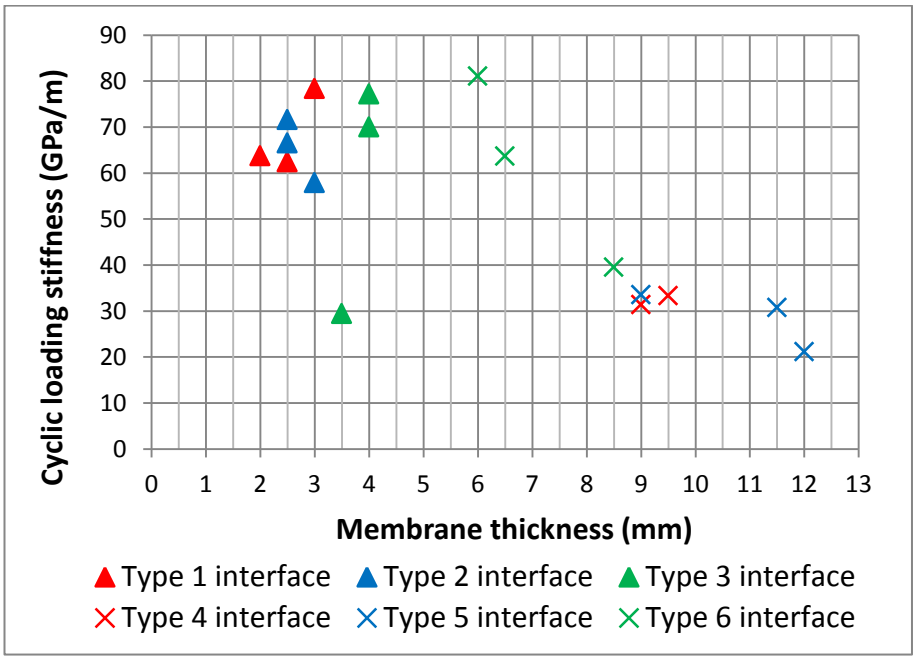

Figure 4-7 Relationship between cyclic loading compressive stiffness, membrane thickness and type of interface

4.3.5 Compressive strain at peak compressive stress

The compressive strain at peak compressive stress is generally between 30% and 50% of measured membrane thickness, with two outliers at 60% and 20% respectively, as shown in Figure 4-8. No clear trend was found between the strain, membrane thickness and type of interface.

As this research focuses on shallow SCL tunnels in soft ground, the distance between the ground surface and the invert level of tunnel should be no more than 50m. Assuming the ground is fully saturated with a density of 20×10^3 kg/m^3, the combined vertical ground and water pressure at 50m depth should be 1.0MPa without taking account of any surcharge. Assuming the interface was over-sprayed with 12mm thick membrane, the first loading stiffness from the tests has been found to be 2.2GPa/m. Therefore, when the full overburden is applied to the extrados of primary lining, an interface deformation of approximately 0.5mm and a compressive strain of about 4% would be expected. This is well below the lowest test result of 20%, therefore failure in compression would not be expected to occur at the sprayed concrete-membrane interface.

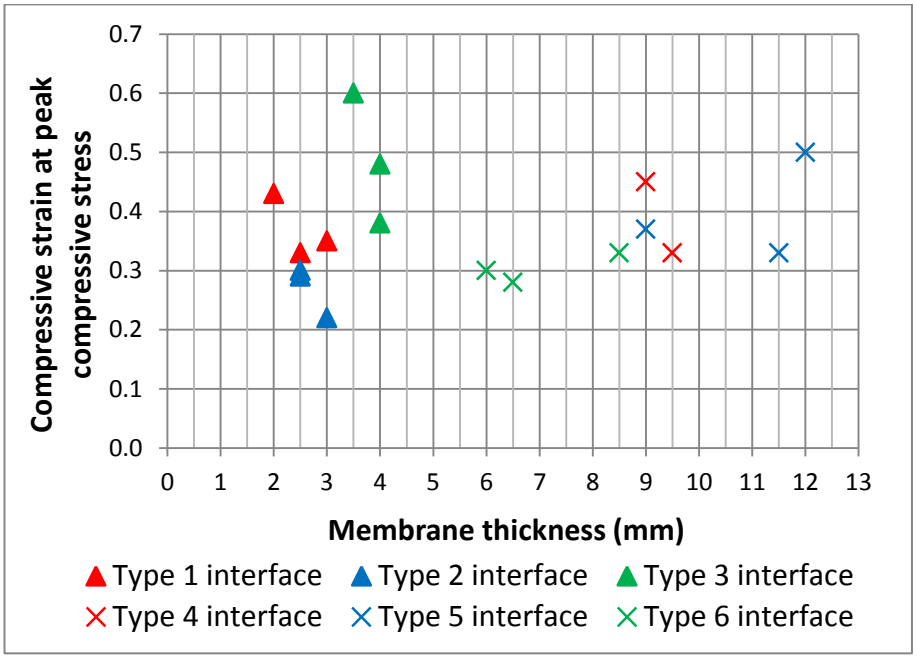

Figure 4-8 Relationship between compressive strain at peak compressive stress and membrane thickness and type of interface

4.3.6 Observed failure modes in compression tests

All compressive interfaces failed in transverse tension, with vertical cracks formed either side of the membrane, as shown in Figure 4-9. For interfaces with a thick membrane application, a significant quantity of membrane was squeezed out at failure, pulling some of the surface concrete away with it (Figure 4-9b). This horizontal deformation of the membrane is likely to have induced horizontal tensile strain at the interface and thus explaining why interface Types 4 to 6 interfaces failed at lower stress levels.

Figure 4-9 Typical compressive failure modes for (a) thin membrane interface (b) thick membrane interface

4.4 Short-term tension tests on pure sprayed concrete cylinder samples

4.4.1 Test results for pure sprayed concrete samples

Direct tension tests for three pure sprayed concrete cylinder samples were carried out to verify the response of sprayed concrete in tension. It was observed that all samples failed with cracks developing horizontally through the cross section, as shown in Figure 4-10, which is the expected failure mode for samples under direct tension. The splitting surfaces after failure were not perfectly flat, probably due to the existence of aggregate in different positions and orientations. The stress-strain relationships for three samples are shown below in Figure 4-11.The tensile strengths for the three samples were 1.95MPa, 1.4MPa and 1.57MPa respectively. The proportional limit was approximately up to 1MPa for all samples with the secant modulus of elasticity ranging from 15-25GPa. This variation is mainly attributed to the difficulty in aligning the test samples perfectly vertical in the machine. The tensile strains at peak stress varied from 60-160 microstrain (10^{-6} strain) of the gauge length and there was no obvious hysteresis during the cyclic loading.

Conventionally, the tensile strength of concrete is obtained using the tensile splitting method or evaluated from the flexural tensile strength (Neville 1995). Although the direct tension test method is thought to be the best method to evaluate the tensile strength, no guidance on its use is currently available in British Standards or Eurocodes due to the difficulty in its execution. It is understood from testing that the determining factor for achieving correct tensile strength is the verticality of the samples in the test, enabling the tensile stress to transfer through the sample cross section uniformly.

4.4.2 Evaluation of test results

The tensile strains of the gauge length at peak stress for sprayed concrete samples were between 60-160 microstrain, smaller than the test results of 200 microstrain from Guo and Zhang (1987) and closer to the RILEM (2003) and Eurocode 2 (BSI 2004) recommended value of 100 microstrain.

The test shows that the verticality between the top and bottom steel plates is very important. Samples 7-5 and 7-6, both of which were in good verticality, achieved higher tensile modulus (25GPa), very close to the compressive modulus presented in previous sections, whilst sample 7-7 showed a "softer" response in tension (15GPa). Therefore, the test results from Samples 7-5 and 7-6 are therefore considered reasonable and can be used as a basis for the following investigation.

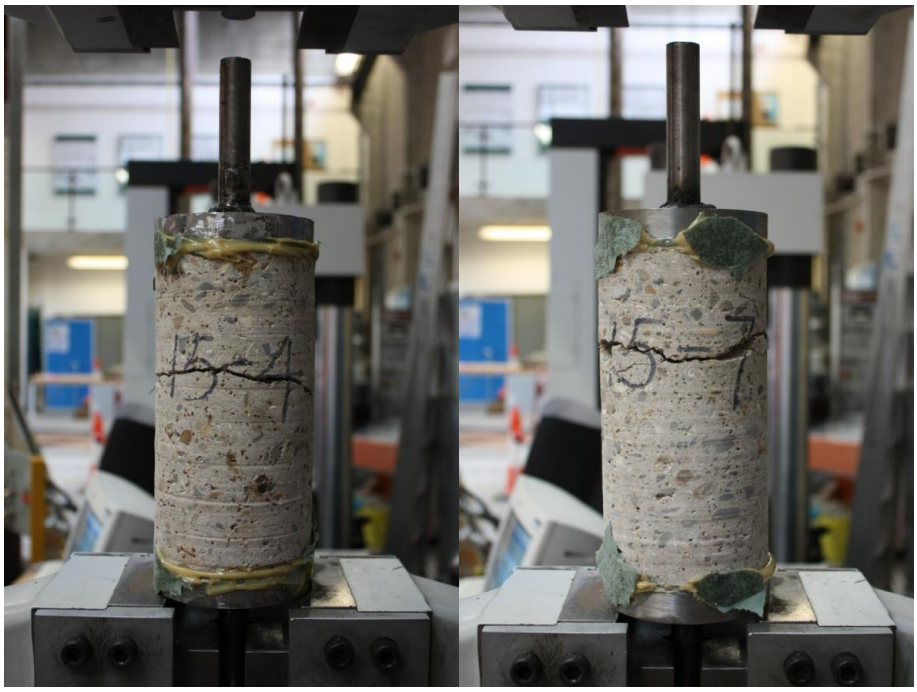

Figure 4-10 Typical failure mode under direct tension tests

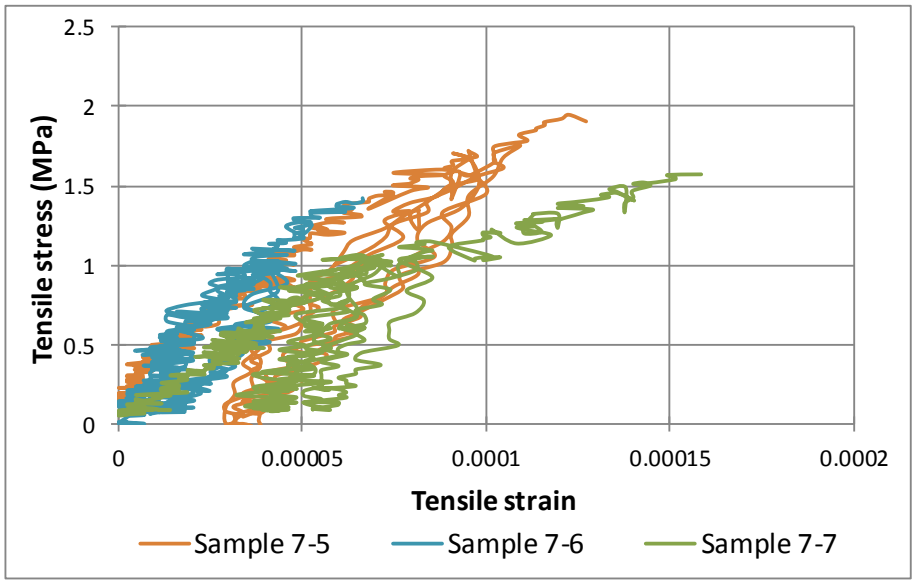

Figure 4-11 Stress-strain relationship for pure sprayed concrete cylinder samples under direct tension test

4.5 Short-term tension tests on composite cylinder samples

4.5.1 Testing overview

Direct tension tests were carried out to investigate the interface response in tension, especially the impact of interface roughness and measured membrane thickness. In line with the testing plan, 18 tests were planned to be carried out on 3 samples from each type for Type 1 to 6. However, only 16 samples were actually tested, with tests omitted for one Type 3 and one Type 6 sample due to damage sustained prior to testing.

4.5.2 Tensile interface stress-deformation relationships

Interface stress-deformation graphs for samples with thin (Type 1 to 3) and thick (Type 4 to 6) membranes are shown in Figure 4-12 and Figure 4-13 respectively.

Thin membrane interfaces, with the exception of 1-6, failed in a ductile manner with stress plateaus over the displacement range 0.1-1.0mm. Even at a tensile displacement deformation of 0.8mm, all other seven interfaces were still able to sustain stress above 0.5MPa, which is the maximum pore water pressure a shallow SCL tunnel is likely to experience. Interface 1-6 failed in a brittle manner, the reason for which is unclear. However, it still achieved a tensile strength of 0.8MPa.

Post-peak performance of thick membrane interfaces is similar to the thin membrane, with seven out of eight interfaces able to sustain 0.4MPa tensile stress at a tensile deformation of 1.5mm with the remaining interface able to sustain 0.3MPa. The post-peak ductile behaviour of both thin and thick membrane interfaces gives confidence to designers because water pressure is more likely to be confined to a small area if it permeates through cracks in the primary lining and reaches the membrane. Numerical data and statistical analysis are presented in Table 4-3 and Table 4-4 respectively.

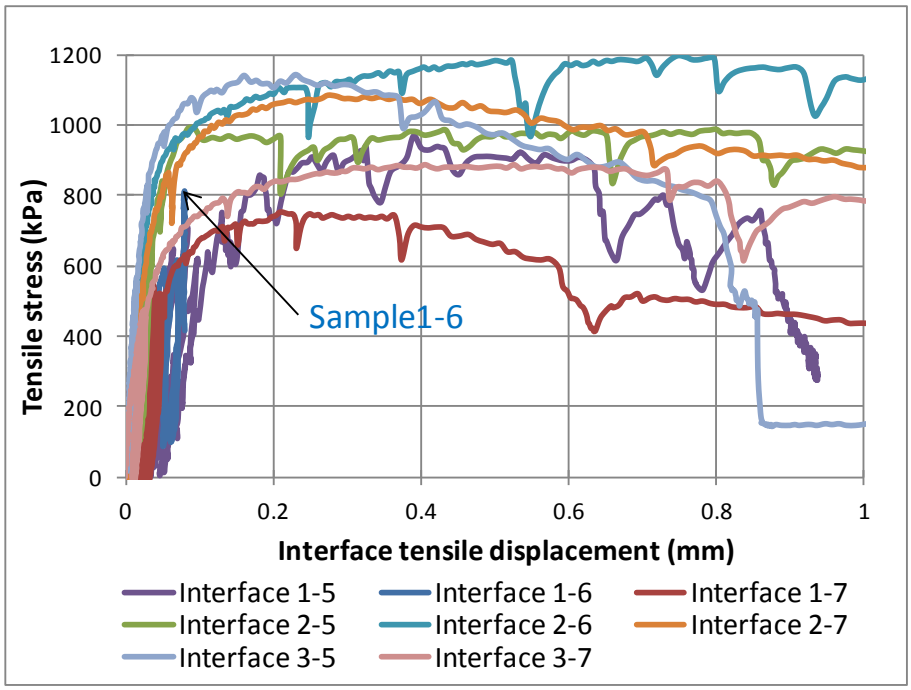

Figure 4-12 Thin membrane interface behaviour under direct tension test

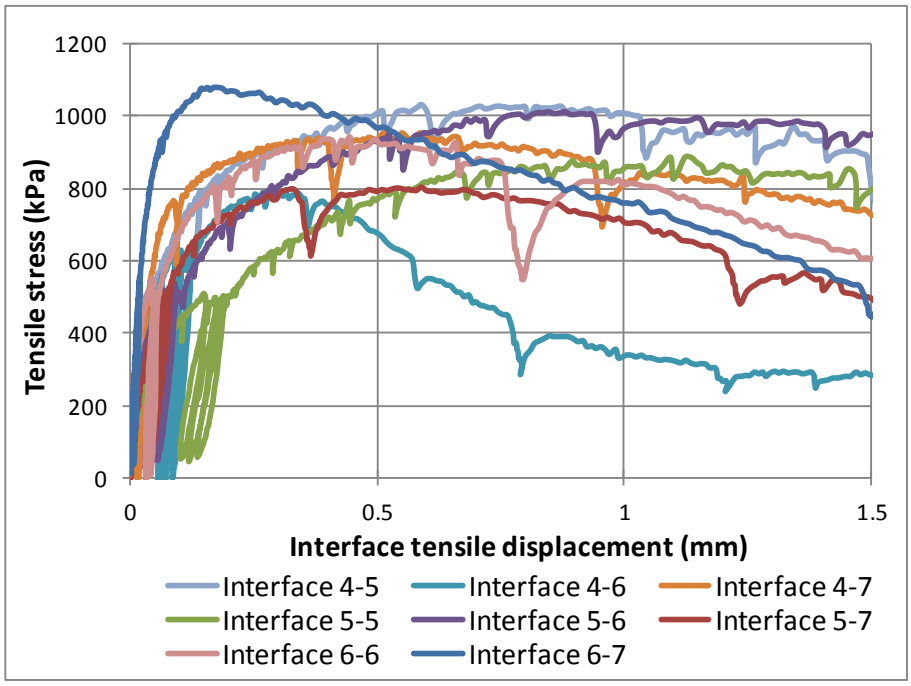

Figure 4-13 Thick membrane interface behaviour under direct tension test

Table 4-3 Direct tension test results

Interface number	Membrane thickness (mm)	Peak stress (MPa)	First loading stiffness (GPa/m)	Cyclic loading stiffness (GPa/m)
1-5	2.0	0.93	10.6	12.1
1-6	2.0	0.80	14.6	46.8
1-7	2.5	0.75	20.4	37.9
2-5	1.0	0.98	59.3	46.2
2-6	1.0	1.13	111.6	100.1
2-7	2.5	1.07	219.1	57.8
3-5	3.0	1.12	399.1	104.0
3-7	3.0	0.88	42.0	43.1
4-5	7.5	1.03	15.0	21.2
4-6	8.0	0.75	7.4	19.0
4-7	8.0	0.93	18.2	37.0
5-5	10.0	0.86	3.4	7.9
5-6	8.0	1.00	7.6	13.1
5-7	9.0	0.80	7.8	13.3
6-6	4.5	0.94	34.7	53.6
6-7	6.0	1.04	34.3	52.6

Table 4-4 Statistical analysis of direct tension test results

Interface Type	Peak stress		First loading stiffness		Cyclic loading stiffness	
	Mean (MPa)	Standard deviation (MPa)	Mean (GPa/m)	Standard deviation (GPa/m)	Mean (GPa/m)	Standard deviation (GPa/m)
Type 1	0.83	0.09	15.2	4.9	32.3	18.0
Type 2	1.06	0.08	130.0	81.5	68.0	28.4
Type 3	0.96	0.17	220.6	252.5	73.5	43.1
Type 4	0.90	0.14	13.5	5.5	25.7	9.8
Type 5	0.89	0.10	6.3	2.5	11.4	3.1
Type 6	0.99	0.07	34.5	0.3	53.1	0.7

4.5.3 Peak tensile stress

The relationships between peak tensile stress, measured membrane thickness and type of interface are shown in Figure 4-14. It shows peak tensile stress for all interfaces exceeded 0.75MPa, greater than the maximum hydrostatic water

pressure a 50m deep SCL tunnel could experience. Therefore, no interface debonding should occur due to water pressure alone.

The mean peak tensile stress for Type 2 interfaces was higher than for Type 1 and 3 interfaces, whilst the standard deviation of peak tensile stress for Type 2 interfaces was smaller than for Type 1 and 3 interfaces. Figure 4-14 also shows the membrane thickness and interface roughness do not change the interface peak tensile stress significantly.

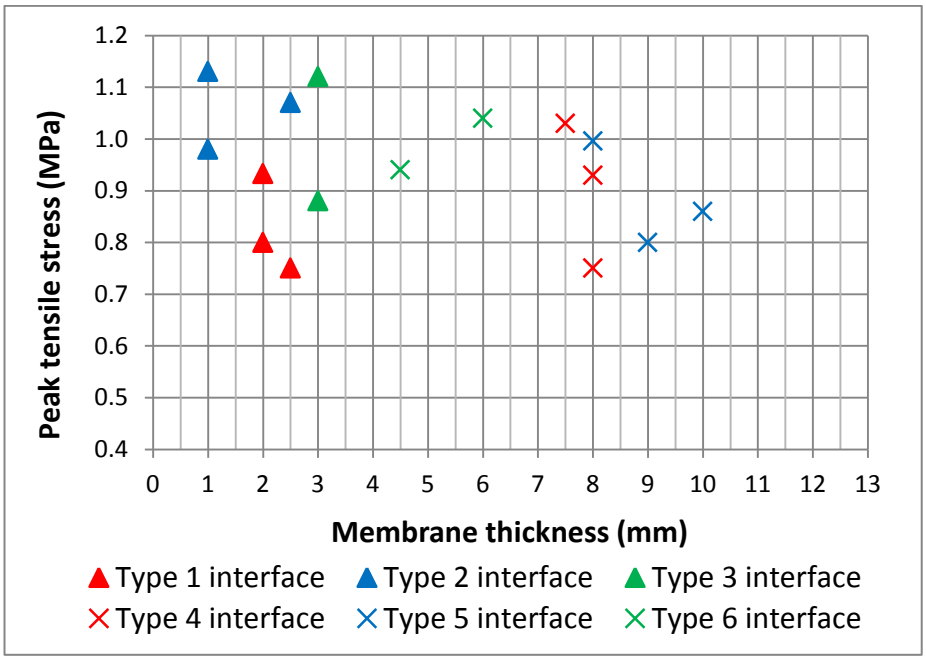

Figure 4-14 Relationship between peak tensile stress, membrane thickness and type of interface

4.5.4 First and cyclic loading tensile stiffnesses

The relationship between first loading tensile stiffness, membrane thickness and type of interface is shown in Figure 4-15. It shows that with the exception of three outliers (interfaces 2-6, 2-7 and 3-5), first loading stiffness for all interfaces was below 60GPa/m, mostly between 10-40GPa/m and reducing with increased membrane thickness. The very high first loading stiffness for the three outliers was probably caused by imperfect vertical alignment of test samples as well as the very thin membrane thickness (between 1-3mm).

The relationship between cyclic loading tensile stiffness, membrane thickness and type of interface is shown in Figure 4-16. It shows that except for two outliers (interfaces 2-6 and 3-5), the cyclic loading stiffness for all interfaces was below

60GPa/m, very similar to the first loading stiffness, and again reducing with increased membrane thickness.

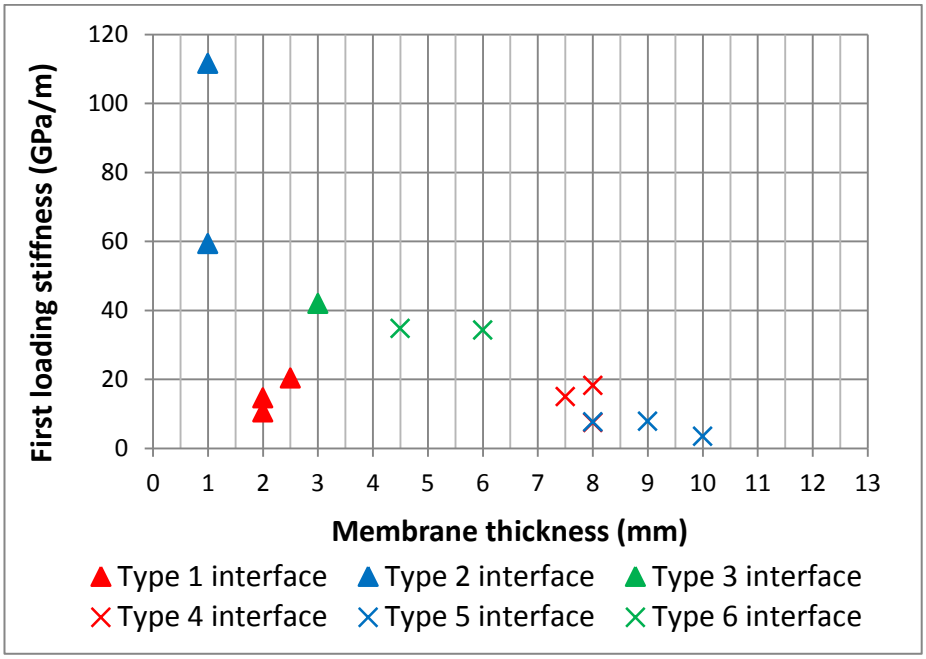

Figure 4-15 Relationship between first loading tensile stiffness, membrane thickness and type of interface (Interfaces 2-7 and 3-5 not shown)

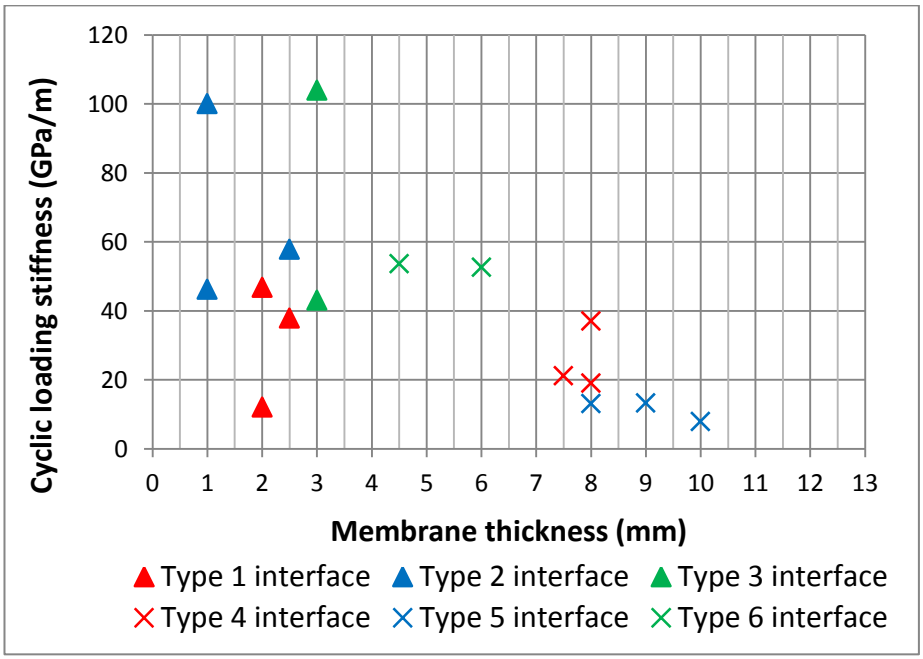

Figure 4-16 Relationship between cyclic loading tensile stiffness, membrane thickness and type of interface

4.5.5 Tensile strain at peak tensile stress

The tensile strain of measured membrane thickness at peak tensile stress was generally between 5% and 10% with three outliers between 15% and 30%. No clear trend was found between the strain, membrane thickness and type of interface, as shown in Figure 4-17.

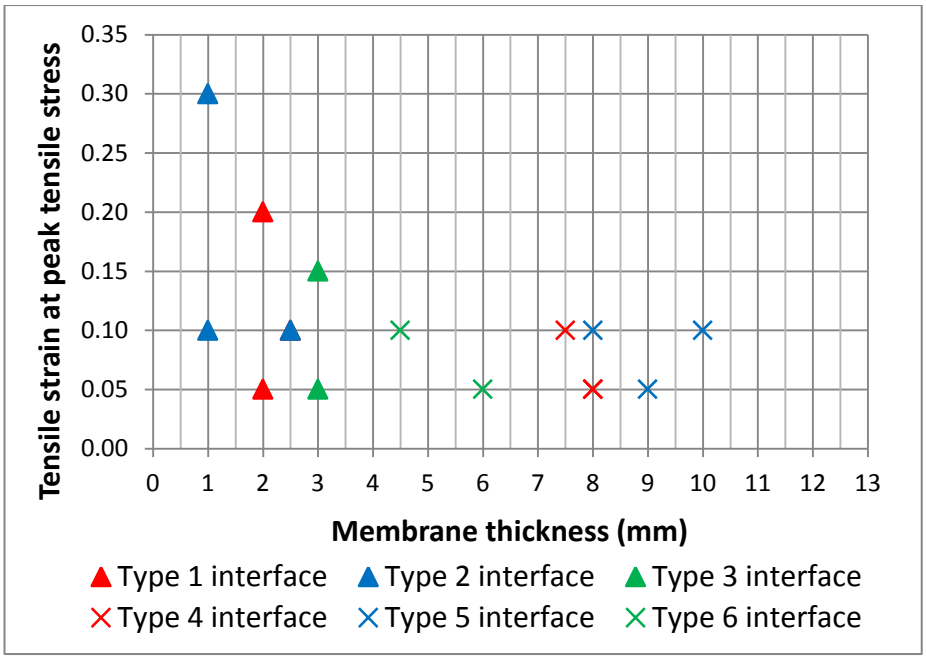

Figure 4-17 Relationship between compressive strain at peak compressive stress and membrane thickness and type of interface

4.5.6 Observed failure modes in tension tests

The typical failure mode for interfaces under direct tension was debonding between the sprayed concrete and membrane. Neither tensile failure of the sprayed concrete nor the membrane was observed as their tensile strengths are both above the interface tensile strength of between 0.75-1.15MPa. A very thin layer of mixed membrane and cement material was normally observed on the sprayed concrete interface after the debonding with either primary lining (red membrane) or secondary lining (grey membrane) as shown in Figure 4-18.

For Type 2 and Type 5 regulated interface finishes, debonding of the membrane occurred at the interface with the secondary sprayed concrete layer, suggesting the chemical bond strength between the membrane and regulating layer is higher than the mechanical bond between the membrane and secondary lining. For other types of interface, there was equal probability the membrane debonding from

either the primary or secondary linings, suggesting similar chemical and mechanical bond strengths between the membrane and the primary and secondary linings respectively. Typical debonded surfaces of primary and secondary layers are shown in Figure 4-19.

Figure 4-18 Organic/inorganic bond of membrane left on the interface

Figure 4-19 Different types of samples with debonded interfaces

4.6 Short-term shear tests under 500kPa normal pressure

4.6.1 Testing overview

Direct shear tests with 500kPa normal pressure were carried out to investigate the impact of interface roughness and membrane thickness on interface response. In line with the testing plan, 18 tests were due to be carried out on 3 samples from each type for Types 1 to 6. However, the cyclic test was not carried out for interface 2-21 as it was the first trial sample.

4.6.2 Shear interface stress-deformation relationships

Thin and thick membrane interface behaviours under direct shear with 500kPa normal pressure are shown in Figure 4-20 and Figure 4-21 respectively. For thin membrane interfaces, peak shear stress occurred at a displacement of 8-10 mm and all interfaces failed in a ductile mode. For thick membrane interfaces, the peak shear strength occurred at 10-15 mm displacement and also exhibited ductile failure, with a stress plateau sustained for an additional 5-7mm of shear displacement.

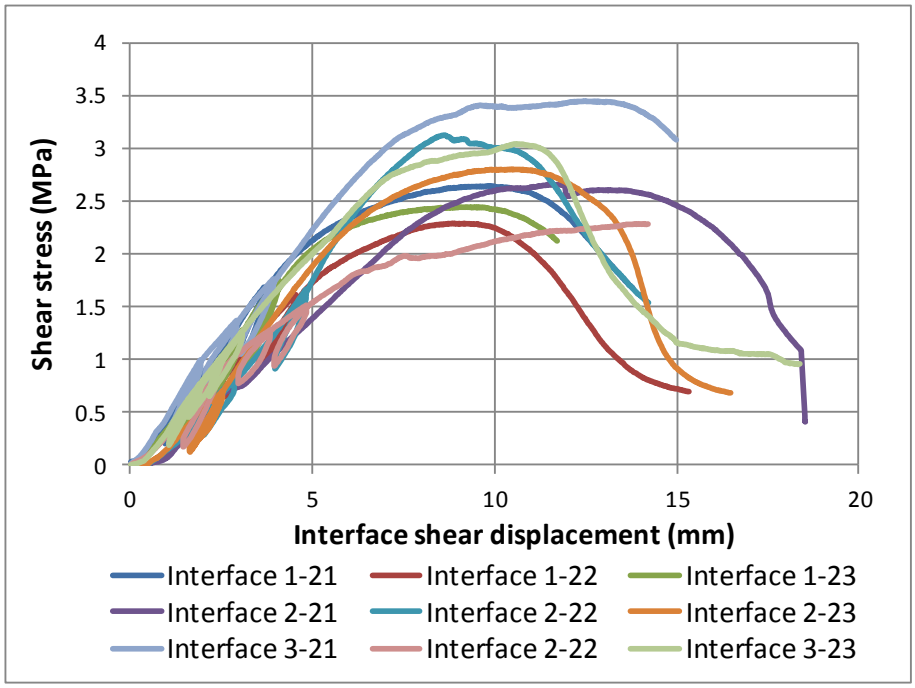

Figure 4-20 Thin membrane interface behaviour under direct shear test with 500kPa normal pressure

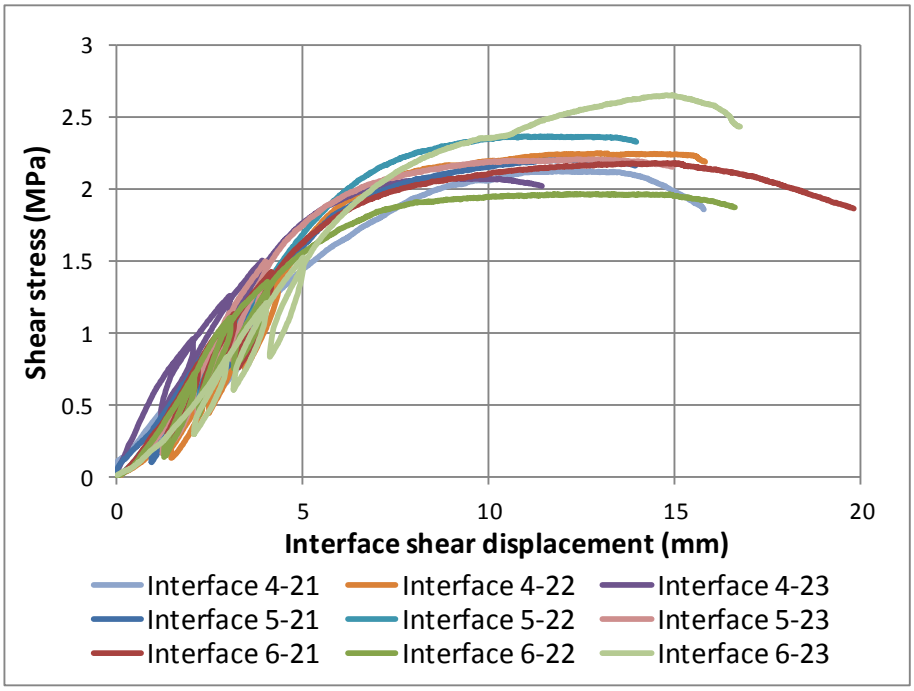

Figure 4-21 Thick membrane interface behaviour under direct shear test with 500kPa normal pressure

4.6.3 Peak shear stress

Numerical test results and statistical analysis are presented in Table 4-5 and Table 4-6 respectively. Table 4-6 suggests that, for thin membrane samples, peak stress increases with interface roughness. Whilst the magnitude of the peak stress is generally lower for thicker membrane samples, the same interface roughness effect is observed.

Table 4-5 Direct shear test results under 500kPa normal pressure

Interface number	Membrane thickness (mm)	Peak shear stress (MPa)	Shear displacement at peak stress (mm)	First loading stiffness (GPa/m)	Cyclic loading stiffness (GPa/m)
1-21	3.0	2.64	9.8	0.58	4.07
1-22	4.0	2.29	8.8	0.50	2.05
1-23	3.0	2.44	9.5	0.82	4.95
2-21	4.0	2.35	10.0	0.74	N/A
2-22	4.0	3.12	8.6	0.69	3.70
2-23	4.0	2.80	10.3	0.51	5.51
3-21	3.0	3.41	9.6	1.01	7.70
3-22	4.0	2.28	14.2	0.93	2.96

3-23	3.0	3.04	10.6	1.05	5.48
4-21	6.0	2.12	12.5	0.73	1.97
4-22	5.0	2.24	14.1	0.48	2.78
4-23	5.0	2.07	10.2	0.98	1.85
5-21	6.0	2.20	12.7	0.61	1.28
5-22	8.0	2.36	13.2	0.38	1.82
5-23	8.0	2.20	13.0	0.52	1.74
6-21	8.0	2.18	15.0	0.59	1.41
6-22	8.0	1.94	9.4	0.62	1.56
6-23	9.0	2.64	14.4	0.58	2.96

Table 4-6 Statistical analysis of direct shear test results under 500kPa normal pressure

Interface Type	Peak shear stress		First loading stiffness		Cyclic loading stiffness	
	Mean (MPa)	Standard deviation (MPa)	Mean (GPa/m)	Standard deviation (GPa/m)	Mean (GPa/m)	Standard deviation (GPa/m)
Type 1	2.46	0.18	0.64	0.17	3.69	1.49
Type 2	2.76	0.39	0.65	0.12	4.61[a]	1.28
Type 3	2.91	0.57	1.00	0.06	5.38	2.37
Type 4	2.14	0.09	0.73	0.25	2.20	0.50
Type 5	2.26	0.09	0.50	0.12	1.61	0.29
Type 6	2.25	0.36	0.59	0.02	1.98	0.85

[a] Mean cyclic loading stiffness based on two test results

4.6.4 First and cyclic loading shear stiffnesses

The relationships between first and cyclic loading shear stiffness, membrane thickness and type of interface under 500kPa normal pressure are shown in Figure 4-22 and Figure 4-23 respectively. For thin membrane interfaces, mean first loading stiffnesses for Types 1 and 2 were smaller than for Type 3. For thick membrane interfaces, mean first loading stiffness for Type 4 was bigger than for Types 5 and 6, possibly due to the thicker measured membrane thickness for the latter two interface types. The same trend was also observed for cyclic loading stiffness values for thick membrane samples.

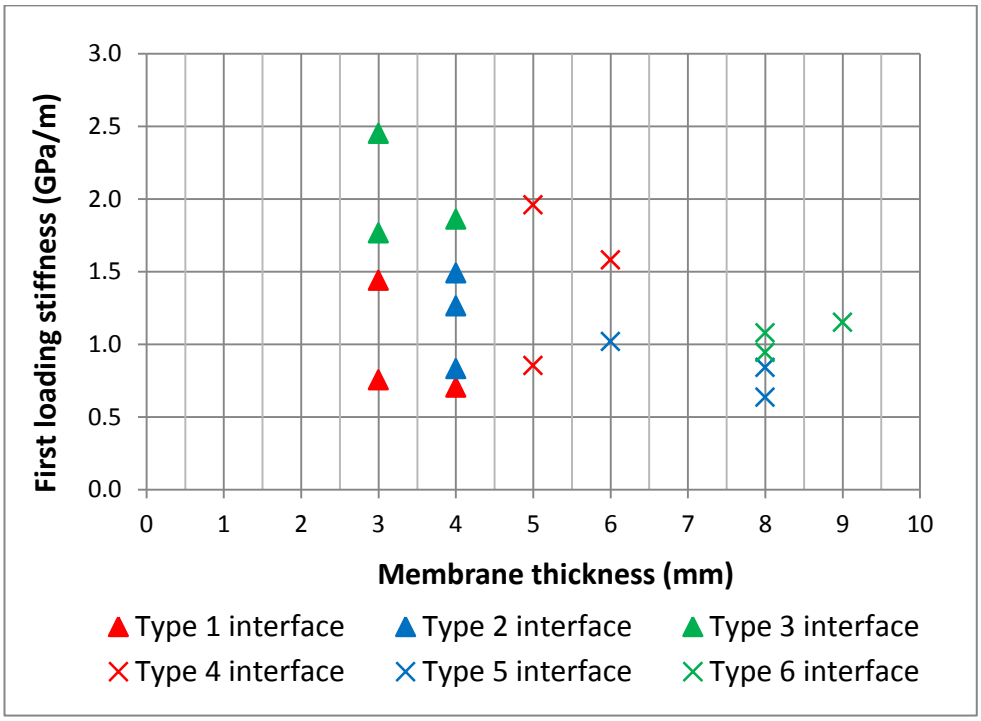

Figure 4-22 Relationship between first loading shear stiffness, membrane thickness and type of interface under 500kPa normal pressure

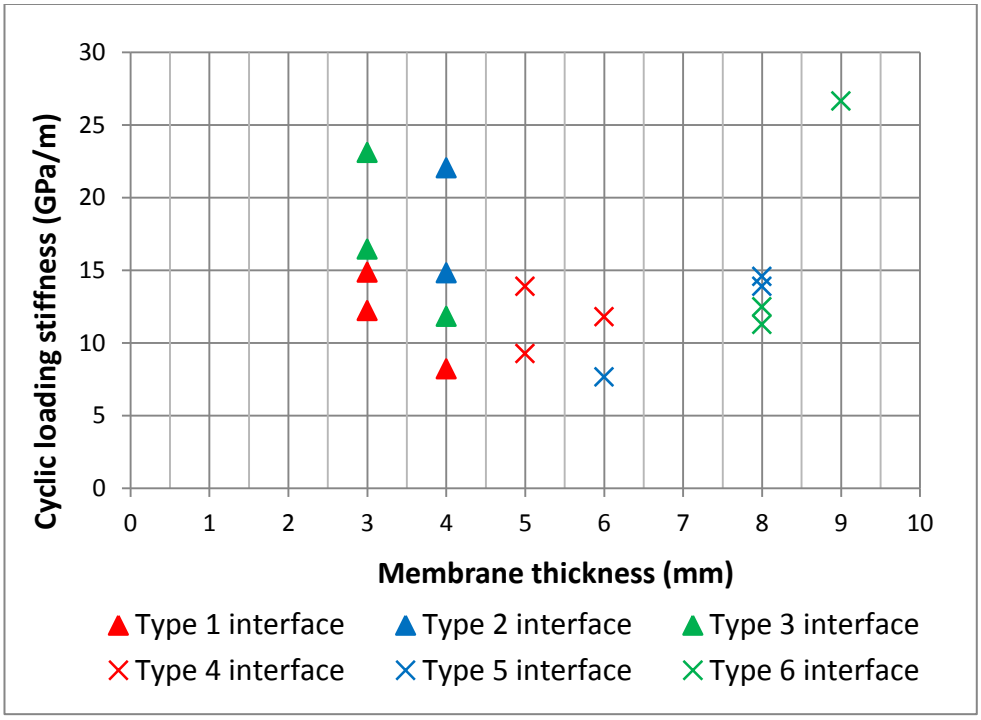

Figure 4-23 Relationship between cyclic loading shear stiffness, membrane thickness and type of interface under 500kPa normal pressure

4.6.5 Shear displacement at peak shear stress

Figure 4-24 shows that the shear displacement at peak shear stress generally increases with the membrane thickness, demonstrating the thicker the membrane, the greater deformation the interface is able to sustain.

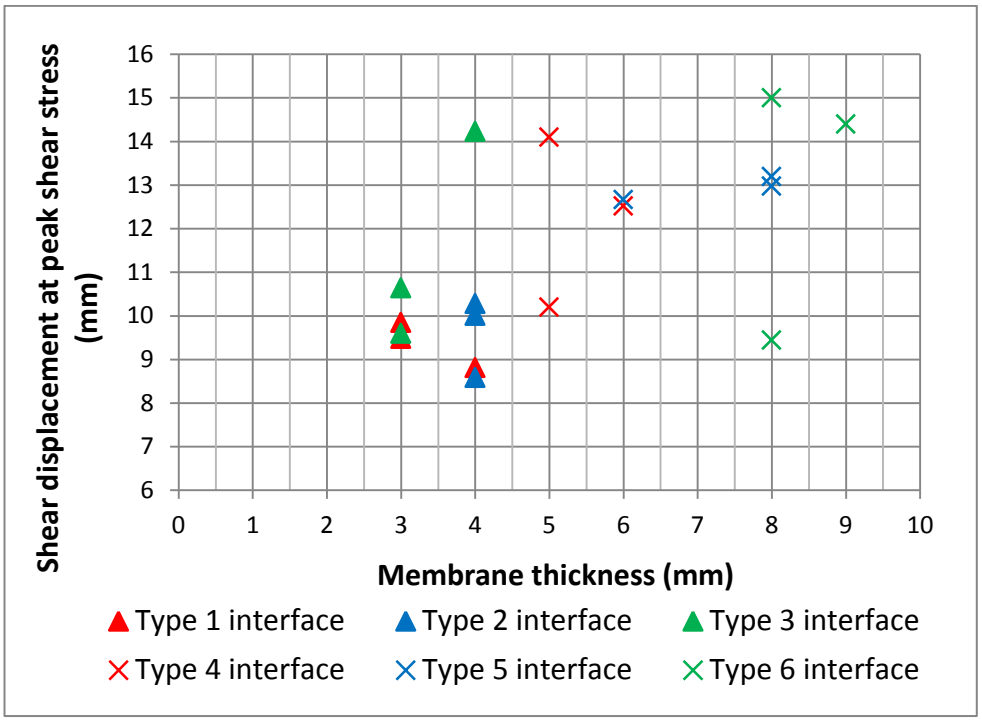

Figure 4-24 Relationship between shear strain at peak shear stress and membrane thickness and type of interface under 500kPa normal pressure

4.6.6 Observed failure modes in shear tests

A number of varying failure modes were observed in the testing samples. For those with smooth or regulated interface finishes and a thin membrane application, the membrane slid along one interface (with no preference as to which one). For samples with smooth or regulated interface finishes and a thick membrane application, the membrane slid along one interface in some cases, as shown in Figure 4-25 (a), or sheared with cracks in the membrane in others, as shown in Figure 4-25 (b). Samples with a rough as-sprayed interface typically demonstrated a mixed failure mode, sliding over the relatively smooth part of the interfaces and shearing within the membrane at the rougher parts, as shown in Figure 4-25 (c) & (d).

For samples with smooth or regulated interface finishes and a thin membrane, the interface always failed at the interface itself (*i.e.* the membrane slid along one interface). For samples with a rough as-sprayed interface, a mixed failure mode was observed. In the relatively smooth parts of the interfaces, the "sliding over" failure mode was identified, whilst in the "rougher" sections shearing with the membrane itself occurred. This suggests that the dominating failure mode is that of the interface and not that of the material. The shearing within the membrane can be considered a "by-product" of the interface failure. Based on this, it is possible that, for samples such as Figure 4-25b, the membrane cohesive failure was a "by-product" of an interface failure which occurred within the membrane and cannot be seen from the outside of the test sample.

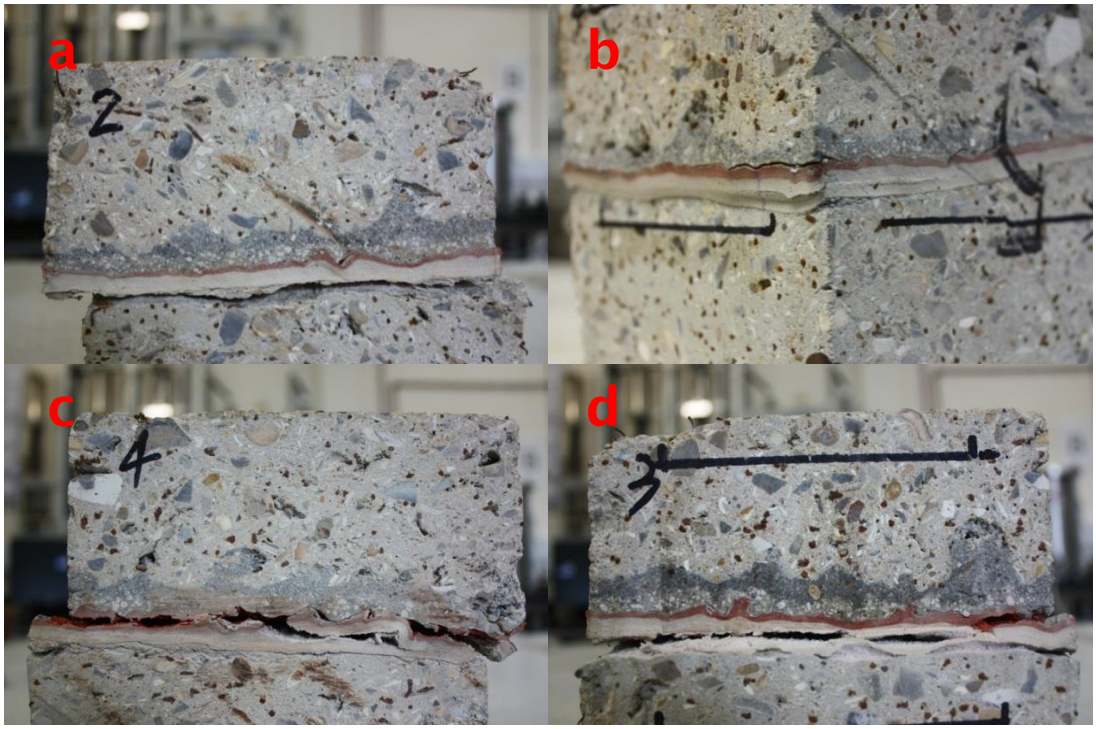

Figure 4-25 Typical failure modes under direct shear test (a) interface failure (b) membrane cohesive failure (c) & (d) mixed failure

4.7 Comparison of the Type 2 interface test results under different normal pressures

Direct shear tests with 250kPa and 750kPa normal pressure were also carried out and the results are presented in Appendix C. This section compares the behaviour of the Type 2 regulated interface under three different normal pressures. Test results and their statistical analysis are presented in Table 4-7

and Table 4-8 respectively. There is no certain trend of the shear displacement at peak shear stress for Type 2 interfaces.

Table 4-7 Direct shear test results for Type 2 interfaces under different normal pressures

Interface number	Normal pressure (kPa)	Membrane thickness (mm)	Peak shear stress (MPa)	Shear displacement at peak stress (mm)	First loading stiffness (GPa/m)	Cyclic loading stiffness (GPa/m)
2-21	500	4.0	2.35	10.0	0.74	N/A
2-22	500	4.0	3.12	8.6	0.69	3.70
2-23	500	4.0	2.80	10.3	0.51	5.51
2-24	250	3.0	2.56	13.1	0.65	12.29
2-25	250	3.0	2.57	15.7	0.47	14.68
2-26	250	3.0	2.21	16.7	0.56	6.55
2-27	750	3.0	3.35	13.2	0.48	3.93
2-28	750	3.0	2.93	11.6	0.59	5.42
2-29	750	3.0	2.73	13.0	0.61	3.80

Table 4-8 Statistical analysis of direct shear test results for Type 2 interfaces under different normal pressures

Normal pressure (kPa)	Peak shear stress		First loading stiffness		Cyclic loading stiffness	
	Mean (MPa)	Standard deviation (MPa)	Mean (GPa/m)	Standard deviation (GPa/m)	Mean (GPa/m)	Standard deviation (GPa/m)
250	2.45	0.21	0.56	0.09	11.17	4.18
500	2.76	0.39	0.65	0.12	4.61*	1.28
750	3.00	0.32	0.56	0.07	4.38	0.90

* Cyclic loading stiffness based on two test results

4.7.1 Peak shear stress

Figure 4-26 shows the peak shear stresses for Type 2 interfaces increase with different normal pressures, in a manner typical of Coulomb's friction hypothesis. There are two key parameters in this hypothesis. The first parameter, cohesion, can be explained by the chemical bond between the sprayed membrane and the two layers of lining. The second parameter, friction angle, can be explained as the ratio of mechanical friction of the two undulated concrete lining surfaces and the normal pressure applying to the samples. The thickness of the membrane is of a similar length scale to the undulations in the interface profiles in many cases,

either locally in the case of the rough interface, or over longer length scales for the smoother interface. As the two pieces of concrete linings within one composite sample try to shear past each other under normal pressure, there is a certain degree of interlock between the two undulated concrete lining surfaces through the membrane. This mechanical interlock can be modelled as friction. Therefore, this behaviour can be numerically described by an effective cohesion and friction angle model, which were calculated as 2.17MPa and 48^0 respectively.

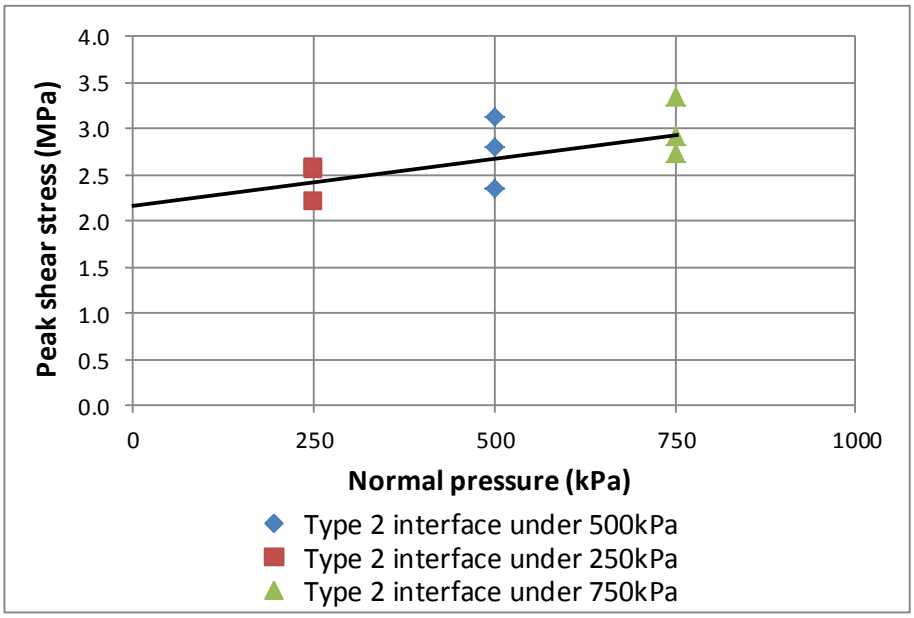

Figure 4-26 Peak shear stresses for Type 2 interfaces under different normal pressures

4.7.2 First and cyclic loading shear stiffnesses

Figure 4-27 shows the normal pressure has little impact on the first loading stiffness for Type 2 interface, with an average value approximately at 0.6GPa/m.

Figure 4-28 shows that the cyclic loading stiffness for samples subjected to a 250kPa normal pressure is greater than those under 500kPa and 750kPa loadings. This is a counterintuitive result.

As stated earlier, external instruments were used to measure displacement. Post-processing includes adjustment for the effect of sample rotation, which may have been excessive for samples under a relatively low normal pressure of 250kPa, leading to exaggerated values. Therefore, it is considered that cyclic loading stiffness test results for Type 2 interfaces under 250kPa are outliers and should not be used for further comparison. Based on other test results, it is concluded

that the normal pressure has little impact on the cyclic loading stiffness for Type 2 interface, with an average value approximately at 4.8GPa/m.

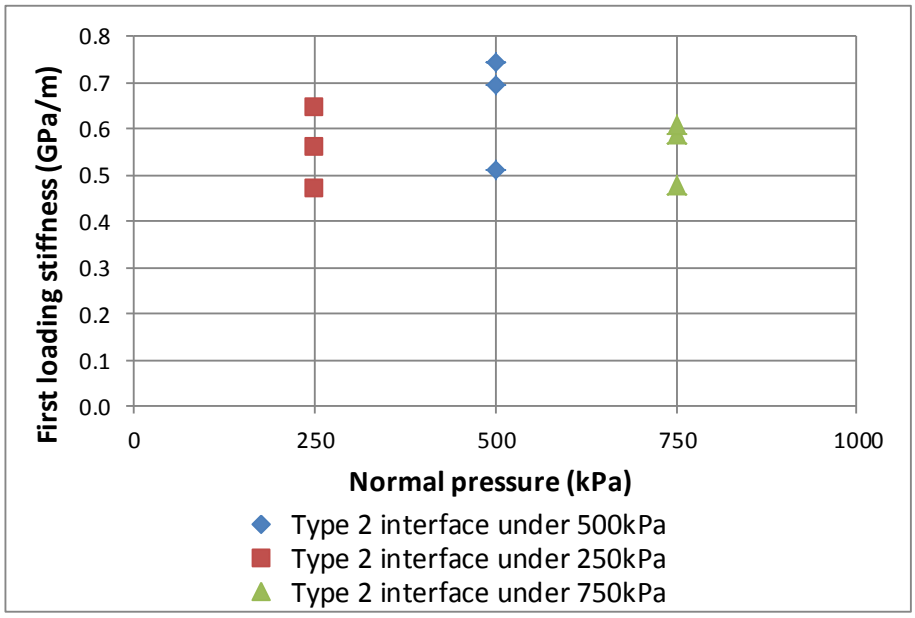

Figure 4-27 First loading stiffness for Type 2 interface under different normal pressures

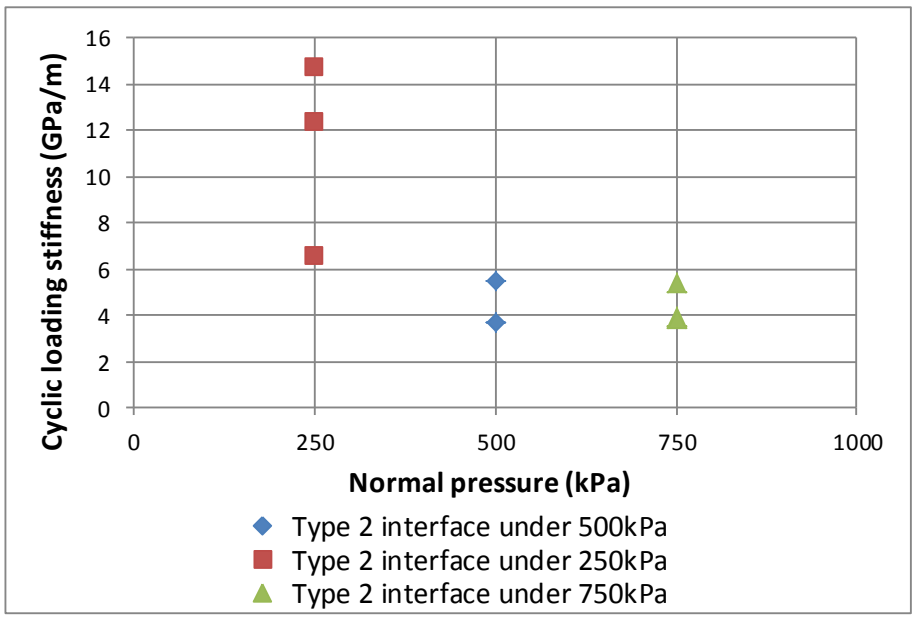

Figure 4-28 Cyclic loading stiffness for Type 2 interface under different normal pressures

4.8 Long-term test results

The composite action between the primary and secondary linings of a CSL tunnel is a long-term phenomenon. Therefore, in order to design such structures, it is essential to obtain the long-term interface stiffness. This section presents the relationship between relaxation percentage and time for each type of test.

It firstly presents the correction for temperature effects with a pure sprayed concrete sample. This is followed by the description of a series of long-term compression, tension and shear relaxation test results for composite samples.

4.8.1 Correction for temperature effects

In a trial long-term compressive test on a pure sprayed concrete cylinder sample (*i.e.* without membrane), it was observed that the test load fluctuation over time correlated with the temperature recorded adjacent to the machine, as shown in Figure 4-29. A temperature reduction of 1°C consistently corresponded to a load reduction of 1.5MPa. This relationship has been used to adjust the raw long-term compression and tension relaxation test data for composite specimens in the following sections.

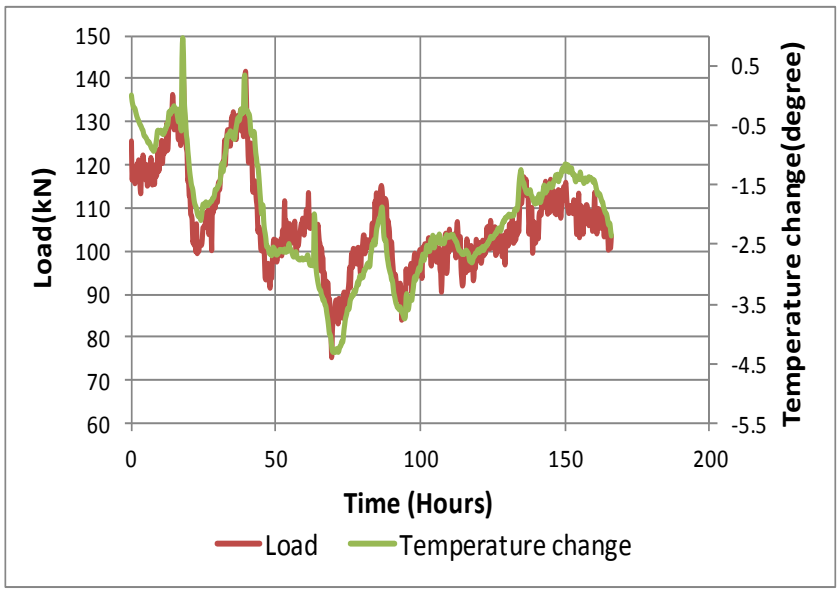

Figure 4-29 Load relaxation-time relationship for pure sprayed concrete sample in the long-term compression test

4.8.2 Long-term compression relaxation test results

Long-term uniaxial compression tests were carried out for just one Type 1 sample (Interface 1-1) at three stress levels (as described in Section 3.1) as relaxation was not expected to be influenced by interface roughness or membrane thickness, but rather only by the molecular structure and physical properties of the membrane polymer (Ashby and Jones 2005). As discussed in Section 4.8.1, corrections were made for temperature-related load fluctuations. The adjusted data showed that the load had relaxed to around 70-80% of its initial value after one week, as shown in Figure 4-30. A logarithmic trend line was obtained, from which a stress relaxation ratio of approximately 0.49 is predicted at 120 years, which is the design life for most underground tunnels in London.

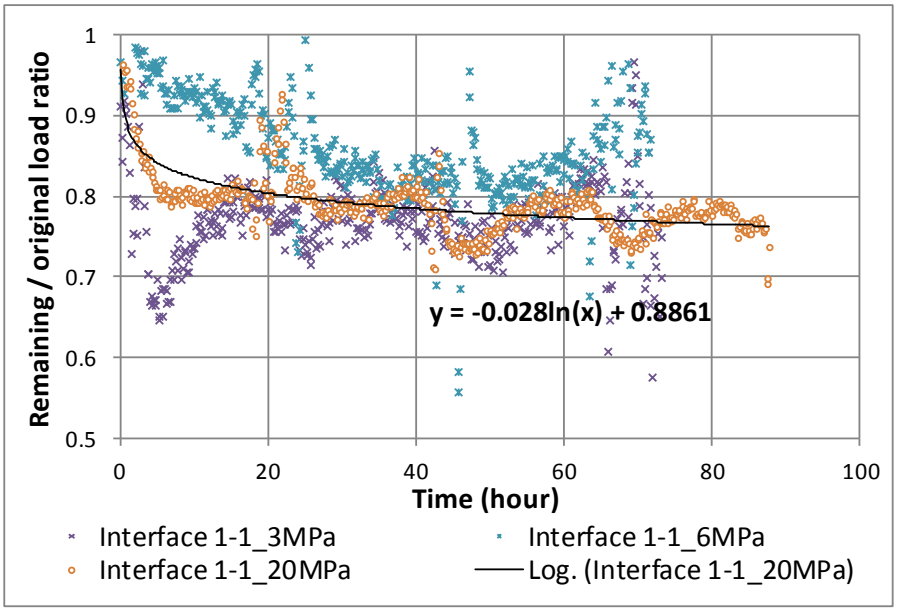

Figure 4-30 Adjusted load relaxation-time relationship for tested interface in the long-term compression relaxation test

4.8.3 Long-term tension relaxation test results

A single Type 2 sample (Interface 2-8) was tested, and the results treated as representative of other interface types, as shown in Figure 4-31. The relationship between test load fluctuation and lab temperature was found to be the same as that for the compression test. By extrapolation of the logarithmic trend line equation, the stress relaxation ratio was calculated as 0.46 at 120 years. Due to limited test number, the variability of this test with respect to this particular

sample is difficult to evaluate. This issue should be addressed by carrying out more tests in future research or construction projects.

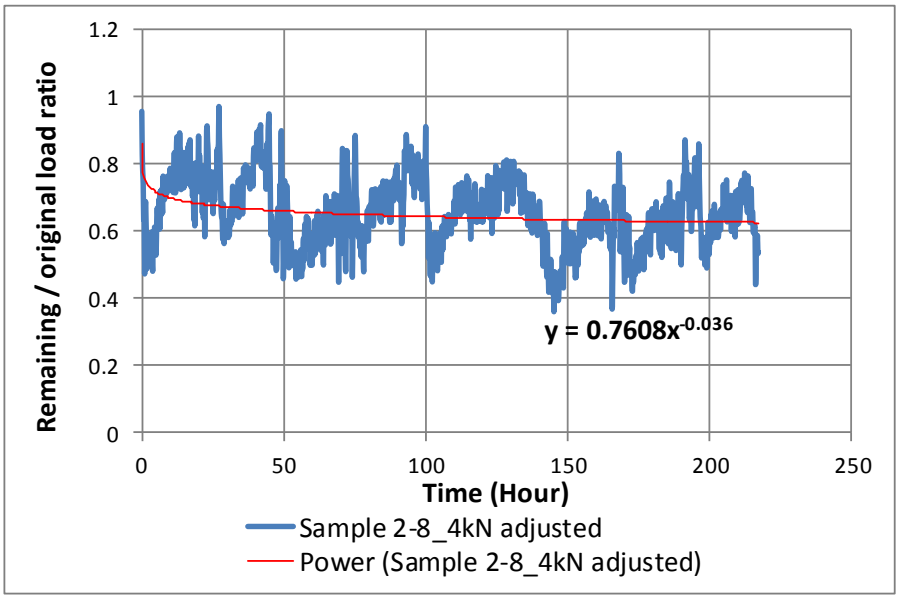

Figure 4-31 Adjusted load relaxation-time relationship for tested interface in the long-term tension relaxation test

4.8.4 Long-term direct shear test results

Long-term direct shear tests were carried out on two Type 2 samples, under normal pressures of 250 and 500kPa respectively and a shear stress of 1MPa. It was observed that the shear stress relaxed from 1MPa to 0.82MPa over 5 days, at which stage there was a sudden drop of stress to about 0.2MPa. The shear stress subsequently continued to relax, but at a much lower rate, presumably because the normal stress had dropped. The stress drop was found to be an artefact of the shear box test machine, which automatically cut its normal stress after five days as a safety feature. By combining the relaxation curves before and after the normal stress drop, two completed long-term stress curves were obtained, one for each normal pressure. A typical long-term shear relaxation test diagram is shown in Figure 4-32.

By extrapolation of the trend to 120 years, a stress relaxation ratio of around 0.59 is found, similar to the compression and tension long-term ratios of 0.49 and 0.46.

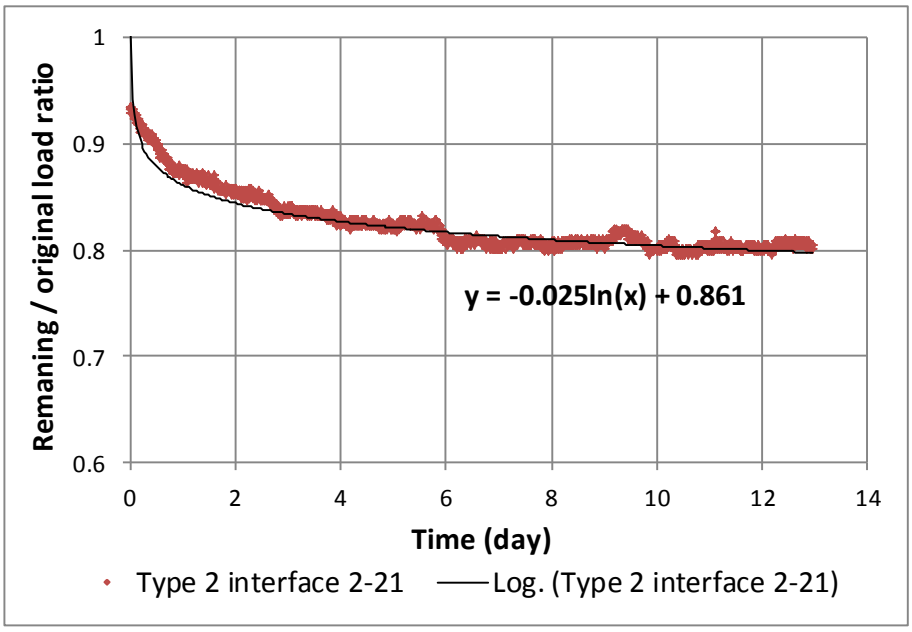

Figure 4-32 Typical load relaxation-time relationship for tested interface in the long-term shear relaxation test

4.9 Summary

This chapter describes the laboratory element tests on the properties of the interface between the sprayed concrete primary and secondary linings when a spray applied waterproofing layer is used. These properties are needed for efficient design of CSL tunnels. There is particular interest in the impact of variance in interface roughness and membrane thickness on stiffness, strength and ductility. The following conclusions are reached based on the results presented:

1. Interface compressive failure will not occur for shallow SCL tunnels because the lowest tested peak compressive stress(*i.e.* 12MPa) is much higher than the stresses on the lining such a tunnel could experience.

2. Similarly, short-term peak interface tensile stress (>0.8MPa) is sufficient to resist the water pressure from debonding the sprayed concrete-membrane interface. Therefore, both short and long-term water pressure may be assumed in design to apply to the extrados of the primary lining.

3. Type 1 & 2 interfaces (thin membrane with either smooth or regulated interface) have higher first loading and cyclic loading compressive and tensile stiffnesses.

4. Peak tensile stress is affected neither by the interface roughness nor the membrane thickness. However, regulated interface is better for producing consistent peak tensile stress. The first and cyclic loading interface tensile stiffnesses are very close to each other, affected mainly by the membrane thickness but not the interface roughness.

5. Peak shear stress (>2MPa) increases with increased interface roughness, reduced membrane thickness and increased normal pressure. Cyclic loading shear stiffness increases with interface roughness and membrane thickness. However, Type 1 & 2 interfaces (thin membrane with either smooth or regulated interface) have more consistent behaviour, improving the quality control of the construction.

6. Long-term stiffness performance in compression, tension and shear is reasonable (approximately 49%, 46% and 59% respectively of the short-term value), enabling reliable interface load transfer during the life of the tunnel.

Having obtained the interface parameters from laboratory testing, the next stage of the research is the calibration of composite beam numerical models. This will allow verification of both the interface parameters and the proposed numerical approach for simulating composite action.

Chapter 5: Calibration of Composite Beam Numerical Models

In order to correctly predict the behaviour of CSL tunnels, it is necessary to establish accurate interface parameters and develop a validated numerical modelling approach for simulating composite action. In Chapter 4, element test interface parameter results were presented and discussed. This chapter focuses on the development of a numerical modelling approach and associated calibration by comparing beam tests against the modelling output.

This chapter comprises three parts. Section 5.1 introduces the theoretical background, calibration plan, laboratory test configuration and corresponding numerical models. The second part, including Sections 5.2 and 0, outlines two rounds of calibration that verified some of the key interface parameters and numerical modelling approach. This is an important step for the next chapter on the numerical modelling of a typical CSL tunnel under practical loadings. The third part, including sections 5.4 to 5.6, presents several numerical sensitivity and lining optimisation studies on composite beams under a four-point bending test configuration.

5.1 Background and calibration plan

5.1.1 Four-point bending tests

The degree of composite action of CSL is a critical parameter for designing such tunnels. Although practical tunnel linings experience both bending moment and axial force, most tunnelling specifications recommended beam testing to evaluate the flexural performance of the lining. The four-point bending test is often used as a standard testing methodology (BSI, 2006), in which a region of constant bending moment is generated between two loading points, enabling assessment of flexural strength and stiffness.

The test configuration and dimensions of the sample beams used in this research are shown in Figure 5-1. Equal loads were applied 250 mm from each end of the beam, giving a 400 mm constant bending zone. This represents a deviation from the BSI standard (BSI, 2006), which specifies a loading point separation of a third

of the total beam length (*i.e.* 300mm for this test configuration). The purposes of this alteration was to make such test samples behaved more like "shallow" beams to reduce the impact of shear and to generate a longer pure bending area for more accurate flexural behaviour.

Two types of sprayed concrete beam were tested. Pure sprayed concrete beams were initially used to validate the Young's modulus value obtained from the element tests. Composite beams were then subsequently tested.

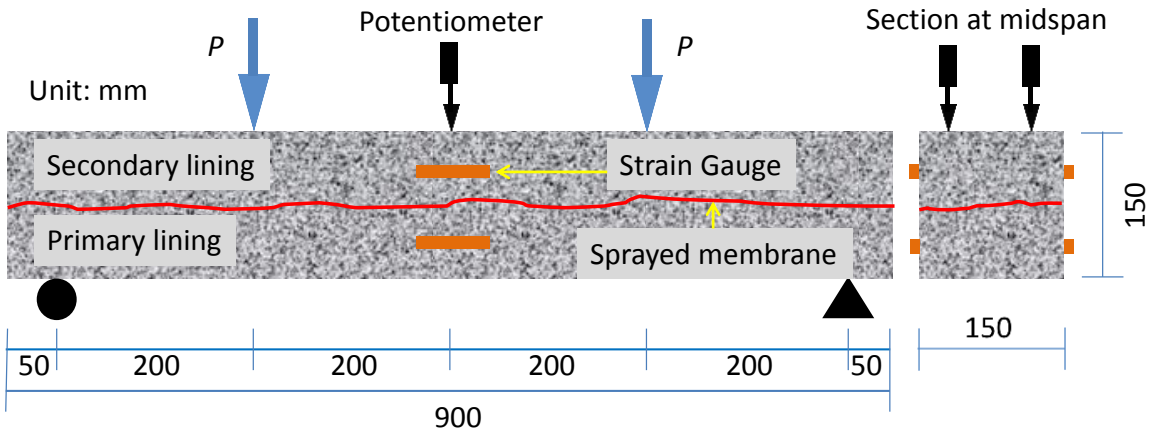

Figure 5-1 The four-point bending test configuration adopted during testing (All dimensions in mm)

5.1.2 Theories and assumptions for pure concrete beams

The test results for the pure concrete beams were used to back-calculate the Young's modulus of the concrete. Euler-Bernoulli beam theory was used to model the beams' deflection characteristics. The following assumptions are made:

- The beams are relatively "shallow", so that shear deformation is not significant compared to bending.
- Beams are supported on one pin support and one roller, so that arching and membrane action cannot occur.
- The concrete exhibits linear elastic material properties are assumed for the concrete.

These assumptions lead to the following relationship between beam displacement $w(x)$ as a function of position x along the beam, applied load $q(x)$, Young's modulus E and second moment of area I of the beam cross-section:

$$EI\frac{d^4\omega}{dx^4} = q(x)$$ Equation 5-1

A schematic figure of the four-point bending test is shown in Figure 5-2, and the maximum vertical displacement ω_{max} at midspan can be calculated by using Equation 5-2:

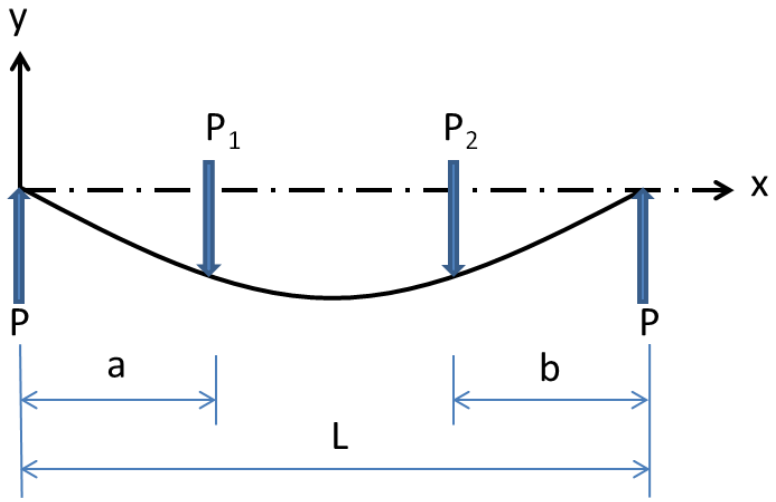

Figure 5-2 Schematic figure of the four-point bending test

$$\omega_{max} = \frac{Pb}{48EI}[3L^2 - 4b^2] + \frac{Pa}{48EI}[3L^2 - 4a^2]$$ Equation 5-2

By substituting the actual test beam dimensions, Equation 5-2 can be simplified to

$$\omega_{max} = 11PL^4/396EI$$ Equation 5-3

Where:

P: Vertical load at each position (*P*=5kN)

L: Beam length between two supports (*L*=800mm)

a: The distance between P_1 loading to its nearest support (*a*=200mm)

b: The distance between P_2 loading to its nearest support (*b*=200mm)

E: testing measured Young's modulus

I: Second moment of inertia (I =4.21E^{-5}m^4)

5.1.3 Theories and assumptions for composite beams

In composite beams the stress and strain distributions through the cross-section are likely to be different from those in a pure concrete beam, due to the existence of interfaces with the sandwiched spraying waterproofing membrane. This is illustrated in Figure 5-3 for four different levels of composite action. As the composite action reduces from full composite to non composite, the neutral axes for each component beam (top and bottom) move away from the membrane and towards half-depth of each component beam. Applying Euler-Bernoulli beam theory leads to the following conclusions for composite beams:

- The lower the degree of composite action, the lower the load (calculated from the stress blocks) for a given deformation (curvature) the beam can take, and hence the lower the flexural stiffness
- The lower the degree of composite action, the lower the ratio between the horizontal strain at half-depth of either component beam and the strain at the top/bottom surface. (The ratio is 0.5 at full composite action and zero for non composite)
- The lower the degree of composite action, the smaller the longitudinal displacement of beam ends at half-depth of each component beam for a given load

Based on the conclusions above, there are three ways to quantify the degree of composite action, designated by *Rc*, the composite action ratio:

- Method 1: Based on vertical displacements: $Rc = \frac{\delta_{non} - \delta_{comp}}{\delta_{non} - \delta_{full}}$ (δ_{comp}, δ_{non} & δ_{full} are vertical displacements of the composite, non composite and full composite beam respectively
- Method 2: Based on horizontal strains: $Rc = \frac{(\epsilon_{1/2} / \epsilon_{top\ (bottom)\ extreme\ fibre})}{0.5}$ ($\epsilon_{1/2}$ & $\epsilon_{top\ (bottom) extreme\ fibre}$ are longitudinal strains for composite beams at half-depth and top (bottom) of respective component beams)
- Method 3: Based on beam end relative displacement: $Rc = \frac{\delta_{1/2comp}}{\delta_{1/2full}}$ ($\delta_{1/2comp}$ & $\delta_{1/2full}$ are longitudinal beam end displacements for composite and full composite beams)

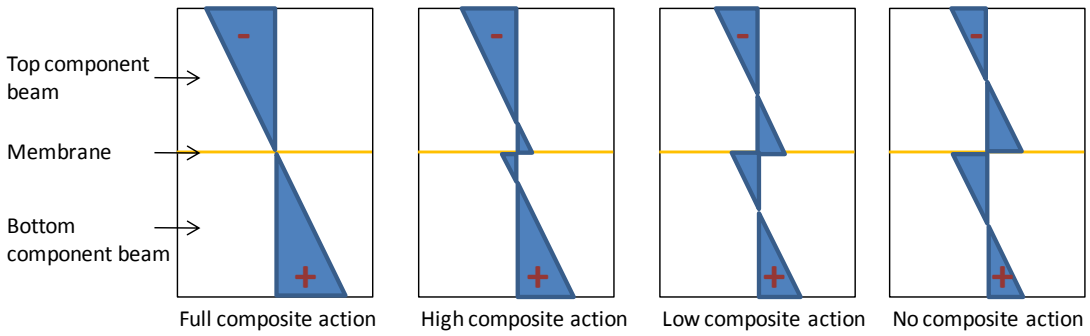

Figure 5-3 Stress-strain distributions through beams subjected to a sagging moment for different degrees of composite action

5.1.4 Calibration plan

Validation of the numerical models comprised of the following stages:

<u>The first round (Section 5.2):</u>

(1) Validate a model of a pure sprayed concrete beam against both laboratory test results and theoretical equations assuming linear elastic behaviour of concrete and taking account of the test setup. This enabled verification of the sprayed concrete material parameters.

(2) Validate models of composite beams, in which interface properties that depend on membrane thickness and interface roughness have been input from the element testing described in Chapter 4, against laboratory test results for the composite beams.

It was found that the composite beam numerical model results did not match the laboratory test results. Consequently, a second round calibration was carried out with a few modifications made to the testing configuration.

<u>The secondary round (Section 5.3):</u>

(3) Validate the laboratory test results of two pure sprayed concrete beams with closed-form equations to examine the consistency between the displacement and strain results. It was found the displacement and strain results did not comply with the beam theory, indicating that one of test results was wrong. Therefore, additional validation of the testing machine compliance was carried out.

(4) Validate the behaviour of a steel beam with a standard cross-section under

the same testing configuration. This verified the compliance of the testing machine, which could then be taken into account for all beam tests.

(5) Validate composite beam models by comparing against laboratory test results for the additional tested beams, which took into account the compliance of the testing machine. This verified the accuracy of the composite beam models as well as the interface stiffnesses used in the validation.

The laboratory test setup and corresponding numerical models used for the calibration are described in the following sections.

5.1.5 Laboratory test setup

The configuration of the laboratory four-point bending test is shown in Figure 5-4 (a). Machine loading was firstly applied to a yellow crossbeam and then equally transferred to two rods, each embedded in a loading pad thus ensuring uniform load distribution to the beam. A potentiometer was positioned at beam midspan to measure the vertical displacement at the top of the beam. Figure 5-4 (b) and (c) show the four strain gauges which were attached to the two sides of the beam, each positioned at half-depth of the top and bottom component beam (*e.g.* top ½ and bottom 1/2), measuring longitudinal strain during the test. Figure 5-4 (d) shows the two potentiometers which were positioned at the right end of the beam, measuring relative beam end displacement. Machine loading was controlled in stroke mode and was applied in increments of 0.1mm every 10s in increments until a crack occurred at the bottom of the beam. The loading was continued until the vertical displacement reached 8mm. No loading/unloading cycles were performed during the short-term four-point bending test.

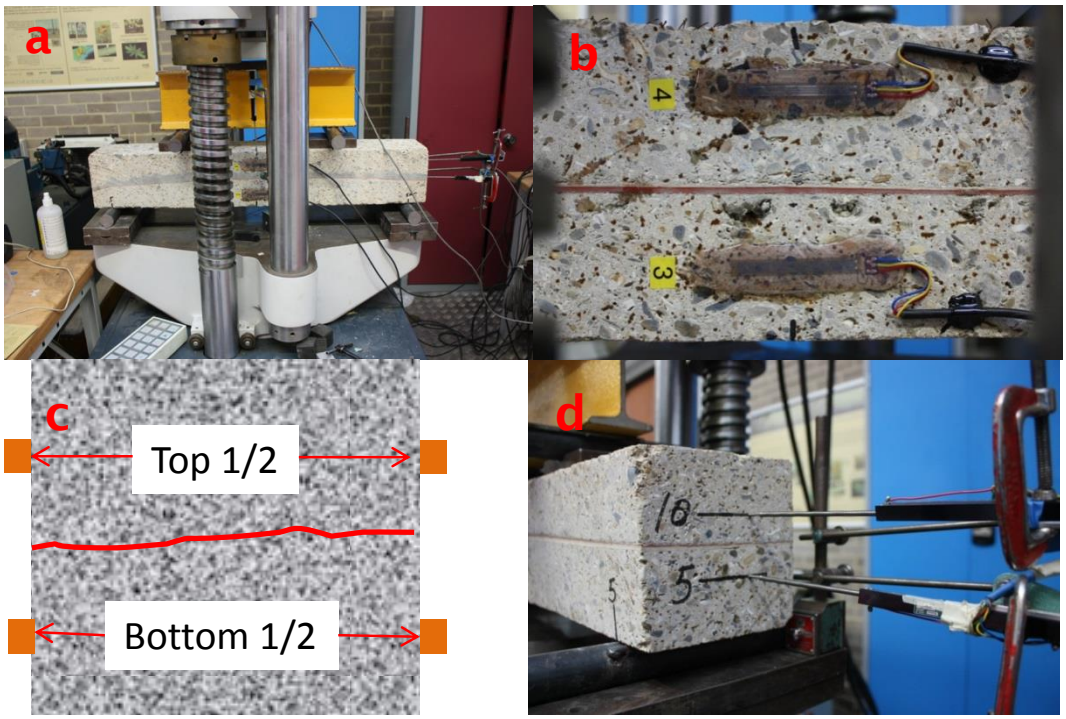

Figure 5-4 (a) Setting up for four-point bending test (b) (c) Strain gauges measuring horizontal strain for composite beams (d) Potentiometers measuring beam end displacement

5.1.6 Modelling strategy

As part of the calibration plan and for the numerical analysis in the following Chapter 6, it is important to define the appropriate modelling strategy for simulating composite action. There are two aspects that need to be considered: (1) how to simulate composite action, and (2) how to take into account the variance at the membrane interface.

The first question is how to simulate composite action. Traditionally, 2D beam or 3D shell elements are used to represent tunnel linings. Several advantages were identified for this approach, such as ease in creating model geometry and obtaining internal forces for design purposes (*e.g.* bending moment and axial force). However, this approach cannot simulate composite action because neither element type has physical thickness, which is a key requirement for simulating composite action. In contrast, elements with physical thickness, such as 2D zones or 3D solid elements, should be used to represent tunnel linings when simulating composite action.

The second question is how to take into account the variance at membrane interface. The variances of the interface focused on in this research are (1) membrane thickness, and (2) primary lining substrate roughness, the origin of which is the different workmanship to the primary lining surface on site. There are two methods to simulate the interface with the consideration of these variances.

Method one uses either 2D zones or 3D solid elements to represent sprayed membrane material only and that the properties of the interfaces between the sprayed membrane material and the concrete on either side would also need to be explicitly defined. In this method, in addition to the membrane material parameters E, G and υ, the primary lining substrate roughness and variance in membrane thickness need to be simulated explicitly. This procedure could be labour-intensive and time-consuming. Besides, there is a lack of statistical analysis on site data to determine what substrate roughness and membrane thickness should be used in numerical simulation. Moreover, the tensile and shear interface strengths for the two interfaces in this case (1.Between primary lining or regulating layer and membrane and 2.Between membrane and secondary lining) need to be specified individually, as they are the key parameters to determine when the composite lining will experience tensile or shear failure.

Method two uses interface elements to represent the whole primary lining substrate-membrane-secondary lining surface interface. Parameters that need to be defined for such an interface are the normal and shear strengths and stiffnesses. The effect of variation in membrane thickness and primary lining substrate surface roughness can be taken into account by specifying a suitable range for each parameter. The use of interface elements instead of 2D zones or 3D solid elements and the associated work in specifying membrane thickness and substrate roughness significantly saves the modelling time. Therefore, method two is recommended in practical CSL tunnel design and has been adopted for this research. The following section discusses the selection of numerical analysis package to deliver this method of analysis.

5.1.7 Selection of numerical analysis package

There were two phases of numerical analysis involved in this research. Firstly in this Chapter, a series of numerical analyses of CSL beam behaviour were

undertaken, from which the interface parameters and the modelling approach for simulating composite action were validated. The second part, described in Chapter 6, involved a series of numerical analyses of a typical CSL tunnel with surrounding ground, adopting the validated interface parameters and modelling approach. The CSL tunnel behaviour is examined and compared with full CSL (CSL with full composite action) and non CSL (DSL) tunnels with the same dimensions and in the same ground.

The need to assess both composite structure behaviour and soil-structure interactions has driven the numerical analysis package selection for this analysis.

FLAC (Fast Lagrangian Analysis Continua) is a two-dimensional explicit finite difference program based on the plane strain theory for engineering mechanics computation. It has the capability to simulate the nonlinear behaviour of London Clay as well as the performance of composite structures. It also has the 2D zone element and interface element that are needed in method two as discussed in section 5.1.6. Additionally, FLAC has been used for many years by both the industrial and academic partners in this research – Mott MacDonald and University of Southampton (Thomas 2003). Consequently the soil constitutive models used have been well optimised by extensive calibration against data from a wide range of underground projects, eliminating the need for further baselining.

5.1.8 Numerical model for four-point bending tests

2D beam models were created to simulate the behaviour of pure sprayed concrete and composite beams under the four-point bending test. As plane strain was assumed in the FLAC2D analysis, the FLAC model was essentially modelling a plate of 1m width. Therefore, the applied load was proportionately increased in the model.

The height and the length of the FLAC beam were 150mm and 900mm respectively. The beam was supported with pinned supports at both ends, with vertical movement restricted at the left support and both vertical and horizontal movement restricted assumed at the left support. The beam consisted of 288 zones, each of 25mm in length and 18.75mm in height. Beam elements, which were set with the same cross-section area and second moment of inertia as the beam but with a Young's modulus a thousand times smaller, were attached to the

zones at the half-depth of the beam, from which the bending moment and vertical displacement could be determined for validation.

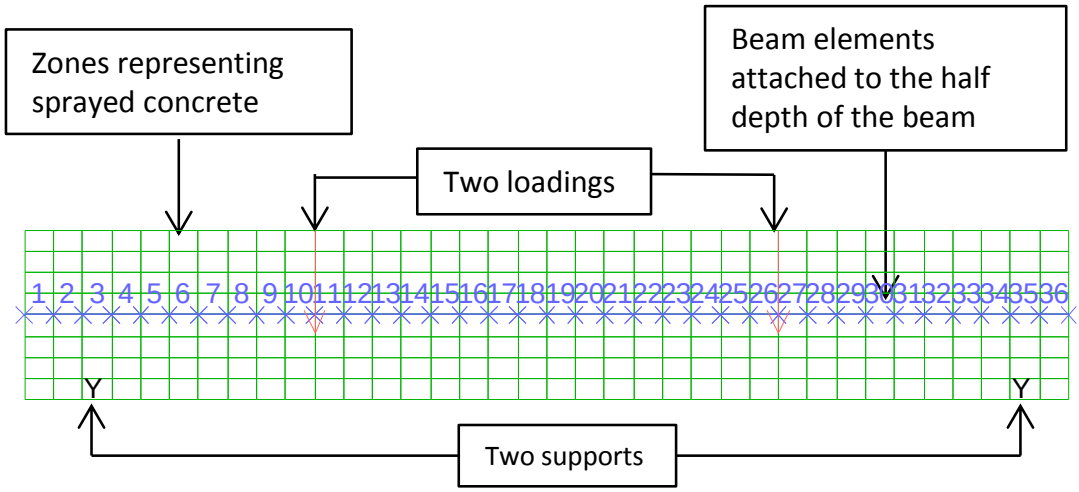

Figure 5-5 FLAC model for a pure sprayed concrete beam

5.2 First round calibration

5.2.1 Validation of pure shotcrete beam model

The first step of the calibration was to carry out a four-point laboratory bending test for a pure sprayed concrete beam, the result of which was then used to compare with the analytical value calculated using equation 5-3. This would enable the Young's modulus and isotropy of sprayed concrete to be confirmed for this study.

The load-displacement curve for the tested beam 7-11 is shown in Figure 5-6. It can be seen that a "bedding" effect inducing a "softer" curve occurs at lower load levels (<10KN). A "stiffer" curve is observed at higher load levels (>10KN) – this is considered to represent the true flexural stiffness with a displacement of 0.137mm occurring over a 10kN loading interval indicated in Figure 5-6 as a black line between 10 and 20kN. By substituting the test results into Equation 5-3, the concrete Young's modulus is determined at around 10GPa. By substituting this value into the FLAC beam model, a maximum displacement of 0.135mm was obtained, very close to the 0.137mm observed in the test. This confirms that the proposed FLAC beam model is able to accurately predict the current behaviour of a beam under a four-point bending test setup. However, it also raised a question about whether the sprayed concrete is anisotropic. This issue is resolved in the

second round of calibration. The sprayed concrete Young's modulus of 10GPa was used as a base value for the calibration of composite beams.

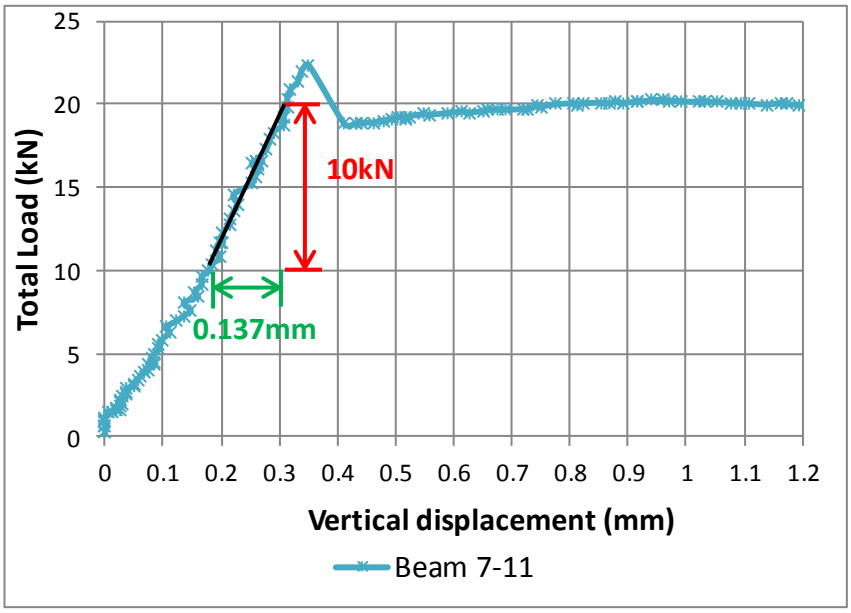

Figure 5-6 Load-displacement curve for pure shotcrete beam 7-11

5.2.2 Composite beam samples

Following the validation of the pure sprayed concrete beam, the second step was to validate the composite beam models. Prior to the numerical analysis, five composite beams were tested. Samples were designated according to the primary layer interface finish and membrane thickness as described in Section 3.2.5. Dimensions of the test beams, the measured membrane thickness and thicknesses of top and bottom component beams, are given in Table 5-1. The beam width and overall depth were both 150mm and the length was 900mm for all beams.

Table 5-1 Dimensions of tested composite beams

Beam number	Measured membrane thickness (mm)	Interface type	Thickness of top component beam (mm)	Thickness of bottom component beam (mm)
1-11	4	smoothed	77	69
2-11	3	regulated	70	77

3-11	3	As-sprayed	67	80
4-11	6	smoothed	69	75
5-11	10	regulated	70	70

5.2.3 Flexural response

The load-displacement diagram for the beams is shown in Figure 5-7 and the vertical downward displacement results under 10kN and 20kN total load are shown in Table 5-2. It was found that:

- The three beams 1-11, 2-11 and 3-11 were unusual because their initial flexural responses to loading were stiffer than the pure concrete beam. This is possibly due to a fault with the potentiometers.
- The composite beams with 6 mm (4-11) and 10 mm (5-11) membranes had noticeable proportional limits (15kN for beam 4-11 and 11kN for beam 5-11) followed by nonlinearity up to peak load.

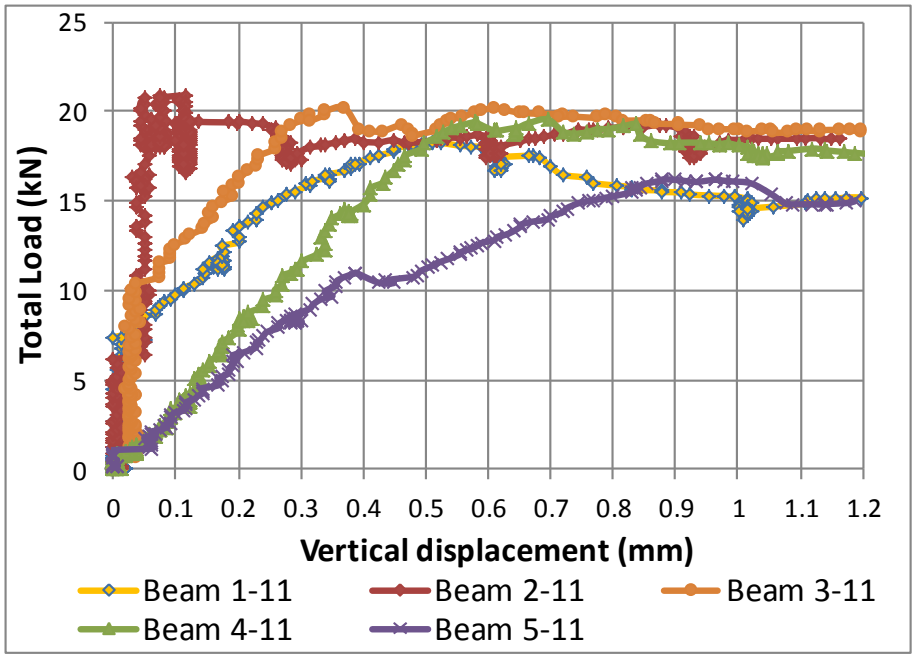

Figure 5-7 Load-displacement relationships for first series test beams

Table 5-2 Vertical displacement for tested composite beams

Beam number	Membrane thickness (mm)	Total vertical load (kN)	Laboratory tested vertical displacement (mm)
1-11	2	10	0.111
		18.2	0.500
2-11	2	10	0.055
		20	0.043
3-11	2	10	0.031
		20	0.338
4-11	6	10	0.26
		20	0.58
5-11	9	10	0.34
		20	0.68*

* projected value

5.2.4 Horizontal strains

The average of the two strain readings on the two sides of the top and bottom component beams of each composite beam are shown in Figure 5-8. The average values under 10kN total load for each composite beam are shown in Table 5-3. The non-zero strain readings demonstrated that the top and bottom component beams were working compositely. There is a bigger difference in the top ½ and bottom ½ strains of beam 3-11 in comparison to other composite beams, which is due to a larger variation of membrane position from half-depth of the whole beam (*i.e.* larger variation in depth for top and bottom component beams).

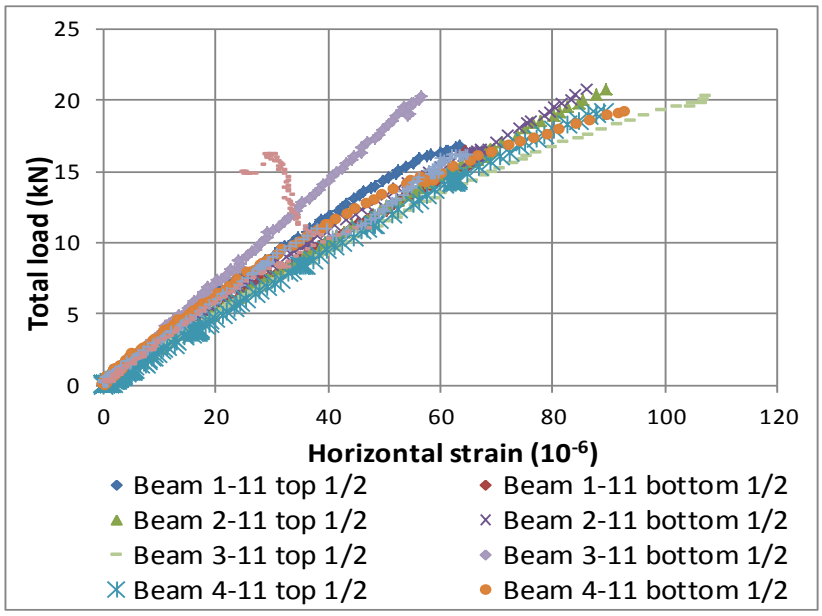

Figure 5-8 Longitudinal strain diagram

Table 5-3 Horizontal strain at mid-span for beams under 10 kN total load

Beam number	Membrane thickness (mm)	Strain gauge position	Strain gauge readings (microstrain)
1-11	4	top	33.7
		bottom	39.7
2-11	3	top	39.8
		bottom	36.5
3-11	2	top	43.5
		bottom	28.1
4-11	6	top	42.5
		bottom	34.8
5-11	10	top	35.7
		bottom	39.8

5.2.5 Crack development

A similar crack development process was observed for all beams, as shown in Figure 5-9. A detailed description of the crack propagation is given below with particular reference to beam 2-11.

- A visible crack was first observed when the load reached 19kN (90% of peak load)
- The crack was continuing to develop and approaching the membrane when the peak load was reached
- When the crack had extended to 3/4 of overall beam depth the beam could still sustain 18.5kN (88% of peak load), and at 4/5 of overall beam depth it could still sustain 10kN (50% of peak load)
- Steel fibres were observed to fail in the desired pull-out mode rather than by fibre breakage
- A single flexural crack was observed in all the tests

Comparing the load-displacement diagram and crack development observations, it is evident that the beams entered nonlinear behaviour before visible cracks were observed, implying invisible cracking occurred much earlier than development of visible cracks [Bloodworth *et al*. 2014].

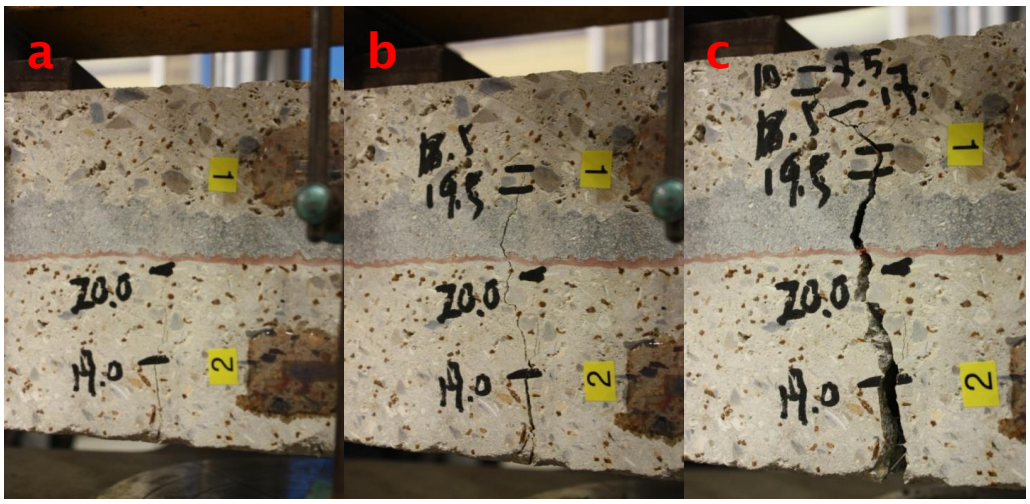

Figure 5-9 Crack development during the test for beam 2-11(a) approaching peak load (b) passing peak load (c) residual strength

5.2.6 Beam end displacements

The test results show that all beam end relative displacements were below 0.2mm, suggesting all beams demonstrated a high degree of composite action.

5.2.7 Calculation of composite action ratios

Section 5.1.3 proposed three methods to calculate the composite action ratios for composite beams. Methods (1) and (2), which are based on the beam displacements and strains, are used in this study. Method (3) is not used because the magnitude of the test data is too small.

Table 5-4 shows that composite action ratios calculated from strain readings are mostly around 42%, showing a good consistency between results. Composite action ratios calculated from the vertical displacements of two of the composite beams (4-11 and 5-11) follow the expected trend, reducing with increased membrane thickness. However, values for the other three beams (1-11, 2-11 and 3-11) do not, due to implausible displacement readings: This raises the question whether the theoretical assumptions behind the data manipulation (*i.e.* application of Euler-Bernoulli theory) and/or whether the measured beam vertical displacements are correct.

Table 5-4 Calculated composite action ratios (*Rc*) based on vertical displacement and strain readings

Beam number	Vertical displacement at 10 kN (mm)	Rc based on vertical displacement	Average Strain reading	Rc based on average strain
7-11	0.178	100%	88.5	
1-11	0.111	113%	36.7	41%
2-11	0.055	123%	38.15	43%
3-11	0.031	128%	35.8	40%
4-11	0.26	85%	38.65	44%
5-11	0.34	70%	37.75	43%

5.2.8 FLAC analysis of composite beams

A sensitivity study was first carried out which found that using an interface element to simulate a relatively thick membrane interface (*i.e.* ≥6mm) could lead to noticeably large difference in the results. This is because the depth of each component beam (*i.e.* approximately 75mm) is relatively thin in comparison to

the membrane interface thickness. Therefore, thin (<6mm) and thick (≥6mm) membrane interfaces were simulated by using interface elements and zones respectively. For the numerical modelling of a full composite SCL tunnel, only interface elements were used due to the thick primary and secondary lining thickness (*e.g.* 300mm for each and 600mm for total).

The FLAC model of the composite sprayed concrete beam under four-point bending is shown in Figure 5-10. The model composition is similar to that of the pure sprayed concrete beam described in Section 5.1.8, but with the addition of interface elements (for membrane thickness less or equal to 6mm) or zones (for membrane thickness bigger than 6mm) to the beam at its half-depth, simulating the sprayed membrane-concrete interface. The overall depth of beam was kept constant at 150mm regardless of the measured membrane thickness.

Similar to previous practice, very low Young's modulus beam elements were modelled at the half-depth of the top and bottom component beams, as an additional validation of the composite action.

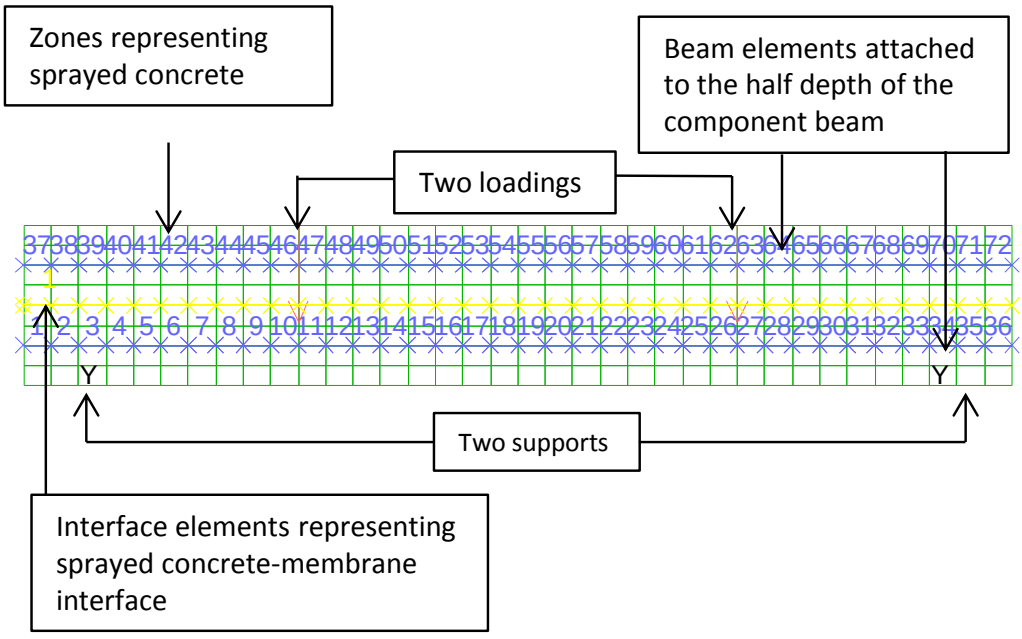

Figure 5-10 FLAC model for a composite sprayed concrete beam

Validation of the beam bending moment was firstly carried out. It was found that, under the same loading, when the interface stiffnesses (*e.g.* the composite action ratios) were increased, both the vertical displacement and bending moment of the beam elements reduced. This was due to the fact that the beam elements were attached to the zone and thus deformed to a smaller curvature, in turn generating a smaller bending moment. Therefore, the actual bending moment

should be the 'nominal' bending moment multiplied by an amplification factor, which is the ratio of vertical displacements between a non composite and a composite beam. This value can be calculated once the normal and shear interface stiffnesses are confirmed.

Validation of beam displacements and strains were also carried out. It was found that the predicted displacements and strains from the FLAC model matched the test results only when the sprayed concrete Young's modulus was assumed as 15GPa, slightly higher than the 10GPa value determined from the testing. The results are shown in Table 5-5.

Table 5-5 Comparison of numerical predictions and test results

Beam number	Strain gauge position	Component Beam depth (mm)	Laboratory measured strains (microstrain)	Kn (GPa/m)	Ks (GPa/m)	Numerical predicted strains (microstrain)
1-11	top	77	33.7	8	4	36.5
	bottom	69	39.7			40.7
2-11	top	70	39.8	8	4	40.8
	bottom	77	36.5			37.0
3-11	top	67	43.5	6	3	35.2
	bottom	80	28.1			28.1
4-11	top	69	42.5	8	4	42.3
	bottom	75	34.8			36.3
5-11	top	70	35.7	4.8	2	35.7
	bottom	70	39.8			35.7

The first round calibration produced contradictory results for the value of Young's modulus of sprayed concrete and the composite action ratios. Comparing with the strain gauge reading data, the quality of the displacement data was in doubt. Imperfect beam dimensions caused beam rotation during initial loading and the compliance of the testing machine may have both affected

the data. Therefore, a second round of calibration was carried out with a different measuring arrangement and the compliance of the testing machine was investigated.

5.3 Second round calibration

5.3.1 Calibration with pure shotcrete beam

In order to resolve the contradictory results obtained in the first round of calibration, the initial step of the second round of calibration was to double check the value of sprayed concrete Young's modulus. This was done by checking the compliance between the vertical displacement and strain readings from pure sprayed concrete beams.

Two additional pure sprayed concrete beams (7-12 and 7-13) were tested using the test dimensions and configuration. In this round of testing the locations of the strain gauges was changed. Four strain gauges were attached to each beam, two at half-depth of the top component beam, one on the top surface and one on the bottom. This arrangement provided a clearer picture of the strain distribution for each component beam, reducing the uncertainty in the strain values at the top and bottom. In addition, a dial gauge was used to give confirmation of potentiometer reading.

The test was undertaken using the same procedures as before. The load-displacement curve and strain readings are shown in Figure 5-11 and Figure 5-12 respectively. A Young's modulus value of 8-9GPa has been back-calculated from the load-displacement curves. This is very close to the 10GPa value obtained from the first round calibration. In contrast, the Young's modulus determined from the strain readings is around 22-24GPa - very close to the value obtained from uni-axial compression element tests. The strain position of top ¼ for sprayed concrete beams in Figure 5-12 is the same as the position of top ½ for composite beams as shown in Figure 5-4.

It was thought that strain gauge value (a local measurement) should be more accurate than the vertical displacement results obtained from the potentiometer (a global measurement). Therefore, detailed investigation on the possible error source was undertaken. Two error sources were identified to have contributed to the additional measured displacement: (1) a layer of compressible rubber sheet

under the pin supports and (2) the compliance of the machine system as a whole, including "bedding" effects at the supports. In order to assess the level of additional displacement, it was decided to test a steel beam with standard cross-section, whose second moment of inertia and Young's modulus (of steel) was known.

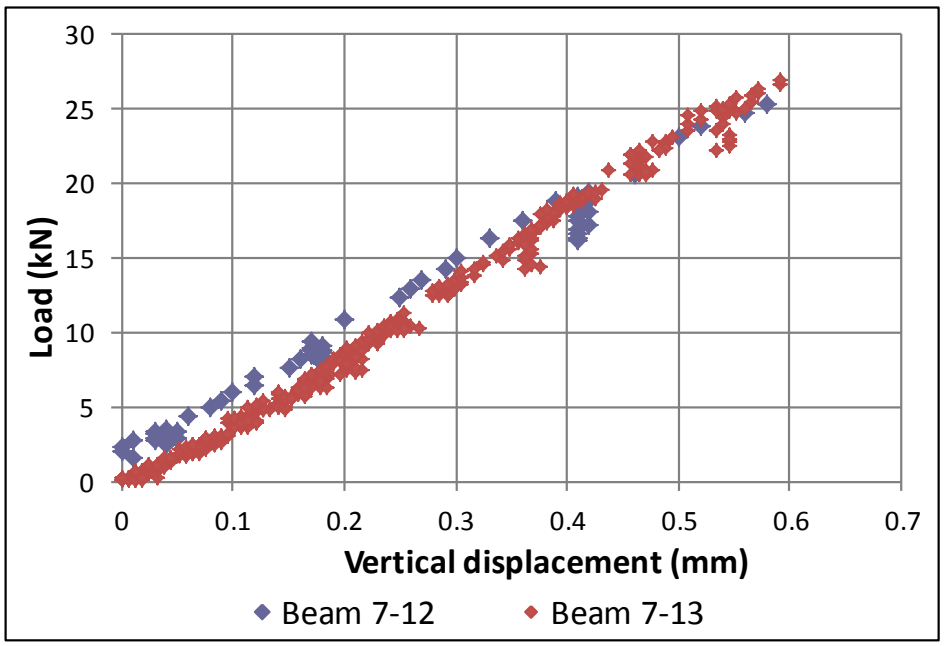

Figure 5-11 Load-displacement curve for pure shotcrete beams 7-12 and 7-13

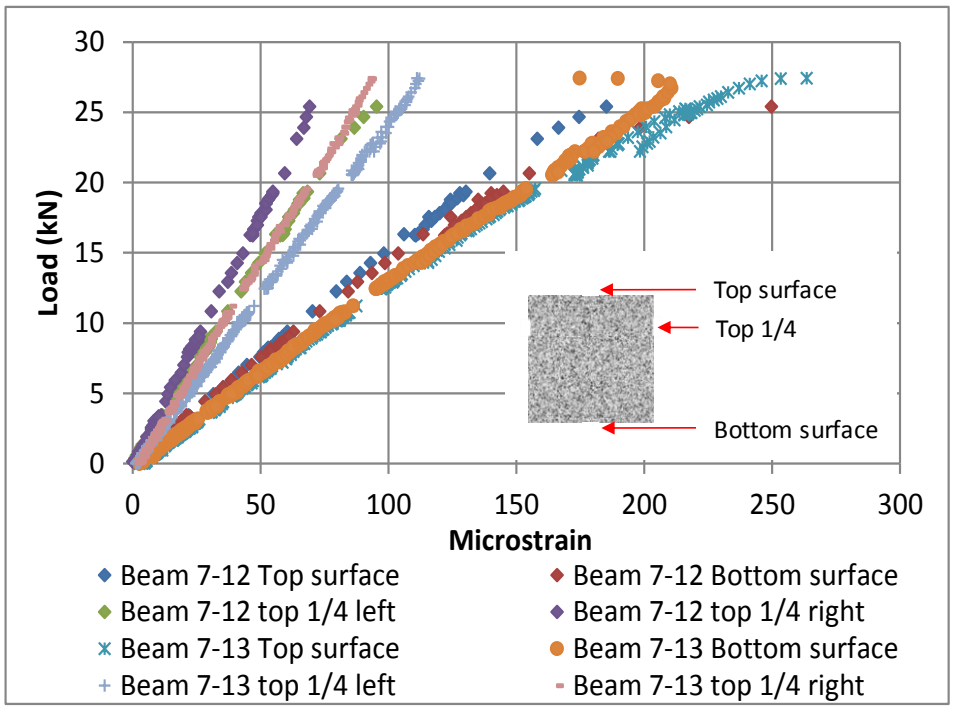

Figure 5-12 Strain readings for pure shotcrete beams 7-12 and 7-13

5.3.2 Correction for test setup compliance

A rolled steel I shape beam of the similar length and cross-section depth as the sprayed concrete beams was tested twice in the same test configuration and under the same loading procedure, as shown in Figure 5-13. The dimensions of the steel beam are provided in Table 5-6. Closed-form equations based on beam theory were used to examine the compliance.

Figure 5-13 Test configuration for the steel beam

Table 5-6 Dimensions of the steel beam

Cross-section	Length (mm)	Depth (mm)	Flange width (mm)	Flange thickness (mm)	Web thickness (mm)
I - shape	917	152	76	8	7

The laboratory tested and closed-form equation calculated load-displacement curves for the steel beam are shown in Figure 5-14. It was found that (1) the curves for the two laboratory tests were almost identical, (2) the initial "bedding" effect was occurred at lower load levels (<3kN) and "stiffer" curves were developed at higher load levels (>3kN) and (3) even the "stiffer" curves exhibited "softer" behaviour than that predicted by the closed-form calculated curve in red. This demonstrates the compressive rubber sheet and the compliance of machine

system did cause additional displacement to the results. The displacement/load ratio calculated for the laboratory test results at higher load levels and that calculated theoretically are 0.0179mm/kN and 0.00366mm/kN respectively. The difference of 0.0142mm/kN can be attributed to the additional displacement that arises from the compressible rubber sheet and the compliance of machine system.

The original and adjusted load-displacement curves for beams 7-12 and 7-13 are shown in Figure 5-15. A theoretical line calculated from the closed-form equation using a Young's modulus value of 22GPa is also shown in red. It can be seen that the adjusted curve for beam 7-13 is slightly "stiffer" than the theoretical curve, whilst the other curve for beam 7-12 is slightly "softer" than the theoretical curve. The range of the Young's modulus for two beams is between 20-24GPa, consistent with the test results from the uni-axial compression element test and the back-calculated values from strain readings. Therefore, it can be concluded that (1) the Young's modulus of sprayed concrete for this study is between 20-24GPa, (2) Young's modulus of sprayed concrete was the same in tension and compression, and (3) sprayed concrete is isotropic.

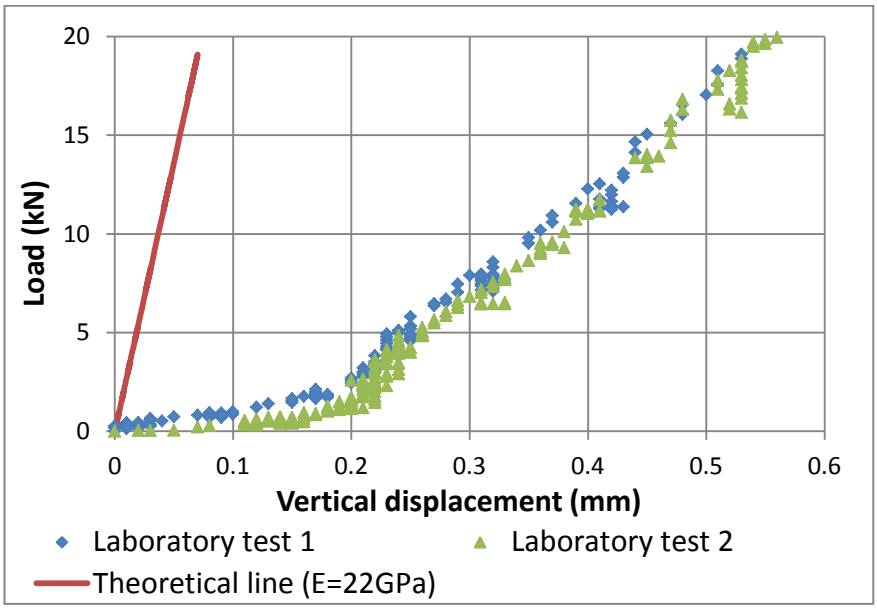

Figure 5-14 Test and theoretical calculation results for the steel beam

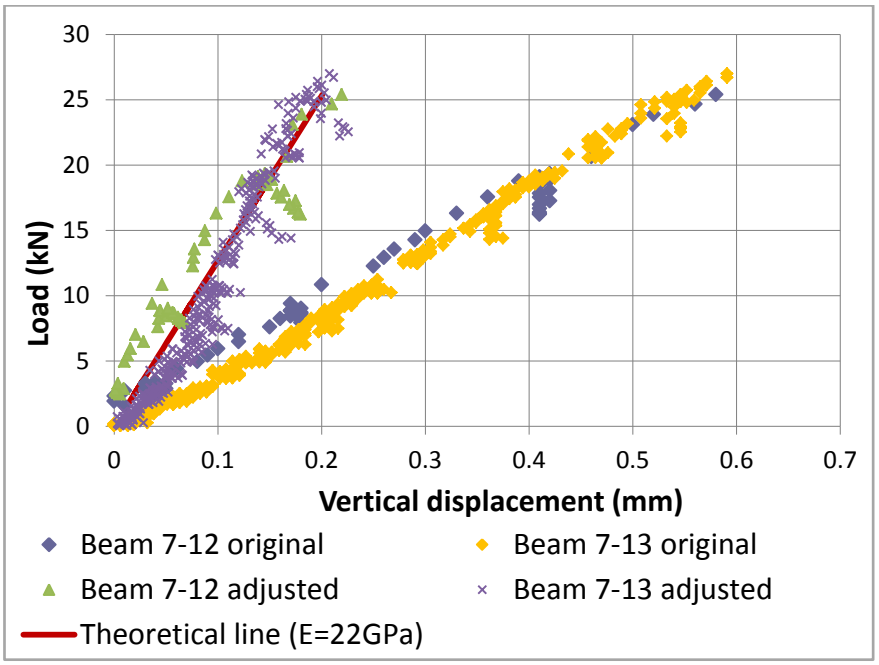

Figure 5-15 Original and adjusted load-displacement curves for pure shotcrete beams

5.3.3 Calibration using additional composite beams

Having established the value of sprayed concrete Young's modulus, the next step was to calibrate the models for the composite beams. Two additional composite beams were tested with new strain gauge arrangements and a dial gauge. The dimensions of these two beams are shown in Table 5-7.

Table 5-7 Dimensions of 2nd round tested composite beams

Beam number	Measured membrane thickness (mm)	Interface type	Thickness of top component beam (mm)	Thickness of bottom component beam (mm)	Beam width (mm)	Beam length (mm)
4-12	6	regulated	65	79	150	900
4-13	4	regulated	66	80		

The adjusted load-displacement curves is shown in Figure 5-16, in which the "softer" behaviour of beam 4-12 was mostly attributed to the initial "bedding" effect. It then exhibits a "stiffer" response at higher load level (>8kN).

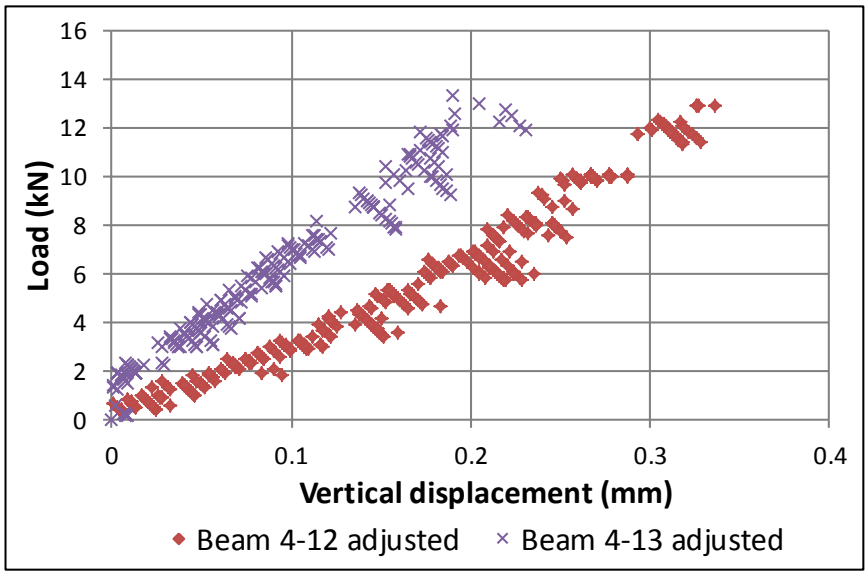

Figure 5-16 Load-displacement curve (adjusted) for 2nd round tested composite beams

The selected strain readings (top surface and top ½ right) for these two composite beams are shown in Figure 5-17. For both cases, the top surface strains are more than double of the top ½ right strains, demonstrating the existence of composite action.

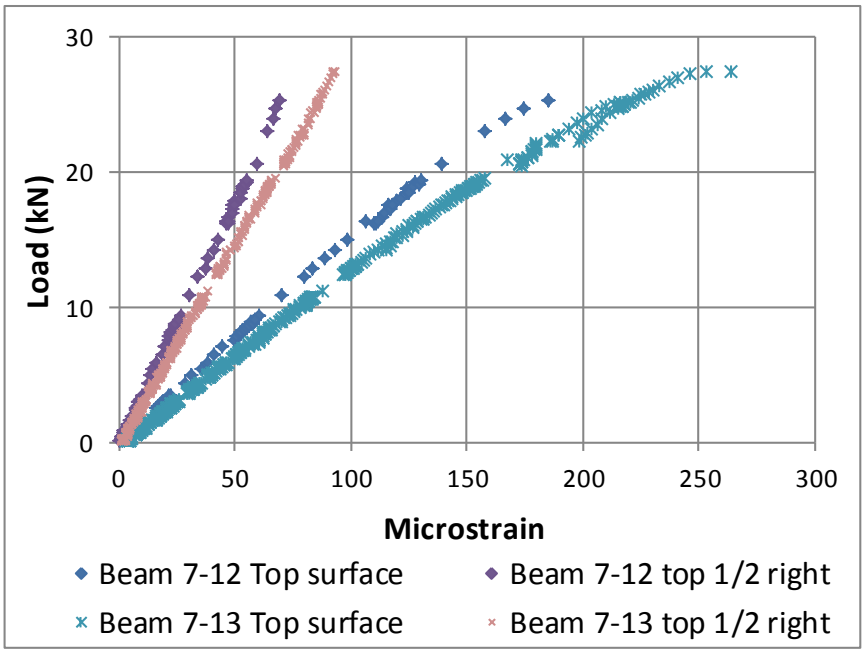

Figure 5-17 Selected strain readings for 2nd round tested composite beams

Numerical analysis using the previously calibrated FLAC model was carried out for these two composite beams. The predicted displacements and strain results are compared with those from laboratory tests and are shown in Table 5-8 and Table

5-9 respectively. It can be seen that the two sets of results are very close to each other - the differences between the two results are all within 8% when against the laboratory test results. Therefore, it can be claimed that the proposed numerical modelling approach is able to reasonably simulate the behaviour of composite beams. This approach is used in the next chapter for the numerical modelling of a typical CSL tunnel.

Table 5-8 Comparison of displacement from numerical predictions and test results

Beam number	Laboratory measured displacement (mm)	Sprayed concrete Young's modulus (GPa)	Kn/Ks (GPa/m)	Numerical predicted displacement (mm)	Differences against the laboratory results
4-12	0.200	20	8/4	0.218	1.0%
4-13	0.176	23	16/8	0.170	3.4%

Table 5-9 Comparison of strains from numerical predictions and test results

Beam number	Strain gauge position	Laboratory measured strains (microstrain)	Numerical predicted strains (microstrain)	Differences against the laboratory results
4-12	top	-82.02	-88.5	7.9%
	½ top beam	-28.0	-29.5	5.3%
	Bottom	114.6	113.3	1.1%
4-13	top	-73.4	-69.2	5.7%
	½ top beam	-48.4	-50.1	3.5%
	½ top beam	-23.77	-23.87	0.4%
	Bottom	78.71	78.85	0.1%

5.3.4 Reanalysis of first round composite beams

Following the successful calibration of the second round composite beams, reanalysis was carried out for the first set of beams with displacement values adjusted for the machine compliance.

Table 5-10 shows that the strains predicted by the FLAC model are reasonably close to those obtained from the laboratory tests, demonstrating its ability to simulate composite action between two layers of lining. There are a few occasions when the differences from the laboratory results are more than 10%, which may be attributed to many factors, such as continued variation of component beam thickness (and hence the membrane thickness) and strain gauges not perfectly positioned in the half-depth of component beams. These variations are inherent to the construction and monitoring of SCL tunnels, so cannot be totally avoided. With most difference ratios less than 10%, the level of accuracy is acceptable.

Table 5-11 shows the FLAC model predicted displacements are slightly different from those obtained from laboratory tests. It should be noted that there was only one potentiometer measuring the displacement in the first round of beam test. Therefore, it was possible that some of those beams were experiencing rotation at the initial loading stage, mostly due to their imperfect dimensions. The rotation could lead to either enlarged or reduced displacement readings, depending on the rotation direction and potentiometer position. Overall, considering the high degree of match between the beam strains and the small discrepancy (<0.1mm) between the beam displacements, it can again be confirmed that the proposed composite beam model is able to simulate the behaviour of composite beams.

Table 5-10 Comparison of strains for the first set of beams

Beam number	Strain gauge position	Laboratory measured strains (microstrain)	Sprayed concrete Young's modulus (GPa)	Kn/Ks (GPa/m)	Numerical predicted strains (microstrain)	Differences against the laboratory results
1-11	top	-33.7	20	16/8	-31.4	6.8%
	bottom	39.7			35.0	11.8%

2-11	top	-39.8	20	16/8	-37.9	4.8%
	bottom	36.5			34.4	5.8%
3-11	top	-43.5	20	32/16	-39.3	9.7%
	bottom	28.1			32.8	16.7%
4-11	top	-42.5	20	10/5	-35.3	16.9%
	bottom	34.8			32.4	6.9%
5-11	top	-35.7	20	8/4	-39.8	11.5%
	bottom	39.8			36.1	9.3%

Table 5-11 Comparison of displacement for the 1st round composite beams

Beam number	Laboratory measured displacement (mm)	Sprayed concrete Young's modulus (GPa)	Kn (GPa/m)	Ks (GPa/m)	Numerical predicted displacement (mm)
1-11	N/A	20	16	8	0.178
2-11	N/A	20	16	8	0.157
3-11	N/A	20	32	16	0.156
4-11	0.12	20	10	5	0.205
5-11	0.20	20	8	4	0.282

5.3.5 Examination of interface stiffnesses

Table 5-12 shows that the calibrated interface stiffnesses are all within the range of test results from element tests presented in Chapter 4 and generally demonstrated the expected trend: (1) the thicker the measured membrane thickness, the lower the interface stiffness, and (2) the rougher the primary lining interface surface, the higher the interface stiffness. Therefore, it was concluded that the validated interface parameters can be used for modelling a typical CSL tunnel under practical loading as described in Chapter 6.

Table 5-12 Interface parameters used in the numerical modelling of composite beams

Beam number	Measured membrane thickness (mm)	Interface type	Kn (GPa/m)	Ks (GPa/m)
1-11	4	smoothed	16	8
2-11	3	regulated	16	8
3-11	3	As-sprayed	32	16
4-11	6	smoothed	10	5
4-12	4	regulated	8	4
4-13	4	regulated	16	8
5-11	10	regulated	8	4

5.4 Sensitivity study of CSL beams

A numerical sensitivity study using the same composite beam model was carried out to investigate the impact of normal interface stiffness Kn and shear interface stiffness Ks both individually and simultaneously, on the composite action ratio Rc based on displacement. The sprayed concrete Young's modulus is assumed as 15 GPa and Kn and Ks were varied by a factor of 10 either side of their base values (Kn=8GPa/m and Ks=4GPa/m). It should be noted that the sprayed concrete Young's modulus does not affect the composite action ratio.

The modelling results for the sensitivity of Rc to Kn are shown in Figure 5-18. It shows that when Kn is increased by a factor of 10 from its base value, the composite action ratio increases by only 0.02, whereas it reduces by 0.12 when Kn is reduced to a tenth of its base value. It also shows that the composite action ratio increases by 0.23 or reduces by 0.40 when Ks is increased or decreased by a factor of 10 respectively, demonstrating that the composite action ratio is more sensitive to the variance of Ks.

The modelling results for the sensitivity of Rc to Kn and Ks simultaneously are shown in Figure 5-19 and Table 5-13. It can be seen that varying Kn and Ks simultaneously changes the composite action ratio significantly. In a range

between 0.1 and 10 times the base case Kn and Ks values, the composite action ratio varies from 0.07 to 0.96. However, within a practical range of Kn and Ks (highlighted in yellow in Table 5-13), the composite action ratio varies from 0.71 to 0.56 and a change in Ks has a much bigger influence than variation of Kn on the degree of composite action.

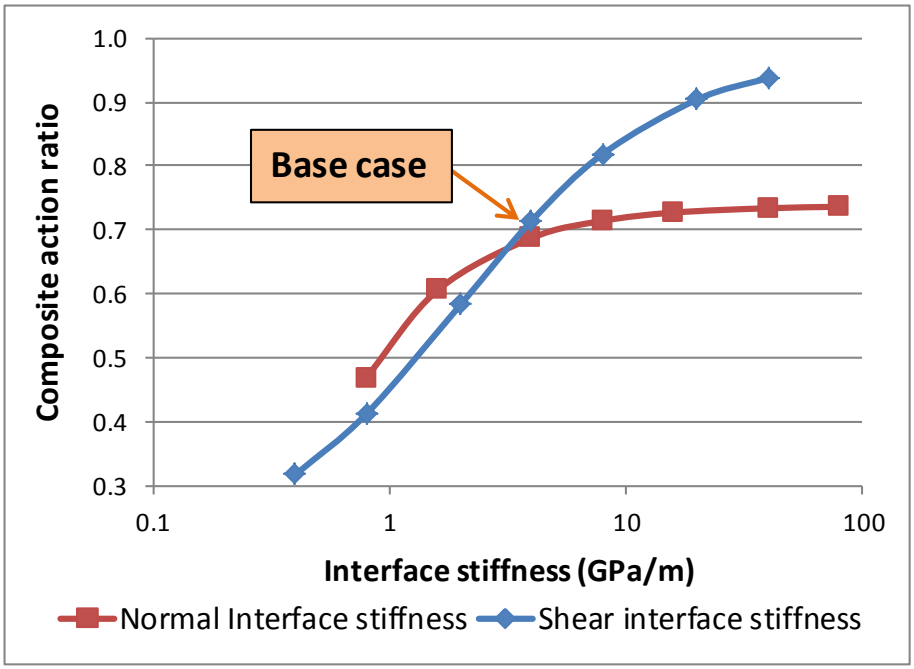

Figure 5-18 Sensitivity of composite action ratio to Kn and Ks

Table 5-13 Composite action ratio from sensitivity study when Kn and Ks vary simultaneously

Composite action ratio		Ks (GPa/m)						
		0.4	0.8	2	4	8	20	40
Kn (GPa/m)	80	0.34	0.43	0.60	0.74	0.84	0.93	0.96
	40	0.34	0.43	0.60	0.73	0.84	0.92	0.96
	16	0.33	0.42	0.60	0.73	0.83	0.92	0.95
	8	0.32	0.41	0.58	0.71	0.82	0.90	0.94
	4	0.29	0.39	0.56	0.69	0.79	0.88	0.91
	1.6	0.21	0.30	0.47	0.61	0.71	0.80	0.83
	0.8	0.07	0.17	0.34	0.47	0.57	0.66	0.69

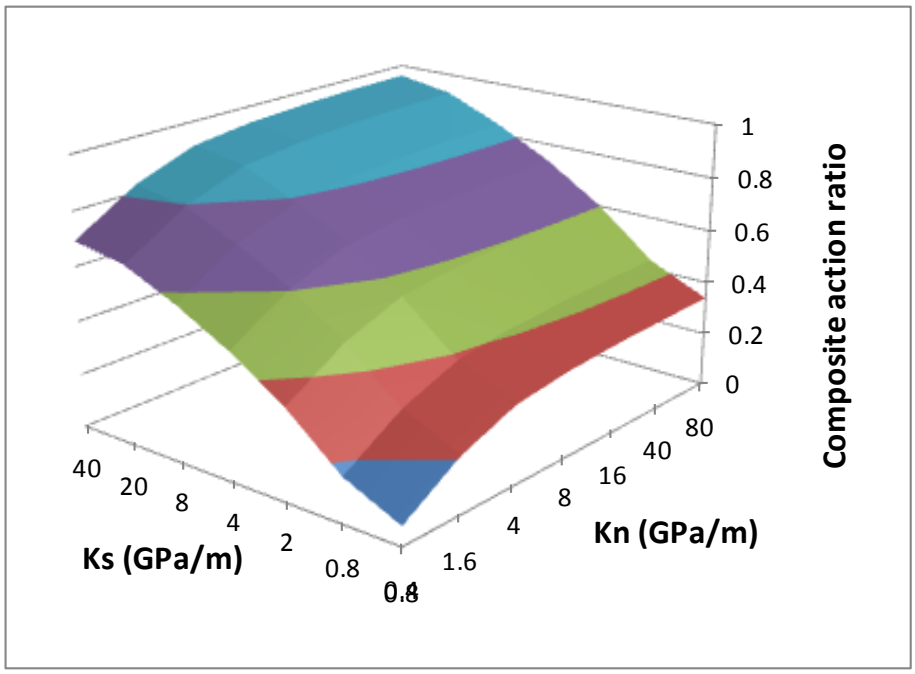

Figure 5-19 Composite action ratio from sensitivity study when Kn and Ks vary simultaneously

5.5 The impact of different position of sprayed waterproofing membrane

The impact of membrane position on the composite action ratio was also investigated. Keeping the overall beam depth constant, vertical location of the waterproofing interface was varied between near the bottom surface of the beam to near the top surface (18.75mm from beam surface).

Figure 5-20 shows that the composite action ratio is biggest when the membrane is at mid-depth of the beam and reduces as the membrane position moves towards the extreme fibre in either direction. This follows the beam theory that the shear stress is highest at the mid-depth of the beam when it is under bending. Consequently, the greater the shear stress utilised at the interface, the higher the composite action ratio.

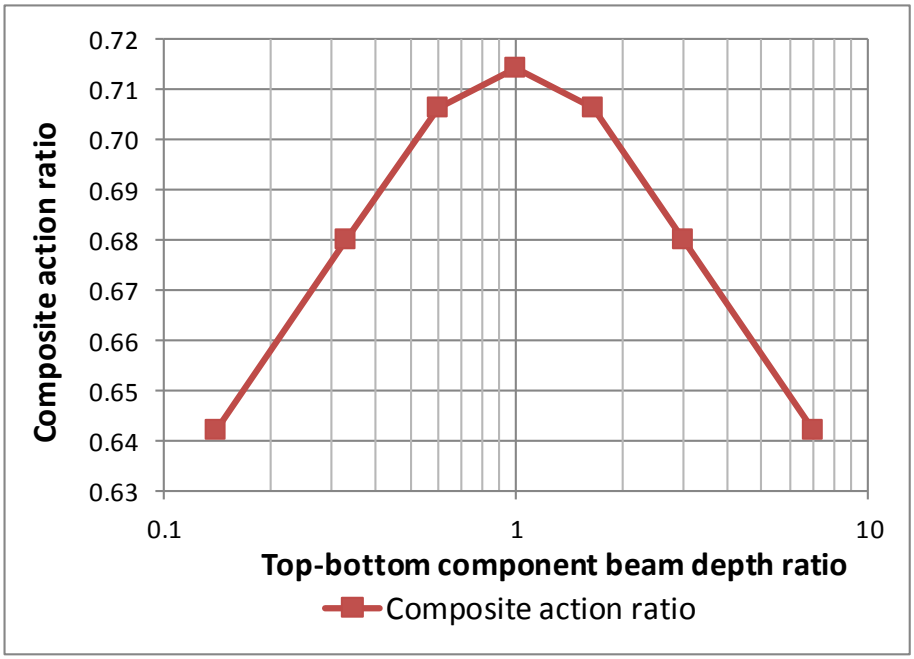

Figure 5-20 Composite action ratios for composite beam with membrane at different positions

5.6 Composite beam thickness optimisation

The sensitivity studies described so far have focused on composite beams with fixed overall thickness. In this section, the primary lining is held constant at 75 mm and secondary lining thickness is varied (reduced). The vertical displacement is compared with that of a non composite double shell beam with primary and secondary lining thicknesses both equal to 75 mm, hence demonstrating the benefit in terms of lining saving of including composite action.

The base case non composite beam has a composite action ratio of 0.0 (top line of Table 5-14). This is compared with five composite beams with top component beam thickness also 75 mm but bottom beam thickness varying from 15mm to 75mm in 15mm intervals. Base case interface properties of Kn=8GPa/m and Ks= 4GPa/m were used.

Table 5-14 shows that the composite beam with a bottom component beam thickness of 20 mm (*i.e.* overall thickness 95 mm) has the closest vertical displacement to that of the non composite beam. This corresponds to a 37% reduction in overall thickness and 73% secondary lining thickness reduction.

It should be noted that the main purpose of this study was to demonstrate an overall lining thickness reduction is possible from a structural engineering point

of view. However, this conclusion has been drawn from structural composite beam models without considering many other factors which influence the behaviour of a CSL tunnel. These include soil-structure interaction effect, sequential excavation and long-term ground behaviour, which are investigated in detail in next chapter. Therefore, given the limitations of this particular comparison study, this conclusion should not directly inform CSL tunnel design without further investigation.

Table 5-14 Secondary lining optimisation study for fixed primary lining thickness

t_{top} (mm)	t_{bottom} (mm)	t_{total} (mm)	Vertical displacement (mm)	Composite action ratio
75	75	150	0.4716	0.00
	15	90	0.5601	-0.25
	20	95	0.4747	-0.01
	30	105	0.4386	0.09
	45	120	0.3467	0.35
	60	135	0.2749	0.56
	75	15	0.2190	0.71

5.7 Summary

A calibration process for a composite beam numerical model against laboratory test data and associated sensitivity studies have been presented. The main findings are:

- The composite action of composite beams can be simulated by using the proposed numerical modelling approach and verified interface parameters
- It is confirmed that the sprayed concrete is an isotropic material and its Young's modulus is the same in tension and compression, ranging from 20GPa to 25GPa for this research.
- Shear interface stiffness has much bigger impact than normal interface stiffness on the degree of composite action.

- Within the practical range of interface stiffness with spray-applied waterproofing membrane, based on the TamSeal 800, the degree of composite action for composite beams under four-point bending tests varies by about 15%.
- The degree of composite action is maximised when the interface is at half-depth of the composite lining.
- The sprayed membrane interface induced composite action could lead to a 37% reduction in overall beam thickness for a composite beam in pure bending.

This chapter validated a numerical modelling approach that can simulate the composite action for composite beams as well as key material and interface parameters, all of which will be used for the next stage of research.

Chapter 6: Numerical Analysis of a Composite SCL Tunnel

This Chapter comprises three main parts and a summary. The first part, including Sections 6.1 and 6.2, introduces the background and numerical modelling plan of this chapter. Sections 6.3 and 6.4 go on to introduce the adopted numerical modelling methodology and presents the results for the base case CSL tunnel. The third part, from Section 6.5 to 6.9, presents a series of parametric study results. A summary of the findings is provided in Section 6.10.

6.1 Background

6.1.1 Load sharing between the primary and secondary linings

Historically, SCL tunnels were mostly designed so that the primary lining takes all the short-term loads and then degrades to "grey rock" in the long-term (Hurt 2002). The secondary lining was assumed to take all the long-term loads, with no load sharing between the sacrificial primary and permanent secondary linings. Due to the complexity of staged construction and soil-structure interactions, monitoring of SCL tunnels focused mostly on the performance of primary linings, using load cells to measure lining forces (Clayton *et al.* 2000, 2006) in most cases and also more recently fibre optics to measure lining strains (Devriendt 2012). Therefore, there is a lack of literature on the load sharing between the permanent primary and secondary linings due to the fact that the CSL tunnel configuration is fairly new to the tunnelling industry.

In this study, numerical modelling has been adopted to investigate the load sharing between the permanent primary and secondary linings and the concrete-membrane interface stresses for a typical CSL tunnel in the long term. The composite action is simulated using the previously validated interface parameters and modelling approach. The load sharing effect is evaluated by examining the long-term consolidation load effects (*e.g.* axial force and bending moment) between the short and long-term (*e.g.* 120 years) stages in the primary and secondary linings.

6.1.2 Capacity evaluation for CSL tunnel lining

One of the common methods of evaluating the performance of a CSL tunnel is to assess whether the primary and secondary linings have sufficient capacity to sustain the lining forces. The use of the thrust-moment capacity curve in SCL tunnel design was introduced in the early 1990s by Dr. Sauer *et al.* (1994) and has now become a standard practice in the tunnelling industry. The capacity curve is derived as a function of the maximum allowable bending moment and axial force for a certain concrete cross-section, which is a powerful tool for designing primary or secondary linings individually. However, it cannot be used directly for the design of a CSL tunnel lining because the bending moment in each component beam is not easily determined due to the asymmetrical compressive and tensile stresses at both extreme fibre surfaces. This section presents the derivation of a modified capacity curve that can be used for the design of CSL tunnels.

Although practical tunnel linings experience both bending moment and axial force, in most tunnelling specifications, beam tests have been used to evaluate the pure flexural performance of the lining, such as the four-point bending test (BSI, 2006). Assuming there are three beams: full composite beam (*i.e.* exhibiting full composite action), composite beam (*i.e.* partial composite action) and non composite beam (*i.e.* two adjacent beams without shear transfer at the interface), each consists of a top and a bottom component beam of height h and width b. According to beam theory, the flexural stiffnesses of the top (or bottom) component beams are $4bh^3/12$ (half of the stiffness for the whole beam at $8bh^3/12$), $Rbh^3/12$ and $bh^3/12$ respectively, where R is the flexural stiffness ratio for the composite component beam versus that of the non composite component beam. It is also understood from beam theory that the bending capacity of a beam is proportional to its flexural stiffness, Young's modulus of the material and the maximum curvature. Therefore, if the three beams are made of the same material and are able to deform to the same maximum curvature, their individual bending moment capacities are purely proportional to their respective flexural stiffnesses. Therefore, the composite beam flexural stiffness ratio is equivalent to its bending capacity ratio.

As it has been difficult to directly measure flexural stiffness, an alternative approach was adopted by measuring the vertical displacement of the beam

instead. The flexural stiffness ratio (bending capacity ratio) between the composite beam and the non composite beam could then be calculated by inversing the respective vertical displacement ratio.

In Chapter 5, the vertical displacement for a composite beam with a short-term base interface stiffness (Kn=8GPa/m and Ks=4GPa/m) was calibrated using the numerical prediction and laboratory test results. Following the same method, the vertical displacement ratio between a composite beam with the long-term base interface stiffness (Kn=4GPa/m and Ks=2GPa/m) and a non composite beam has been numerically determined as 0.56 (0.26400mm/0.4716mm). By inversing the vertical displacement ratio, the flexural stiffness ratio (bending moment ratio) between the two beams has been determined as 1.78, as this can be used as an amplification factor to generate the capacity curve for the composite component beam. It should be noted that the bending capacity ratio arises for different primary/secondary lining thickness ratios and different interface stiffnesses, which have both been taken into account in the following analysis.

Figure 6-1 shows two capacity curves. The black curve reflects that of a 300mm thick non composite component beam with concrete grade of 32MPa and a material partial factor of 1.5, which allows for material variability and a reduction in strength and stiffness resulting from material degradation. The green curve is for a 300mm thick partial composite component beam with the same grade of concrete and partial factor but has an interface that is able to transfer the normal and shear interface stiffnesses (composite action). This therefore allows allowing the component beam to carry extra bending at the same level of axial force when compared with the non composite component beam. No capacity contribution from either steel rebar or structural fibers is included. The former has been excluded such that “out of capacity” area on the lining can be identified and reinforcement requirements established. The latter has been neglected due to the small capacity contributed by the structural fibers.

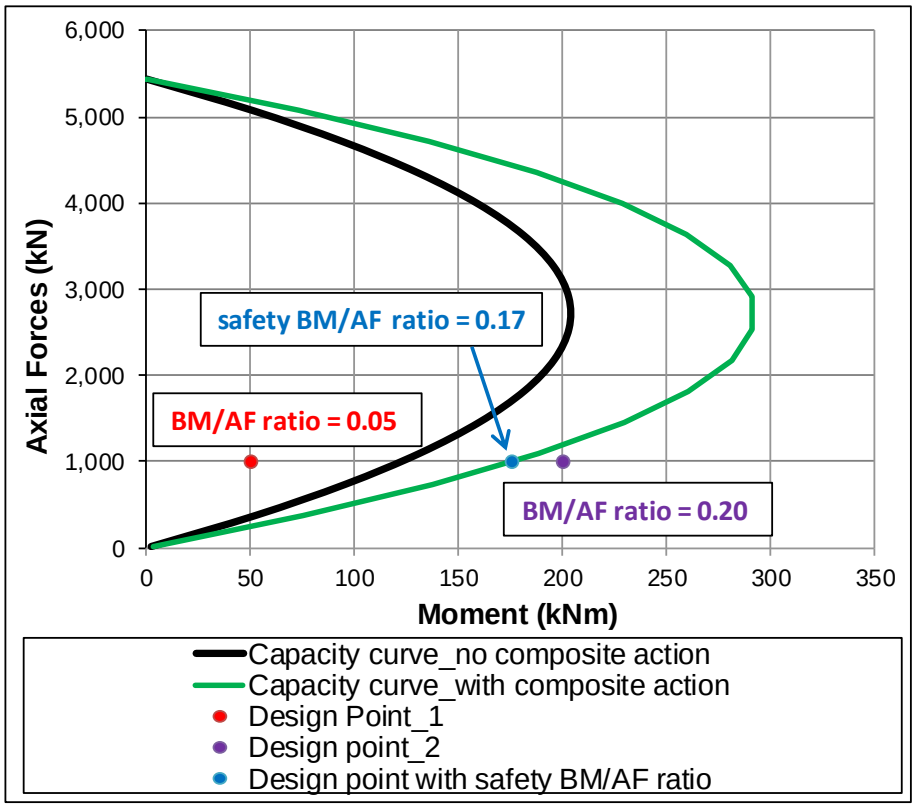

Figure 6-1 Capacity curves for non composite (black) and composite (green) sprayed concrete linings

6.1.3 Bending moment/axial force ratio

For SCL tunnel lining design, the axial force in the lining is usually limited to half that which corresponds to the peak axial force (*i.e.* below the bulge tip point level of the capacity curve). Therefore, the capacity of the lining (*e.g.* whether reinforcement is needed) can be assessed by the bending moment/axial force (BM/AF) ratio, defined as follows:

$$R_{BM/AF} = M/(N \times 1m) \qquad \text{Equation 6-1}$$

Where

$R_{BM/AF}$: BM/AF ratio for either lining

M: bending moment for either lining

N: axial force for either lining

In this chapter, the lining capacity is evaluated by comparing the component beam BM/AF ratio from the analysis results with the safety BM/AF ratio, at which no additional steel reinforcement is needed. For example, Figure 6-1 shows that

the safety BM/AF ratio for the composite component beam (green curve) is around 0.17. The design point 1 has a BM/AF ratio of 0.05 – this is within the limit of the capacity curve and therefore, no steel reinforcement is required in this case. The design point 2 has a BM/AF ratio of 0.20 which exceeds the safety ratio of 0.17, is outside of the capacity curve and, therefore, additional steel reinforcement is needed. The advantage of this method over the traditional approach using a capacity curve is the out of capacity section of tunnel lining can be more easily identified, as shown in Figure 6-2.

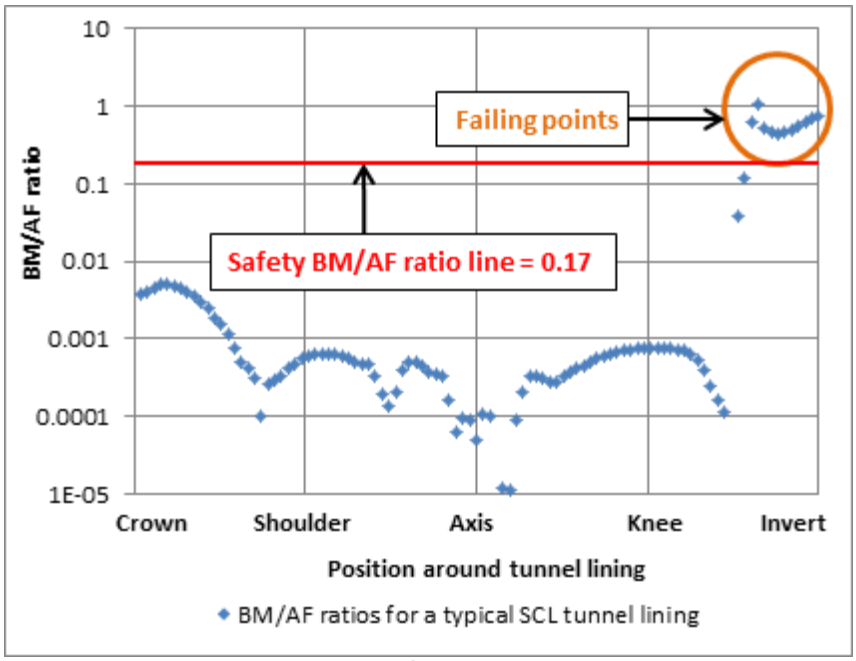

Figure 6-2 BM/AF diagram for a typical SCL tunnel lining.

6.1.4 Criteria of an efficient and robust CSL tunnel design

Chapters 1 and 2 have described the current trend of using steel fibres instead of traditional steel bars as the main structural reinforcement for SCL tunnels and the desire to utilise composite action to reduce the overall lining thickness. Therefore, for this study, the criteria for an efficient and robust CSL tunnel design are (1) minimised use of traditional reinforcement, a practice that leads to prolonged construction programme, additional costs and installation associated Health & Safety issues, and (2) reduced overall lining thickness, and (3) increased robustness of CSL tunnels (*i.e.* whether the interface is able to maintain the integrity of CSL tunnels under external loadings).

6.2 Numerical Modelling Plan

In this Chapter, a series of numerical analyses was carried out to investigate how to produce an efficient and robust CSL tunnel design.

This numerical analysis programme first investigated the base case scenario, adopting a model with the long-term base normal and shear interface stiffnesses from Chapter 4. The results, including the absolute magnitude of consolidation lining forces, the evaluation of lining and interface capacities are presented and used as a basis for further comparison. The lining capacity is checked to see if additional reinforcement is needed in any part of the lining. The interface capacity is checked to see if any debonding or slippage could occur at the interface.

Following the base case investigation, three series of parametric studies were carried out. The first series investigates the impact of variance in interface stiffnesses on the behaviour of CSL tunnels, especially the requirements of reinforcement in the lining. These parametric studies include:

(1) Variance in normal interface stiffness, Kn

(2) Variance in shear interface stiffness, Ks

(3) Variance simultaneously in Kn and Ks

The second series investigates whether an overall lining thickness reduction can be achieved for CSL tunnels and its impact on the reinforcement requirement in the lining. These parametric studies include:

(4) Variance in primary lining thickness (with secondary lining thickness held constant)

(5) Variance in secondary lining thickness (with primary lining thickness held constant)

The third series of parametric studies examines the robustness of the composite SCL tunnel to external impacts, including:

(6) Nearby construction on one side of the SCL tunnel

(7) Nearby construction beneath the SCL tunnel.

6.3 Modelling strategy for CSL tunnel

For this study, the modelling approach calibrated in Chapter 5 was used.

6.3.1 Long-term plane strain condition

SCL tunnel excavation is a complex soil-structure interaction problem and 3D modelling has been used to understand the excavation-induced ground deformations and lining forces (Thomas, 2003, Jones, *et al.* 2008). For this study, since composite action is a long-term phenomenon and the SCL tunnel sequential excavation is not the key focus, plane strain 2D analysis is used.

6.3.2 Model geometry and boundary conditions

A typical 2D plane strain FD mesh used in this study is shown in Figure 6-3. To represent the soil strata of the London basin, the model was assumed to have a depth of 58 m and a width of 140 m, and consisted of two materials, as indicated in Table 6-1. The top and bottom boundaries of the model represent the ground surface and the top of the Chalk bedrock (acting as a relatively incompressible boundary) respectively. The side model boundaries were set at a distance required to reliably predict lining forces and ground deformation around the tunnels. The detailed CSL tunnel model showing the different parts of the lining and the five key locations at which the results from the model will be analysed are shown in Figure 6-4.

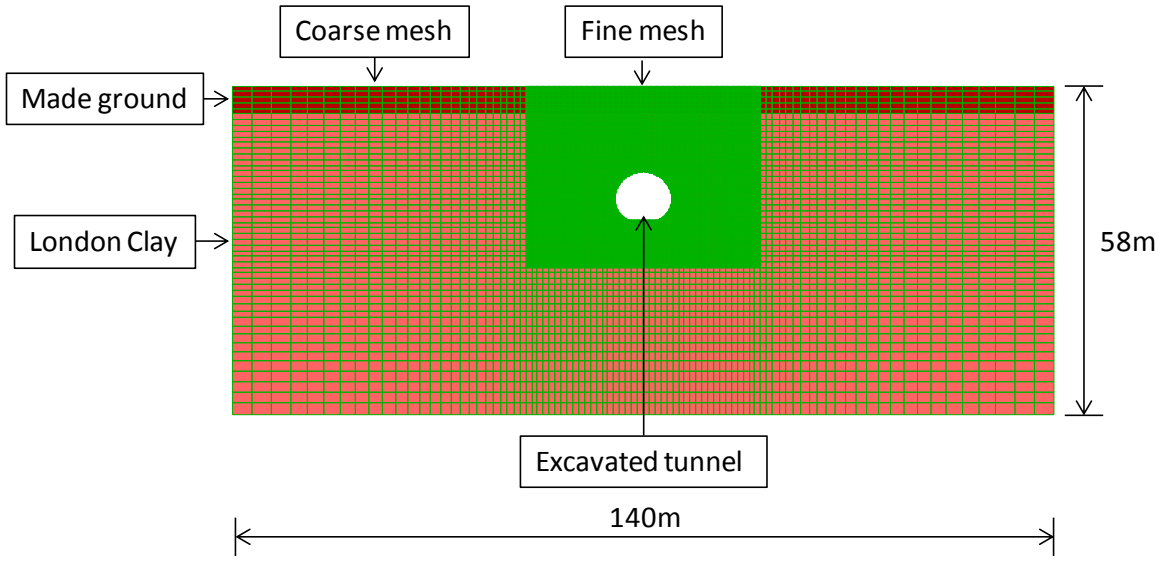

Figure 6-3 Global Model mesh

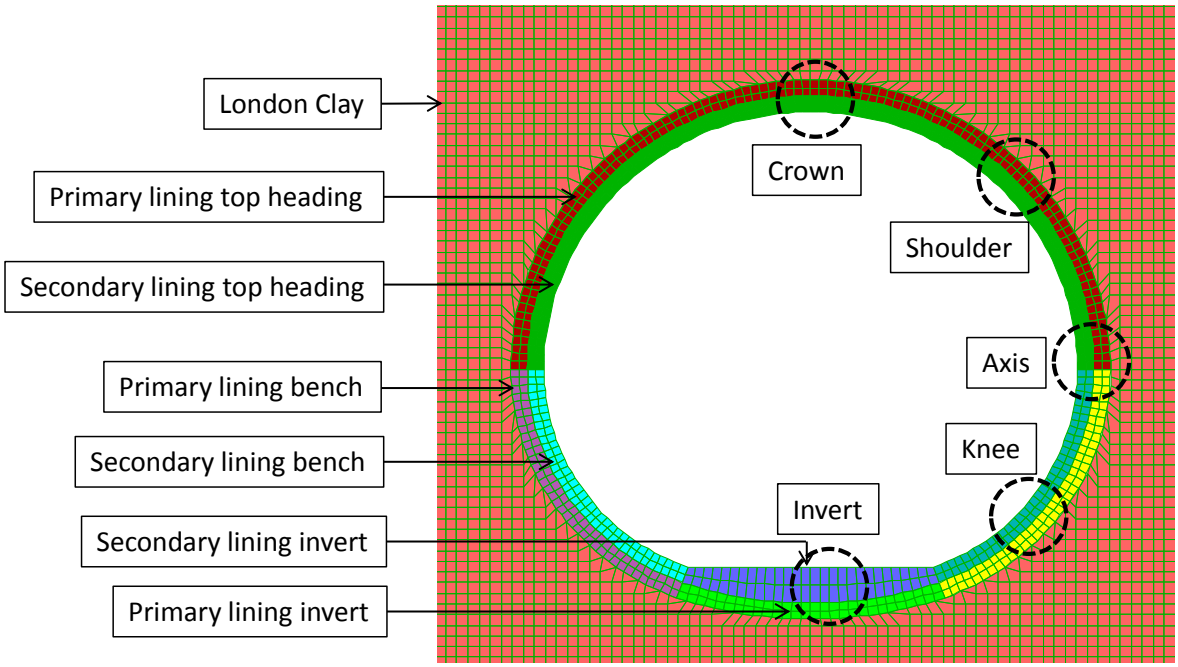

Figure 6-4 CSL tunnel and surrounding ground mesh

Table 6-1 Geological stratigraphy

Depth from [mATD]	Base [mATD]	Thickness [m]	Description
120.00	113.00	7.00	Made Ground (MG)
113.00	62.00	51.00	Upper London Clay (ULC) – unit B/A3

The model representing the ground consists of 28,500 finite difference zones in total, organised into two main areas. The area of high stress and strain gradients around the tunnel is represented by a fine mesh of 25,000 zones, each with dimensions of 0.2m by 0.2m. The rest of the model is represented by a coarse mesh of 3500 zones, continuously refined towards the tunnel. The model vertical boundaries are fixed horizontally and the bottom boundary is fixed in both vertical and horizontal directions. Overground development is simulated as a 75kPa surcharge applied at the ground surface. The model representing the lining consists of 688 finite difference zones, half for the primary lining and half for the secondary lining. The dimensions of most lining zones are approximately 0.15m by 0.15m, with slightly bigger zones defined for the thick secondary lining invert area.

6.3.3 Ground model

Geotechnical parameters of the ground used in this study are summarised in Table 6-2. They were derived from a series of site investigation and laboratory tests (Mott MacDonald 2009c). Made Ground stiffness was modelled as linear, constant with depth and independent of stress and strain. Previous calibration at Heathrow has demonstrated that the behaviour of London Clay is best represented by an anisotropic soil model with a higher stiffness in the horizontal plane (Chang *et al.* 2001, Scott *et al.* 2003). However, the anisotropy of the soil model is not important for investigation of the long-term load sharing between primary and secondary linings. Thus an isotropic elastic perfectly plastic model was adopted in this study. Nonlinear stiffness of London Clay was simulated by the Jardine A* function (Eadington and Brian 2011, O'Brian and Harris 2013), developed by the geotechnical team within Mott MacDonald. These parameters are summarized in Table 6-3, in which z is the depth below top of London Clay. The short-term (prior to and during construction) and long-term pore water pressure profiles used in modelling are the same. The groundwater table is taken at the top of London Clay, 7m below ground surface, and the water pressure increases linearly to the bottom of the London Clay at a rate of 70% of hydrostatic pressure.

Table 6-2 Geotechnical ground parameters

Soil stratum	Made Ground	Upper London Clay
Bulk unit weight [kNm^{-3}]	20	20
Coefficient of earth pressure at rest K_0	0.5	1.2
Undrained shear strength c_u [kPa]	-	70+11z
Effective cohesion c' [kPa]	0	10
Effective friction angle ϕ' [deg]	25	20
Porosity n [%]	35	45
Drained Poisson's Ratio ν'	0.3	0.1
Drained Elastic Modulus E' [kPa]	5000	ε_s and p' dependant using Jardine function

Table 6-3 Jardine A* parameters for Upper London Clay

A*hh0 [kPa]	A	B	C	α	γ	ε_{amin}	ε_{amax}	G_{min} [kPa]
5,500+60*z	0.43	0.27	$5.0*10^{-5}$	1.76	0.81	5.0*10-5	$2.0*10^{-3}$	6,000

6.3.4 SCL tunnel geometry and sprayed concrete models

The base case SCL tunnel primary and secondary lining geometries are shown in Figure 6-5. The primary and secondary linings are both 300mm thick, except where the secondary lining invert increases from 300mm at the edge to 650mm in the middle. The tunnel is first excavated with a 5.3m diameter circular section pilot tunnel, followed by enlargements in three steps: top heading (TH), bench (BCH) and invert (INV). All the stated dimensions are extrados to extrados. Tunnel axis level is set at 100m ATD. The lining is modelled using elastic zones attached directly to the excavated ground. The primary lining joints between steps (e.g. between TH & BCH) are assumed to be rigidly connected (full normal and shear forces and bending moment transfer using FLAC command 'attach'). Low stiffness beams attached to the half-depth of zones were used to obtain lining axial force and bending moment, as verified in Chapter 5. Discontinuities of plots will be shown at the primary lining joints between steps because beam elements cannot be used in zones in which 'attach' are also used.

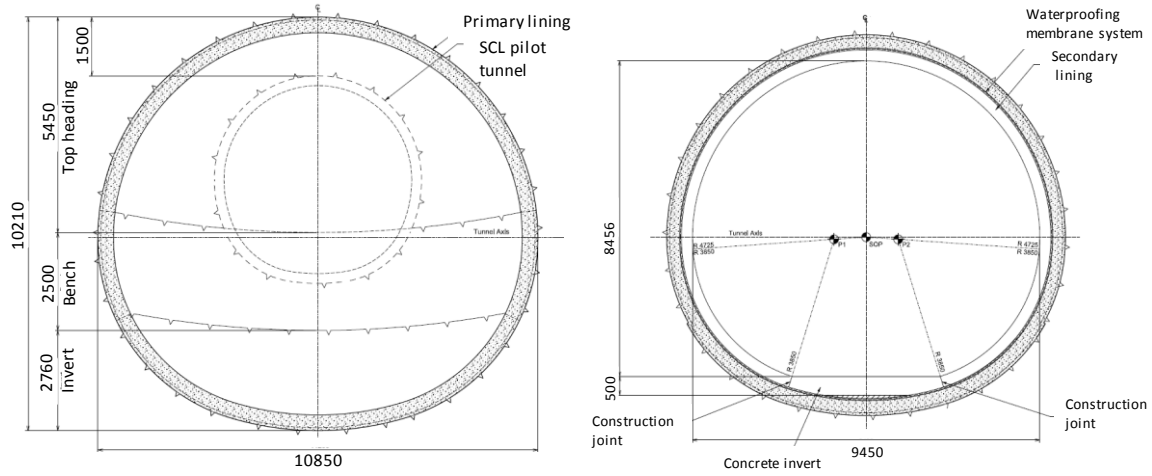

Figure 6-5 SCL tunnel primary and secondary lining geometry

To simulate the time dependent early age properties of sprayed concrete, Chang and Stille's equation (1993) has been used to obtain the development of stiffness

under immediate loading within the first 28 days, shown as the red curve in Figure 6-6. A corresponding stiffness curve for the long-term loading shown in blue on the same figure was derived by adopting a creep factor of 2 based on Eurocode 2 (BS EN 1992-1-1, 2004). After rapid development in the first day, the long-term stiffness starts to increase more linearly with time.

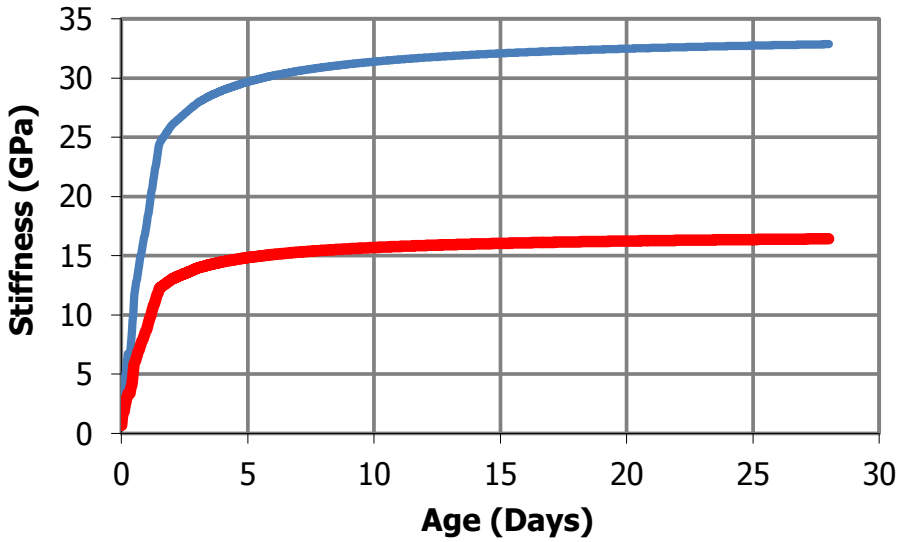

Figure 6-6 Sprayed concrete stiffness development curve

It was assumed for the numerical analysis that the tunnel construction adopted the following construction sequences; (1) two top heading, (2) double bench and (3) double invert. Construction of each top heading was assumed to take 12 hours. Construction of the double bench and double invert were assumed 6 hours each. The sprayed concrete stiffness used in the analysis was calculated according to the age when the next construction step starts. For example, the age of the tunnel crown lining is assumed as 24 hours following completion of the two top headings, 30 hours following double bench excavation and 36 hours at ring closure.

6.3.5 Modelling SCL Tunnel Construction in Soft Ground

The SCL tunnel construction-induced short-term ground deformation and lining forces were simulated using the stress reduction method (Panet and Guenot 1982). This method assumes a fictitious tunnel internal pressure that is firstly set equivalent to the initial ground stress and is then reduced by a certain percentage to model the sequential tunnel excavation, allowing the lining to deform and

carry a proportion of the initial ground stress. The specific stress relaxation ratios have been calibrated against monitoring data for previous SCL tunnel construction in London (Mott MacDonald 2010b) and are reproduced in Table 6-4.

The ground is assumed to behave in an undrained condition and the sprayed concrete lining is modelled as an impermeable material. Tresca theory is used to predict the shear strength of the soil. After installation of the primary lining, undrained equilibrium of loads in the ground and tunnel lining is obtained. After that, the interface elements, representing the sprayed concrete-membrane interface and the zones, representing the secondary lining, are installed and assigned their long-term properties. Drained equilibrium is executed and Mohr-Coulomb theory used to predict the shear strength of the soil.

Table 6-4 Stress relaxation ratios

Tunnel	Stage	TH	BCH	INV
SCL Pilot tunnel	Full face excavation	100%-50%		
	Lining installation	50%-0%		
SCL tunnel enlargement	Enlarge whole tunnel	100%-75%	100%	100%-75%
	Install TH lining	75%-50%	100%-75%	75%-50%
	Install BCH lining	50%-25%	75%-50%	50%-25%
	Install INV lining	25%-0%	50%-0%	25%-0%

6.3.6 Interface parameters

Interface elements had been used in the CSL tunnel to enable the simulation of composite action between the two layers of tunnel lining as well as the sandwiched layer of sprayed membrane. Previous research concluded that for a nominal membrane thickness between 2mm and 4mm, the best fit base value short-term normal (kn) and shear (ks) interface stiffnesses are 8GPa/m and 4GPa/m respectively. It also found that long-term stress after relaxation for the interface under compression, tension and shear is between 46% and 59% of initial stress. For this study, a creep factor of 2 was assumed to calculate the base long-term interface parameters (kn=4GPa/m and ks=2GPa/m). The interface was assumed to be linear elastic-perfectly plastic with tensile and shear strengths of 0.8MPa and 2.0MPa respectively, both of which were the minimum values

obtained from the laboratory tests. These interface parameters were used in the base case analysis.

6.4 Base case results

6.4.1 Short-term lining forces

Figure 6-7 shows the primary lining short-term axial force and bending moment. The axial force gradually increases from 850kN at the crown to around 1100kN above the axis, and then reduces to around 450kN at the invert. This is attributed to the fact that the lining at the top heading is the first part to be built and thus takes more axial force when compared to the bottom half of lining. The biggest bending moment occurs between the axis and the knee, with values around 25kNm, attributed to the reduced radius of lining curvatures.

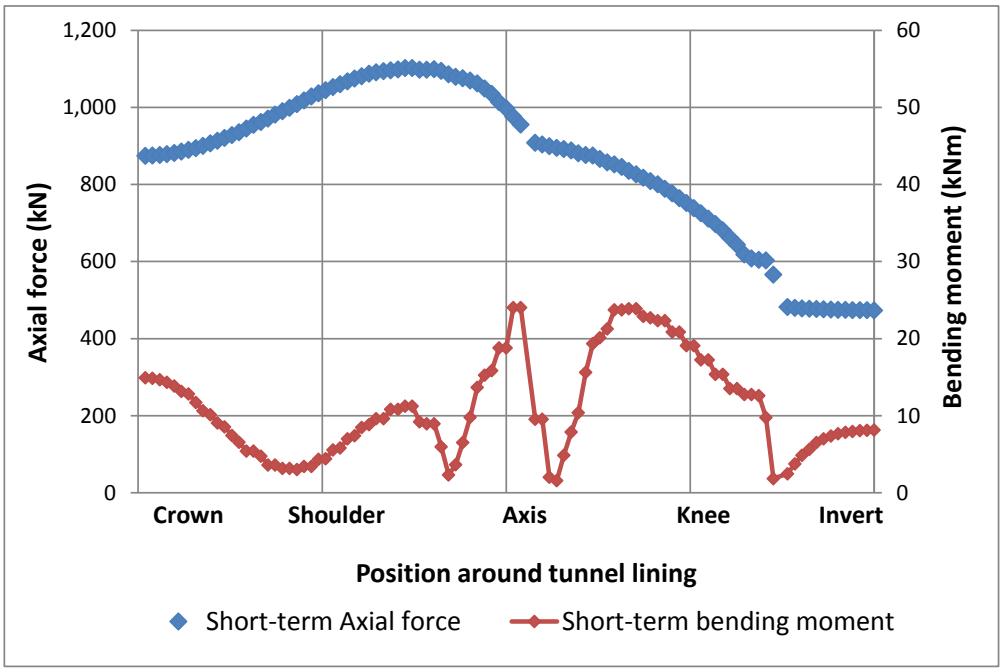

Figure 6-7 Primary lining short-term axial force and bending moment

6.4.2 Load sharing for the consolidation loads

Figure 6-8 shows the long-term consolidation axial force and bending moment for the primary and secondary linings. The primary lining shares more axial force above the shoulder and below the knee whilst sharing less between the shoulder and the knee. It is noteworthy that 50kNm of pure tension occurs at the secondary lining crown. The reason for this is discussed in the following sections.

The secondary lining shares more bending moment at all positions except around the knee. This is due to the complex ground-structure interaction and the composite actions between the primary and secondary linings, and is further discussed in the following sections.

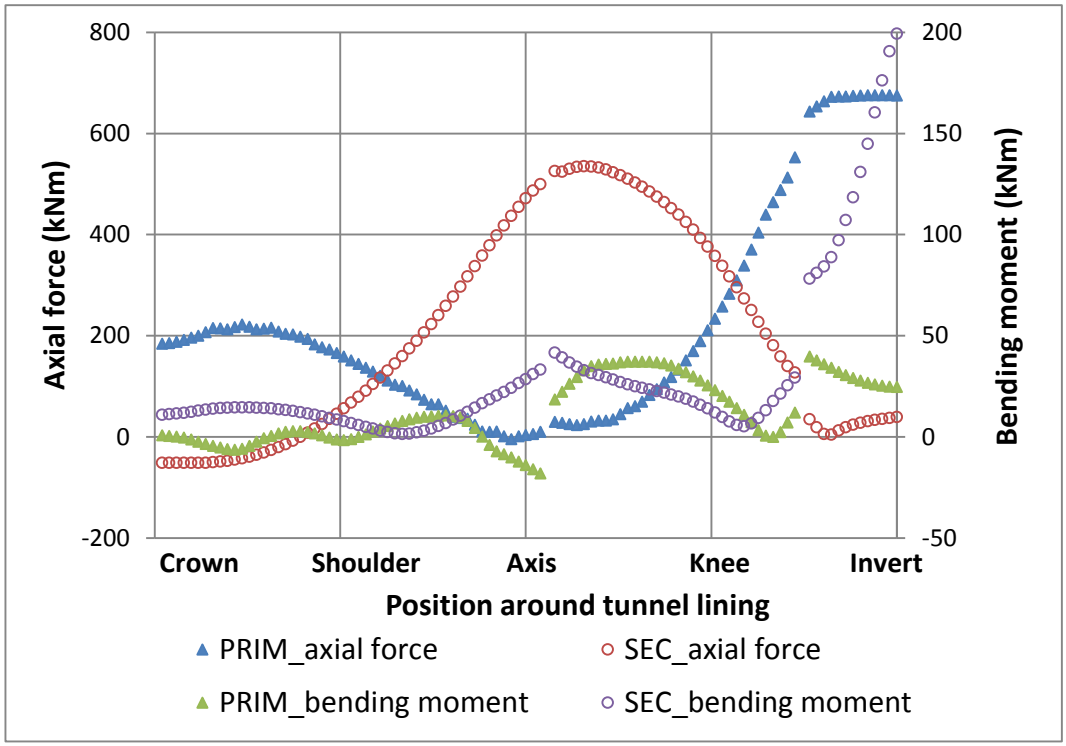

Figure 6-8 Long-term consolidation axial force and bending moment for the primary and secondary linings

6.4.3 Lining capacity and BM/AF ratio

Figure 6-9 shows two lining capacity curves, from Figure 6-1, superimposed with the total lining forces for the primary and secondary linings. It shows the primary lining forces are well within the capacity curve whilst some of the secondary lining forces are outside the capacity curve. The BM/AF ratio diagram is used to explore the lining positions with insufficient capacity (Figure 6-10). The primary lining BM/AF ratios at all positions are below 0.1, lower than the safety ratio of 0.17 by the red line in Figure 6-9, so no reinforcement is needed. In contrast, the BM/AF ratios for the secondary lining above the shoulder and below the knee are either greater than the safety ratio of 0.17 (bending failure) or less than 0 (tension failure), meaning reinforcement is needed at these two positions. No reinforcement is needed for the other parts of the secondary lining.

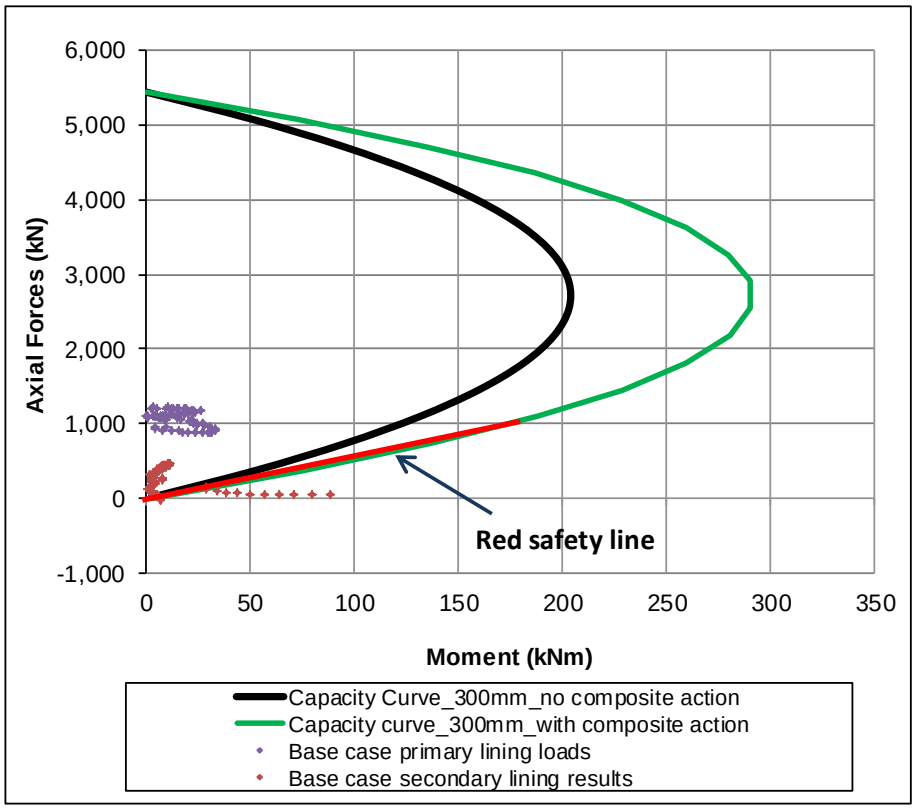

Figure 6-9 Composite component lining loads and capacity curves

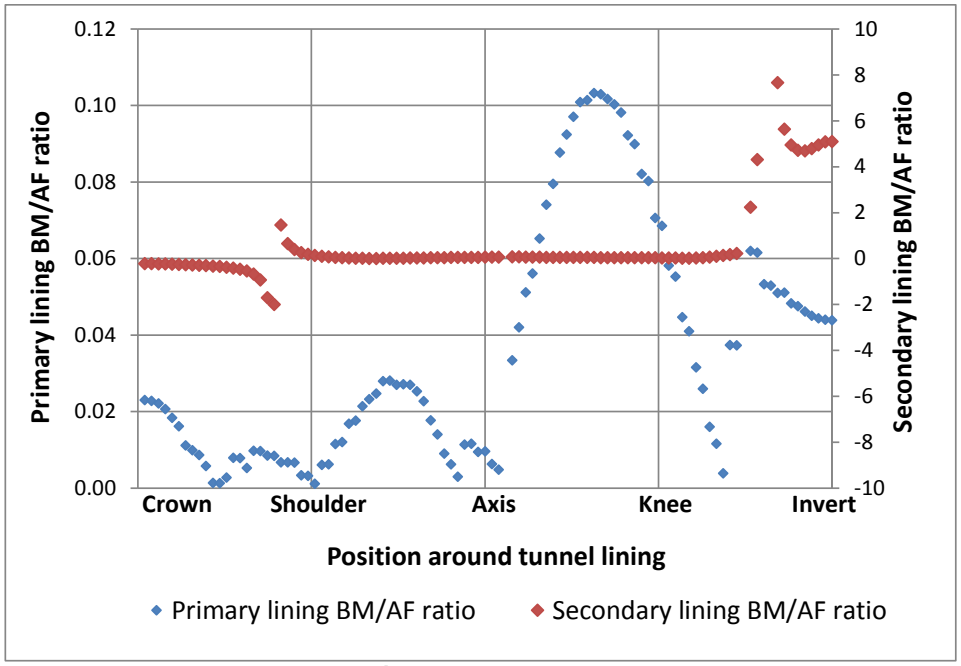

Figure 6-10 BM/AF ratios for base case primary and secondary lining

6.4.4 Behaviour of the interface

Figure 6-11 shows the base case normal and shear interface stresses. The maximum normal interface stress is around 20kPa in compression (positive value) at the crown and changes almost linearly to the maximum tension around -150kPa (negative value) at the axis. It then reduces to around zero at the construction joints between the knee and the invert before increasing back to -70kPa (tension) at the centre of the invert, well below the tension limit of 0.8MPa.

The tension interface stresses at the axis indicate the secondary lining has been stretched horizontally outwards, pulling the crown into tension. The normal interface stress at the invert was in tension, mostly due to the bigger bending moment in the secondary lining invert introducing greater deformation than that in the primary lining invert. This is consistent with the lining deformation as shown in Figure 6-12, in which a red circle shows the (approximate) original tunnel profile prior to the deformation.

The shear interface stress varies between 0 and 150kPa from crown and axis and changes to -170kPa (opposite direction) at the knee, before returning to zero at the centre of the invert. These values are all below the shear stress limit of 2MPa. The two biggest shear interface stresses (biggest bending curvatures) occur at the shoulder and knee, corresponding with the lining deformation as shown in Figure 6-12.

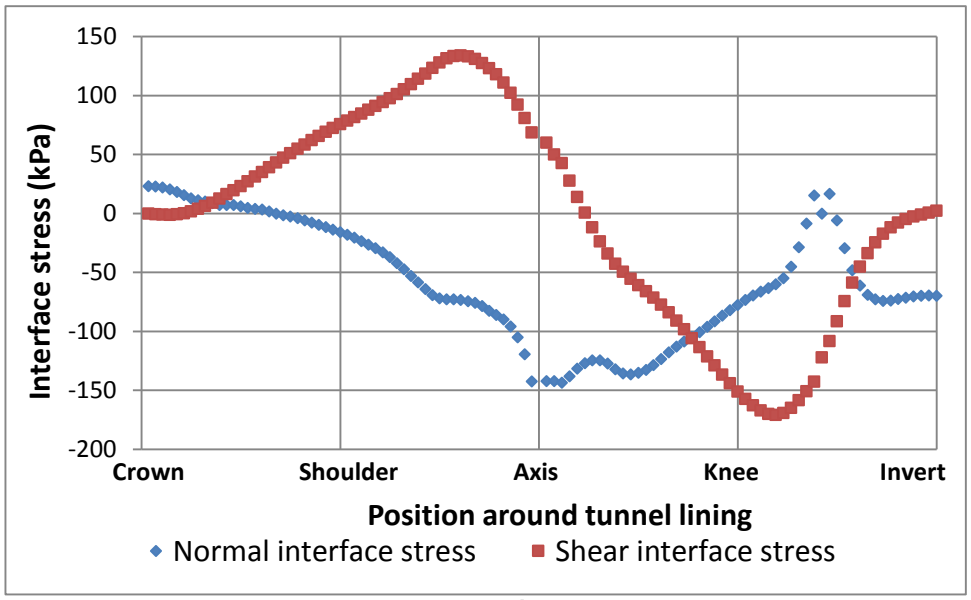

Figure 6-11 Normal and shear interface stresses

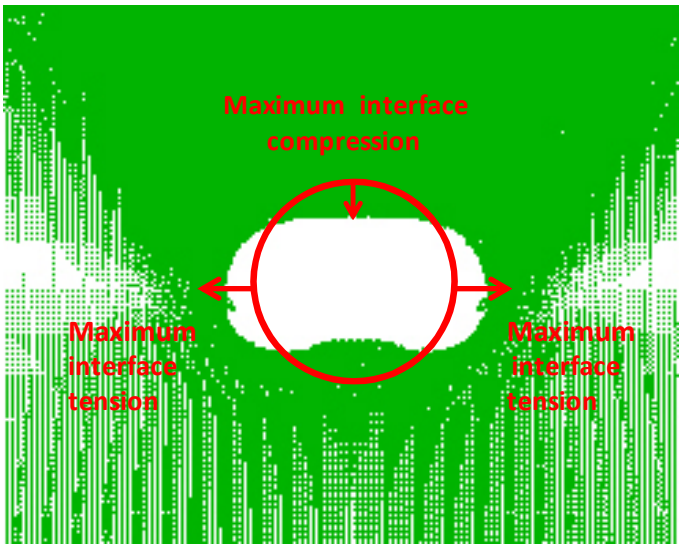

Figure 6-12 Deformation of a CSL tunnel

6.4.5 Degree of composite action

Figure 6-13 and Figure 6-14 compare the axial force and bending moment of the base case CSL with that of full CSL (*i.e.* CSL tunnel with full composite action) and non CSL (DSL) tunnels of the same dimensions and ground conditions, to quantify its degree of composite action. It can be seen that the axial forces of the base case are very close to those of the full CSL tunnel whilst the bending moment of the base case varies between the corresponding full and non CSL tunnel values.

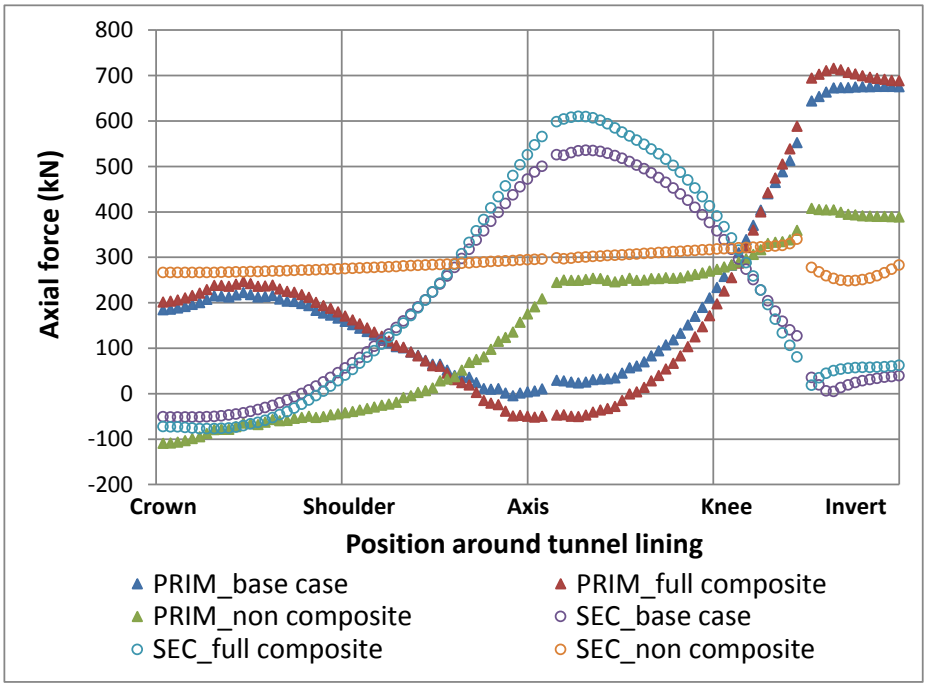

Figure 6-13 Long-term consolidation axial force for primary lining and the axial force for secondary lining.

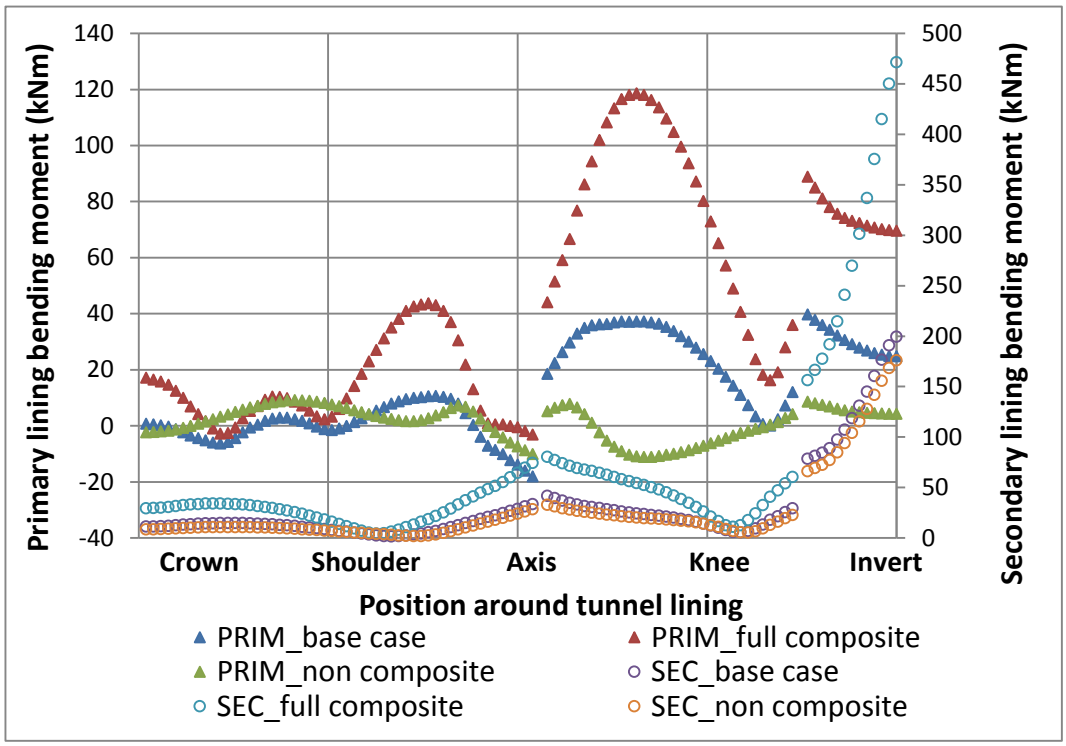

Figure 6-14 Long-term consolidation bending moment for primary lining and the bending moment for secondary lining.

6.5 Influence of normal interface stiffness Kn

This and the following two sections investigate the impact of variance in interface stiffnesses on the behaviour of the CSL tunnel. These analyses address the following scenarios; (1) use of a different membrane product with different interface parameters and (2) variance of workmanship during the membrane interface preparation.

For this study, the interface normal stiffness Kn was magnified by 10 and 100 times as well as reduced to 1/10 and 1/100 of the base value. The results have then been compared with the base value to evaluate their sensitivity.

6.5.1 Axial force

Figure 6-15 shows that the primary lining long-term consolidation axial force decreases and the secondary lining axial force increases with an increase in normal interface stiffness prior to reaching the base Kn value of 4GPa/m at all positions except the crown and the invert. This follows the trend that the greater

the normal interface stiffness, when Kn is less than the base value more consolidation loads are taken by the secondary lining. When Kn is at the base value, the primary lining has transferred all of its transferable forces to the secondary lining, mostly due to the tunnel deformation. Therefore, further increase in the Kn value does not correspond to a further increase the transferred lining forces.

The biggest axial force transfer occurs at axis level. It is noteworthy that no tension occurs at the secondary lining crown and less compression is experienced at the axis for the lowest normal interface stiffness case (Kn=0.04GPa/m). This is mainly because the weak interface stiffnesses allow the secondary lining to deform more freely, reducing the "stretching" effect at the crown.

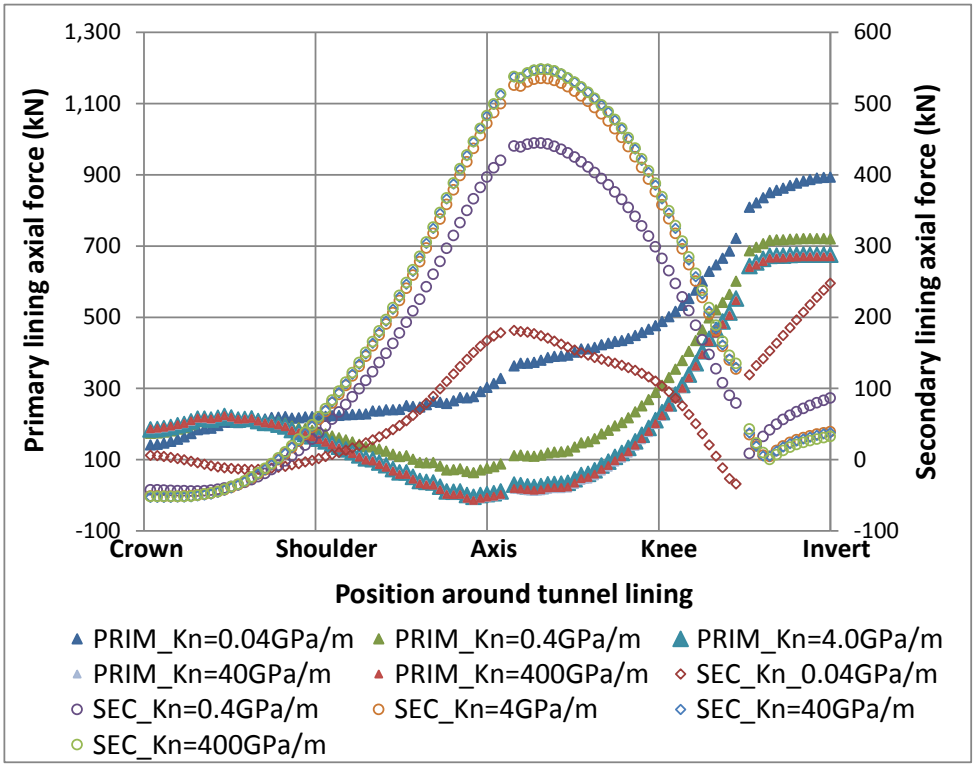

Figure 6-15 Sensitivity of primary and secondary lining axial force to normal interface stiffness Kn

6.5.2 Bending moment

Figure 6-16 shows that, prior to the base value, the higher the normal interface stiffness, the higher the long-term consolidation bending moment in the primary and secondary linings.

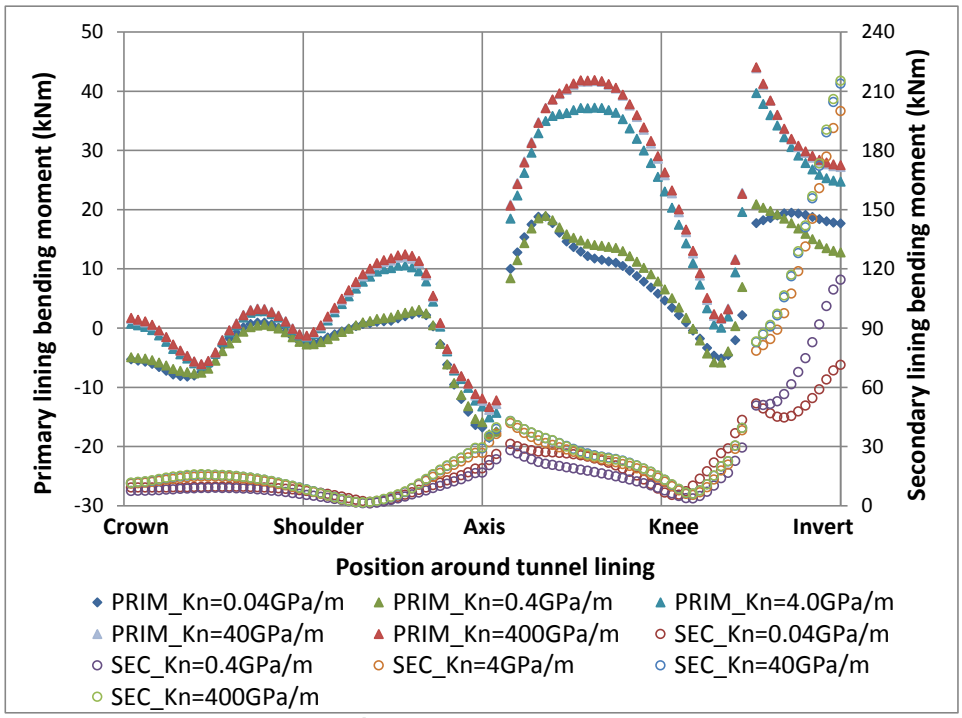

Figure 6-16 Sensitivity of primary and secondary lining bending moment to normal interface stiffness Kn

6.5.3 Evaluation of lining capacity

Similar to the base case, the capacity of the primary lining is not a concern as the normal stiffness is varied. A calculation shows the safety BM/AF ratios for these five cases are between 0.12 (lowest Kn case) and 0.18 (highest Kn case). Figure 6-17 shows that all cases for the secondary lining exceed the safety BM/AF ratios above the shoulder and below the knee but also below the safety ratio between the shoulder and the knee. The lower the normal interface stiffness, the lower the BM/AF ratio. This trend does not apply to the Kn=0.04GPa/m case because its secondary lining axial force is much lower than the other cases but its bending moment is similar to that of the Kn=0.4GPa/m case, leading to a higher BM/AF ratio.

6.5.4 Interface stresses

Figure 6-18 and Figure 6-19 show that the normal and shear interface stresses increase significantly when the normal interface stiffness Kn increases from 0.04GPa/m to 0.4GPa/m but only slightly when Kn further increases. This corresponds with previous observations on the axial force and bending moment. The maximum normal and shear interface stresses are 20kPa (compression),

130kPa (tension) and 160kPa (shear) respectively, all of which are well within the interface stress limits.

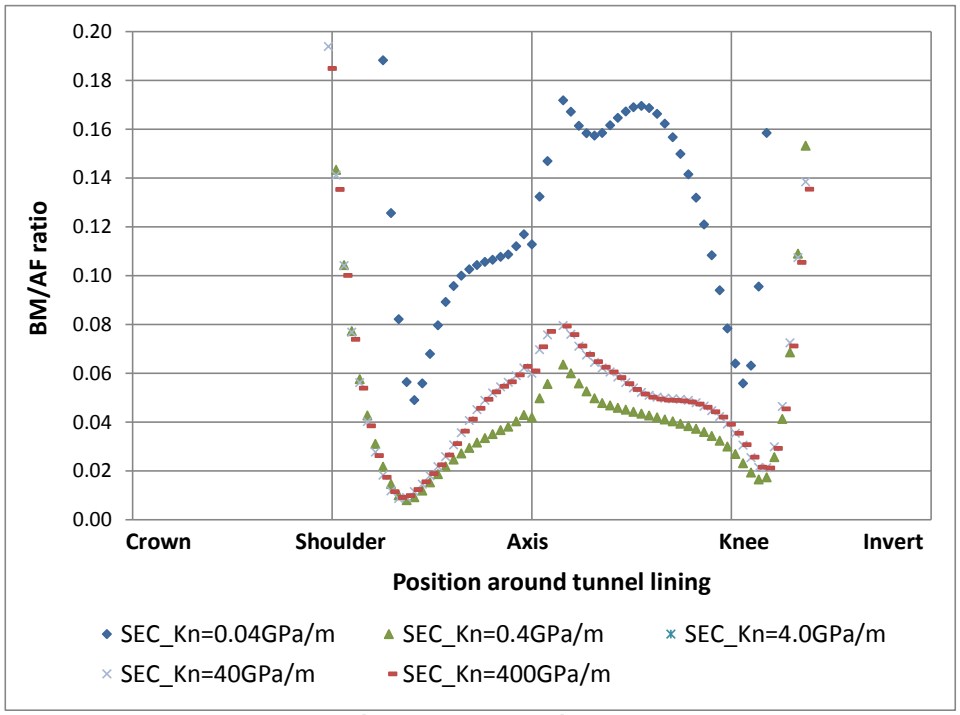

Figure 6-17 Sensitivity of BM/AF ratio for secondary lining to normal interface stiffness Kn

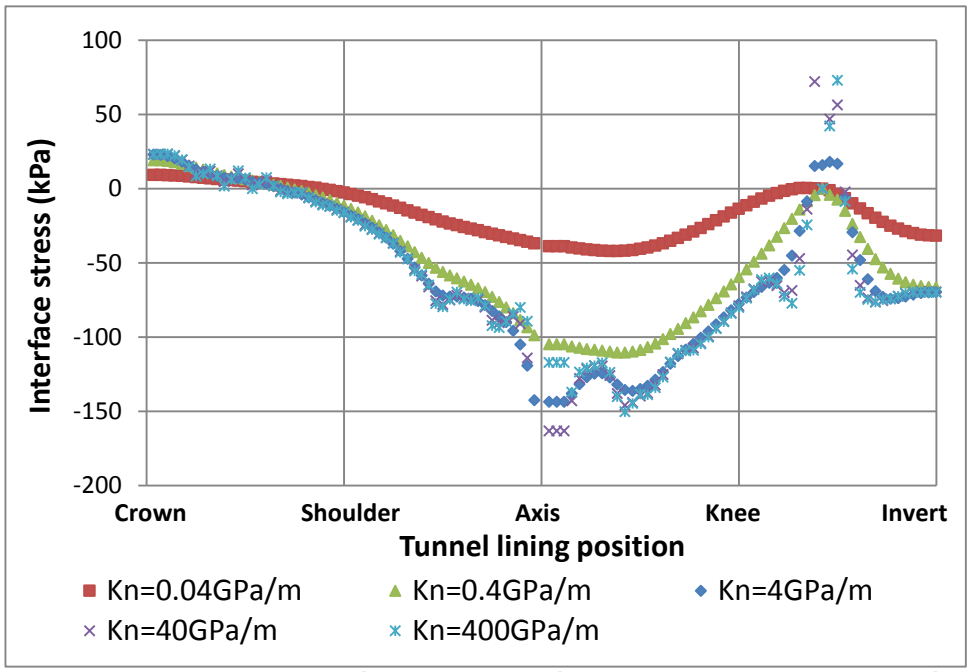

Figure 6-18 Sensitivity of normal interface stress to normal interface stiffness Kn (compression is positive)

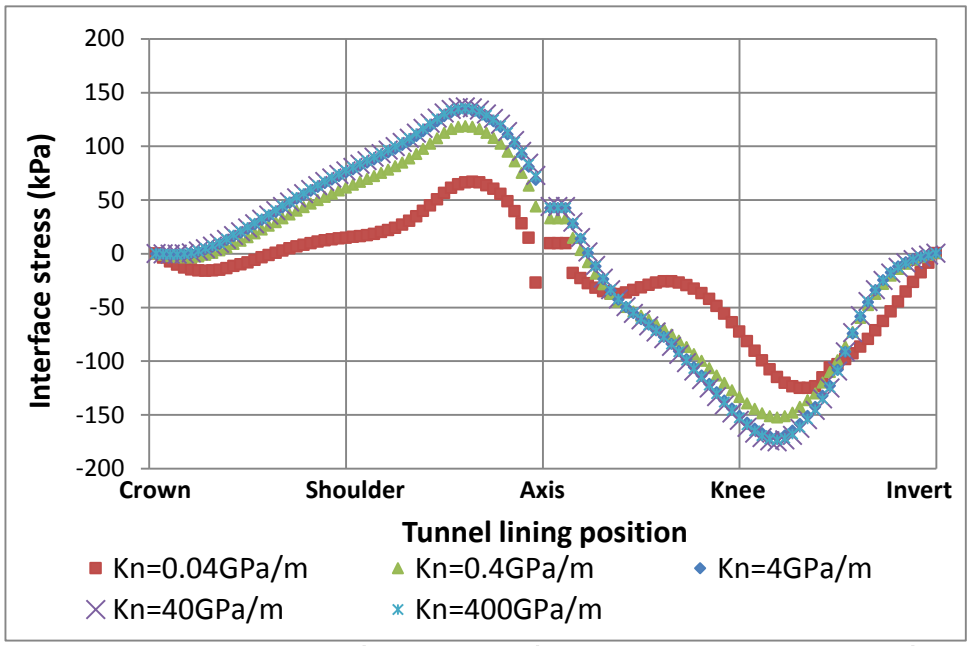

Figure 6-19 Sensitivity of shear interface stress to normal interface stiffness Kn

6.6 Influence of shear interface stiffness Ks

For this study, the interface shear stiffness Ks was varied using the same magnification and reduction factors used in the Kn investigation. The results have then been compared with the base value to evaluate their impact.

6.6.1 Axial force

The trend in Figure 6-20 is very similar to that in Figure 6-15 in that the biggest secondary lining axial force occurs at the axis. The lower the shear interface stiffness, the higher the compression axial force observed at the secondary lining crown.

6.6.2 Bending moment

The trend in Figure 6-21 is also very similar to that observed in Figure 6-16 in that the higher the shear interface stiffness, the higher the bending moment in the primary and secondary linings. One noteworthy point is that the maximum primary and secondary lining bending moments are around 95kNm and 80kNm for the Kn=4GPa/m and Ks=200GPa/m cases. This is approximately double the corresponding maximum bending moments for the Kn=400GP/m and

Ks=2GPa/m cases respectively. This confirms the previous conclusions that Ks has a bigger impact on the degree of composite action.

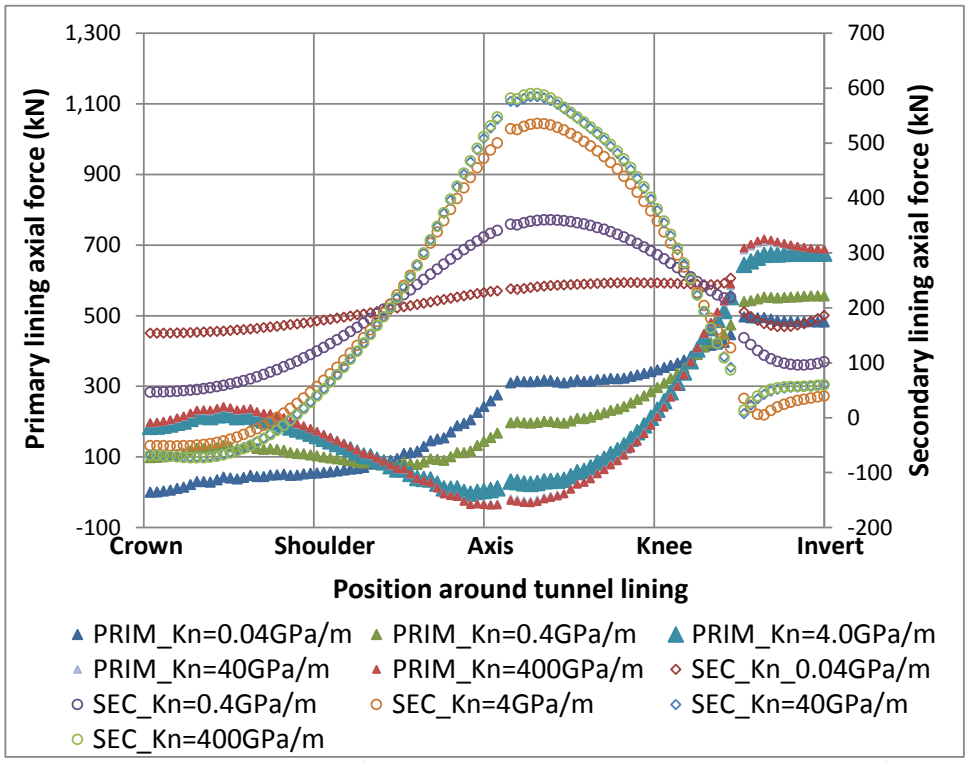

Figure 6-20 Sensitivity of primary and secondary lining axial force to shear interface stiffness Ks

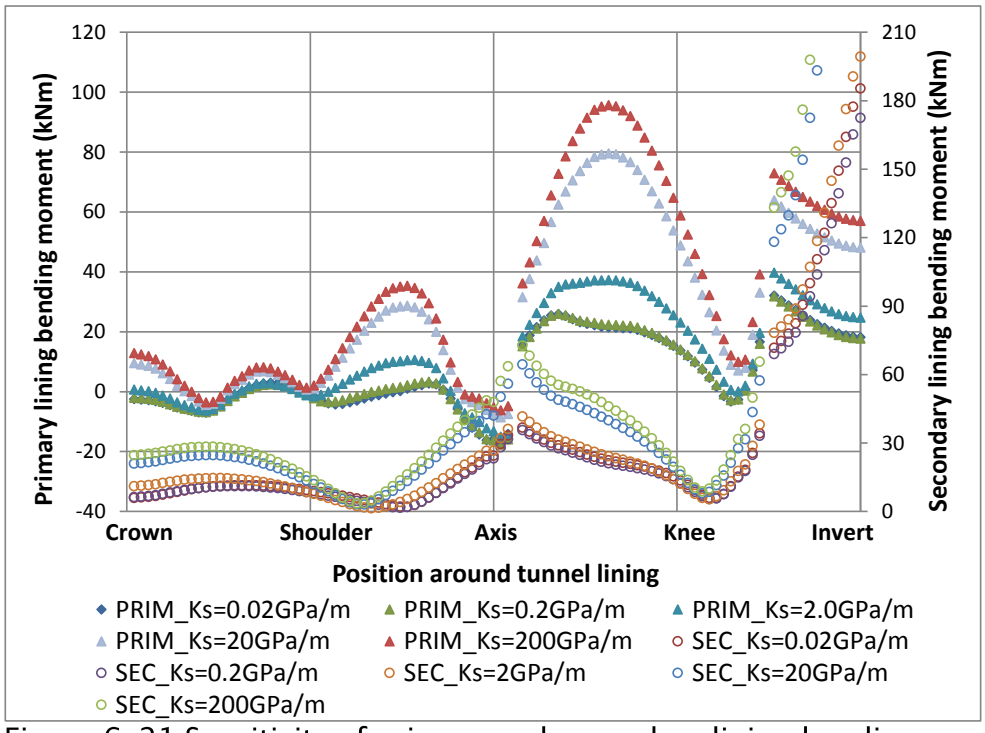

Figure 6-21 Sensitivity of primary and secondary lining bending moment to shear interface stiffness Ks

6.6.3 Evaluation of lining capacity

A calculation shows the safety BM/AF ratios for these five cases are between 0.12 (lowest Ks case) and 0.28 (highest Ks case). Figure 6-22 shows that all cases exceed the safety BM/AF ratios above the secondary lining shoulder and below the knee, as also observed in the Kn sensitivity study results. All other lining positions are within the safety ratio. It also shows that the lower the Ks value, the safer the secondary lining, except for Ks=0.02GPa/m case, as discussed previously.

6.6.4 Interface stress

The shapes of the normal and shear interface stress plots of this Ks parametric study are very similar to those for Kn. The interface stresses increase significantly when the shear interface stiffness Ks increases from 0.02GPa/m to 2GPa/m, but only slightly when Ks further increases. The maximum normal and shear interface stresses are 30kPa (compression), 160kPa (tension) and 220kPa (shear) respectively, well within the interface stress limits.

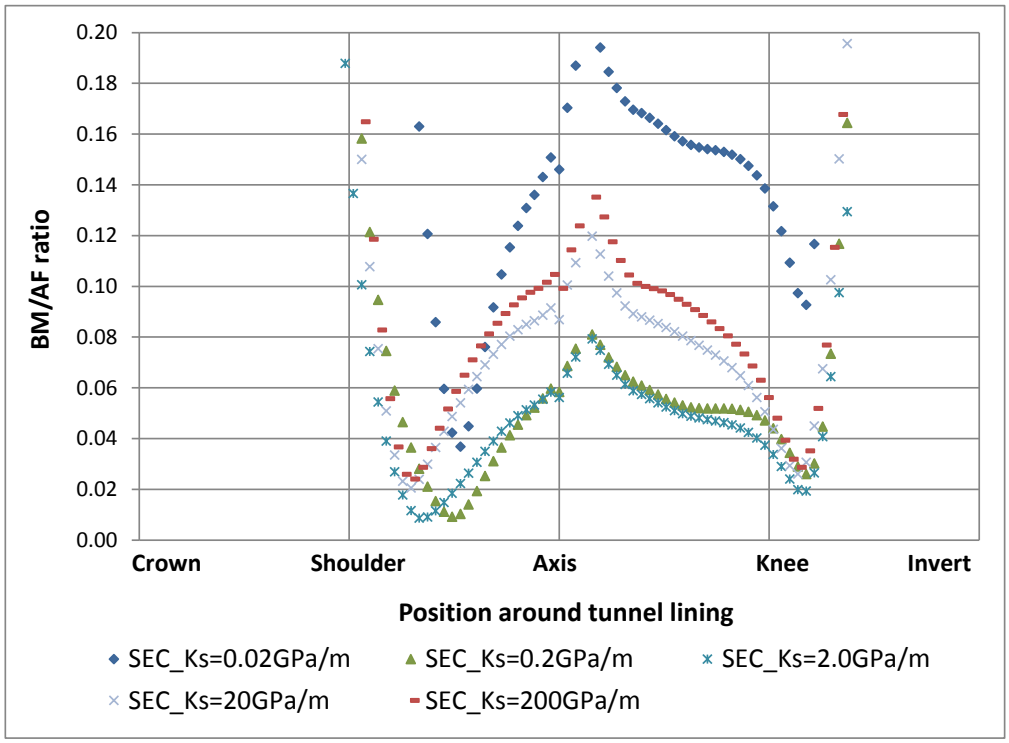

Figure 6-22 Sensitivity of BM/AF ratios for secondary lining to shear interface stiffness Ks

6.7 Simultaneous influence of Kn and Ks

The effect of varying Kn and Ks simultaneously was established by multiplying the previously stated multiplication factors. The results will then be compared with the base value to evaluate their impact. Only the conclusions are presented here and the plots for this Section are shown in Appendix D.

6.7.1 Axial force

The results confirm the previous observation that (1) the higher the normal and shear interface stiffness, the higher proportion of load that is transferred from the primary to the secondary lining, (2) a tension force would occur at the secondary lining crown when Kn and Ks are equal to or bigger than the base values and (3) there is little change in axial force for further increase in Kn and Ks above the base values.

6.7.2 Bending moment

The results confirm the previous observation that (1) the higher the normal and shear interface stiffness, the higher the bending moment for both the primary and secondary linings, (2) increasing both interface stiffnesses simultaneously from the base values significantly increases the magnitude of bending moment, and (3) Reducing the two interface stiffnesses simultaneously from the base values would reduce the magnitude of the bending moment, but to a much lesser extent than that compared with the stiffness increase scenarios.

6.7.3 Evaluation of lining capacity

Calculation shows that the safety BM/AF ratios for these five cases are between 0.12 (lowest Kn & Ks case) and 0.30 (highest Kn & Ks case). Results show that the primary lining is safe for all cases, whilst the secondary lining is safe only between the shoulder and knee, as previously observed.

6.7.4 Interface stress

The maximum normal and shear interface stresses are very close to those values in the Ks sensitivity study and are all within the interface stress limits.

6.8 Influence of lining thickness

This section investigates the impact of variance in lining thickness on the performance of both linings and the interfaces, from which recommendations for an efficient CSL tunnel design can be drawn.

This investigation consisted of two analysis parts. In the first stage, the primary lining thickness was varied from 50mm to 300mm at 50mm intervals, whilst the secondary lining thickness was kept constant at 300mm. Therefore the primary/secondary lining thickness (P/S) ratio ranged from 1/6 to 1. In the second stage, the secondary lining thickness was varied from 50mm to 300mm at 50mm intervals, whilst the primary lining thickness was kept constant at 300mm, leading to ratio ranges from 1 to 6. For the purpose of this investigation, only the BM/AF ratio and interface stress results are presented and discussed. Other results are shown in Appendix E.

6.8.1 Evaluation of lining capacity (P/S≤ 1)

Figure 6-23 shows the sensitivity of the primary lining BM/AF ratio to varying P/S ratios (P/S ratio≤1). Similar to previous observations, the primary lining in all cases is safe. The smaller the P/S ratio, the “safer” the primary lining. This is mostly attributed to a faster reduction in bending moment than the corresponding reduction in axial force.

Figure 6-24 shows the sensitivity of the secondary lining BM/AF ratio to varying P/S ratios (P/S ratio≤1). The smaller the P/S ratio, the “safer” the secondary lining. Similar to previous observations, the secondary lining between the shoulder and the knee is safe for all cases and the secondary lining at the invert always demonstrates a need for reinforcement. When the P/S ratio is smaller than 0.5, the secondary lining crown does not require reinforcement.

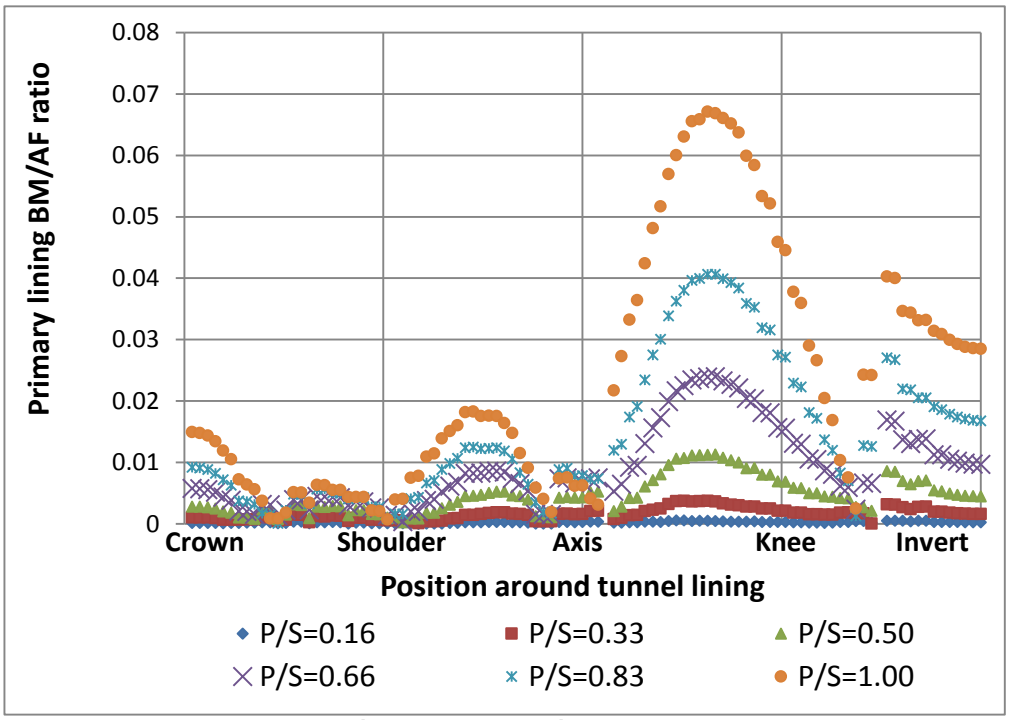

Figure 6-23 Sensitivity of BM/AF ratio for primary lining to varying primary/secondary lining thickness ratio (P/S ratio≤1)

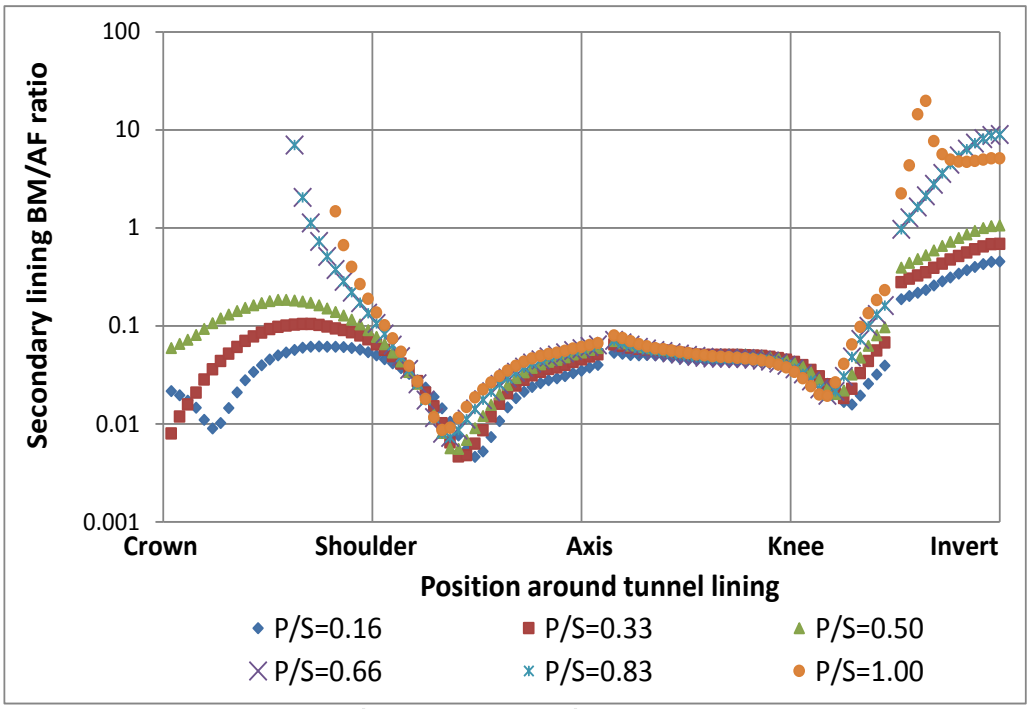

Figure 6-24 Sensitivity of BM/AF ratios for secondary lining to varying primary/secondary lining thickness ratio (P/S ratio≤1)

6.8.2 Evaluation of lining capacity (P/S≥1)

Figure 6-25 shows the sensitivity of the primary lining BM/AF ratios to varying P/S ratio (P/S ratio≥1). Similar to previous observation, in all cases the entire primary lining ring is safe. The greater the P/S ratio, the "safer" the primary lining. This is mostly attributed to a faster increase in axial force than the corresponding increase in bending moment.

Figure 6-26 shows the sensitivity of the secondary lining BM/AF ratios to varying P/S ratio (P/S ratio≥1). The bigger the P/S ratio, the "safer" the secondary lining. Similar to previous observation, the secondary lining between the shoulder and the knee is safe for all cases and the secondary lining at the invert always demonstrates a need for reinforcement. When the P/S ratio is bigger than 3.0, the secondary lining crown does not require reinforcement.

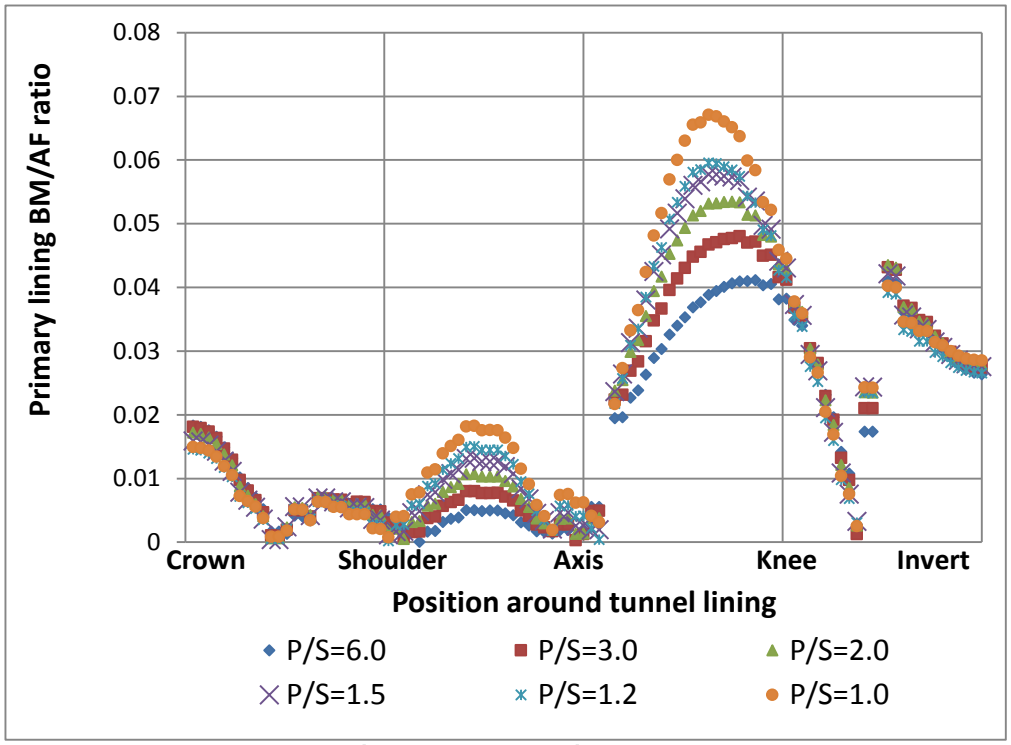

Figure 6-25 Sensitivity of BM/AF ratios for primary lining to varying primary/secondary lining thickness ratio (P/S ratio≥1)

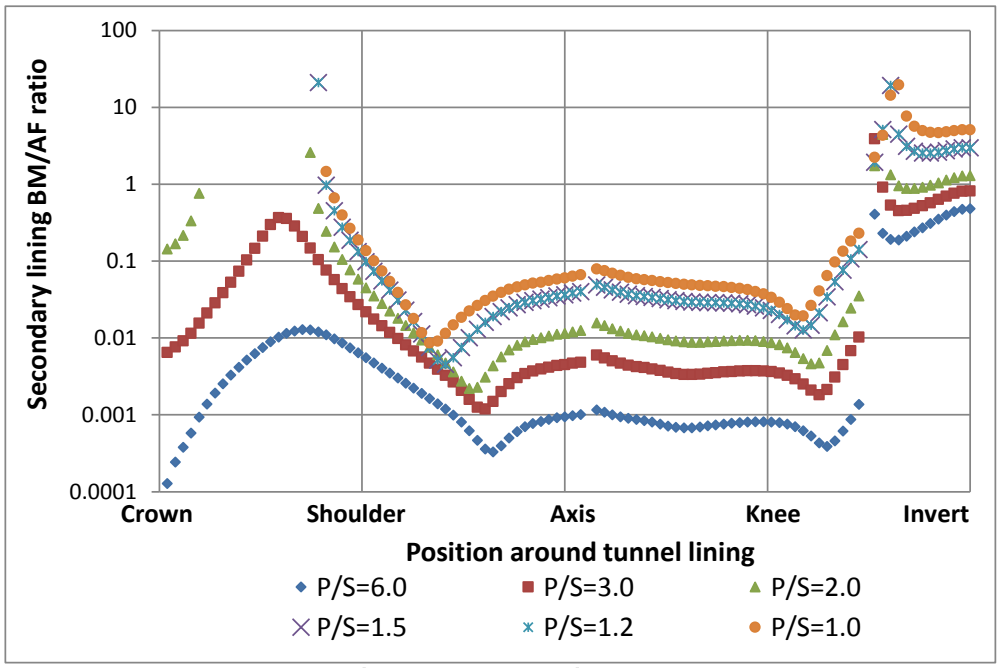

Figure 6-26 Sensitivity of BM/AF ratios for secondary lining to varying primary/secondary lining thickness ratio (P/S ratio≥1)

6.8.3 Interface stress (P/S≤1)

Figure 6-27 shows the sensitivity of normal interface stress to varying P/S ratio (P/S≤1). The smaller the P/S ratio, the bigger the normal interface stress. This is mainly due to the thicker secondary lining sharing more consolidation loading.

Figure 6-28 shows the sensitivity of shear interface stress to varying P/S ratio (P/S≤1). The closer to 1 the P/S ratio, the bigger the shear interface stress, confirming the principle established in Chapter 5 that the degree of composite action (*i.e.* the magnitude of shear interface stress) is most significant when the interface is located at the half-depth of composite linings.

All shear interface stresses are less than 170kPa, well below the shear stress limit of 2MPa.

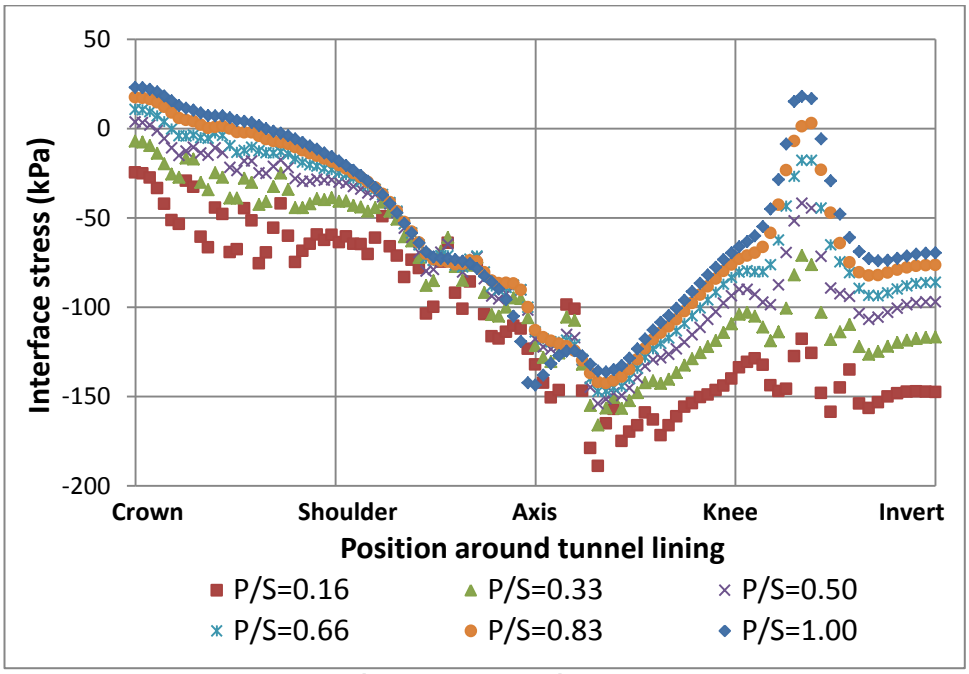

Figure 6-27 Sensitivity of normal interface stress to varying primary/secondary lining thickness ratio (P/S ratio≤1)

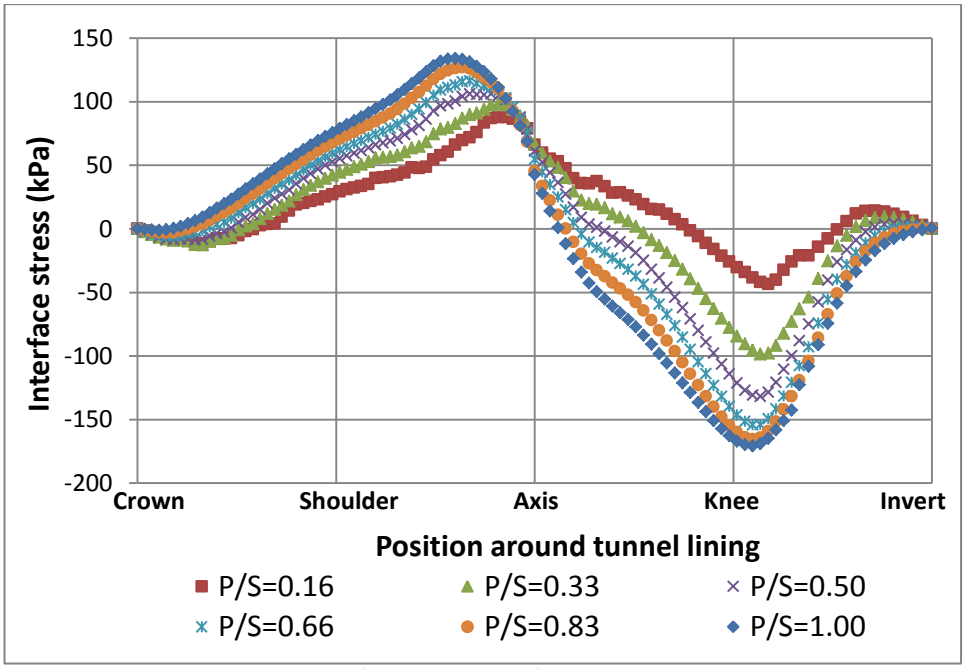

Figure 6-28 Sensitivity of shear interface stress to varying primary/secondary lining thickness ratio (P/S ratio≤1)

6.8.4 Interface stress (P/S≥1)

The sensitivity of normal and shear interface stresses to P/S ratio (P/S ratio≥1) are very similar to those for P/S ratio≤1. The smaller the P/S ratio, the bigger the normal interface stress, mainly attributed to a bigger stiffness of the thicker secondary lining. The highest normal interface stress is around 150kPa in tension at axis level. The closer to 1 the P/S ratio is, the bigger the shear interface stress. This again confirms the principle that the degree of composite action (*i.e.* the magnitude of shear interface stress) is most significant when the interface is located at the half-depth of composite linings. All shear interface stresses are less than 170kPa, well below the shear stress limit of 2MPa.

6.9 Influence of nearby construction

6.9.1 Investigation and modelling strategy

Two investigations into the effect of nearby construction were carried out; simulating works adjacent to the CSL tunnel and those directly beneath it.

For these investigations, rather than modelling the actual underground construction operations (*e.g.* tunnelling or diaphragm wall construction), notional forces were applied in the nearby ground to introduce shear strains of the magnitude that could reasonably be generated by such activities. Atkinson and Salfors (1991) and Mair (1993) reported the shear strain ranges for different types of underground construction, from which the tunnel construction usually generates shear strains of between 0.1 and 1%.

For each investigation, five cases were analysed with different clear distances between the notional forces and the closest tunnel linings: 2m, 4m, 6m, 8m and 10m. In each case, 100kPa pressure was applied to a linear boundary acting either away towards the right or away beneath the tunnel. This generated a shear strain of around 1% in the ground at the notional force linear boundary at the upper half of the tunnel level and smaller values when the depth increases. The shear strain generated in this study therefore represents a conservative case (*e.g.* the upper limit of shear strain). The linear boundary has the same length as the tunnel diameter. A schematic diagram for this parametric study is shown in Figure 6-29.

The SCL tunnel diameter is approximately 10m and the gap between the tunnel and stress linear boundary is between 2m–10m, therefore, the analysed cases could be generalised by introducing a gap distance to tunnel diameter ratio:

$$R_g = \frac{D_g}{D_t} \qquad \text{Equation 6-1}$$

Where:

R_g: clear gap distance to tunnel diameter ratio (abbreviated as GT ratio)

D_g: clear gap distance from the extrados of tunnel to the nearby construction (*i.e.* stress linear boundary) (unit: m)

D_t: tunnel diameter (unit: m)

As the main purpose of this study is to investigate the robustness of the CSL tunnel, only interface stress results are presented and discussed here. All other results are shown in Appendix F.

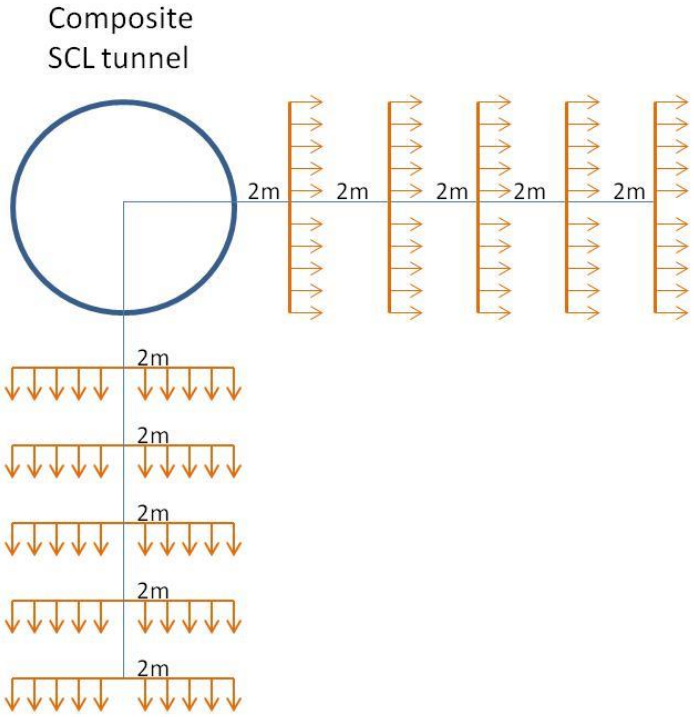

Figure 6-29 Schematic diagrams of notional forces applied to the CSL model simulating nearby construction (the arrows represent the direction of applied force)

6.9.2 Interface stress – beneath construction

Figure 6-30 and Figure 6-31 show that the smaller the GT ratio, the greater the change in the normal and shear interface stress at all lining positions. However, all the interface stresses are less than 50kPa and therefore, well within the interface stress limit.

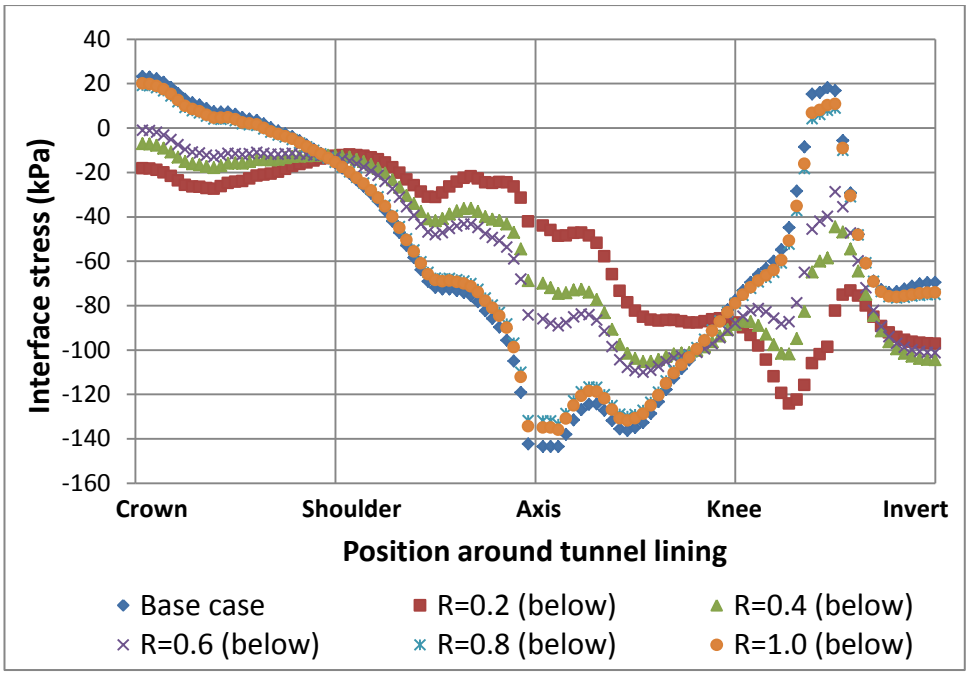

Figure 6-30 Sensitivity of normal interface stress to the underneath construction

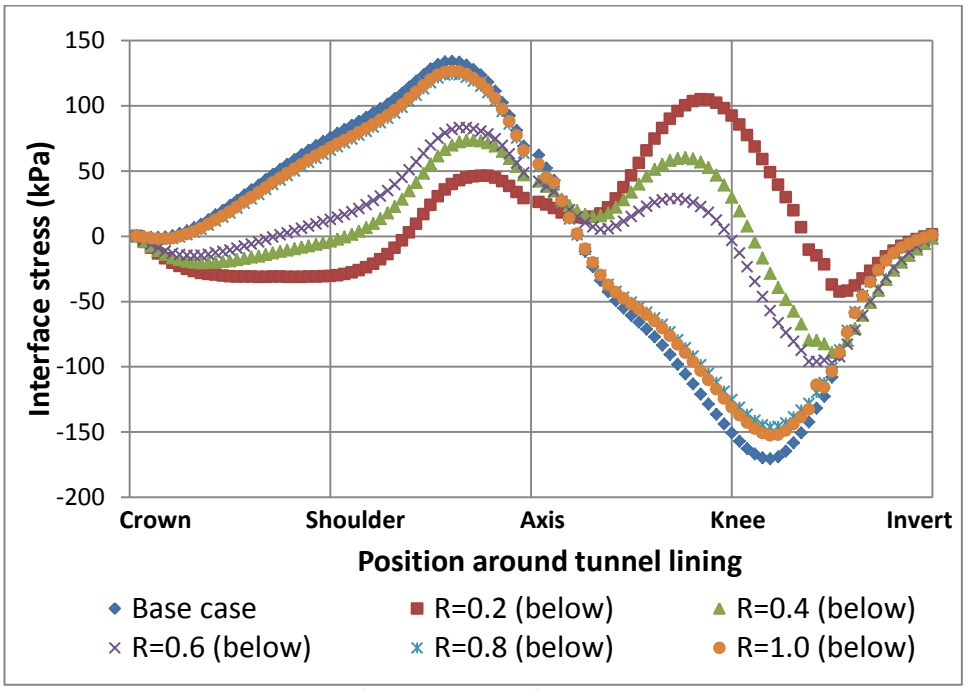

Figure 6-31 Sensitivity of shear interface stress to the underneath construction

6.9.3 Interface stress – right hand side construction

Figure 6-32 shows that the maximum compression occurs at the connection between knee and invert and the maximum tension occurs at axis, both at a magnitude of 400kPa. This represents 50% of the tensile stress limit (800kPa established in Chapter 4).

Figure 6-33 shows that the maximum shear stress occurs between the axis and the knee, with a magnitude of about 650kPa. This is significantly lower than shear stress limit of 2MPa established in Chapter 4. Both Figures show that the closer the proximity of the RHS construction, the greater the interface stresses.

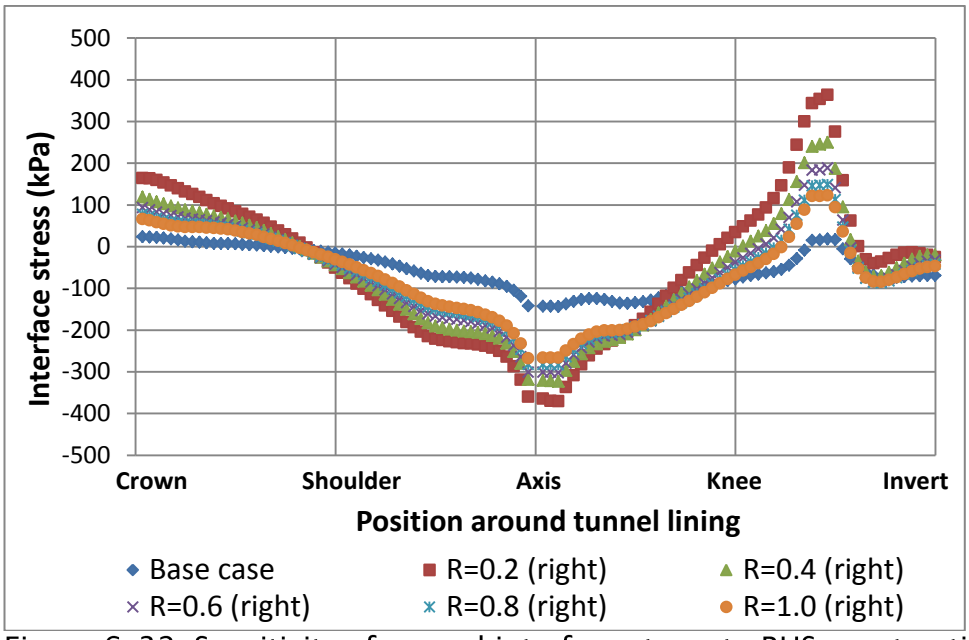

Figure 6-32 Sensitivity of normal interface stress to RHS construction

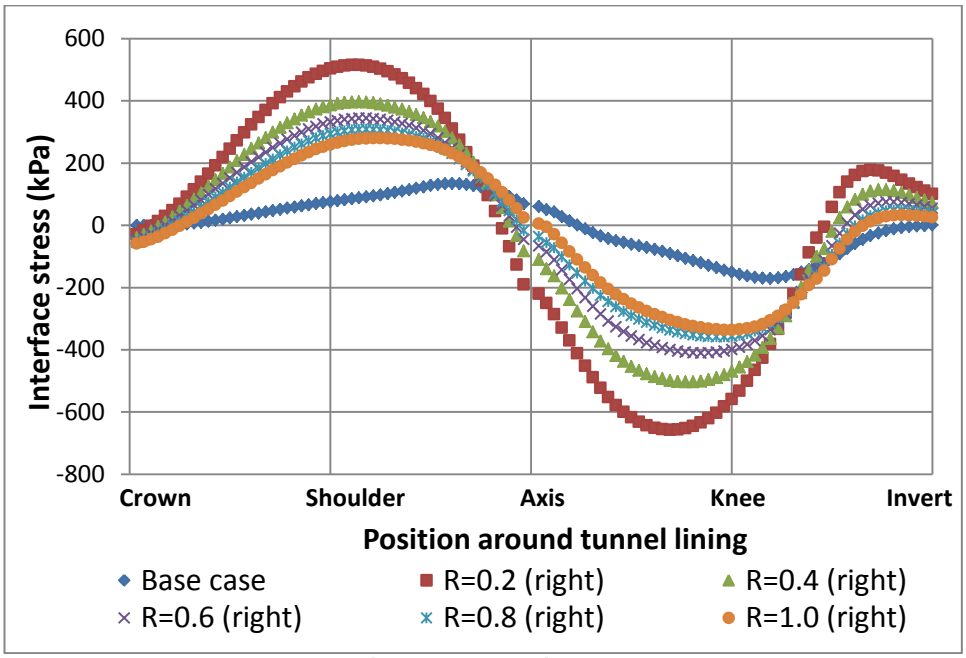

Figure 6-33 Sensitivity of shear interface stress to RHS construction

6.10 Summary

This Chapter has investigated efficient and robust CSL tunnel design by presenting the results obtained from a series of numerical modelling analyses on a typical CSL tunnel. The impact of variance in interface stiffness, primary and secondary lining thicknesses and external loadings was evaluated. The following has been established:

1. The base case CSL tunnel, adopting the long-term base interface stiffnesses, demonstrates a certain degree of composite action.
2. The real benefits of CSL tunnels when compared with the traditional SPL and more recent unbonded DSL tunnels is that the interface tensile and shear bonds prevent the long-term water pressure from only applying to the secondary lining, instead it acts mostly on the primary lining, leading to a possible reduction in secondary lining thickness.
3. The high degree of composite action (*i.e* high normal and shear interface stiffnesses) may introduce high bending moments to the secondary lining, resulting in additional reinforcement required in the secondary lining

crown. It is therefore not conservative to design a CSL tunnel as a DSL tunnel without taking account of the shear interface stiffness.

4. For CSL tunnels, when the secondary lining thickness is less than or equal to half of the primary lining thickness (or the primary lining thickness is more than or equal to three times of the secondary lining thickness under special circumstances), no reinforcement is needed for the secondary lining crown. This results in an efficient CSL tunnel design from both reinforcement saving and lining thickness reduction perspectives.
5. The interface compressive, tensile and shear stress limits obtained from previous element tests are sufficient to resist interface stresses that occur in the parametric cases investigation in this chapter, and are able to maintain the integrity of CSL tunnels.
6. The numerical analyses presented in this chapter demonstrate that CSL tunnels can be designed using the tested interface parameters and validated numerical modelling approach, resulting in an efficient CSL tunnel design.

Chapter 7: Summary of Discussions

7.1 Background to this project

SCL tunnelling is an established method which is able to generate underground spaces in a wide range of shapes and sizes. The tunnelling industry has long been seeking to understand, if it can be demonstrated to exist, the performance of the CSL tunnels. Being able to answer these questions would open the door for more efficient design of CSL tunnels. In response to this urgent call, the author has carried out extensive laboratory experimentation and numerical modelling on this topic and the findings have been presented in this thesis.

7.2 Contribution to the knowledge of CSL

In order to take advantage of the potential composite action at the membrane interface between the primary and secondary linings, reliable interface parameters are required. Prior to this research, only a few "unpublished" documents on the properties of different sprayed membranes were produced by their manufacturers.

There were uncertainties regarding the data presented in those documents. Firstly, only small numbers of samples were tested, which does not provide sufficient statistical evidence for determining the interface properties. Secondly, most of the data presented were either for the material properties of the sprayed membrane itself or the interface properties between the sprayed membrane and steel. Application of the former requires further consideration of primary lining surface finish roughness and the latter does not apply to the sprayed concrete-membrane interface. Furthermore, there was no long-term data available, a key requirement for the design of CSL tunnels to the common design life of 120 years.

This research presents the first published results on the interface properties of a sprayed waterproofing membrane, based on a systematic testing programme and verification process. The test results are for samples cut from CSL panels and both short and long-term results are presented.

It should be noted that the CSL panels used in this research were produced in an industrial yard owned by a SCL specialist contractor, who was involved in the construction of Crossrail SCL tunnels. The sprayed concrete and sprayed

membrane mixes both complied with the Crossrail specifications and are therefore representative of materials currently used in the UK tunnelling market. The impact of variation of workmanship is not within the scope of this research and all CSL panels were sprayed by a single nozzleman who had achieved the SCL spray certification (EFNARC) required by Crossrail.

One of the significant features of this research is that some of the test results outlined in this thesis have already been used in the design of the SCL tunnels in Crossrail itself – Europe's biggest construction project.

7.3 Laboratory testing for Interface parameters

The degree of composite action at the interface between the primary and secondary linings in CSL tunnels is mainly controlled by the normal and shear interface stiffness. This research has used some well-established testing methods to determine these parameters and has also developed some innovations in testing, including the use of steel plates and epoxy resin to apply normal tensile stresses to the test samples directly. This research has involved both the (1) test and verification of interface parameters using different testing configurations on a large number of CSL samples (with one specific brand of membrane), and (2) presentation of both short and long-term relaxation test results for the interface parameters.

Two factors were evaluated for their impact on the normal and shear interface stiffnesses: primary lining surface finish and measured membrane thickness.

The primary lining surface finish has a significant impact on the compressive interface strength and first loading stiffness, shear interface strength, first loading and cyclic loading stiffnesses, but not on compressive interface cyclic loading stiffness, tensile interface strength, first loading and cyclic loading stiffnesses.

The measured membrane thickness has a high degree of influence on the compressive interface strength, first loading and cyclic loading stiffnesses, tensile interface first loading and cyclic loading stiffnesses, shear interface strength, first loading and cyclic loading stiffness. However, it does not exhibit a significant effect on the tensile interface strength of the tested samples.

Statistical analysis of test results was carried out. It was identified that (1) the interface stiffnesses for samples with smooth and regulated primary lining surface finishes were similar, (2) a thicker membrane interface is weaker than a thin membrane interface in compression and shear but equally strong in tension and (3) the extent of interface stiffness reduction introduced by an increase in the membrane thickness is greater than that caused by an increase in primary lining surface finish roughness (interface roughness). Therefore, it is concluded that membrane thickness has a bigger impact on the degree of composite action for a CSL structure than primary lining surface finish.

7.4 Verification of interface parameters and modelling technique

This research has presented and verified a proposed finite difference numerical modelling approach for composite action in a sandwiched structure, using zones to model the sprayed concrete lining and interface elements or zones to model the sprayed concrete–membrane interface. The verification included two steps.

The first step was to compare the results from laboratory four-point bending tests on a pure shotcrete beam with numerical analysis and a closed-form equation. This step was required to confirm (1) the sprayed concrete Young's modulus (by comparing it with the results from previous element tests), (2) the testing configuration (whether the beam is deformed in pure bending and the boundary condition effect), and (3) the accuracy of the laboratory beam test readings (from potentiometers and strain gauges).

Following verification of the model for the pure shotcrete beam, the second step was to compare the results from laboratory four-point bending tests of a series of composite beams with corresponding numerical analyses to verify the interface parameters used in the CSL beam models. This verification step demonstrates the proposed modelling approach is able to simulate the behaviour of composite beams.

A method for quantifying the degree of composite action was established and used to assess the laboratory tested and numerical analysed CSL beams. The results of an interface stiffness parametric study showed that the shear interface stiffness has a larger influence than the normal interface stiffness on the degree of composite action. The interface optimal position investigation showed that the

maximum degree of composite action is achieved if the interface is located at the mid-depth of the CSL beam. The beam thickness optimisation study showed that a 37% overall CSL beam thickness reduction can be achieved when composite action for a CSL beam in pure bending is considered.

7.5 Investigation of the performance of a CSL tunnel

In order to investigate and establish an efficient and robust design for CSL tunnels, a typical CSL tunnel, consisting of permanent primary and secondary linings separated by a sprayed waterproofing membrane, was modelled within typical soft ground at shallow depth in plane strain. This model includes the following key features: soil-structure interaction, staged construction and a calibrated modelling approach for composite action. The base long-term interface stiffnesses previously verified against laboratory data were used in the base case model.

The performance of the base case CSL tunnel was compared with that of a full CSL (*i.e.* CSL tunnel with full composite action) and a non CSL (DSL) tunnel and a certain degree of composite action was identified.

A parametric study on the impact of interface stiffness variation on the performance of the CSL tunnel was carried out to explore the simulated effect of different membrane materials. It was found that a reduction of normal and/or shear interface stiffnesses from the base case long-term values significantly reduced the axial force transferred from the primary to the secondary lining. The bending moment in both linings was also significantly reduced. An increase of normal and/or shear interface stiffness had little impact on the axial force and bending moment transfer between the two linings. It was also found, with the base case CSL tunnel configuration, that no matter how the interface stiffnesses vary, reinforcement is not needed in the primary lining but always needed above the shoulder and below the invert for the secondary lining.

A parametric study on the impact of primary/secondary lining thickness ratio (*i.e.* keeping one lining thickness constant at 300mm and reducing the thickness of the other lining gradually from 300mm to 50mm at 50mm intervals) the performance of CSL tunnels was carried out to investigate what overall lining thickness reduction can be achieved if composite action at the interface is utilised. It was also found that the ratio has a major impact on the reinforcement

requirement in the secondary lining above the shoulder but has no impact on it in other lining positions. When the ratio is less than 0.5 or more than 3.0, no reinforcement is needed in the secondary lining above the shoulder. The result of the former case was attributed to the faster increase in axial force than the corresponding increase in bending moment in the secondary lining. Conversely, the result of the latter case was attributed to the faster reduction in bending moment than the corresponding reduction in axial force in the secondary lining when compared with the base case. The reinforcement requirement for other lining positions (*i.e.* below the shoulder) is the same as the base case configuration tunnel.

A parametric study on the impact of nearby construction beneath or to the side of a CSL tunnel on the performance of the lining was carried out, with the intention of investigating its ability to maintain composite integrity under external loading. It was found that construction to the side has much greater impact on interface stresses than construction beneath the tunnel and can generate a relative high interface tensile stress. However, the interface strength is sufficient to resist this tensile stress and the integrity of the CSL tunnel is maintained.

7.6 Implications for CSL tunnel design

This research shows that the key to ensuring an efficient CSL tunnel design (*i.e.* not requiring reinforcement above the tunnel shoulder in the secondary lining is to choose suitable primary and secondary lining thicknesses that lead to a primary/secondary lining thickness ratio of either less than 0.5 or bigger than 3.0. This will maximise the axial force but minimise the bending moment in the secondary lining whilst ensuring the CSL configuration.

For a CSL tunnel in an urban environment, the primary lining usually takes not only the ground and water loads, but also additional compensation grouting pressures and additional lining forces caused by the construction of cross passages. It is therefore suggested to install a relatively thicker primary lining (*e.g.* primary/secondary lining thickness ratio bigger than 3.0) to take all short-term loads as well as a significant proportion of the long-term loads, whilst applying a thinner secondary lining for fireproofing and internal load support purposes.

This research also highlights that the "way of thinking" for CSL tunnel design may be somewhat counter-intuitive when compared to SPL or DSL approaches. For CSL tunnels, reducing the lining thickness may lead to a safer lining as the tunnel design process is more about achieving an optimum BM/AF ratio in the lining rather than just varying the bending moments. With particular reference to the base case tunnel, when the results show that reinforcement is needed above the secondary lining shoulder, the traditional resolutions would be (1) thicken the lining and (2) add reinforcement. These approaches are typical of a traditional structural engineering frame of reference and focus purely on increasing the bending moment capacity of the lining. This research demonstrates that an alternative effective way to resolve the issue is to reduce the secondary lining thickness, hence reducing the BM/AF ratio in the secondary lining.

For CSL tunnels that are designed as bonded DSL tunnels, although a certain degree of tensile bond is assumed at the sprayed concrete-membrane interface, which in turn leads to a large proportion of the long-term water and ground loads taken by the permanent primary lining, ignoring the interface shear stiffness could result in a lower estimation of the bending moment in both the primary and secondary linings, resulting in an unsafe tunnel design.

7.7 Advantages over other SCL tunnel configurations

The main advantage of using the CSL tunnels over other SCL tunnel configurations is outlined in this section.

For SPL tunnels, the primary and secondary linings have been traditionally designed specifically for the short and long-term loads respectively. The primary lining was treated only as a temporary structure, mainly due to concerns about the long-term durability of sprayed concrete as well as the unknown lining forces. This in turn raised several concerns about material wastage for the primary lining, as described in Chapter 2.

For unbonded DSL tunnels (*e.g.* where sheet membrane is installed between a sprayed primary and a cast *in situ* secondary lining), the lack of tensile and shear bond at the sprayed concrete-membrane interface means ground water which penetrates the primary lining construction joints will apply long-term water pressure directly onto the secondary lining, resulting in a reduction in the primary lining axial force. Meanwhile, the primary lining will take additional consolidation

bending moment arising from the further long-term lining deformation, leading to a bigger BM/AF ratio and, thus, the possible formation of cracks in the primary lining. The current design of a permanent primary lining in a DSL tunnel usually uses steel fibre as structural reinforcement. The assumed strain softening post-crack behaviour means a single crack would occur and continue to develop if the lining forces reach and exceed the lining capacity. The crack development will introduce durability issues (*i.e.* corrosion of the steel fibres) and possibly lead to a degradation of the permanent primary lining to a sacrificial lining in the long-term, raising the same material wastage issue.

This research has demonstrated that, by using the CSL tunnel configuration, the wastage of concrete material in other SCL tunnel configurations can be avoided. This advantage arises mostly from the changed axial force and bending moment distribution between the primary and secondary linings.

7.8 Interface property implications

In order to achieve the desired design effect for the CSL tunnel, there are two "desired properties"' for the sprayed concrete-membrane interface. Firstly, the interface should have strong tensile and shear bonds. This will ensure the integrity of the CSL tunnel is maintained under external loading and will lead to the stiffer primary lining (*i.e.* bigger axial force than that in the secondary lining) taking most of the long-term loads. Secondly, the interface should have low normal (*i.e.* in compression and tension) and shear stiffnesses that reduce the load transfer from the primary lining to the secondary lining.

Chapter 8: Conclusions and Recommendations

8.1 Conclusions

The main conclusions from this project are as follows;

(1) There is significant composite action at the interface between the primary and secondary lining for a CSL tunnel with sandwiched spray applied waterproofing membrane. The degree of composite action for the CSL tunnel is mainly controlled by the nominal membrane thickness. Variation in primary lining surface finish has little impact on the degree of composite action for a CSL tunnel.

(2) The CSL tunnel with sandwiched spray applied waterproofing membrane is able to maintain its integrity and functionality under the variations of external loading, such as long-term water pressure and nearby construction. No tensile debond or shear slippage occurs for the analysed scenarios.

(3) The representation of sprayed concrete lining by zones and spray concrete-sprayed membrane interface by either interface elements or zones in the composite CSL numerical model was found to be a successful approach for predicting its behaviour. The composite beam model could provide detailed information on stresses and strains through the beam depth, out-performing traditional tunnel models using beam elements.

(4) For the CSL tunnel in the base case configuration, no matter how the interface stiffnesses vary, reinforcement is always required in the secondary lining above the shoulder and below the knee. No reinforcement is required in other lining positions.

(5) The key for an efficient CSL tunnel design is to select suitable primary and secondary lining thicknesses rather than fine tuning the interface parameters.

8.2 Recommendations for further work

CSL is a new type of tunnel lining configuration, which has only recently been adopted in practice. This research has investigated the impact of some interface characteristics on the behaviour of the composite SCL tunnel. However, it should be noted that this research has involved many simplifications when compared with real SCL tunnel design and construction. In order to further the understanding of CSL tunnels performance, the following recommendations for further work have been identified:

(1) Detailed interface roughness characterisation should be carried out to understand at a fundamental level the impact of interface roughness and membrane thickness on the interface normal and shear stiffnesses and whether it is possible to achieve the combination of strong tensile and shear bounds and low normal and shear stiffnesses that would give optimal CSL lining performance

(2) Adopt advanced linear elastic perfectly plastic sprayed concrete and sprayed membrane interface constitutive models to better predict the performance of CSL tunnels. A particular interest is the cracked lining situation where reinforcement is not present (some clients allow for the occurrence of cracks of low crack width under certain circumstances)

(3) Use monitoring data (*e.g.* data from pressure cells and fibre optics) from Crossrail CSL tunnels to verify the CSL tunnel numerical modelling approach and interface parameters

Appendices

Appendix A Sample Cutting Plan

Panels No. 1-12 were prepared in two sets with each set consisting of 6 panels, differentiated by interface roughness (*e.g.* smooth, regulated and as-sprayed) and target membrane thickness (*e.g.* 3mm and 6mm). The six types of panels are shown in Figure A-1.

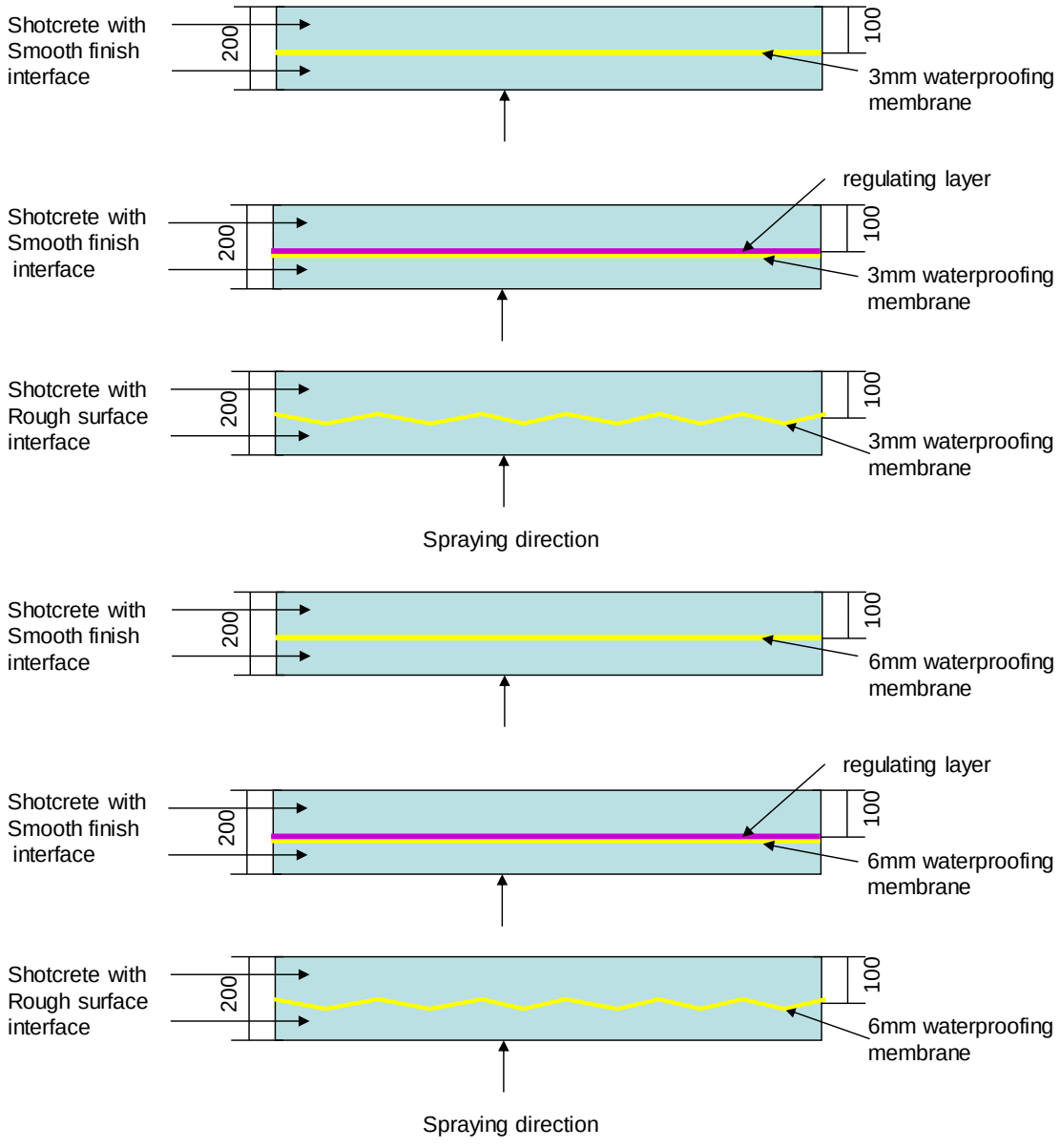

Figure A-1 Panels with 6 types of interfaces

Appendix A

The two sets of panels were cut to obtain different types of samples according to the two diagrams in Figure A-2.

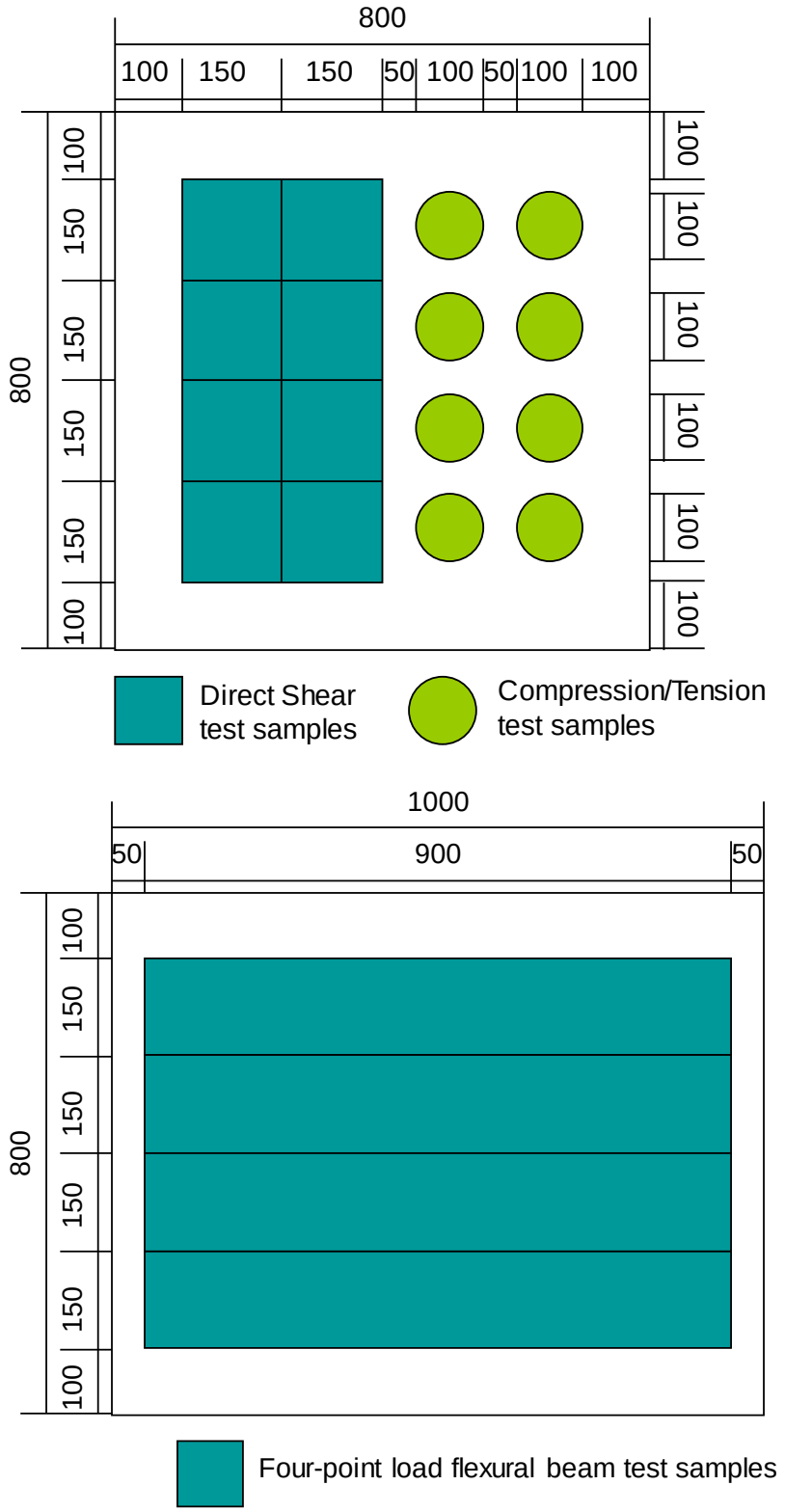

Figure A-2 Two sample cutting plans

Panel No.13 was prepared with a regulated interface and 3mm target membrane thickness. 16 block samples were cut for direct shear testing, as shown in Figure A-3.

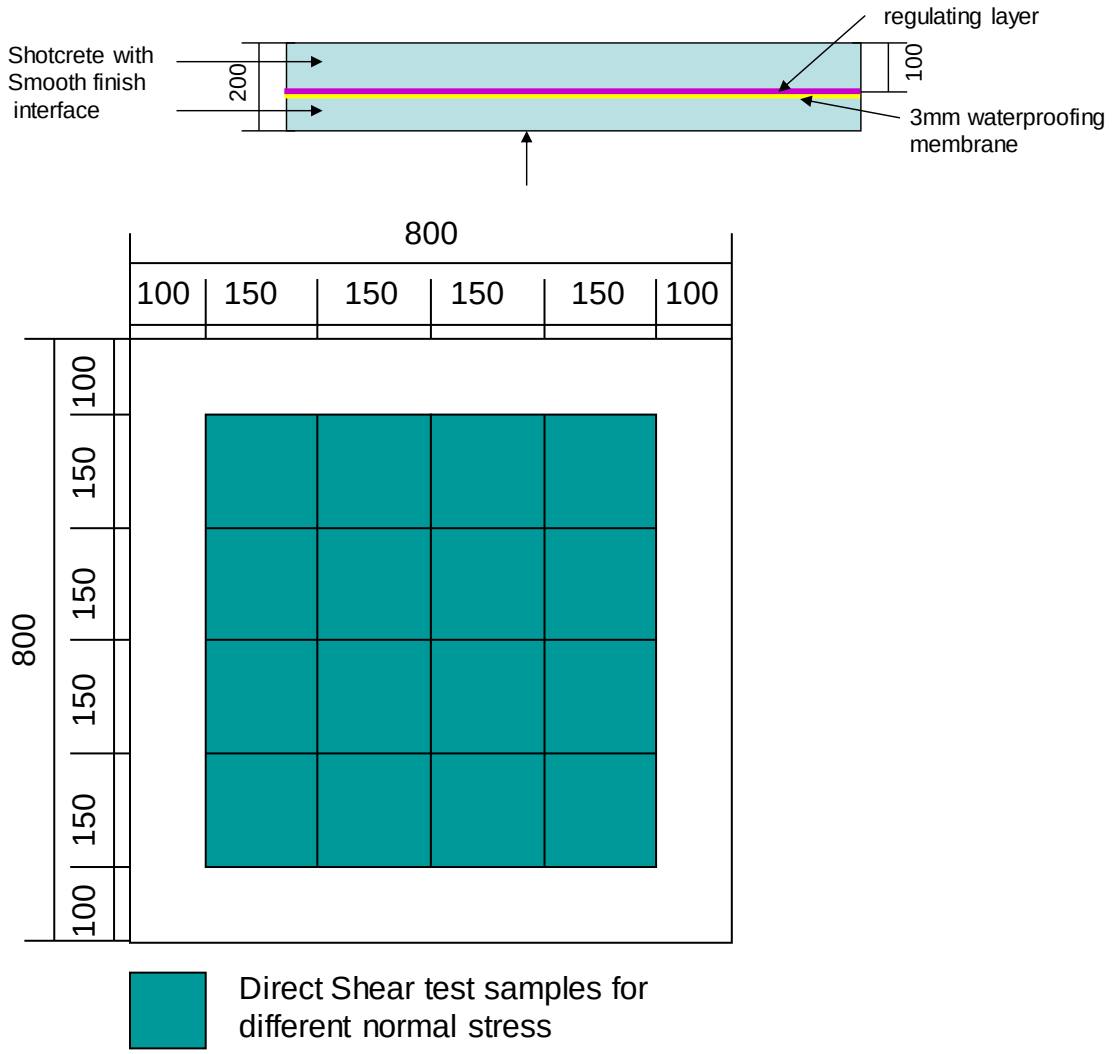

Figure A-3 Sample preparation and cutting plan for panel No.13

Panels 14 and 15 were prepared with only sprayed concrete. Panel No.14 has a smaller dimension (*i.e.* 600mm×600mm) when compared with other panels. 9 pure sprayed concrete cores were cut off for the compression and tension test. 4 pure sprayed concrete beams were cut off from panel No. 15 for the four-point bending test. The panel preparation and cutting plans for both panels are shown in Figure A-4.

Appendix A

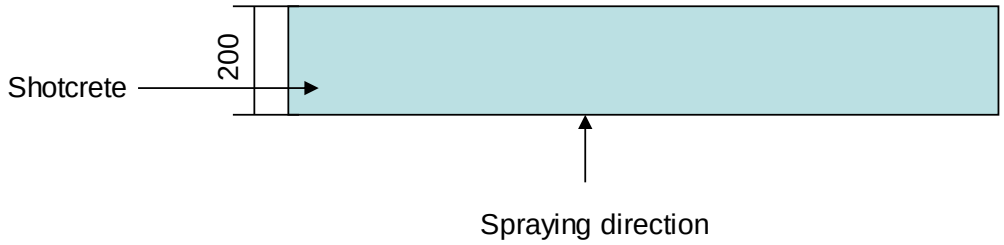

Spraying direction

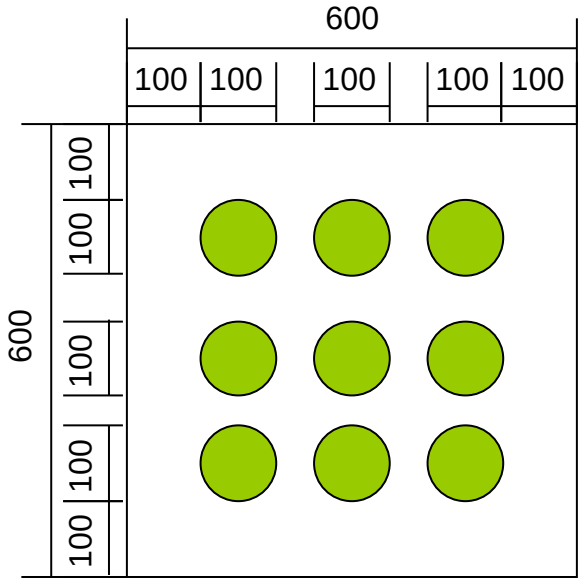

Compression/Tension test samples

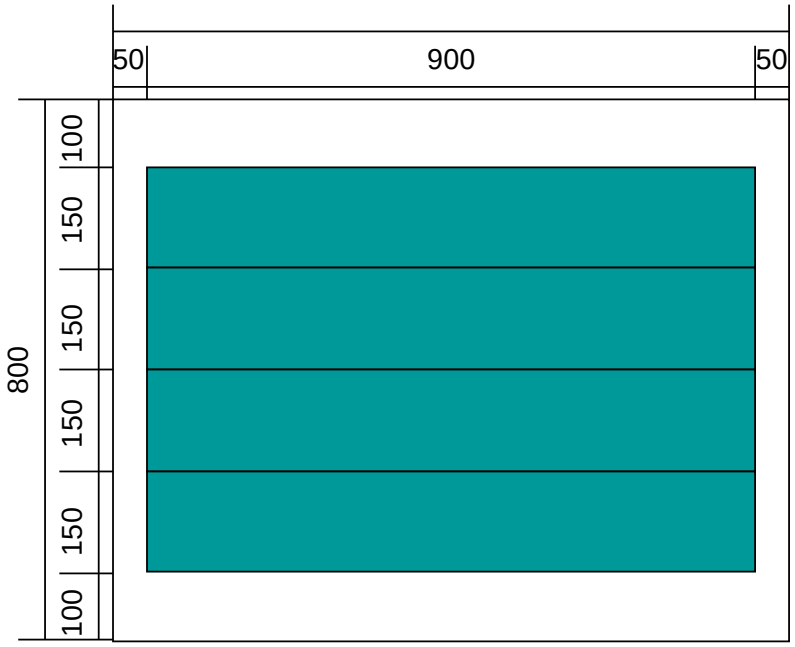

Four-point load flexural beam test samples

Figure A-4 Sample preparation and cutting plan for panels No.14 and No.15

Appendix B Calculation for adjusted shear interface stiffness

This Appendix explains how the adjusted shear interface stiffness was derived from the raw test data. A calculation example is also provided.

Due to limitations of the testing equipment, external measurement was used during the direct shear test, the results of which therefore need to be corrected for the compliance of the test apparatus and the sample rotation effect. To correct for the compliance of the test, the cyclic loading shear interface stiffness, which increased with the shear stress, is extrapolated from the shear stress level when the cyclic loading was performed to the peak shear stress level, to obtain a value closer to the 'true' shear interface stiffness value.

This value has then been corrected again to compensate for the sample rotation that occurred during the test, a diagram of which is shown in Figure B-1. This sample rotation induces a rigid body (vertical) movement (same as the rigid body horizontal movement). This should be deducted from the horizontal displacement recorded and hence used to determine a higher value of interface shear stiffness.

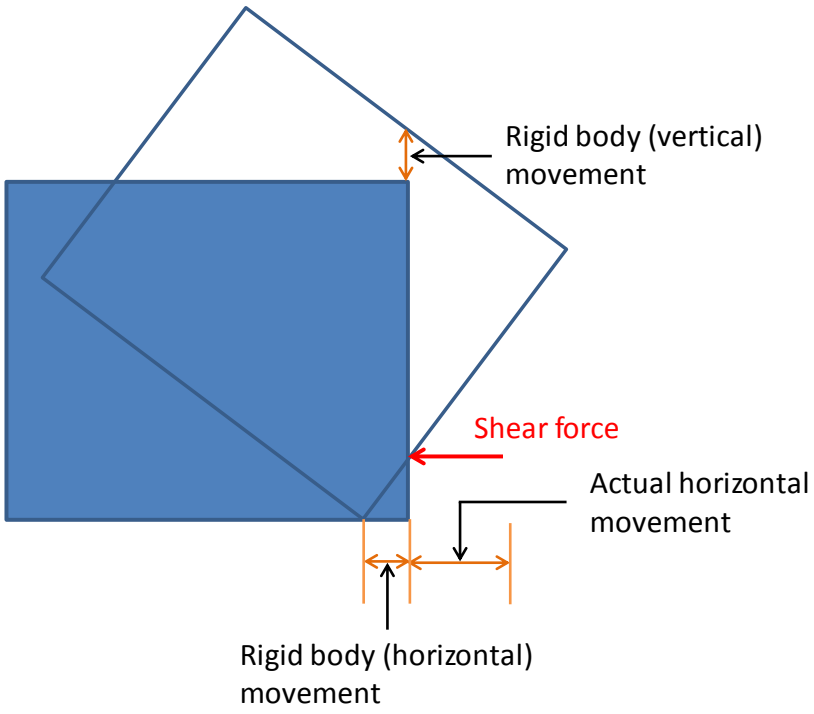

Figure B-1 Relationship between rigid body and actual horizontal movements

Appendix B

A typical calculation example for interface 1-23 is given below. Firstly, the rotation factor was calculated, as shown in Table B-1 and based on the test results shown in Figure B-2.

Table B-1 Calculation of rotation ratio

Interface number	Horizontal movement reading from potentiometer (mm)	Vertical movement reading from potentiometer (mm)	Calculated actual horizontal movement (mm)	Rotation factor
1-23	2.30	1.50	0.80	2.87

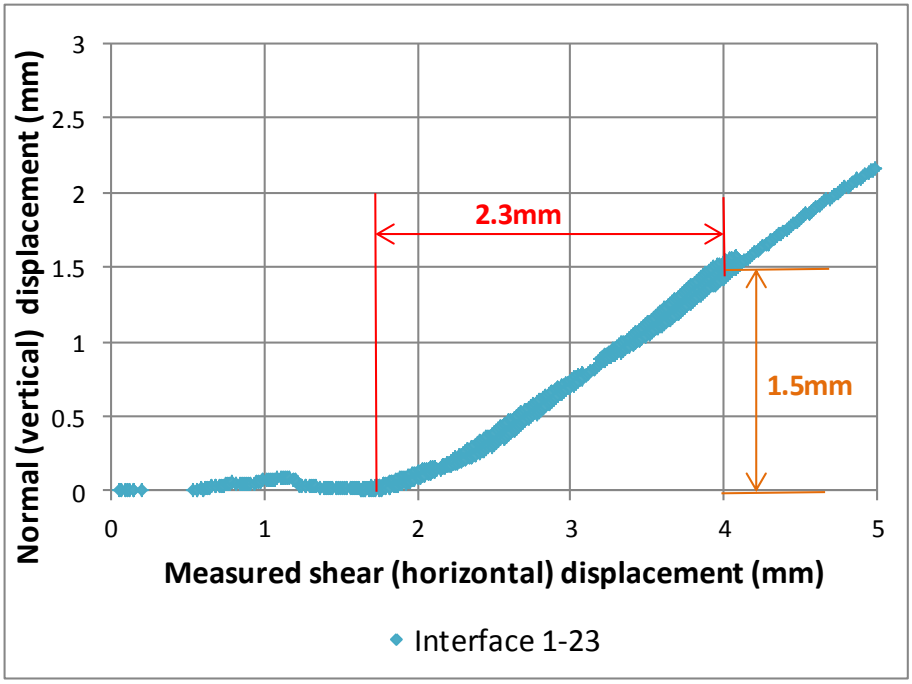

Figure B-2 Measured normal and shear displacements for interface 1-23

Following that, the shear interface stiffness at the peak shear stress was extrapolated from the mean cyclic loading shear interface stiffness and then multiplied by the rotation factor to obtain the adjusted shear interface stiffness. The calculation procedure is shown in Table B-2 and the cyclic loading loop for interface 1-23 is shown in Figure B-3.

Table B-2 Calculation of adjusted shear interface stiffness

Calculation procedure	Shear stress level (MPa)	Shear interface stiffness (GPa/m) at corresponding stress levels
cyclic loading 1	0.84	0.82
cyclic loading 2	1.35	0.93
cyclic loading 3	1.71	1.01
Mean cyclic loading	1.30	0.92
Peak shear stress	2.44	1.72
Adjusted for Rotation factor	2.87	4.95

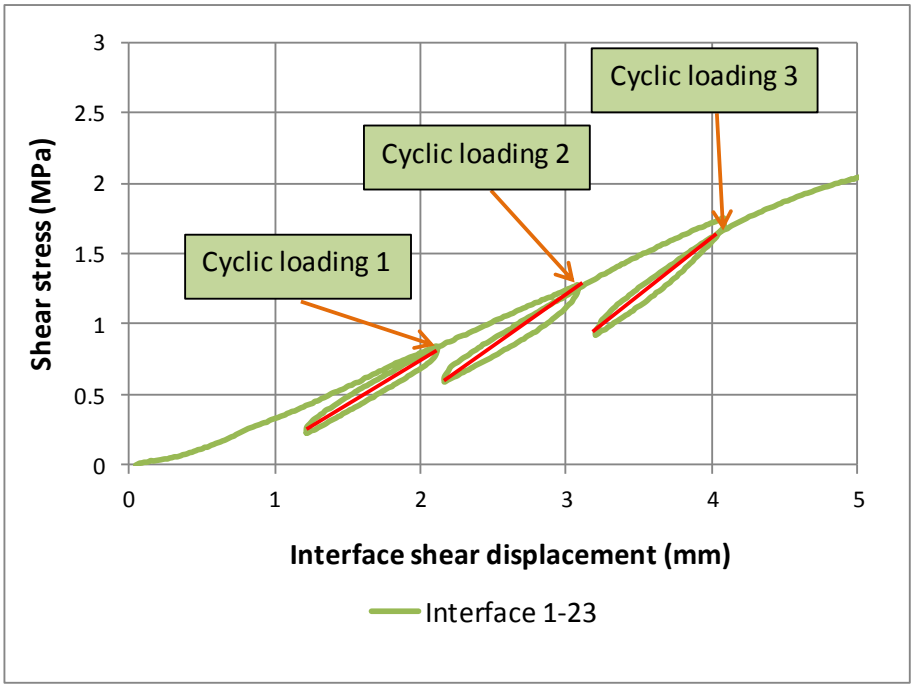

Figure B-3 Cyclic loading loops for interface 1-23

Appendix C Test results for samples under 250kPa and 750kPa normal pressures

250kPa normal pressure testing overview

Direct shear tests with 250kPa normal pressure were also carried out. Due to the limited number of samples and the main focus on smooth and regulated interface samples, tests were only carried out on 12 samples – 3 samples from each of Types 1, 2, 4 and 5.

Shear interface stress-deformation relationships

Relationships for selected Type 1, 2, 4 and 5 samples are shown in Figure C-1 and Figure C-2 respectively. Peak shear stresses occurred at displacements between 10 and 15mm. All samples failed in a ductile manner.

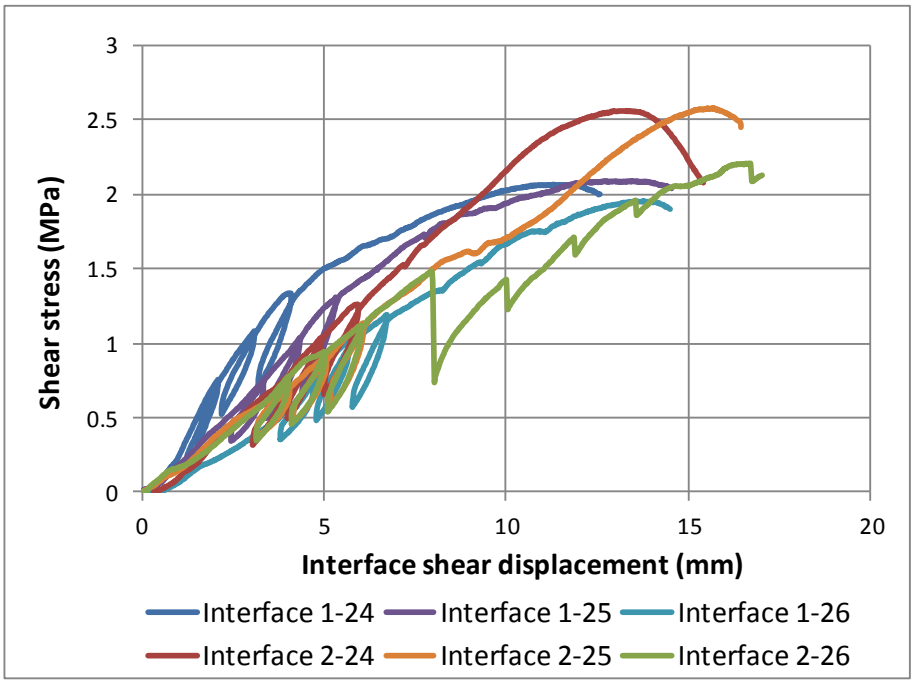

Figure C-1 Thin membrane interface behaviour under direct shear test with 250kPa normal pressure

Appendix C

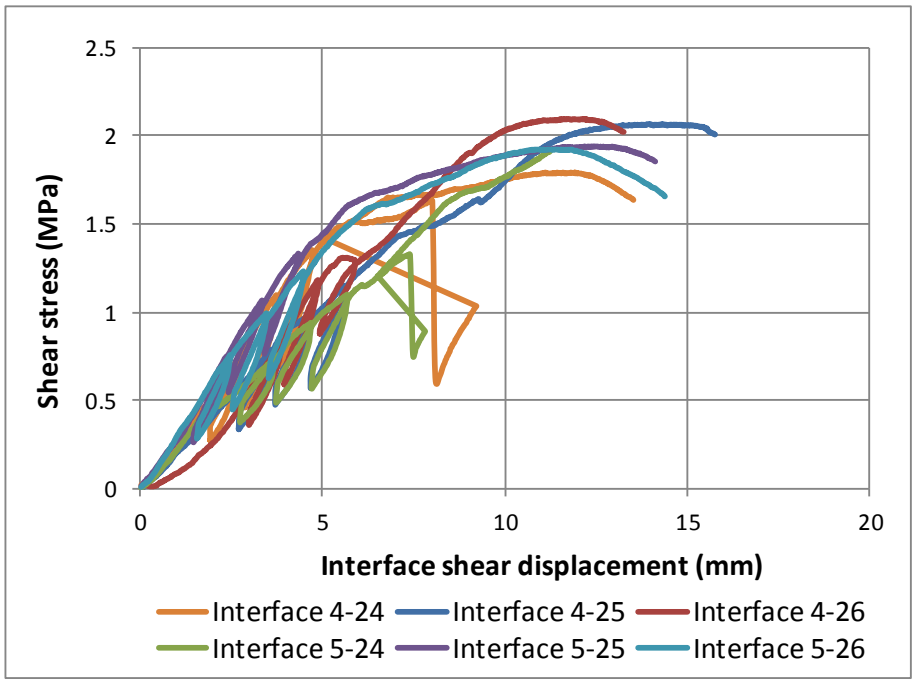

Figure C-2 Thick membrane interface behaviour under direct shear test with 250kPa normal pressure

Peak shear stress

Numerical test results and their statistical analysis are presented in Table C-1 and Table C-2 respectively. Values of peak shear stress for samples with thin and thick membranes are very close within their respective groups, confirming the two conclusions drawn from the 500kPa normal stress results. Peak shear stress shows a slight reduction with increased membrane thickness.

Table C-1 Direct shear test results under 250 kPa normal pressure

Sample designation	Membrane thickness (mm)	Peak shear stress (MPa)	Shear displacement at peak stress (mm)	First loading stiffness (GPa/m)	Cyclic loading stiffness (GPa/m)
1-24	2.0	2.0	9.7	0.94	8.26
1-25	2.0	2.0	11.0	0.73	17.45
1-26	2.0	1.9	13.5	0.70	26.68
2-24	3.0	2.6	13.1	0.65	12.29
2-25	3.0	2.6	15.7	0.47	14.68
2-26	3.0	2.2	16.7	0.56	6.55
4-24	8.0	1.8	11.6	0.51	1.69
4-25	7.0	2.1	13.9	0.61	4.42
4-26	7.0	2.1	12.1	0.57	3.82
5-24	8.0	1.9	10.1	0.50	3.07

5-25	8.0	1.9	12.4	0.40	0.91
5-26	9.0	1.9	11.4	0.52	1.43

Table C-2 Statistical analysis of direct shear test results under 250 kPa normal pressure

Sample Type	Peak shear stress		First loading stiffness		Cyclic loading stiffness	
	Mean (MPa)	Standard deviation (MPa)	Mean (GPa/m)	Standard deviation (GPa/m)	Mean (GPa/m)	Standard deviation (GPa/m)
Type 1	2.0	0.0	0.79	0.13	17.47	9.21
Type 2	2.4	0.2	0.56	0.09	11.17	4.18
Type 4	2.0	0.2	0.57	0.05	3.31	1.43
Type 5	1.9	0.0	0.47	0.06	1.80	1.12

First loading and cyclic loading shear stiffnesses

Values of first loading and cyclic loading stiffnesses for samples with thin and thick membrane are very close within their respective groups, as shown in Figure C-3 and Figure C-4, also confirming the two conclusions drawn from the 500kPa normal stress results.

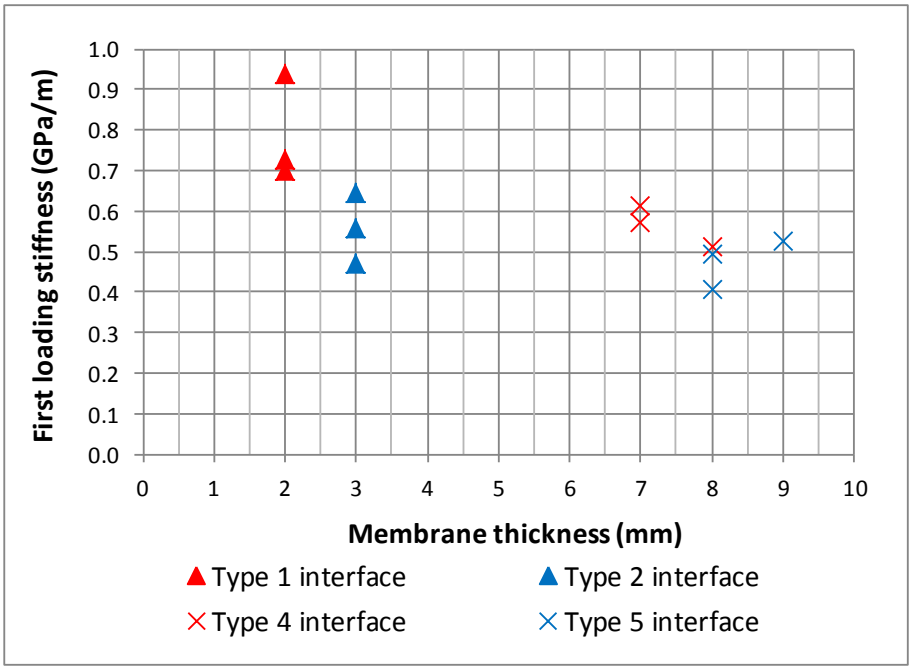

Figure C-3 Relationship between first loading shear stiffness, membrane thickness and type of interface under 250kPa normal pressure

Appendix C

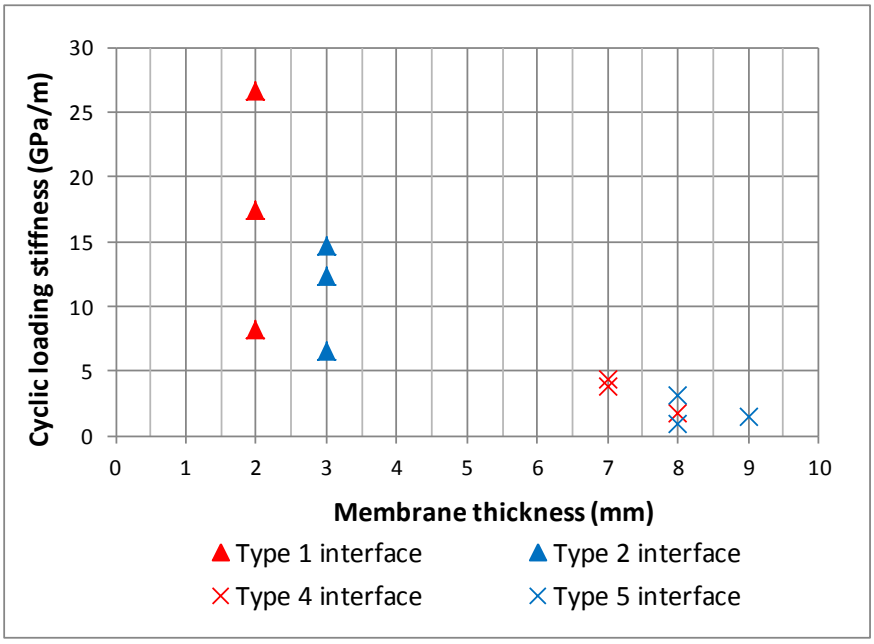

Figure C-4 Relationship between cyclic loading shear stiffness, membrane thickness and type of interface under 250kPa normal pressure

Shear displacement at peak shear stress

Figure C-5 shows a different trend to that of the direct shear tests under 500kPa normal pressure. In this case the shear displacement at peak shear stress does not increase with the membrane thickness, probably due to the unknown membrane thickness inside of the sample.

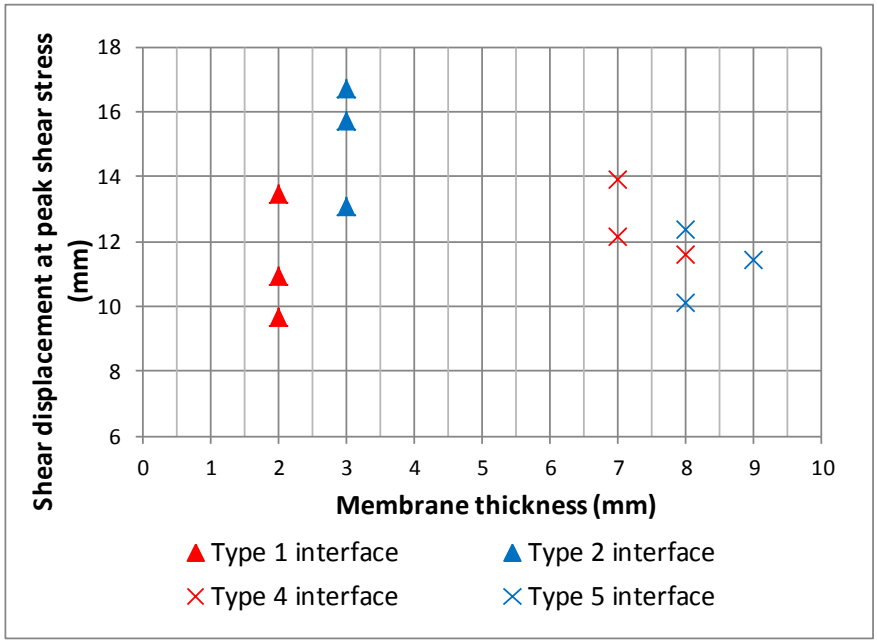

Figure C-5 Relationship between shear displacement at peak shear stress and membrane thickness and type of interface under 250kPa normal pressure.

Observed failure modes in shear tests

The failure mode for samples under 250kPa normal pressure was similar to that for samples under 500kPa vertical pressure. One significant difference between these two cases is that the samples under 250kPa vertical pressure were more likely to rotate than samples under 500kPa vertical pressure. This effect has been taken into account during the result post-processing stage, especially for the cyclic loading stiffness values.

750kPa normal pressure testing overview

Direct shear tests with 750kPa normal pressure were carried out only on three Type 2 samples. The shear stress-shear displacement relationships are shown in Figure C-6. Peak stress occurred again when the samples were sheared to a displacement of 10-15mm. All samples failed in a ductile mode, similar to previous observations. Numerical test results and their statistical analysis are presented in Table C-3 and Table C-4 respectively.

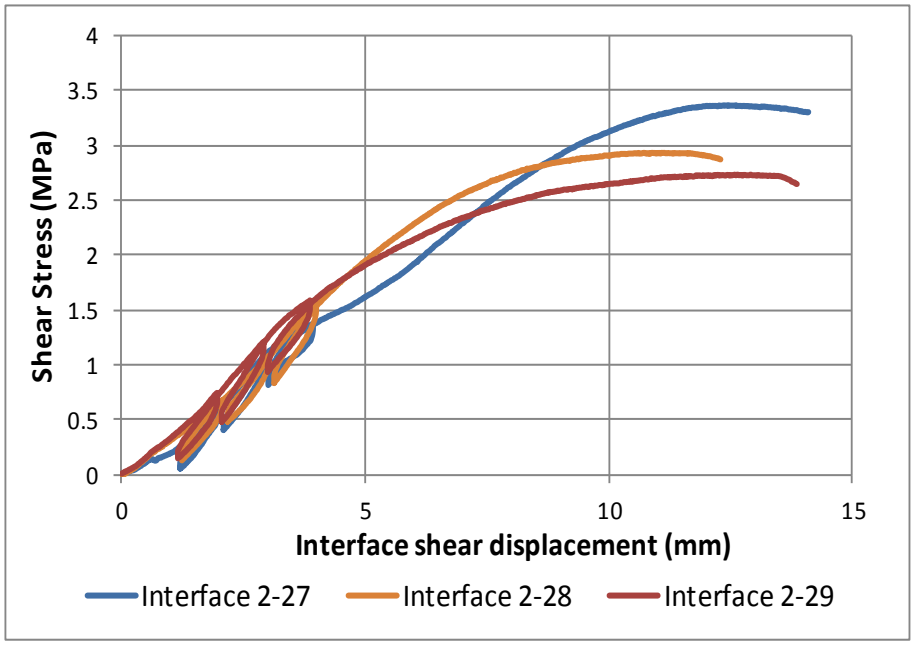

Figure C-6 Type 2 interface behaviour under direct shear test with 750kPa normal pressure

Appendix C

Table C-3 Direct shear test results under 750 kPa normal pressure

Sample designation	Membrane thickness (mm)	Peak shear stress (MPa)	Shear displacement at peak stress (mm)	First loading stiffness (GPa/mm)	Cyclic loading stiffness (GPa/mm)
2-27	3.0	3.4	13.2	0.48	3.93
2-28	3.0	2.9	11.6	0.59	5.42
2-29	3.0	2.7	13.0	0.61	3.80

Table C-4 Statistical analysis of direct shear test results under 750 kPa vertical pressure

Sample Type	Peak shear stress		First loading stiffness		Cyclic loading stiffness	
	Mean (MPa)	Standard deviation (MPa)	Mean (GPa/m)	Standard deviation (GPa/m)	Mean (GPa/m)	Standard deviation (GPa/m)
Type 2	3.0	0.3	0.56	0.07	4.38	0.90

Appendix D Plots for simultaneous influence of Kn and Ks parametric study

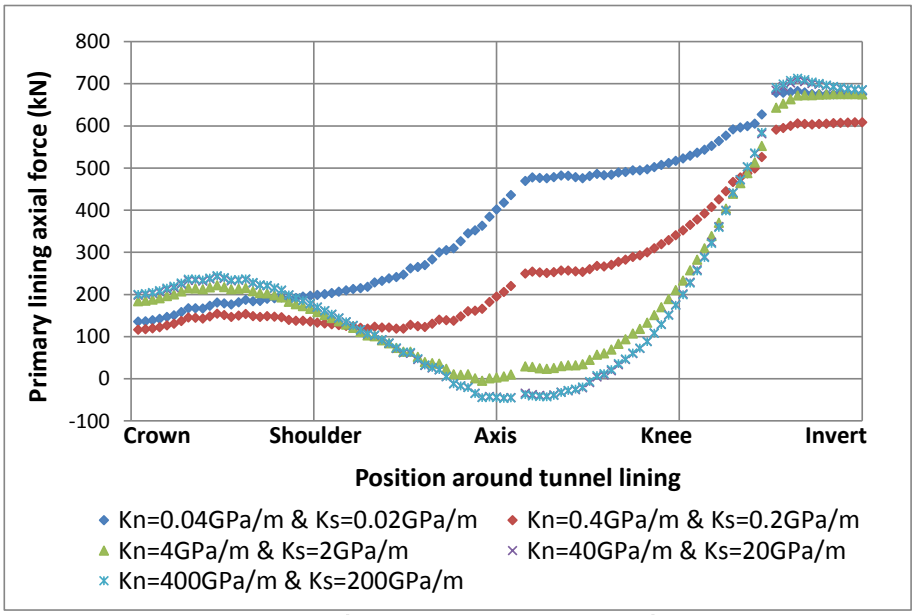

Figure D-1 Sensitivity of primary lining axial force to simultaneously varying Kn and Ks values

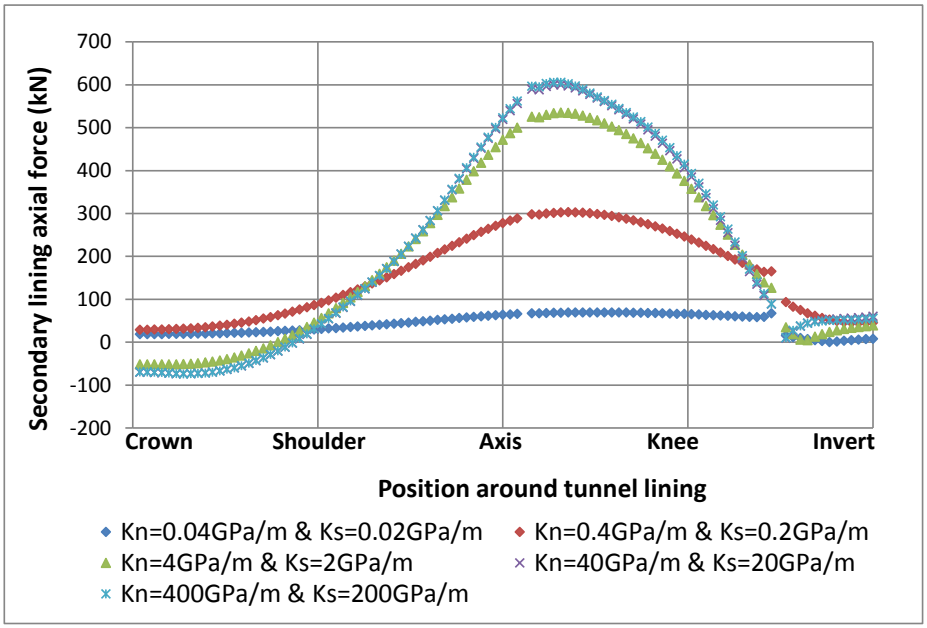

Figure D-2 Sensitivity of secondary lining axial force to simultaneously varying Kn and Ks values

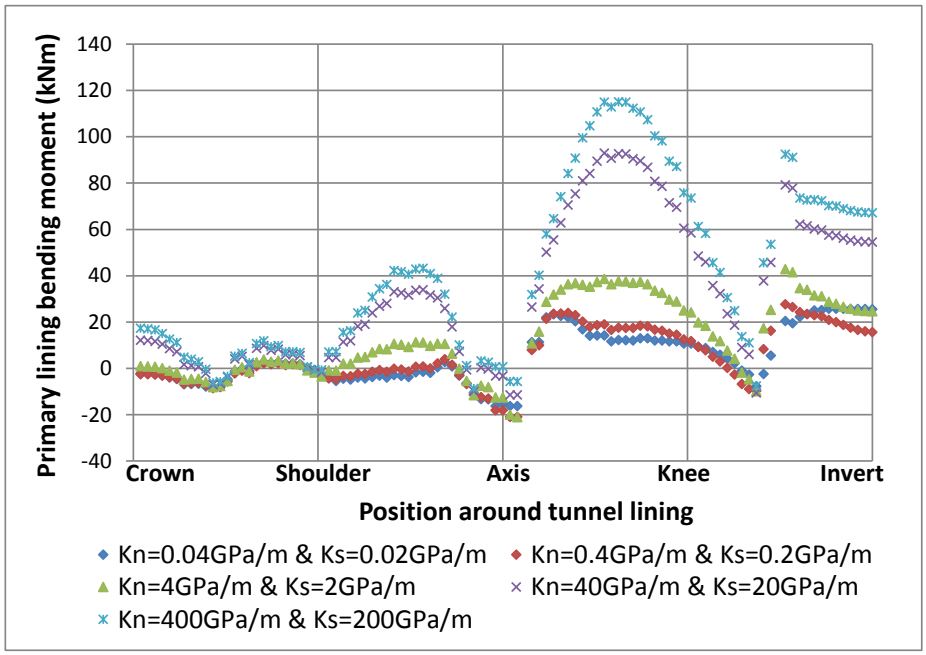

Figure D-3 Sensitivity of primary lining bending moment to simultaneously varying Kn and Ks values

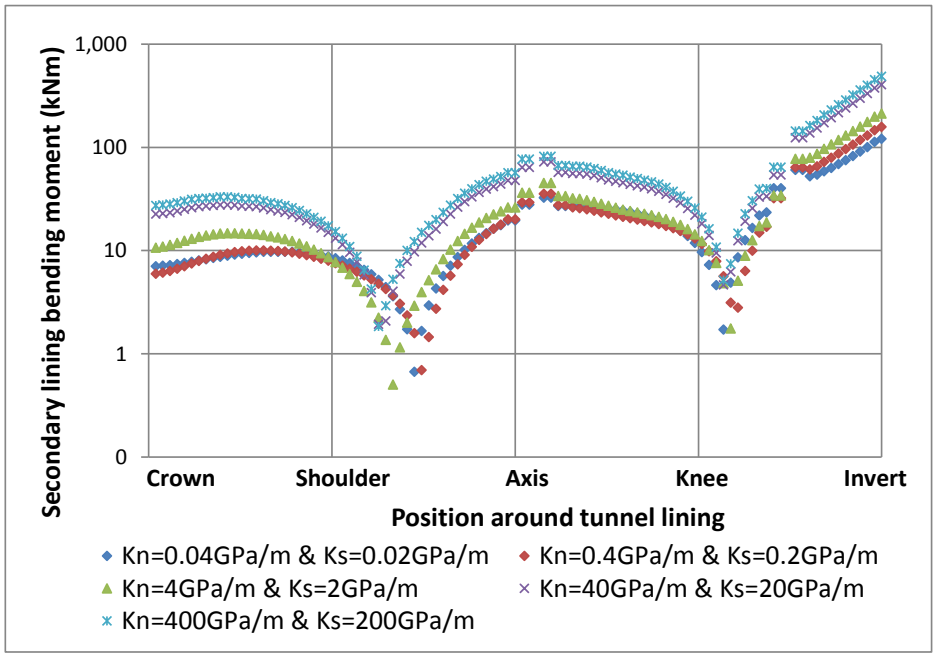

Figure D-4 Sensitivity of secondary lining bending moment to simultaneously varying Kn and Ks values

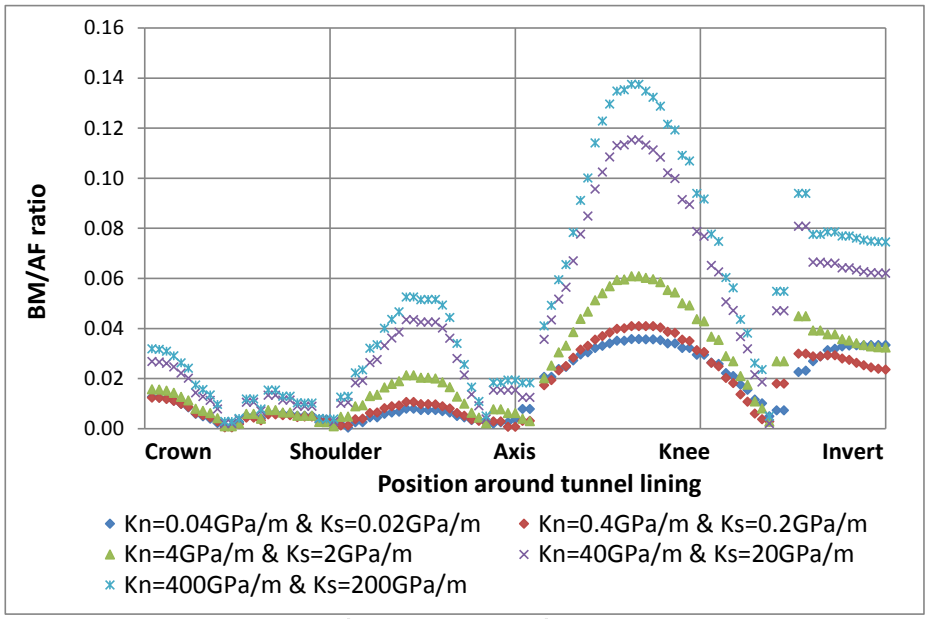

Figure D-5 Sensitivity of BM/AF ratio for primary lining to simultaneously varying Kn and Ks values

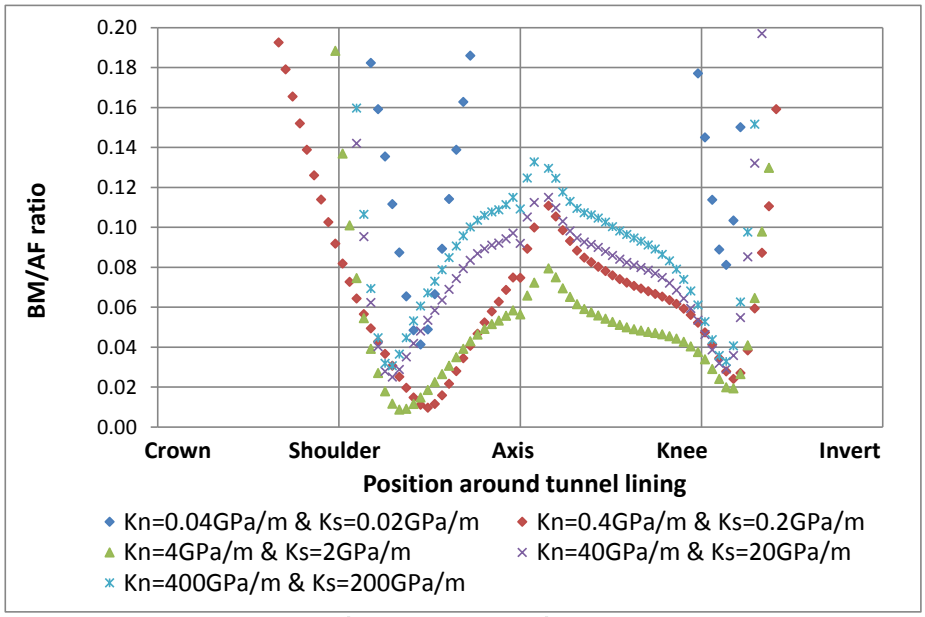

Figure D-6 Sensitivity of BM/AF ratio for secondary lining to simultaneously varying Kn and Ks values

Appendix E Plots for lining thickness parametric study

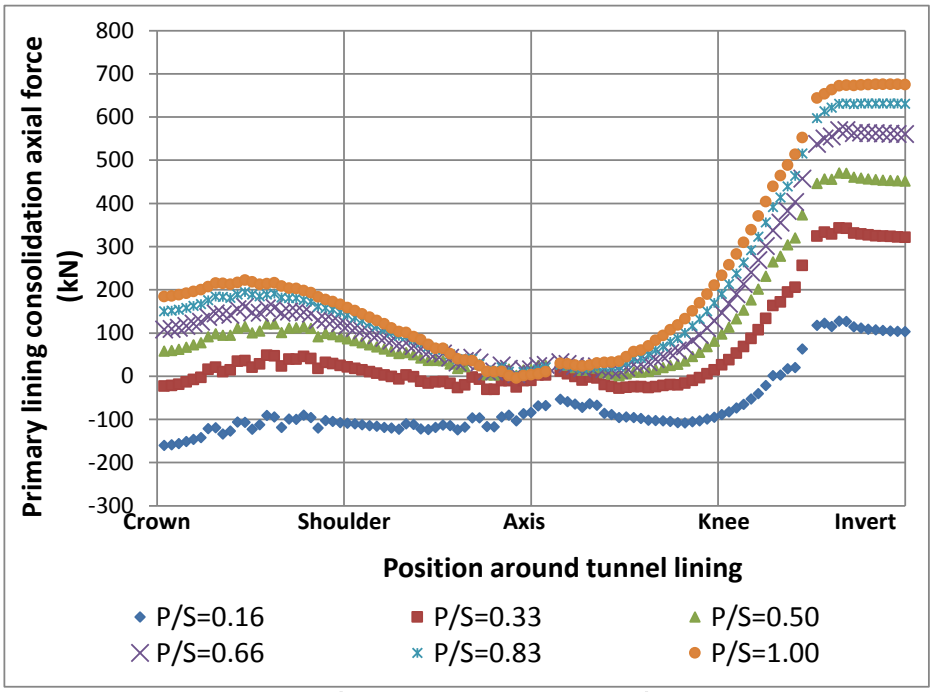

Figure E-1 Sensitivity of primary lining axial force to varying primary/secondary lining thickness ratio (P/S ratio≤1)

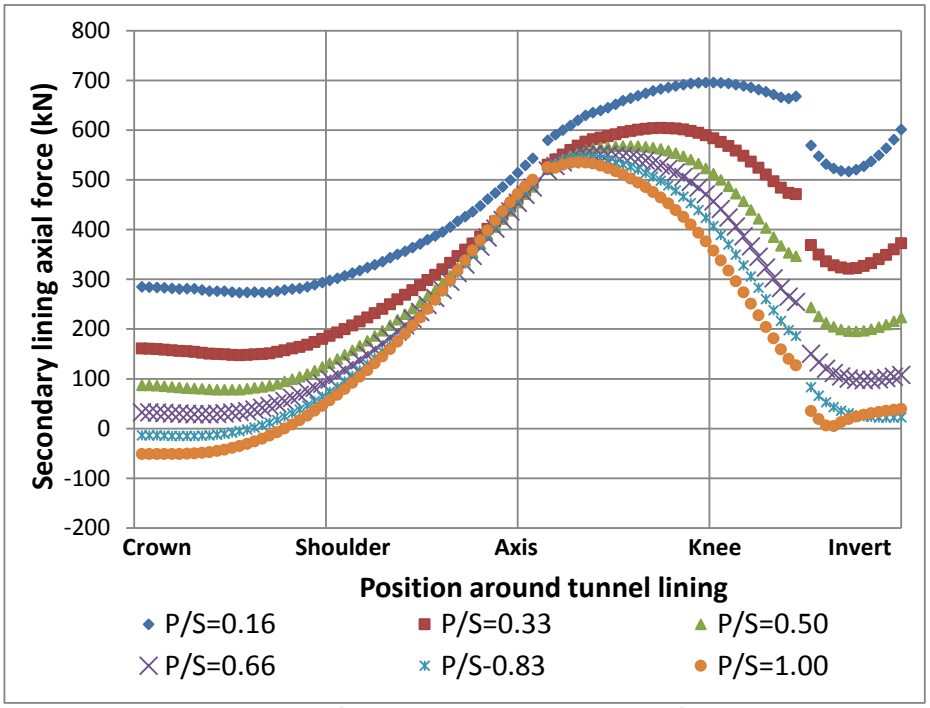

Figure E-2 Sensitivity of secondary lining axial force to varying primary/secondary lining thickness ratio (P/S ratio≤1)

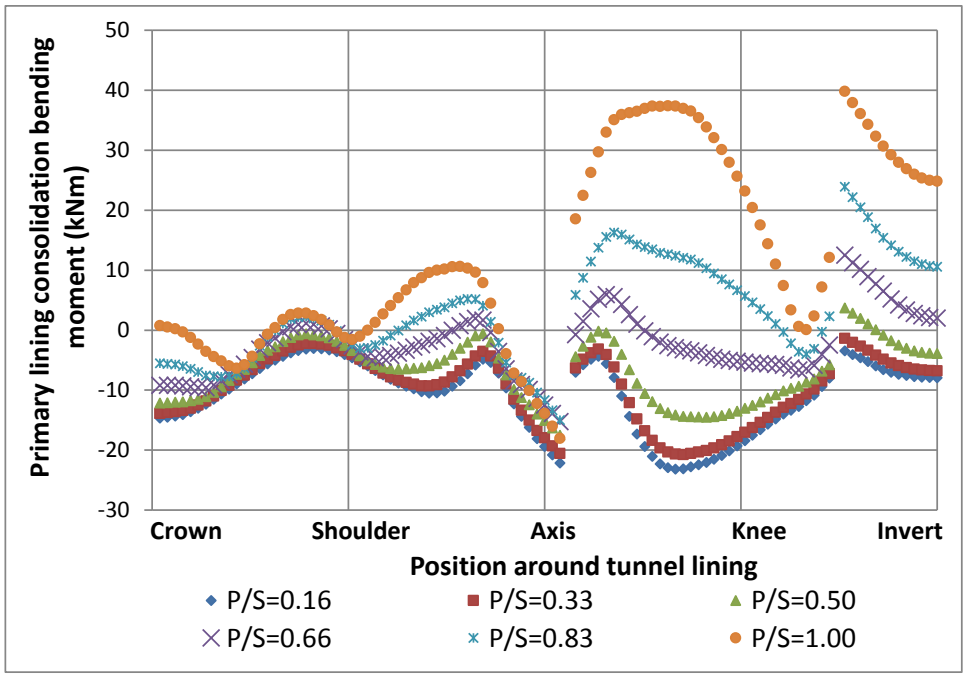

Figure E-3 Sensitivity of primary lining bending moment to varying primary/secondary lining thickness ratio (P/S ratio≤1)

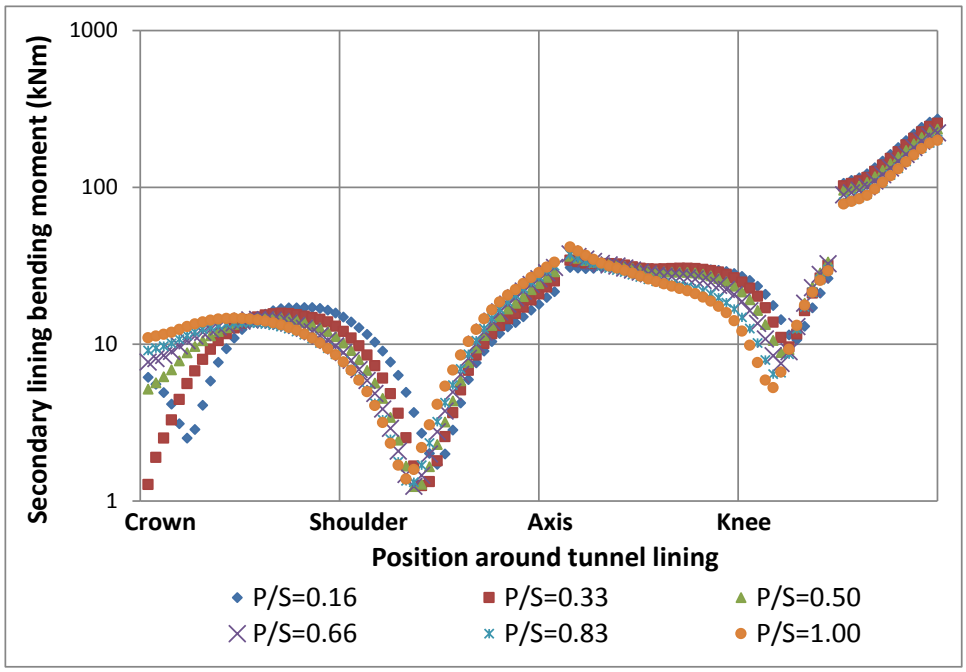

Figure E-4 Sensitivity of secondary lining bending moment to varying primary/secondary lining thickness ratio (P/S ratio≤1)

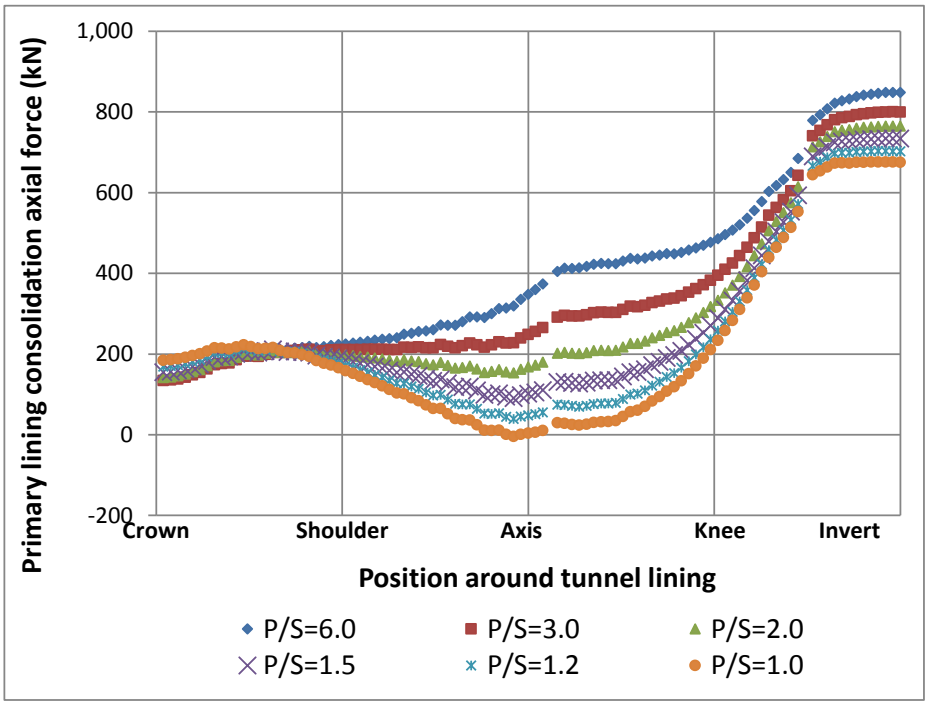

Figure E-5 Sensitivity of primary lining axial force to varying primary/secondary lining thickness ratio (P/S ratio≥1)

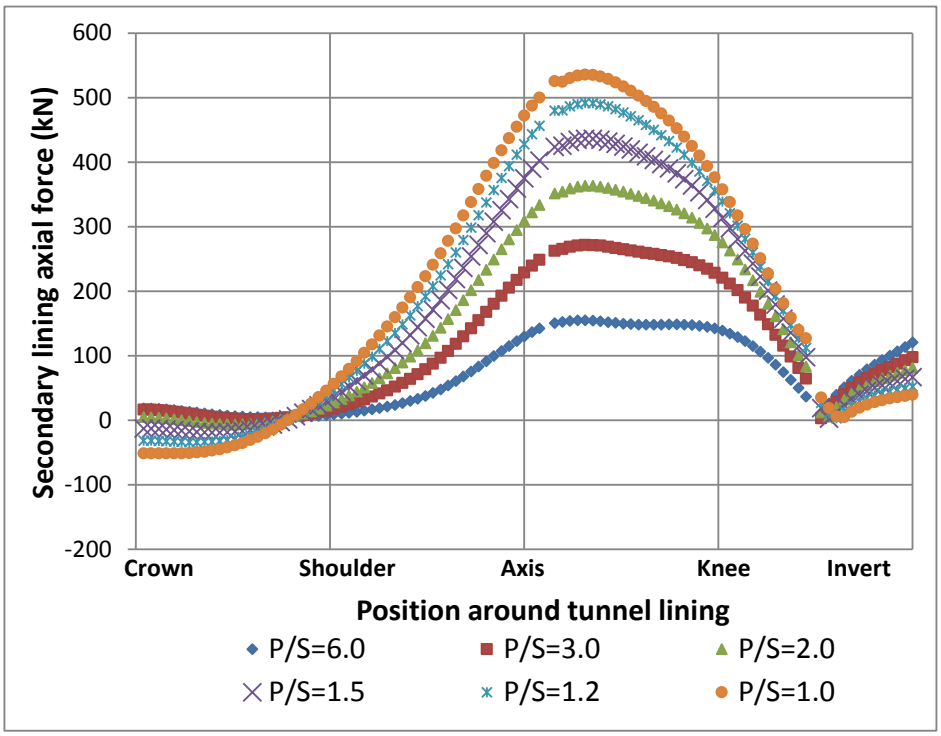

Figure E-6 Sensitivity of secondary lining axial force to varying primary/secondary lining thickness ratio (P/S ratio≥1)

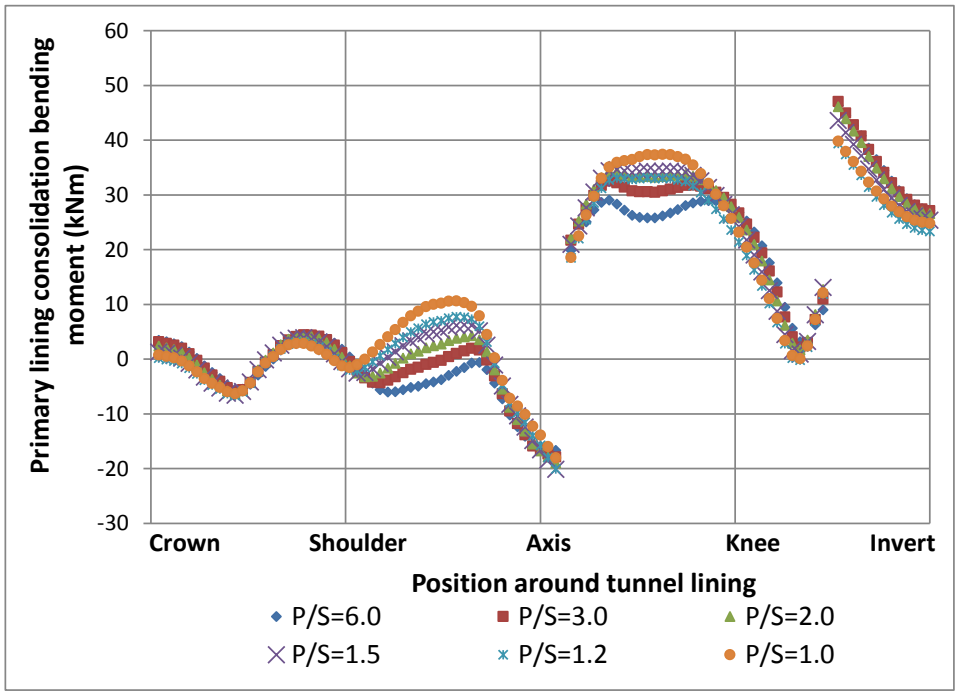

Figure E-7 Sensitivity of primary lining bending moment to varying primary/secondary lining thickness ratio (P/S ratio≥1)

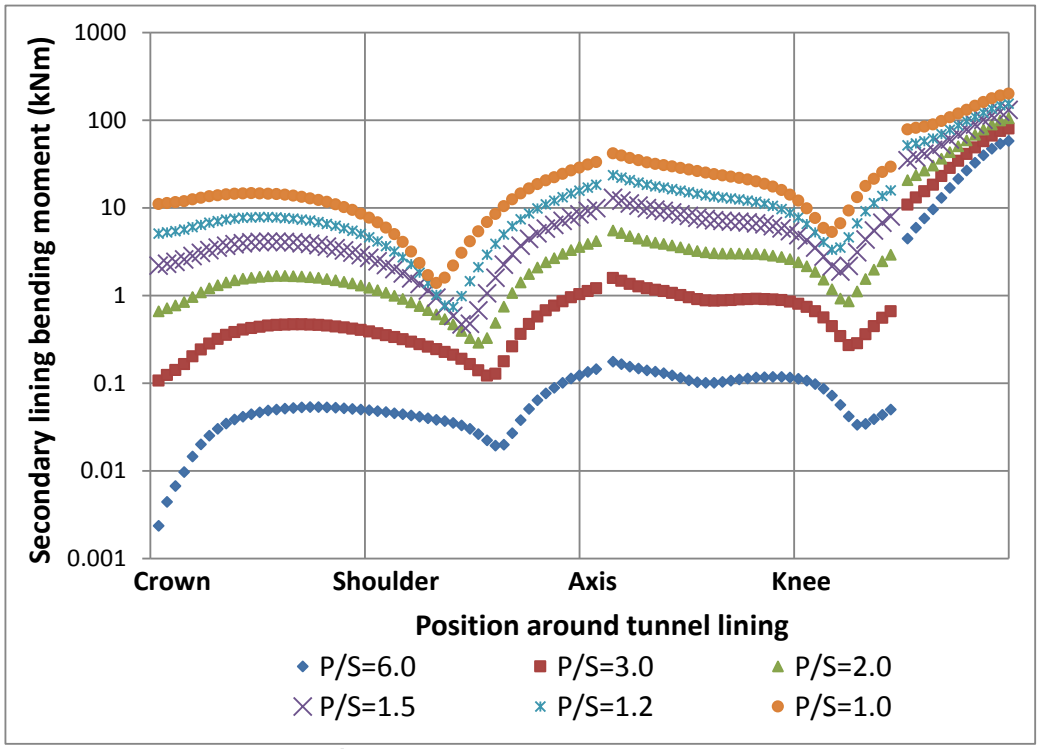

Figure E-8 Sensitivity of secondary lining bending moment to varying primary/secondary lining thickness ratio (P/S ratio≥1)

Appendix F Plots for nearby construction parametric study

In the following plots, R is the ratio between the clear distance between the nearby construction and tunnel extrados to the tunnel diameter.

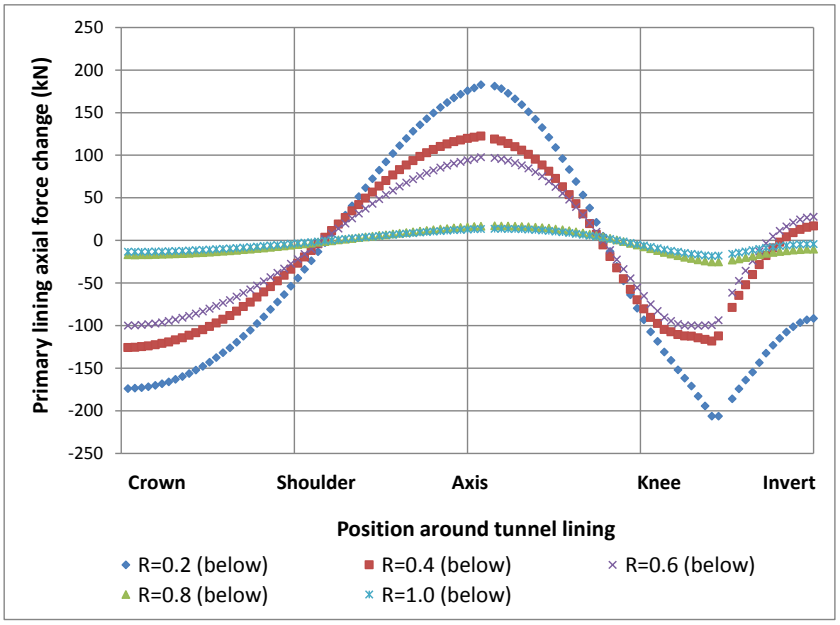

Figure F-1 Primary lining axial force changes to the beneath construction

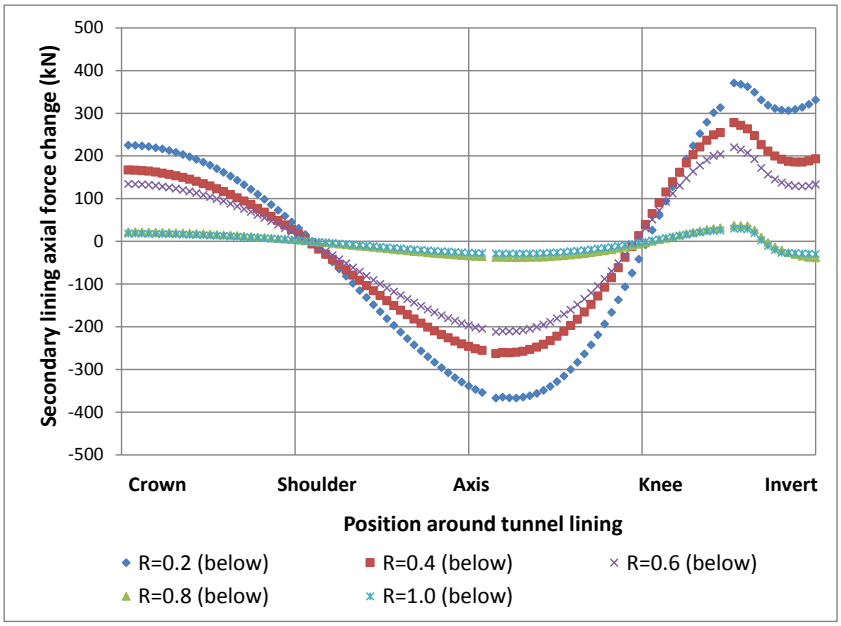

Figure F-2 Secondary lining axial force changes to the beneath construction

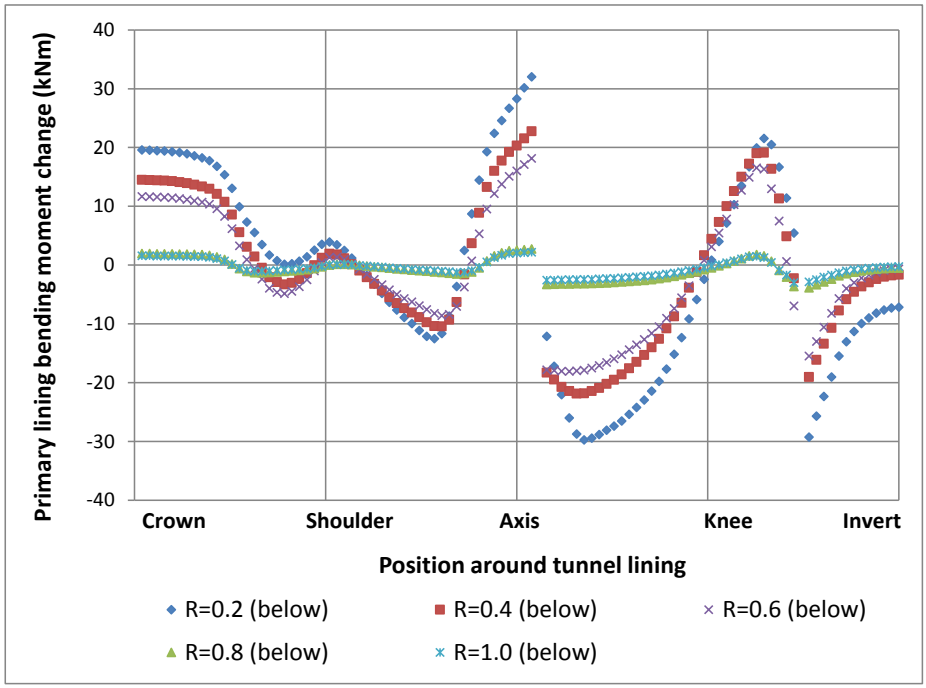

Figure F-3 Primary lining bending moment changes to the beneath construction

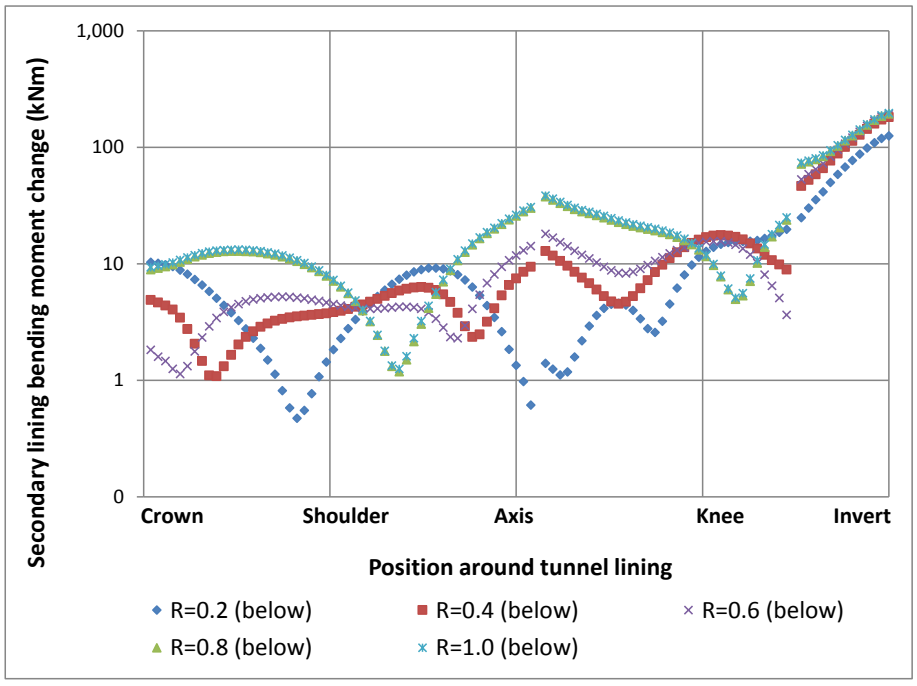

Figure F-4 Secondary lining bending moment changes to the beneath construction

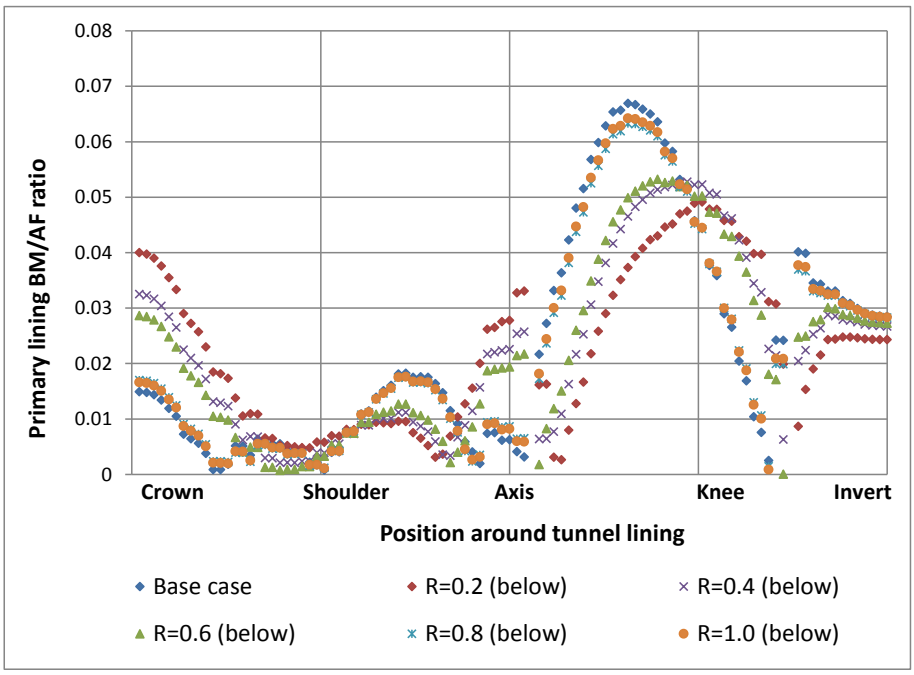

Figure F-5 BM/AF ratio for the primary lining with beneath construction

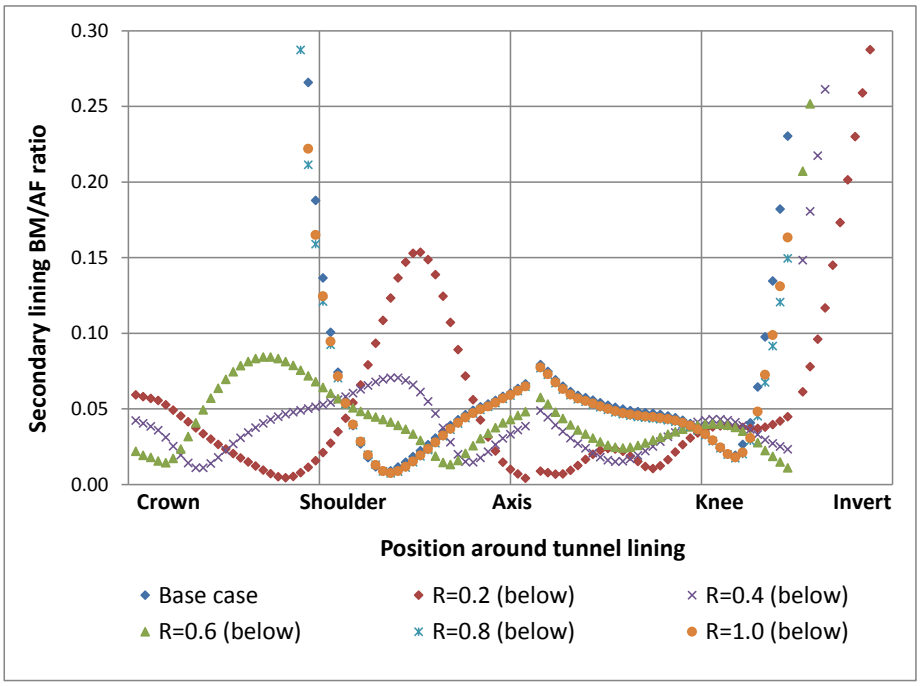

Figure F-6 BM/AF ratio for the secondary lining with beneath construction

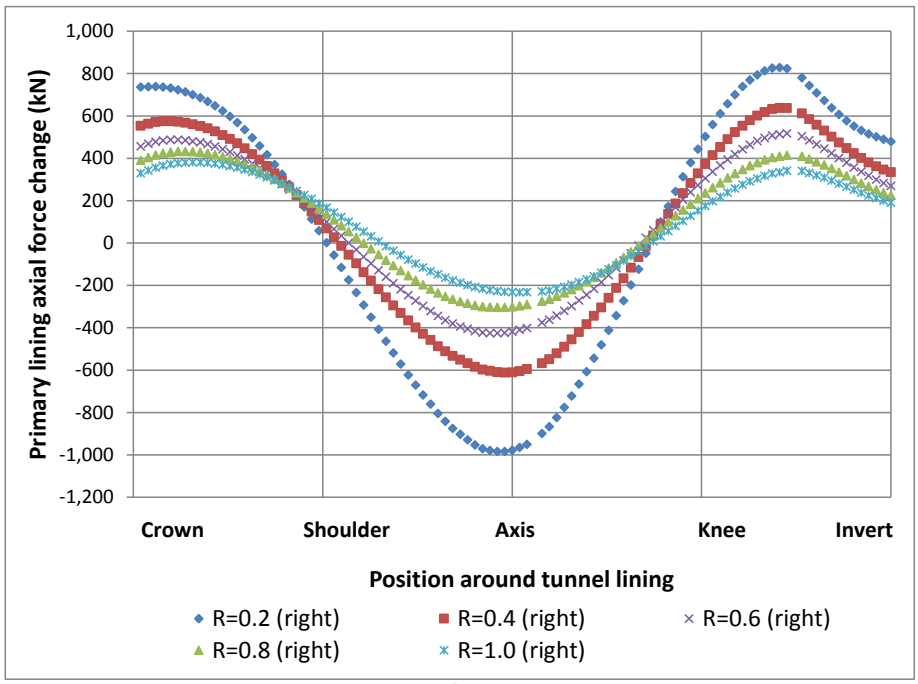

Figure F-7 Primary lining axial force changes to right hand side construction

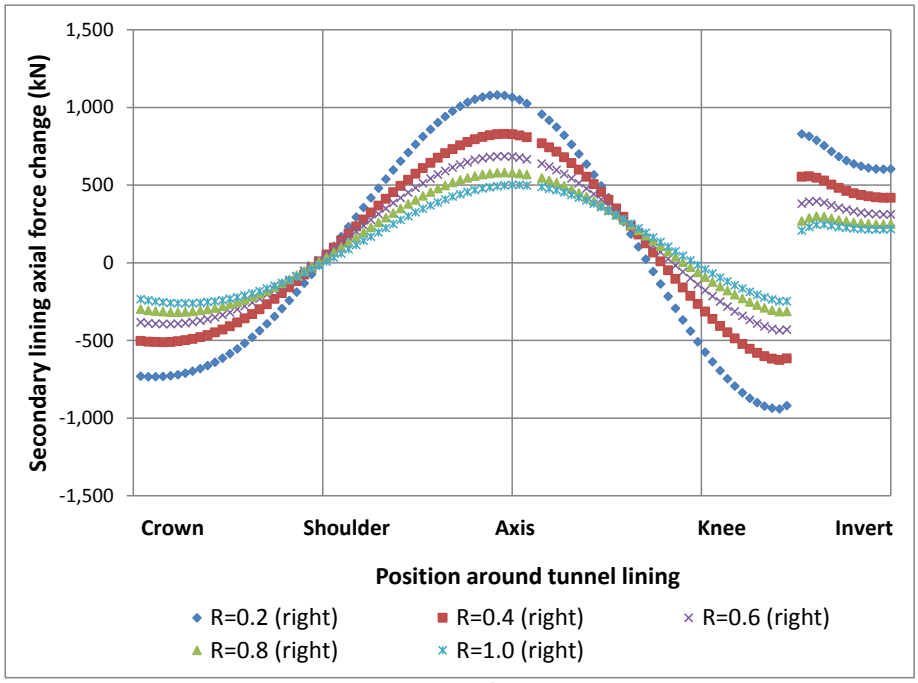

Figure F-8 Secondary lining axial force changes to right hand side construction

Figure F-9 Primary lining bending moment changes to right hand side construction

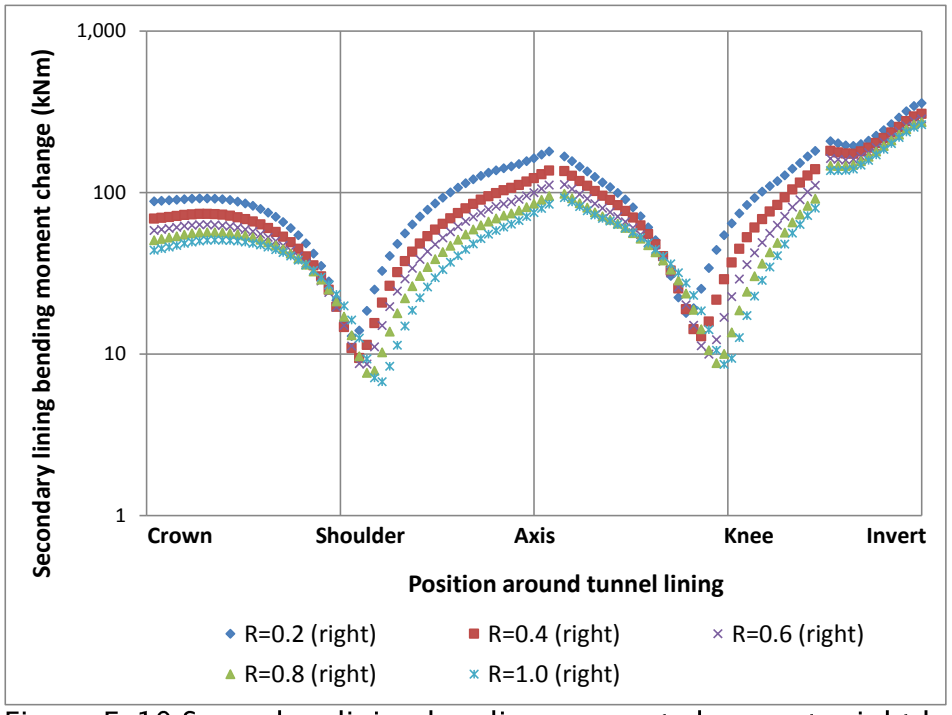

Figure F-10 Secondary lining bending moment changes to right hand side construction

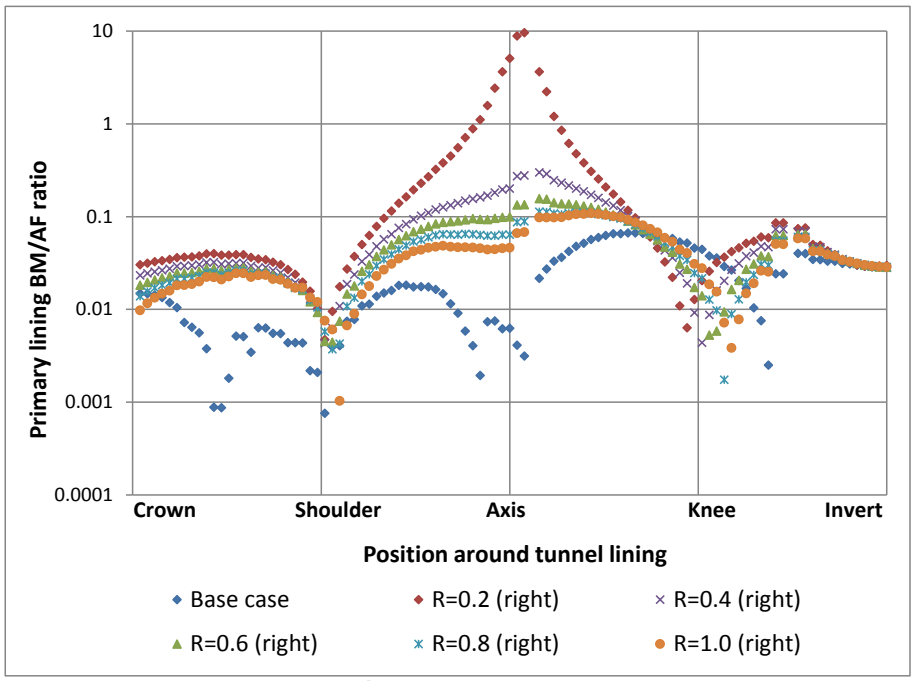

Figure F-11 BM/AF ratio for the primary lining with right hand side construction

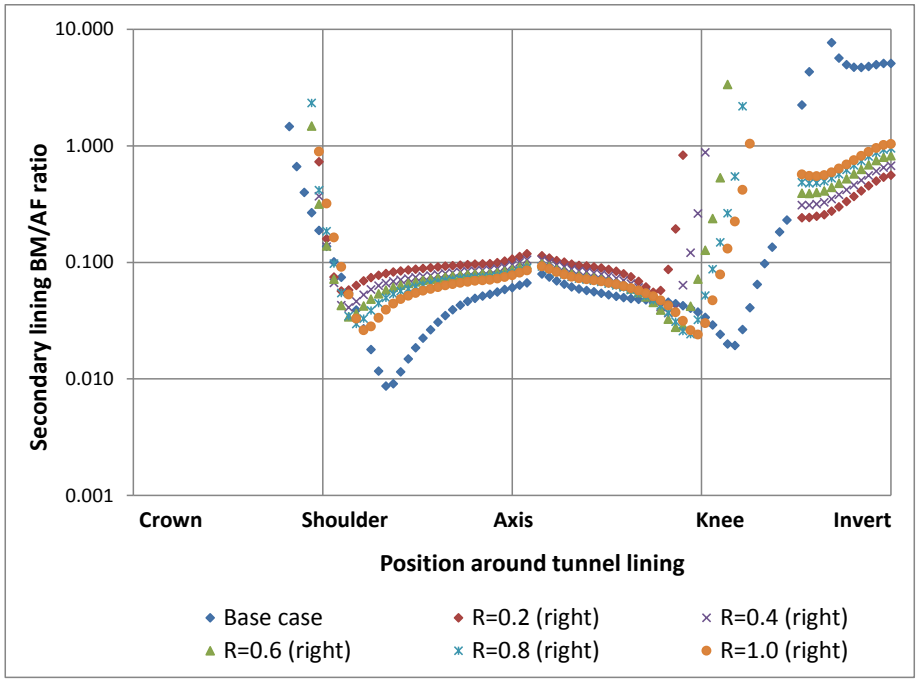

Figure F-12 BM/AF ratio for the secondary lining with right hand side construction

List of References

Addenbrooke, T.I. (1996). *Numerical analysis of tunnelling in stiff clay*, PhD Thesis, Imperial College, London.

Addenbrooke, T.I., Potts, D.M. and Puzrin, A.M. (1997). The influence or pre-failure soil stiffness on the numerical analysis of tunnel construction. *Géotechnique,* 47(3), 693-712.

Annett, M.F., Earnshaw, G. and Leggett, M. (1997). Permanent sprayed concrete linings at Heathrow Airport. *Proceedings of the Tunnelling 97*, Institution of Mining & Metallurgy, London, 517-534.

ASCE (1984), *Tunnel Lining Design*, American Society of Civil Engineers.

Ashby, M.F. and Jones, DRH. (2005) *Engineering Materials 2: An Introduction to Microstructures, Processing and Design*, 3rd Edition, Butterworth-Heinemann Publishing.

Atkinson, J. (2000). Non-linear soil stiffness in routine design. Géotechnique, 50(5), 487-508.

Atkinson, J. (2007). The mechanics of soils and foundations. CRC Press.

Atkinson, J. H. and Sallfors, G. (1991). Experimental determination of soil properties. General Report to Session 1. *Proceedings of the 10th ECSMFE*, Florence, 915-956.

Austin, S. and Robbins, P. (1995). *Sprayed Concrete: Properties, design and application*, Bristol: Whittles Publishing.

Babendererde, S. (1980). Application of the new Austrian Tunnelling Method for Metro Construction in the Federal Republic of Germany, *Proceedings for Eurotunnel '80*, Basle, Switzerland, Institution of Mining and Metallurgy, London, 54-58.

Barton, N.R. and Choubey, V. (1977). The shear strength of rock joints in theory and practice. *Rock Mechanics* 10(1-2), 1-54.

Barton N. and Grimstad E. (1994). Rock mass conditions dictate the choice between NMT and NATM, *Tunnels & Tunnelling*, Oct. 1994, 26, 39-42.

BASF (2008). Flexural strength test data for Masterseal 345. Unpublished Report. BASF Construction Chemicals Europe AG. Zurich.

Bernard, E.S. (2004). Creep of cracked fibre-reinforced sprayed concrete panels, *Sprayed concrete: More Engineering Developments*, Taylor & Francis, London, 47-58.

Bernard, E.S. (2008). Early-age load resistance of fibre reinforced sprayed concrete linings. *Tunnelling and Underground Space Technology,* 23, 451-460.

Bolton, M. D. (1991). A guide to soil mechanics. Universities Press.

Brown, E.T., Bray, J.W., Ladanyi, B. and Hoek, E. (1983). Ground response curves for rock tunnels, *Journal of Geotechnical Engineering. ASCE* (109), 15-39.

Brown, E.T. (1990). Putting the NATM into perspective. *Tunnels & Tunnelling*, Summer 1990, special issue, 22, 9-13.

BS EN 1992-1-1 (2004). *Design of concrete structures — Part 1-1: General rules and rules for buildings*, British Standards Institution, London.

BS EN 12390-1 (2000). *Testing Hardened Concrete – Part 1: Shape, dimensions and other requirements for specimens and moulds.* British Standards Institution, London.

BS EN 12390-3 (2009). *Testing Hardened Concrete – Part 3: Compressive strength of test specimens.* British Standards Institution, London.

BS EN 12390-5 (2000). Testing harden concrete. Flexural strength of test specimens. British Standard Institution, London.

BS EN 14488-3 (2006). Testing Sprayed Concrete – Part 3: Flexural strengths (first peak, ultimate and residual) of fibre reinforced beam specimens. British Standard Institution, London.

BTS (2004). *Tunnel lining design guide*. Thomas Telford Publishing, London.

Chang, J., Scott, J.M. and Pound, C. (2001). Numerical study of Heathrow cofferdam, *Proceedings of the 2nd International Symposium FLAC and Numerical Modelling in Geomechanics*. Lyon, 163-169.

Chang, Y. and Stille, H. (1993). Influence of early age properties of sprayed concrete to tunnel construction sequence, *Proceedings of Sprayed concrete for Underground Support VI*, American Society of Civil Engineers, Reston, 110-17.

Clayton, C. R. I., Van der Berg, J. P. and Thomas, A. H. (2006). Monitoring and displacements at Heathrow Express Terminal 4 station tunnels. *Géotechnique,* 56(5), 323–334.

Clayton, C.R.I., Hope, V.S., Heymann, G., Van der Berg, J.P. and Bica, A.V.D (2000). Instrumentation for monitoring sprayed concrete lined soft ground tunnels. *Proceedings of the ICE, Geotechnical Engineering*, 143(3), 119-130.

Crossrail (2009a). *Crossrail Central Section – Tunnels: Materials and Workmanship Specification Sprayed Concrete Linings*. Unpublished report.

Crossrail (2009b). *Crossrail SCL Tunnels – MDC2/3 Sprayed Secondary Lining Study*. Unpublished report.

Crossrail (2010), *Civil Engineering Design Standard – part 2: Tunnels and Shafts*. Unpublished report.

Curtis, D. J. (1976). Discussion on the circular tunnel in elastic ground, *Géotechnique,* 26(1), 231-237.

List of References

Curtis, D. J. (2010). The Curtis-Muir-Wood Formulea. *Proceedings of Sir Alan Wood Memorial Symposium*. London. https://www.britishtunnelling.org.uk/ajax/functiongrabber.asp?loadfunction=downloadfile&f=downloads&filename=10-john-curtis-the-curtis-muir-wood-formulae.pdf.

Deane, A.P. and Bassett, R.H. (1995). The Heathrow Express Trial Tunnel, *Proceedings of the ICE, Geotechnical Engineering*, 113(3), 144 -156.

Deane, A.P., Myers, A.G. and Tipper, G.C. (1997). Tunnels for Heathrow Express, *Proceedings of Tunnelling 97*, Institution of Mining & Metallurgy, London. 535-550.

Devriendt, M. (2012). Crossrail, CSIC and using instrumentation to make savings in design and assessment, *JSPS/CSIC international symposium on Smart Infrastructure and Construction*, Cambridge. http://www-smartinfrastructure.eng.cam.ac.uk/20121112CSICJSPS/20121113devriendt

Dimmock, R.H., Haig, B. and Su, J. (2011). Spray Applied Waterproofing Membranes – Key Success Factors and Development of Efficient Sprayed Concrete Tunnel Linings. *Proceedings of 6th international symposium on sprayed concrete.* Tromso, Norway, 110-124.

Eadington, J. and O'Brien, T. (2011). Stiffness parameters for a deep tunnel – Developing a robust parameter selection framework. *Proceedings of. 15th European Conference on Soil Mechanics and Geotechnical Engineering*. Athens, Greece.

EFNARC (1996). *The European Specification for sprayed concrete*. European Federation of Producers and Applicators of Specialist Products for Structures.

Franzén, T. (1992). Sprayed concrete for underground support: a state-of-the-art report with focus on steel-fibre reinforcement. *Tunnelling and Underground Space Technology*, 7(4) 383-391.

Fuenkajorn, K. (2011). Experimental assessment of long-term durability of some weak rocks. *Bulletin of Engineering Geology and the Environment*, 70(2), 203-211.

Gasparre, A. (2005) *Advanced laboratory characterisation of London Clay*. PhD Thesis. University of London.

GE, *Undercover operation on Crossrail's Whitchapel tunnels*, October 2013, http://www.nce.co.uk/features/geotechnical/undercover-operation-on-crossrails-whitchapel-tunnels/8653502.article?sm=8653502

Golser, J. (1976). The New Austrian Tunnelling Method (NATM) (theoretical background – practical experiences). *Proceedings of the Engineering Foundation Conference*, Easton, Maryland, USA. 675-712.

Golser, J. (1978). History and development of the New Austrian Tunnelling Method. *Proceedings of. Engineering Foundation Conference Sprayed concrete for Underground Support III*, St. Anton am Arlberg, Austria, 1-13.

Grose, W.J. and Eddie, C.M. (1996). *Geotechnical aspects of the construction of the Heathrow transfer baggage system tunnel*. Unpublished Paper, Ove Arup Ltd.

Graz (2008). *Laboratory Report: Direct Shear Test Results for Masterseal 345*. Unpublished Report. BASF Construction Chemicals Europe AG. Zurich.

Guo, Z.H. and Zhang, H.Q. (1987). Investigation of complete stress-deformation curves for concrete in tension. *ACI Materials Journal*, 84(4), 278-285.

Hagenhofer, F. (1990). NATM for tunnels with high overburden. *Tunnels and Tunnelling*, 22(5), 2.

Hoek, E. and Brown, E. (1980). *Underground Excavation in Rock*, Institution of Mining and Metallurgy, London.

Holter, K.G. and Nermoen, B. (2011). Permanent Waterproof Tunnel Lining Based on Sprayed Concrete and Spray-Applied Double- Bonded Membrane. *Proceedings of the World Tunnel Congress 2011, Underground Space in the Service of a Sustainable Society:* Helsinki: ITA-AITES. 330-340.

HSE (2000), The collapse of NATM tunnels at Heathrow Airport. Health and Safety Executive Books, HMSO, Norwich.

Hurt, J. (2002). Primary Ways to Save – Harding Prize Paper. *Tunnels & Tunnelling International*, Polygon Media, Sevenoaks, 2. 44-45

ICE (1996). *Sprayed concrete linings (NATM) for tunnels in soft ground, ICE design and practice guide*, Thomas Telford Publishing, London.

ITA (1996). Health and safety in shotcreting: ITA working group report, *Tunnelling and Underground Space Technology*, Vol. 11. 391-409.

ITA (2013). *ITAtech design guidance for spray applied waterproofing membranes*. http://www.ita-aites.org/en/wg-committees/committees/itatech/publications

Jardine, R.J., Potts, D.M., Fourie, A.B., *et al.* (1986). Studies of the influence of non linear stress-strain characteristics in soil-structure interaction, *Géotechnique,* 36(3), 377-396.

Jardine, R.J., Symes, M.J.P.R. and Burland, J.B. (1984). The measurement of soil stiffness in the triaxial apparatus, *Géotechnique,* 34(3), 323-340.

Jones, B.D. (2007). *Stress in Sprayed Concrete Tunnel Junctions*. PhD thesis, University of Southampton.

Jones, B.D., Thomas, A.H., Hsu, Y.S. and Hilar, M. (2008). Evaluation of innovative sprayed-concrete-lined tunnelling. *Proceedings of the Institution of Civil Engineers, Geotechnical Engineering*, 161, 137-149.

Kovári, K. (1994). Erroneous concepts behind the New Austrian Tunnelling Method, *Tunnels &Tunnelling*, November. 38-42.

Kovári, K. (2003a). History of the sprayed concrete lining method – part I: milestones up to the 1960s. *Tunnelling and Underground Space Technology*, 18(1), 57-69.

Kovári, K. (2003b). History of the sprayed concrete lining method – part II: milestones after the 1960s. *Tunnelling and Underground Space Technology*, 18(1), 71-83.

Kusterle, W.A. (1997). New ecologically desirable sprayed concrete. *Proceedings of Tunnelling 97*. Institution of Mining & Metallurgy, London, 263-274.

Linney, L.F. and Essler, R.D. (1994). Compensation grouting trail works at Redcross Way, London. *Grouting in the ground.* Thomas Telford, London, 313-326.

LUKAS, W. (2003). *Practical effectiveness of cement-bonded sealing layers for single-shell tunnel construction project*. Unpublished Report. University of Innsbruck.

Lyons, B., Kumpfmueller, S., Sleath, M. and Terry, D. (2014). Development of Sprayed Concrete Linings for London Underground Bond Street Station Upgrade Project, London, UK. *Proceedings of North American Tunnelling 2014*, Society for Mining, Metallurgy & Exploration, 76-85.

Mair, R.J. (1993). Developments in geotechnical engineering research: applications to tunnels and deep excavations. *Unwin Memorial Lecture 1992, Proceedings of the Institution of Civil Engineering*, *Civil Engineering*, 3, 27-41.

Mair, R.J. and Jardine, F.M (2001). *Tunnelling methods. Building Response to Tunnelling*, Vol. 1. 127-134.

List of References

Mar, A. and Eddie, C. (2013). Modelling the influence of compensation grouting sing advanced three-dimensional finite element analysis. Proceedings of the NAFEMS World Congress 2013, Austria. http://www.nafems.org/downloads/nwc13/abstracts/292_Mar.pdf

Meriam, J.L. and Kraige, L.G. (2011). *Engineering Mechanics: Statics. 7th Edition.* John Wiley & Sons;

Mašın, D. and Herle, I. (2005). Numerical analyses of a tunnel in London clay using different constitutive models. *Proceedings of 5th International Symposium TC28 Geotechnical Aspects of Underground Construction in Soft Ground*. Amsterdam, The Netherlands.

Mott MacDonald (2008). *Product evaluation of MASTERSEAL 345: assessment, application and specification.* Unpublished report.

Mott MacDonald (2009a). *SCL Numerical Modelling Guidelines.* Unpublished report.

Mott MacDonald (2009b). *Numerical Modelling of Composite Shell Lining.* Unpublished report.

Mott MacDonald, (2009c). *Crossrail C121 isotropic nonlinear stiffness moduli for numerical modelling.* Unpublished report.

Mott MacDonald, (2010a). *SCL tunnel lining optimisation study.* Unpublished report.

Mott MacDonald, (2010b). *Heathrow Express SCL Tunnel – Calibration Report for Relaxation Methodology.* Unpublished report.

Mott MacDonald, (2010c). *Kings Cross back analysis.* Unpublished report.

Mott MacDonald, (2010d). *London Bridge Calibration.* Unpublished report..

Mott MacDonald, (2011). *3D Analysis of SCL tunnel junctions.* Unpublished report.

Mott MacDonald, (2012), *Secondary Lining at Junctions – 3D analysis.* Unpublished report.

Mott MacDonald, (2013a). *Bond Requirement between Sprayed-applied waterproofing membrane and SCL linings.* Unpublished report.

Mott MacDonald, (2013b). *Compensation grouting review.* Unpublished report.

Muir Wood, A.M. (1975). The circular tunnel in elastic ground. *Géotechnique*. 25(1), 115-127.

Müller-Salzburg, L. (1977). The use of deformation measurements in dimensioning the lining of subway tunnels. *Proceedings of International Symposium on Field Measurements in Rock Mechanics*. Zurich, Switzerland, Vol. 1. 451-471.

Neville, A.M. (1995). *Properties of Concrete*. 4th Edition, Addison Wesley Longman Limited. England.

O'Brien, A. and Harris, D. (2013). Geotechnical characterisation, recent development and applications. *Proceedings of the 12th International Conference on Underground Construction*, Prague.

Panet, M. and Guenot, A. (1982). Analysis of convergence behind the face of a tunnel. *Proceedings of Tunnelling 82*, Institution of Mining & Metallurgy, London, 197-204.

Peck, R.B. (1969). Deep excavations and tunneling in soft ground. *Proceedings of the 7th International Conference on Soil Mechanics and Foundation Engineering,* Mexico City, 225-281

Pickett, A. (2013). Crossrail sprayed concrete linings design. Underground. The Way to the Future. *Proceedings of World Tunnel Congress 2013*, Abingdon, GB, CRC Press.593-600.

Powell, D.B., Sigl, O. and Beveridge, J.P. (1997) Heathrow Express - design and performance of platform tunnels at Terminal 4, *Proceedings of Tunnelling 97*, Institution of Mining & Metallurgy, London, 565 -593.

Rabcewicz, L.V. (1954a). Bolted support for tunnels – part one. *Water Power*, April, 150-155.

Rabcewicz, L.V. (1954b). Bolted support for tunnels – part two. *Water Power*, May, 171-175.

Rabcewicz, L.V. (1964a). The New Austrian Tunnelling Method – part one. *Water Power*, November, 453-457.

Rabcewicz, L.V. (1964b). The New Austrian Tunnelling Method – part two. *Water Power*, December, 511-515.

Rabcewicz, L.V. (1965). The New Austrian Tunnelling Method – part three. *Water Power*, January, 19-24.

Rabcewicz, L.V. (1969a). Stability of tunnels under rock load – part one. *Water Power*, June, 225-229.

Rabcewicz, L.V. (1969b). Stability of tunnels under rock load – part two. *Water Power*, July, 266-273.

Rabcewicz, L.V. (1969c). Stability of tunnels under rock load – part three. *Water Power*, August, 297-302.

Rabcewicz, L.V. and Golser, J. (1973). Principles of dimensioning the supporting system for the “New Austrian tunnelling method”. *Water Power*, March, 88-93.

Rabcewicz, L.V. and Golser, J. (1974a). Application of the NATM to the underground works at Tarbela – part one. *Water Power*, September, 314-321.

Rabcewicz, L.V. and Golser, J. (1974b). Application of the NATM to the underground works at Tarbela – part two. *Water Power*, October, 330-335.

Raphael, J. M. (1984). Tensile strength of concrete. *ACI Journal Proceedings* Vol. 81, No. 2, 158-165.

RILEM (2003) RILEM TC 162-TDF 2003 Test and design methods for steel fibre reinforced concrete, *Materials and Structures*, 36, 560-567.

Sauer, G. (1988). Further insights into the NATM. The 23rd Sir Julius Wernher Memorial Lecture of the Institution of Mining and Metallurgy, London.

Sauer, G., Gall, V., Bauer, E. and Dietmaier, P. (1994). Design of tunnel linings using capacity limit curves. *Proceedings of the 8th international conference on computer methods and advances in geomechanics*. http://www.dr-sauer.com/technical-info/938

Scott, J.M, Pound, C. Shanghavi, H.B. (2003) Heathrow airside road tunnel: wall design and observed performance. *Proceedings of the International Conference on Underground Construciton*. London. 281-292.

Shuttleworth, P. (2001) Fire Protection of Concrete Tunnel Linings, *Proceedings of the Third International Conference on Tunnel Fires, Oct. 9-11, 2001*, Washington, DC, 157-165.

Simpson, B. (1993). Development and application of a new soil model for prediction of ground movements. *Predictive Soil Mechanics. Proceedings of the Wroth Memorial Symposium,* Oxford, 628-643.

Spyridis, P., Nasekhian, A. and Skalla, G. (2013). Design of SCL structures in London. *Geomechanics and Tunnelling*. 6(1), 66-80.

Thomas, A.H. (2008). *Sprayed Concrete Lined Tunnels*. Abingdon: Taylor and Francis Publishing.

Thomas, A.H. (2003). *Numerical Modelling of Sprayed Concrete Lined (SCL) tunnels*. PhD thesis, University of Southampton.

Thomas, A.H. and Pickett, A.P. (2011). The design of composite sprayed linings. Proceedings of the 6th international symposium on sprayed concrete, Tromso, 2011, 402-413.

TRL (1998). *Single Pass Tunnel Linings Final Report*. Unpublished Project Report. Transport Research Laboratory.

Van der Berg, J.P., Clayton, C.R.I. and Powell, D.B. (2003). Displacements ahead of an advancing NATM tunnel in the London clay. *Géotechnique*, 53(9), 767-784.

Watson, P., Warren, C.D., Eddie, C. and Jäger, J. (1999). CTRL North Downs Tunnel, *Proceedings of the Tunnel Construction and Piling Symposium*, London, 301-323.

Whittle, A. J., & Kavvadas, M. J. (1994). Formulation of MIT-E3 constitutive model for overconsolidated clays. *Journal of Geotechnical Engineering*, 120(1), 173-198

Wongsaroj, J., Soga, K. and Mair, R.J. (2007). Modelling of long term ground response to tunnelling under St James's Park, London. *Géotechnique,* 57(1), 75-90.

Yamamuro, J. A. and Kaliakin, V. N. (2005). *Soil constitutive models: Evaluation, selection, and calibration*. ASCE.

Zhang, L. and Morgan, D.R. (2014) Variability of Compressive Strength of Shotcrete, *Proceedings of 7th International Symposium on Sprayed Concrete*, Sandefjord, Norway, 446-458.

.

Bibliography

ACI (2005). *ACI 506R-05: Guide to Sprayed concrete*, American Concrete Institute, Farmington Hills.

Aldrian, W. and Kattinger, A. (1997). Monitoring of performance of primary support of NATM station at Heathrow Terminal 4, *Tunnels for People*, 71 – 77.

Au, S.K.A., Soga, K., Jafari, M.R., Bolton, M.D. and Komiya, K. (2003). Factors affecting long-term efficiency of compensation grouting in clays. *Journal of Geotechnical and Geoenvironmental Engineering*, 254-262.

Austrian Concrete Society (1999). *Sprayed Concrete Guideline*, Karlsgasse: Osterreichischer Betonverein.

BASF (2009). *Specification for a waterproofinging fully bonded sprayed applied system*. Unpublished Report. BASF Construction Chemicals Europe AG. Zurich.

BS EN 14487-1 (2005). *Sprayed Concrete — Part 1: Definitions, Specifications and Conformity*, British Standards Institution, London.

Brite Euram (1998). *New materials, Design and Construction Techniques for Underground Structures in Soft Rock and Clay Media*, BRE-CT92-0231 Final Technical Report, Mott MacDonald.

Chang, Y. (1994). *Tunnel support with sprayed concrete in weak rock – a rock mechanics study*, PhD Thesis, Royal Institute of Technology, Stockholm.

Clayton, C. R. I., Van Der Berg, J. P., Heymann, G., Bica, A. V. D. and Hope, V. S. (2002). The performance of pressure cells for sprayed concrete tunnel linings. *Géotechnique,* 52(2), 107–115.

Crossrail (2009). *Crossrail Central Section – Tunnels: Materials and Workmanship Specification – Spray Applied Waterproofing Membrane Systems for SCL Tunnels and Shafts*. Unpublished Report. Crossrail.

Dasari, G. R. (1996). *Modelling the variation of soil stiffness during sequential construction*, PhD Thesis, University of Cambridge.

Dasari, G. R., Rawlings, C.G. and Bolton, M.D. (1996). Numerical modelling of a NATM tunnel construction in London clay, *Proceedings International Symposium on Geotechnical Aspects of Underground Construction in Soft Ground*, City University, Balkema, 491–496.

DBV (2001). *Steel fibre reinforced concrete, Code of Practice*, Deutscher Betonund Bautechnik- Verein.

Dimmock, P. and Mair, R.J. (2007). Estimating volume loss for open-face tunnels in London clay. *Proceedings of the Institution of Civil Engineers, Geotechnical Engineering,* 160. 13–22.

Dimmock, P. and Mair, R.J. (2007). Volume loss experienced on open-face London Clay tunnels. *Proceedings of the Institution of Civil Engineers, Geotechnical Engineering*, 160, 3–12.

Franzius, J. N., Potts, D. M. and Burland, J. B. (2005). *The influence of soil anisotropy and K0 on ground surface movements resulting from tunnel excavation*. Géotechnique, 55, No. 3, 189–199.

Golser, J. and Kienberger, G. (1997). Permanente Tunnelauskleidung in Spritzbeton – Beanspruchung und Sicherheitsfragen. *Felsbau*, 1997, Nr6. 416–421.

Golser, J. (1999). Behaviour of early-age sprayed concrete. *Proceedings of. sprayed concrete for Underground Support VII*, São Paulo, Brazil. 11–15.

Golser, J. and Brandl, J. (1996). Die neue Österreichische Tunnelbaumethode als einschalige Bauweise. *Procedings of 5th International Conference Spritzbeton-Technologie 96*, Innsbruck, Austria, 65-69.

Golser, J. & Kienberger, G. (1997). Permanent sprayed concrete tunnel lining – loading and safety issues. *Felsbau* 6, 416-421.

Golser, J., Schubert, P. and Rabensteiner, K. (1989). *Proceedings of International. Congress on Progress and Innovation in Tunnelling*, Toronto, 79-85.

Holter , K.G., Bridge, R. and Tappy, O. (2010). Design and construction of permanent waterproof tunnel linings based on sprayed-applied double-bonded membrane. *Proceedings of international conference: underground construction*, Prague 2010. http://www.basf-cc.cz/cs/novinky/prisadydobetonu/technologiepropodzemnistavby/Documents/navrh_a_kostrukce_trvale_vodeodolneho_osteni.pdf

Holter, K.G., Nilsen, B., Langas, C. and Tandberg, M.K. (2014). Testing of sprayed waterproofing membranes for single shell sprayed concrete linings in hard rock. *Proceedings of 7th International Symposium on Sprayed Concrete*, Sandefjord, Norway, 208-221.

ICE (2010). *BTS-ICE Specification for Tunnelling, 3rd Edition*. London: Thomas Telford.

ITA (2001). Sprayed concrete for final linings: ITA working group report. *Tunnelling and Underground Space Technology*, Vol. 16. 295-309.

Itasca (2013). *FLAC 7.0 manual*.

Johnson, P.R. (2011). *Tests in shear and compression on sheets of 'Integritank' waterproofing material*. Unpublished report, University of Warwick.

Bibliography

London Underground (2007). *Civil Engineering Standard – Deep Tube Tunnels and Shafts.*

Marcher, T., John, M. and Ristic, M. Determination of Load-Sharing Effects in Sprayed Concrete Tunnel Linings. *Proceedings of Underground Construction Conference and Exhibition 2011*, London, BTS, ITA AITES.

Mair, R.J. (2008). Tunnelling and geotechnics: new horizons. *Géotechnique*, 58(9), 695-736

Melbye, T.A. and Dimmock, R. H. (2001). Modern advances and applications of sprayed concrete. *Proceedings of the International Conference on Engineering Developments in Sprayed concrete*, Netherlands: Lisse Publishing. http://www.episkevesold.civil.upatras.gr/selida%20ektoks%20skyrod/arthra%20pdf/MelbyeDimmockTasmania2002.pdf

Muir Wood, D. (2004). Geotechnical Modelling. London: Taylor & Francis.

New, B.M. & Bowers, K.H. (1994) Ground movement model validation at the Heathrow Express trial tunnel, *Proceedings of Tunnelling 94*, Institution of Mining & Metallurgy, London. 301 – 329.

Norris, P. and Powell, D. (1999). Towards quantification of the engineering properties of steel fibre reinforced sprayed concrete. *Proceedings of the 3rd International Symposium on Sprayed Concrete*, Norway, 393 – 402.

Oreste, P. (2007). A numerical approach to the hyperstatic reaction method for the dimensioning of tunnel supports. *Tunnelling and Underground Space Tehchnology,* 22(2), 185-205.

Potts, D.M. and Addenbrooke, T.I. (1997). A structure's influence on tunnelling-induced ground movement. Proceedings of the Institution of Civil Engineers, Geotechnical Engineering, 125, 109-125.

Potts, D.M. and Zdravkovic, L. (1999) *Finite element analysis in geotechnical engineering, Vol. 1: Theory*. London: Thomas Telford.

Potts, D.M. and Zdravkovic, L. (2001) *Finite element analysis in geotechnical engineering, Vol. 2: Application*. London: Thomas Telford.

RILEM (2002) Recommendations of RILEM TC162-TDF: 'Test and Design Methods for Steel Fibre Reinforced Concrete: bending test' (final recommendation), *Materials and Structures*, 35, 579-582.

Rispin, M., Gause, C. and Kurth, T. (2004). Robotic shotcrete applications for mining and tunnelling. Proceedings of North American Tunnelling 2004 conference, CRC publishing, 223-230.

Rossi, P. (2009). Steel or synthetic fibre reinforcement. http://www.structuremag.org/article.aspx?articleID=1184

Rowe, R.K. and Lee, K.M. (1992). An evaluation of simplified techniques for estimating three-dimensional undrained ground movements due to tunnelling in soft soils. Canadian Geotechnical Journal, 29, 39-52.

Sauer, G. and Sharma, B. (1977). A system for stress measurement in constructions in rock. Proceedings of International Symposium on Field Measurements in Rock Mechanics, 1, 317-329.

Schuetz, R., Potts, D.M. and Zdravkovic, L. (2011). Advanced constitutive modelling of shotcrete: Model formulation and calibration, *Computers and Geotechnics*, 38, 834-845.

Shin, J.H., Addenbrooke, T.I. and Potts, D.M. (2002). A numerical study of the effect of ground water movement on long-term tunnel behaviour. *Géotechnique,* 52(6), 391-403.

Swoboda, G. (1979). Finite element analysis of the New Austrian Tunnelling Method (NATM). *Proceedings of the 3rd International Conference on Numerical Numerical Methods in Geomechanics*, Aachen, 581-586.

Shin, J.H., Potts, D.M. and Zdravkovic, L. (2002). Three-dimensional modelling of NATM tunnelling in decomposed granite soil. *Géotechnique,* 52(3), 187-200.

Standing, J.R. and Potts, D.M. (2008). Contributions to Géotechnique 1948-2008: Tunnelling, *Géotechnique*, 58(5), 391-398.

Thomas A.H. (2009) Advance numerical modelling in tunnel design – the example of a major project in the UK. Safe tunnelling for the city and for the environment: *Proceedings of ITA-AITES world tunnel congress 2009*, Budapest, Hungary. http://www.ctta.org/FileUpload/ita/2009/papers/O-03/O-03-21.pdf

Thomas, A.H., Powell, D.B. and Clayton, C.R.I. (2001). Modelling of sprayed concrete tunnel linings. Proceedings of conference on Underground Construction, Institute of Mining & Metallurgy, London, 462-473.

US Army Corps of Engineering (1997). *Tunnels and shafts in rock. Engineering Manual* 1110-2-2901, Washington (USA)

Zdravkovic, L. and Carter, J. (2008). Contributions to *Géotechnique* 1948-2008: Constitutive and numerical modelling, *Géotechnique*, 58(5), 405-412.